

## AN ABSTRACT OF THE DISSERTATION OF

Liping Yang for the degree of Doctor of Philosophy in Chemistry presented on May 14, 2014

Title: Effects of Small Molecule Ligands on the Conformational Dynamics of the Farnesoid X Receptor Ligand Binding Domain (FXR-LBD)

Abstract approved: \_\_\_\_\_

Dr. Claudia S. Maier

The Farnesoid X Receptor (FXR) is a member of the nuclear receptor superfamily of transcription factors that plays a key role in the regulation of bile acids, lipid and glucose metabolisms. The regulative function of FXR is governed by conformational changes of the ligand binding domain (LBD) upon ligand binding. Although FXR is a highly researched potential therapeutic target, only a limited number of FXR-agonist complexes have been successfully crystallized and subsequently yielded high resolution structures. There is currently no structural information of any FXR-antagonist complexes publically available. This dissertation focuses on the development and application of hydrogen-deuterium exchange mass spectrometry (HDX-MS) to characterize the impact of various ligands on the structural dynamics of the FXR-LBD. Additionally, fluorescence spectroscopy is used to complement the HDX studies.

Firstly, we explored the use of amide HDX coupled with mass spectrometry for characterizing conformational changes in the FXR-LBD upon binding of three well known ligands: GW4064, a synthetic non-steroidal high affinity agonist; the bile acid chenodeoxycholic

acid (CDCA), the endogenous low affinity agonist of FXR; and Z-guggulsterone (GG), an *in vitro* antagonist of the steroid chemotype. Ligand-specific deuterium incorporation profiles were obtained for the FXR LBD upon interaction with the diverse ligand chemotypes. Comparison of the HDX profiles of the ligand-bound FXR-LBD complexes revealed a unique mode of interaction for GG. The conformational features of the FXR-LBD-antagonist interaction are discussed.

Secondly, several functional studies focusing on the health promoting effects of prenylflavonoids have suggested that prenylflavonoids, including xanthohumol (XN), isoxanthohumol (IX), and 8-prenylnaringenin (8-PN), are capable of modulating lipid metabolism possibly via modulating expression of FXR target genes. Therefore, we hypothesize that prenylflavonoid-type molecules might be FXR ligands that exert their regulatory effects by binding to the FXR-LBD thereby inducing changes in structural dynamics in a ligand-specific manner. Under identical experimental solution-phase conditions, we determined the effects of binding of prenylflavonoid-type compounds on the structural dynamics of FXR-LBD. Deuterium incorporation profiles were obtained for the four prenylflavonoids: XN, IX, 8-PN, and one derivative of XN, tetrahydroxanthohumol (TX). The HDX protection profiles of the FXR-LBD in presence of the diverse prenylflavonoids indicated partial conformational stabilization of the LBD in particular in regions that would be consistent with a model in which the prenylflavonoids interact with the canonical ligand binding cavity. *In silico* molecular docking studies predicted that the series of prenylflavonoids tested can act indeed as ligands of the FXR-LBD, in agreement with our HDX data. We discuss the prenylflavonoid-induced conformational changes in the context of the conformational changes that were observed with the known agonist (GW4064, CDCA) and *in vitro* antagonist (Z-GG).

Finally, to complement our HDX studies, intrinsic fluorescence titration experiments were conducted to investigate the interactions between the FXR-LBD and the seven ligands studied. The analysis of the quenching data suggested that GG and the prenylflavonoids have a strong ability to quench fluorescence of the tryptophan residues in the hFXR-LBD through a static quenching mechanism. The apparent dissociate constants  $K_d$  of the three prenylflavonoids with hFXR-LBD were  $2.7 \pm 0.1$   $\mu\text{M}$  for XN,  $5.9 \pm 0.3$   $\mu\text{M}$  for IX, and  $2.2 \pm 0.0$   $\mu\text{M}$  for 8-PN, indicating generally low affinity interactions between the prenylflavonoids and FXR. The analysis of the Scatchard plots and Hill plots suggested that hFXR-LBD seems to have more than one ligand binding site for IX and 8-PN. The comparison of the molecular volume between the small molecule compounds studied and eight well known typical FXR agonists suggested that hFXR-LBD has a tendency to offering more than one ligand binding cavity for compounds with smaller volume ( $<350 \text{ \AA}^3$ ).

Taken together, this is the first systematic HDX-MS study of the interaction of prenylflavonoids with the FXR LBD. The ligand-dependent HDX protection profiles provided insights in ligand-specific molecular recognition modes of structurally diverse ligand chemotypes. The current comparative HDX data are consistent with an interpretation in which the apo LBD exhibits rather conformationally flexible properties and that binding of ligand with high affinity exert strongly stabilizing effects. We further may speculate that the partial exchange protections and conformational stabilization observed for the prenylflavonoids may provide a glimpse into the mechanisms of partial agonism. The disparate ligand-specific conformational modulation of the FXR LBD may provide a possible framework for understanding the pleiotropic functions of FXR.

©Copyright by Liping Yang  
May 14, 2014  
All Rights Reserved

Effects of Small Molecule Ligands on the Conformational Dynamics of the Farnesoid X  
Receptor Ligand Binding Domain (FXR-LBD)

by  
Liping Yang

A DISSERTATION

submitted to

Oregon State University

in partial fulfillment of  
the requirements for the  
degree of

Doctor of Philosophy

Presented May 14, 2014  
Commencement June 2014

Doctor of Philosophy dissertation of Liping Yang presented on May 14, 2014

Approved:

---

Major Professor, representing Chemistry

---

Chair of the Department of Chemistry

---

Dean of the Graduate School

I understand that my dissertation will become part of the permanent collection of Oregon State University libraries. My signature below authorizes release of my dissertation to any reader upon request.

---

Liping Yang, Author

## ACKNOWLEDGEMENTS

Firstly, I would like to express my very great appreciation and gratitude to my advisor, Dr. Claudia S. Maier, for the patient guidance, persistent mentorship, and strong support she provided to me during my years of study at Oregon State University. I would also like to thank my committee members, Dr. Victor Hsu, Dr. Staci Simonich, Dr. Neal Sleszynski, and Dr. John Baham for the support and contributions that each of them offered to me while I pursued this final degree. I am particularly grateful for the friendly guidance, valuable suggestions, and assistance given by Dr. Victor Hsu.

Secondly, I would like to offer my special thanks to Dr. William H. Bisson and Dr. Juan Jiang for their timely advice and help in keeping my progress on schedule. My grateful thanks are also extended to Mr. Jeff Morré and Mr. Brian Arbogast, who provided me with lots of assistance in the operation of the instrumentation; and to the other members of the mass spectrometry lab, Dr. Samanthi Wickramasekara and Michelle Romero, for providing a supportive environment. I would like to further express my gratitude to Mr. David Broderick, who provided me with protein of high quality; to Dr. Adrian F. Gombart, Dr. Jan F. Stevens, and Dr. Yan Campbell, for their support; to my group-mates, Shin-Cheng Tzeng and Sasidhar Nirudodhi for their kind advice. I also wish to thank other members in Dr. Maier's group for their help and camaraderie: Fereshteh Zandkarimi, Lin Huang, Ievgen Motorykin, Jeremiah Kelley, and Zifeng Song.

Finally, I would like to express appreciation from the bottom of my heart to my husband, Xinhua Li, for his deep love, support, encouragement, and understanding, all the way from when I was first considering applying to the PhD program through to the completion of this degree.

## CONTRIBUTION OF AUTHORS

Corresponding Author: Dr. Claudia S. Maier

Contribution: Conceived research direction and provided leadership in all aspects of this dissertation.

Author: Liping Yang

Contribution: Implemented research design, conducted all experiments, collected and analyzed data, and wrote the first draft of the thesis and related manuscript.

Co-Author and Co-Corresponding Author of the Chapter 5: Dr. Victor Hsu

Contribution: Aided, conceived and implemented the experimental design, provided expertise for data analysis, reviewed and revised chapter 5; and provided feedback on early drafts of the thesis chapters 3 and 4 and related manuscripts.

Co-Author: David Broderick

Contribution: Purified protein samples and provided feedback on early drafts of the chapters and related manuscripts.

Co-Author: Dr. Yuan Jiang

Contribution: Helped with data analysis, provided statistical advice and comments, and developed the R script for fitting of the deuterium uptake data described in chapters 3 and 4.

Co-Author and Co-Corresponding Author of Chapter 4: Dr. William H. Bisson

Contribution: Performed the molecular docking experiments, aided in data interpretation and wrote the contents relating to the docking study for chapter 4.

Co-Author: Dr. J. Fred Stevens

Contribution: Provided the prenylflavonoids described in chapters 4 and 5.



Co-Authors: Dr. Adrian F. Gombart, and Dr. Yan Campbell

Contribution: Offered biologically experimental data in support of the research direction that led to chapter 4 and the related manuscript.

## TABLE OF CONTENTS

	Page
Chapter 1 .....	1
Introduction.....	1
1.1 FXR ligands: from physiological ligands to natural and synthetic ligands .....	3
1.1.1 The physiological ligands of FXR .....	5
1.1.2 Natural products that act as ligands of FXR .....	6
1.1.3 Synthetic ligands of the FXR.....	7
1.1.4 Co-crystal structures of FXR-LBD-ligand complexes .....	7
1.2 Prenylflavonoids – bioactive polyphenols from hops .....	8
1.2.1 Bioactivities of prenylflavonoids .....	9
1.2.2 Are Prenylflavonoids a novel class of emerging FXR ligands? .....	10
1.3 The methods used to study FXR-LBD-ligand interactions .....	11
1.3.1 Hydrogen-Deuterium Exchange Mass Spectrometry (HDX-MS).....	11
1.3.2 Intrinsic Fluorescence Titration .....	12
1.4 Reference.....	27
Chapter 2.....	37
Methods.....	37
2.1 HDX-MS method .....	38
2.1.1 The theory and mechanisms of HDX.....	38
2.1.2 Mass spectrometry (MS).....	41
2.1.3 HDX-MS analysis .....	45
2.1.3.1 Protein expression and purification .....	45
2.1.3.2 HDX MS workflow.....	46
2.1.3.3 Mass spectrometry setup used for intact protein analysis.....	48
2.1.3.4 HDX-MS data generation .....	48

## TABLE OF CONTENTS (Continued)

	Page
2.1.4 HDX data processing and analysis .....	49
2.1.4.1 Peptide identification .....	49
2.1.4.2 The determination of deuterium uptake levels.....	50
2.1.4.3 The determination of HDX rate constants .....	51
2.1.4.4 The normalization of deuterium up-take level.....	52
2.2 Fluorescence method.....	53
2.2.1 The theory of fluorescence.....	53
2.2.2 Fluorescence analysis.....	54
2.2.3 Fluorescence data analysis .....	54
2.3 Reference.....	63
Chapter 3 .....	67
Conformational dynamics of human FXR-LBD ligand interactions studied by hydrogen/deuterium exchange mass spectrometry: Insights into the antagonism of the hypolipidemic agent Z-guggulsterone .....	67
3.1 Abstract .....	69
3.2 Introduction .....	70
3.3 Materials and Methods .....	72
3.3.1. Materials .....	72
3.3.2. Protein expression and purification .....	72
3.3.3 Fluorescence titration experiment.....	73
3.3.4 HDX-MS analysis .....	74
3.3.5 Mass spectral data analysis .....	76
3.3.6 HDX kinetics .....	76
3.4 Results .....	77

## TABLE OF CONTENTS (Continued)

	Page
3.4.1. Ligand binding studies by intrinsic protein fluorescence measurements .....	77
3.4.2. Global HDX profiles of FXR-LBD. ....	78
3.4.3.1 HDX-MS of the apo FXR-LBD.....	79
3.4.3.2 Peptide-level HDX profiles of FXR-LBD in presence of different ligands .....	80
3.5 Discussion .....	84
3.6 Conclusion.....	88
3.7 References .....	90
3.8 Supplementary data .....	105
Chapter 4.....	125
Probing human FXR LBD – prenylflavonoid interactions by hydrogen/deuterium exchange mass spectrometry.....	125
4.1 Abstract .....	126
4.2 Introduction .....	127
4.3 Materials and Methods .....	128
4.3.1 Materials .....	128
4.3.2 Protein expression and purification .....	129
4.3.4 Hydrogen/deuterium exchange mass spectrometry .....	130
4.3.5 HDX data analysis .....	131
4.3.6 Kinetic Modeling .....	132
4.3.7 The Hierarchical clustering analysis.....	132
4.3.8 Molecular docking study.....	133
4.4 Results .....	133
4.4.1 HDX-MS analysis of intact protein provides indication of molecular recognition of prenylflavonoids by FXR LBD.....	133

## TABLE OF CONTENTS (Continued)

	Page
4.4.2 Peptide-level HDX protection profiles of FXR-LBD in presence of prenylflavonoid ligands .....	134
4.5 Discussion .....	135
4.6 Conclusion.....	138
4.7 Reference.....	149
4.8 Supplementary data .....	153
Chapter 5 .....	169
Human Farnesoid X Receptor Ligand Binding Domain (hFXR-LBD)–prenylflavonoid Interaction Investigated by Intrinsic Fluorescence Quenching.....	169
5.1 Abstract .....	170
5.2 Introduction .....	171
5.3 Materials and methods .....	173
5.3.1 Materials .....	173
5.3.2 Cell growth and purification of hFXR LBD .....	173
5.3.3 Fluorescence quenching experiments .....	174
5.3.4 Data analysis .....	175
5.4 Results .....	176
5.4.1 Intrinsic Fluorescence of apo hFXR-LBD and holo hFXR-LBD .....	176
5.4.2 Binding mechanism of ligand to the hFXR-LBD .....	178
5.4.3 Analysis of hFXR-LBD-ligand equilibrium binding data .....	179
5.5 Discussion .....	180
5.6 Conclusion.....	183
5.7 Reference.....	197
Chapter 6 .....	201

## TABLE OF CONTENTS (Continued)

	Page
Conclusion .....	201
Abbreviation .....	205
Bibliography .....	209

## LIST OF FIGURES

Figure	Page
Figure 1.1 Schematic representation of FXR action.....	15
Figure 1.2 The amino acid sequence and classical modular architecture of the FXR .....	16
Figure 1.3 Chemical structures of bile acids.....	18
Figure 1.4 Chemical structure of the GG.....	19
Figure 1.5 Crystal structure of FXR-LBD with GW4064 (PDB ID 3DCT).....	20
Figure 2.1 Schematic of a Synapt G1 HDMS mass spectrometry instrument.....	58
Figure 2.2 Experimental workflow used for the HDX-MS analyses of FXR LBD in presence of diverse ligands .....	59
Figure 2.3 Pipeline of HDX data analysis .....	60
Figure 2.4 Basic theory of fluorescence .....	61
Figure 2.5 Workflow of fluorescence quenching experiment .....	62
Figure 3.1 Fluorescence spectra of FXR-LBD with structures of the ligands used in the current study: GW4064, CDCA, and GG (Z) .....	96
Figure 3.2 Deuterium levels observed for the FXR-LBD with and without ligands after the following incubation periods: 0.5, 1, 2, 5, 10, 30, 60min.....	97
Figure 3.3 Comparative presentation of the HDX heat maps of FXR-LBD in the presence of ligands .....	98
Figure 3.4 Exchange-in plots of peptides that showed disparate exchange characteristics.....	100
Figure 3.5 Average differences in deuterium uptake (in %) of FXR-LBD with or without ligand overlaid onto crystallographic structures .....	101
Figure 3.6 Differential HDX data of FXR-LBD-agonist and FXR-LBD-antagonist .....	102
Figure S3.1 A SDS PAGE of purified hFXR-LBD; B, MS spectrum of purified hFXR-LBD .....	106
Figure S3.2 Binding of GG to FXR-LBD studied by intrinsic fluorescence titration .....	107
Figure S3.3 Design and schematic flow path diagrams of the UPLC system used in this study	108
Figure S3.4 Peptide coverage map of FXR-LBD .....	109

## LIST OF FIGURES (Continued)

Figure	Page
Figure S3.5 Mass spectra for peptides demonstrating evolution of deuterium incorporation into peptic peptides .....	110
Figure S3.6 Deuterium incorporation levels for each peptide at seven exchange-in time points. ....	115
Figure S3.7 Deuterium exchange data for apo FXR-LBD .....	118
Figure S3.8 Peptide-level HDX profiles of FXR-LBD in the presence of GW4064, CDCA and GG(Z), respectively. ....	119
Figure S3.9 Ligand-dependent deuterium exchange protection plots at the peptide level. ....	120
Figure S3.10 Overlay of the peptide deuterium levels of GW4064-bound hFXR-LBD and the B-factors of the backbone N atoms extracted from the crystal structure, PDB ID 3DCT.....	121
Figure 4.1 Chemical structures of the prenylflavonoids used in the present study .....	143
Figure 4.2 Global HDX uptake plots for the apo FXR-LBD in comparison to the FXR-LBD in presence of ligands.....	144
Figure 4.3 Peptic peptides HDX profiles of the holo FXR-LBD .....	145
Figure 4.4 Comparison of the HDX protection profiles at the peptide level .....	146
Figure 4.5 Cluster analysis of the HDX data for seven FXR-LBD-bound complexes.....	147
Figure 4.6 Top row: Detailed view of the hydrogen bonds formed between ligands and protein .....	148
Bottom row: Average differences in deuterium percentage (D%) of seven time points .....	148
Figure S4.1 Mass spectra for peptides demonstrating evolution of deuterium incorporation into peptic peptides. ....	154
Figure S4.2 Deuterium incorporation level for each peptide at seven exchange-in time points	161
Figure S4.3 The covalent modification of XN with the FXR-LBD. ....	164
Figure 5.1 Chemical structure of the four ligands .....	187
Figure 5.2 Fluorescence emission spectra of hFXR-LBD in the presence of different ligands .	188
Figure 5.3 The Stern-Volmer plots of hFXR-LBD quenching by the different ligands.....	189



## LIST OF FIGURES (Continued)

Figure	Page
Figure 5.4 Modified Stern-Volmer plots for GG and XN quenching of hFXR-LBD .....	190
Figure 5.5 Scatchard plots of the hFXR-LBD-molecule binding data .....	191
Figure 5.6 Hill plots of the hFXR-LBD-molecule binding data.....	192
Figure 5.7 Mass spectra of XN exhibiting covalently binding to hFXR-LBD.....	193

## LIST OF TABLES

Table	Page
Table 1.1 List of marine natural compounds that act as in vitro antagonists of FXR .....	21
Table 1.2 Published crystal structures of FXR-ligand complexes .....	22
Table 1.3 In vitro biological activities of prenylflavonoids.....	26
Table S3.1 Averaged differences in deuterium incorporation levels for each of the 20 peptides used in the current HDX-MS study .....	122
Table S3.2 The amide hydrogen distribution of each peptide in the six-fixed-rate-constant binning model .....	124
Table 4.1 ICM Docking score data into ligand binding pocket of the human FXR-LBD.....	142
Table S4.1 Average differences in deuterium incorporation levels for each of the peptide used in the current HDX-MS study .....	165
Table S4.2. The amide hydrogen distribution of each peptide in the six-fixed-rate-constant binning model .....	167
Table S4.3 Average deuterium exchange-in levels of each peptide for the FXR-LBD with presence and absence of ligands .....	168
Table 5.1 The Stern-Volmer constant ( $K_{SV}$ ), the fraction of fluorophore accessible to the quencher ( $f_a$ ), the bimolecular quenching constants ( $k_q$ ), the dynamic quenching constant ( $K_D$ ) and the static quenching constant ( $K_S$ ) of the hFXR-LBD-ligand .....	194
Table 5.2 Hill coefficient $n_H$ and the apparent dissociation constant $K_d$ ( $\mu\text{M}$ ) for different ligands with hFXR-LBD.....	195
Table 5.3 Comparison of different ligand volumes .....	196

## **Chapter 1**

### **Introduction**

Hydrogen-deuterium exchange mass spectrometry (HDX-MS) is an analytical technology that allows studying protein higher order structures, protein conformational dynamics and interactions under physiologically relevant conditions. This dissertation focuses on the development and application of HDX-MS for investigating the structural dynamics of the ligand binding domain (LBD) of the Farnesoid X Receptor (FXR), a ligand activated transcription factor that regulates bile acid, lipid and glucose homeostasis. FXR has emerged as a highly researched pharmacological receptor for intervention strategies that target metabolic diseases. However, structure activity relationship efforts are hampered by the limited structural information that is at present available for this potentially drugable receptor.

In this study, the HDX-MS technique was used for studying seven protein-ligand systems: FXR-LBD with GW4064 - a well-established high affinity agonist; FXR-LBD with chenodeoxycholic acid (CDCA) – its low affinity endogenous agonist; FXR-LBD with Z-guggulsterone (GG) – there is currently no co-crystal structure available for this low affinity in vitro antagonist; and FXR-LBD modulation by four prenylflavonoid-type compounds which are xanthohumol (XN), isoxanthohumol (IX), 8-prenylneringenin (8PN), and tetrahydroxanthohumol (TX). Prenylflavonoids are emerging new modulators of FXR of which currently no protein structural information is available. This dissertation describes for the first time the conformational structures of prenylflavonoid interactions with FXR LBD. Fluorescence spectroscopy was used to complement the small molecule ligand interaction studies. Computational models, developed in collaboration with Dr. Bisson, provided a first attempt to rationalize the ligand-induced differences in conformational dynamics of FXR LBD. In conclusion, HDX-MS derived conformational structures of small molecule FXR-LBD

interactions deepened our understanding of the mechanisms of action of nuclear receptor ligand interactions.

### **1.1 FXR ligands: from physiological ligands to natural and synthetic ligands**

FXR is one member of the nuclear receptor superfamily and also is a ligand-activated transcription factor. It plays a key role for regulating bile acids, lipoprotein, and glucose metabolisms [1, 2]. FXR has been also identified as a metabolic bile acid receptor which is expressed mainly in the liver, intestine, and kidney. In a proposed model (Figure 1.1) increased levels of bile acids in the liver activates FXR, resulting in an induction of small heterodimer partner (SHP), which in turn represses cytochrome P450 7A1 (CYP7A1) and CYP8B1 - the rate limiting enzymes in the conversion of cholesterol to bile acid [3-5]. Along with FXR activation, FXR up-regulates the bile salt export pump (BSEP) and indirectly down-regulates a transport protein-sodium taurocholate cotransporting polypeptide (NTCP), which is involved in bile acid uptake in the liver. Thus, activation of FXR in the liver inhibits bile acid synthesis and results in a net flux of bile acid from the liver to the intestine [6]. In addition, FXR decreased bile acid toxicity in the liver by increasing bile acid-modifying enzymes, such as sulphotransferase 2A1 (SULT2A1), UDP-glucuronosyltransferase 2B4 (UGT2B4) and CYP3A4 [5]. Similarly, activation of FXR in the intestine increases expression of the intestinal bile acid binding protein (IBABP) - a protein implicated in cellular uptake of bile acids, while decreases expression of intestinal bile acid transport (IBAT) [7]. Within the intestine, FXR downregulates the apical sodium-dependent bile acid transporter (ASBT) to reduce bile acid absorption and promotes recycling of bile acids to the liver via organic solute transporter- $\alpha$  (OST $\alpha$ ) and OST $\beta$  [5]. In the liver, FXR also down-regulates phosphoenolpyruvate carboxykinase (PEPCK) and glucose-6-phosphatase (G6Pase), two key enzymes in the glucose synthesis pathway to reduce

gluconeogenesis [5]. Furthermore, FXR reduces lipogenesis via inhibition of sterol-regulatory element-binding protein 1C (SREBP1C) and fatty acid synthase (FAS) [5].

Like other nuclear receptors, FXR shares the classical modular architecture (Figure 1.2): a ligand-binding domain (LBD) in the C-terminal, a DNA-binding domain in the N-terminal, and a connection hinge region [5, 8]. The LBD (amino acid 241-272), by binding with diverse ligands, controls the release of corepressor proteins and the subsequent recruitment of coactivator proteins. The FXR is a permissive binding partner of the retinoid X receptor (RXR) and the FXR/RXR $\alpha$  heterodimer can be activated by agonists for both RXR and FXR independently or together [9]. FXR/RXR $\alpha$  binds with the FXR elements or bile acid response elements, e.g. the BSEP response element, and further regulates bile acid metabolism [5]. It is required that agonists bind with FXR-LBD and form a coactivator complex, and then activate transcription genes of the FXR (Figure 1.2C). Kassam et al. found that the RXR agonist antagonized induction of BSEP expression mediated by the FXR agonist, which suggested that the FXR/RXR heterodimer functions as conditionally permissive heterodimer [10]. FXR ligands under preclinical investigation strongly suggests that they play a therapeutic role in the treatment of cholestasis, dyslipidemic disorders, and show a potential utility in the treatment of insulin resistance in patients with metabolic syndrome, type 2 diabetes and non-alcoholic steatohepatitis [4, 11]. Several reviews have discussed the physiologically relevant roles of FXR regulation and the potential of FXR as a target for synthetic ligands to prevent, manage or treat metabolic diseases.[4, 11-15].

Three research groups independently reported in 1999 CDCA as the most potent endogenous FXR agonist [16-18]. FXR activation rapidly became the objective of intense research efforts. Synthetic FXR agonists have been developed with the potential to treat

cholestatic liver diseases, including primary biliary cirrhosis, and metabolic disorders [19]. For instance, FXR agonists have been identified that improve myocardial fatty acid metabolism in obese (fa/fa) Zucker rats, and to counteract pro-atherogenic lipoprotein profiles and thereby confer protection against aortic plaque formation in (ApoE<sup>-/-</sup>) mice, a model of accelerated atherosclerosis [20-23]. Hence, the design and development of small molecules targeting FXR is a very promising approach to treat various metabolic diseases[15].

### **1.1.1 The physiological ligands of FXR**

As described previously, FXR is a bile acid nuclear receptor and bile acids are the most important physiological ligands of FXR. The bile acid skeleton is not flat because the C5 hydrogen at the juncture of rings A and B is oriented in the  $\beta$ -configuration forcing the A/B juncture into a cis configuration, which then enables bile acids to fit well into the FXR-LBD. Among bile acids (Figure 1.3), CDCA was identified as the most potent endogenous agonist (EC<sub>50</sub> ~ 8  $\mu$ M) of FXR, while deoxycholic acid (DCA) and lithocholic acid (LCA) showed weaker affinity with EC<sub>50</sub> ~ 50  $\mu$ M [16-18]. Ursodeoxycholic acid (UDCA) is inactive for FXR, however, it is to date the only approved medication by the FDA to treat primary biliary cirrhosis (PBC) [15]. Structure activity relationship research between FXR and bile acids with various chemical structures indicated that the configuration around position 7 is a key determinant of FXR activity, and then yielded a high affinity agonist of FXR, 6 $\alpha$ -ethyl-chenodeoxycholic acid (6ECDCA) [16, 24]. Another study suggested that polyunsaturated fatty acids, including arachidonic acid (AA), docosahexaenoic acid (DA), and linolenic acid (LA), are endogenous and selective FXR modulators that specifically regulate certain target genes of FXR [25].

### 1.1.2 Natural products that act as ligands of FXR

GG (Figure 1.4) has been identified as the key active ingredient in the gum resin of the tree *Commiphora mukul* and is used to treat hypolipidemia in India since 1987 [26]. Subsequent studies proved GG is an *in vitro* antagonist of FXR and that FXR antagonism by GG has been proposed as a mechanism for its hypolipidemic effect and cholesterol-lowering activity [27-29]. A number of studies relating to the biological activity of GG, both in animal models and human clinical trials, have focused primarily on the effects on lipid metabolism [28, 30, 31]. Also, the combination of GG and XN is more potent in exerting anti-obesity effects than additive effects of the individual compounds [32]. Internationally, GG has received considerable attention, and as a result several other biological activities have been uncovered [33, 34].

A recent study suggested that the hop chalcone XN is a ligand for FXR. XN activated FXR in a transient transfection assay. XN also modulated the expression of genes involved in lipid and glucose metabolism regulated by FXR in a diabetic rodent model [35]. However, whether XN can be truly classified as an *in vivo* agonist or a modulator of FXR awaits further investigations.

In recent years, a number of the natural compounds from marine species have been identified as ligands of the FXR to regulate its signaling (Table 1.1). Ten steroidal compounds bearing a 4-methylene group isolated from sponges of the genus *Theonella* antagonized FXR transactivation induced by CDCA in HepG2 cells [36]. The majority of the FXR antagonists contains a steroid skeleton [29, 37] and they might also regulate other steroid receptors. Nonsteroidal FXR antagonists are more suitable for investigating FXR physiology and help us to better understand the regulatory functions of the FXR. Six nonsteroidal compounds from the Korean tunicate *Botryllus tuberatus* are identified as antagonists of FXR [38].



### 1.1.3 Synthetic ligands of the FXR

Extensive research has been focused on steroidal ligand synthesis by modifying the chemical structure of bile acids, and resulted in the discovery of two potent FXR agonists, 6ECDCA and MFA-1 with an EC<sub>50</sub> of 99 nM and 17 nM, respectively [24, 39]. Until now, 6ECDCA is the first synthesized FXR agonist used in the clinical phase II trials among patients with PBC or non-alcoholic fatty liver [40]. Because of the high toxicity of bile acids in pharmacology, the synthesis of non-steroidal ligands of FXR began right after the discovery of FXR. In 2000, distinct stilbene-derivatives, as moderately potent FXR agonists, were discovered by screening a stilbene-based compound library [41]. Subsequently, GW4064 was identified as a highly potent and efficacious FXR agonist with an EC<sub>50</sub> of 70 nM [42]. GW4064 has emerged as the standard non-steroid high affinity agonist for FXR to investigate the role of FXR in regulating diverse signaling pathways. Three other classes of potent synthetic FXR agonists are azepino [4,5-b] indole compounds [43], benzopyran-based compounds [44], and benzimidazole-based compounds [45, 46]. Their chemical structures are shown in Table 1.2.

### 1.1.4 Co-crystal structures of FXR-LBD-ligand complexes

The X-ray structures of agonist-bound FXR complexes show the classical nuclear receptor (NR) fold, consisting of 12 helices that form a three-layer sandwich harboring the LBD (Figure 1.5.). FXR agonists can bind with the LBD in FXR and induce conformational changes that cause the recruitment of the coactivator proteins and keep the helix 12 in an active conformation [24, 42, 44, 47]. Ligand binding is primarily facilitated by interactions with residues located in helices 3 (L287, T288, M290, A291, and H294), 5 (M328, F329, R331, I335, and S342), 6 (L348, and I352), 7 (Y369), and 11 (H447, and W454) (Figure 1.5). Despite FXR's importance as a potentially therapeutically relevant receptor, only a limited number of X-ray

structures of the FXR-LBD bound to high affinity synthetic ligands are available that may guide structure-activity relationship (SAR) studies. The published X-ray crystal structures of FXR-ligand complexes illustrate binding modes of five different ligand chemotypes: three steroid-like agonists [24, 39], ten stilben-based agonists (GW4064 and derivatives) [42, 48-52], seven benzimidazole-based agonists [45, 46], two azepino [4,5-b] indole agonists (XL335 and FXR 450) [53, 54], and one fexaramide y-shaped ligand [44]. A summary of the various X-ray crystal structures of the FXR-LBD-ligand complex is compiled in table 1.2. To date, there are no published crystal structures available for antagonist-bound FXR-LBD complexes or the apo-protein. The conformational plasticity of FXR's LBD has been discussed as one of the possible reasons for the limited success of X-ray structural analyses of FXR-LBD ligand complexes [39].

## **1.2 Prenylflavonoids – bioactive polyphenols from hops**

Prenylflavonoids have been identified as one of the main classes of chemical compounds from the cones of the hop plant (*Humulus Lupulus L.*). The hop cones are widely used in the brewing industry to add bitterness and flavor to beer. Therefore, beer is the most significant dietary source of prenylflavonoids [55]. As a medicinal remedy, hop cones have been widely used over centuries: by Native American tribes as a sedative to treat insomnia and a poultice to treat pneumonia [56, 57]; to treat restlessness as recommended by the Ayurvedic Pharmacopoeia in India [58]; and to treat insomnia, dyspepsia, and acute bacterial dysentery in China [59]. Research has shown that the four major prenylflavonoids, XN, isoxanthohumol (IX), 6-prenylnaringenin (6PN) and 8-prenylnaringenin (8PN), contribute to the use of hop cones as medicinal. Today, XN is the biologically active component in two dietary supplements, MeridumXN<sup>TM</sup> and MeridiumXH<sup>TM</sup>, which have been marketed in the United States to promote general health and relieve metabolic stress ([www.bionovex.com](http://www.bionovex.com)).

### 1.2.1 Bioactivities of prenylflavonoids

An overview of *in vitro* biological activities of prenylflavonoids is given in Table 1.3. Over the past two decades, several studies have suggested that prenylflavonoids function as potential cancer chemopreventive agents. XN has received a great deal of attention as a broad-spectrum chemopreventive agent and is the best studied cancer chemopreventive phytochemical isolated from hops [60-66]. A recent study reported that the consumption of XN by diabetic animals consistently inhibits angiogenesis, inflammation and oxidative stress, allowing control of neovascularization and improving diabetic wound healing [67]. XN also induced apoptosis of human T98G glioblastoma cells with a high degree of malignancy [68, 69]. Besides the very potent anticancer bioactivity of XN, the other three prenylflavonoid compounds (IX, 6-PN, and 8-PN) demonstrated similar potency of inhibiting the angiogenesis and growth of several kinds of human tumor cells, including breast cancer cells, colon cancer cells, ovarian cancer cells, and prostate cancer cells [60, 65, 66].

Besides its anti-cancer activity, estrogenic activity of prenylflavonoids has been demonstrated by several research groups. Among the prenylflavonoids, 8-PN has been identified as one of the most potent phytoestrogens isolated to date based on the following findings: (a) 8PN has a high affinity to bind with the estrogen receptors (ER), and its EC<sub>50</sub> is 4 nM and 40 nM in the Ishikawa cell assay and yeast screen cell assay, respectively [70], and 8PN showed about 100 times more potency than genistein [71]; (b) 8PN is able to improve some menopausal symptoms relating to estrogen deficiency, such as hot flashes, sweating, insomnia, heart palpitations, and irritability [72-74]. Among the other major prenylflavonoids, 6PN showed very weak estrogenic activity, while XN and IX were inactive [70].

XN showed high antioxidant activity in inhibiting human low-density lipoprotein oxidation [75]. As a broad spectrum anti-infective agent, the anti-infective properties of XN are described in detail in a recent review [76]. Additionally, Lee et al reported that XN exhibited potent activity in inhibiting platelet aggregation stimulated by collagen, and this novel role of XN might point to a therapeutic potential of XN in prevention and treatment of cardiovascular diseases [77].

### **1.2.2 Are Prenylflavonoids a novel class of emerging FXR ligands?**

Prenylflavonoids in hops have been researched by Dr. Fred Stevens' group at Oregon State University since the 1990's. Their work significantly contributed to the emergence of prenylflavonoids as highly potent bio-active natural products [78-80]. To date, only a few studies have reported that XN has potential in modulating hyperlipidemia based on the following experimental results: XN inhibits the expression or activity of diacylglycerol acyltransferase [81] and triglyceride synthesis and secretion in HepG2 cells [82]; XN functions as an FXR agonist in a transient transfection assay, and the determination of hepatic gene expression in XN-fed mice suggested that XN acts as an selective bile acid receptor modulator [35]. XN and isoxanthohumol (IX) inhibit lipid accumulation in maturing preadipocytes, possibly partly by modulating FXR target genes [83]. These initial studies implied that XN has a role in modulating lipid metabolism and led to the hypothesis that XN possibly interacts with FXR.

Recently, a study completed by Dr. Adrian Gombart's [84] group at Oregon State University showed that XN did induce BSEP promoter activity in HEK293 cell lines – one of FXR target genes (manuscript in preparation). This induction occurred at a similar level as observed for CDCA and GG in biliary carcinoma cells that express FXR. Also, XN is capable of inducing the expression of FXR target genes in biliary carcinoma cells as well as or better than

current known agonists, which suggests that XN functions as a bona-fide ligand for FXR. These findings prompted us to study FXR–prenylflavonoid interactions by HDX-MS, to obtain the molecular descriptions of these interactions.

### **1.3 The methods used to study FXR-LBD-ligand interactions**

In this dissertation, HDX-MS and fluorescence titration methods were explored for performing FXR-LBD-ligand interaction studies. Motivation for the application of HDX-MS was grounded in the repeatedly reported difficulties of obtaining X-ray crystal structures of the FXR-ligand complexes due to the plasticity of the FXR-LBD [39, 85]. ).

#### **1.3.1 Hydrogen-Deuterium Exchange Mass Spectrometry (HDX-MS)**

Over the last twenty years, hydrogen/deuterium exchange in combination with mass spectrometry (HDX-MS) has emerged as a powerful method to study conformational changes in proteins induced by (un)folding [86-88] and interactions with other proteins, peptides, oligonucleotides, small molecule ligands, post-translational modifications, membrane bilayers and surfaces [89, 90]. The rate of exchange of backbone amide hydrogens is highly sensitive to changes in conformational flexibility, hydrogen bonding strength and solvent accessibility [90]. HDX-MS has been used successfully for studying the conformational properties of diverse nuclear receptors and their conformational changes upon binding to diverse ligands [91-94].

The physiological functions of a nuclear receptor depend on their conformations and dynamics, which can be changed by ligand or a drug binding at specific binding sites. HDX-MS has emerged as a powerful technology to study receptor-ligand (drugs) interaction and to assist in the development of small/large molecule drugs in pharmaceutical industries. Differential HDX-MS studies enable the comparison of apo protein and holo protein and provide distinct deuterium uptake profile, a “HDX fingerprint”, for each protein ligand system studied. “HDX fingerprints”

permit scientists to classify ligands into different clusters. In each cluster, ligands often share a similar binding mode in the ligand binding pocket of proteins and induce similar conformational changes. From a pharmacology point of view, ligands in the same cluster will regulate target genes of a protein in a similar way. Ligand cluster analysis has been applied to the vitamin D receptor (VDR) [95], the estrogen receptor (ER) [93, 96], and the peroxisome proliferator-activated receptor (PPAR) [95].

Chapter 4 describes a comparative HDX-MS study of prenylflavonoid-type ligands on the structural dynamics of the FXR-LBD. We determined the mode of binding of prenylflavonoid-type ligands and how these novel FXR ligands affect the structural dynamics of the FXR-LBD. We also discuss the differences in the mode of conformational modulation of the FXR LBD by the different classes of ligand studied.

### **1.3.2 Intrinsic Fluorescence Titration**

Chapter 5 is devoted to intrinsic fluorescence titration studies to determine the mode of ligand binding to FXR LBD and to complement the HDX-MS-based conformational analyses. This was possible because our FXR-LBD construct contains two tryptophan residues, tryptophan 454 and tryptophan 469, located in helix 11 and helix 12, respectively. We used intrinsic fluorescence quenching methodology to investigate interactions between seven ligands (GW4064, CDCA, GG, XN, IX, 8-PN, and TX) and FXR-LBD. We attempt to clarify quenching mechanisms for the ligands, to determine their apparent dissociation constants, and to identify how the exposure and environment of tryptophan residues in FXR-LBD are impacted by the presence of ligands.

Intrinsic protein fluorescence is a common phenomenon in proteins because of the existence of three aromatic amino acids: phenylalanine (Phe), tyrosine (Tyr), and tryptophan

(Trp). Tyr and Trp are used experimentally as the main intrinsic fluorescence sources in proteins because the quantum yield of Phe is so low that it cannot produce a strong enough fluorescence signal. In order to measure the fluorescence of Trp, the excitation wavelength 295 nm is often selected because no absorption for Tyr at this wavelength is observed. Trp fluorescence is highly sensitive to its local environment in solution and its emission spectrum is often changed because of protein conformational transitions, subunit association, substrate binding, or denaturation [97]. The intrinsic fluorescence quenching method has been used for studying the structures and dynamics of proteins [98] for investigating ligand/receptor interactions [99-102] and determining the dissociation constant and/or the binding affinity of ligands to proteins [103].

## Figures

Figure 1.1 Schematic representation of FXR action.

Figure 1.2 Amino acid sequence and classical modular architecture of the FXR

Figure 1.3 Chemical structures of bile acids

Figure 1.4 Chemical structure of GG

Figure 1.5 Crystal structure of FXR-LBD with GW4064, a high affinity agonist (PDB ID 3DCT)

## Tables

Table 1.1 List of marine natural compounds that act as in vitro antagonists of FXR

Table 1.2 Published crystal structures of the FXR-ligand complexes (as of 2013)

Table 1.3 In vitro biological activities of prenylflavonoids



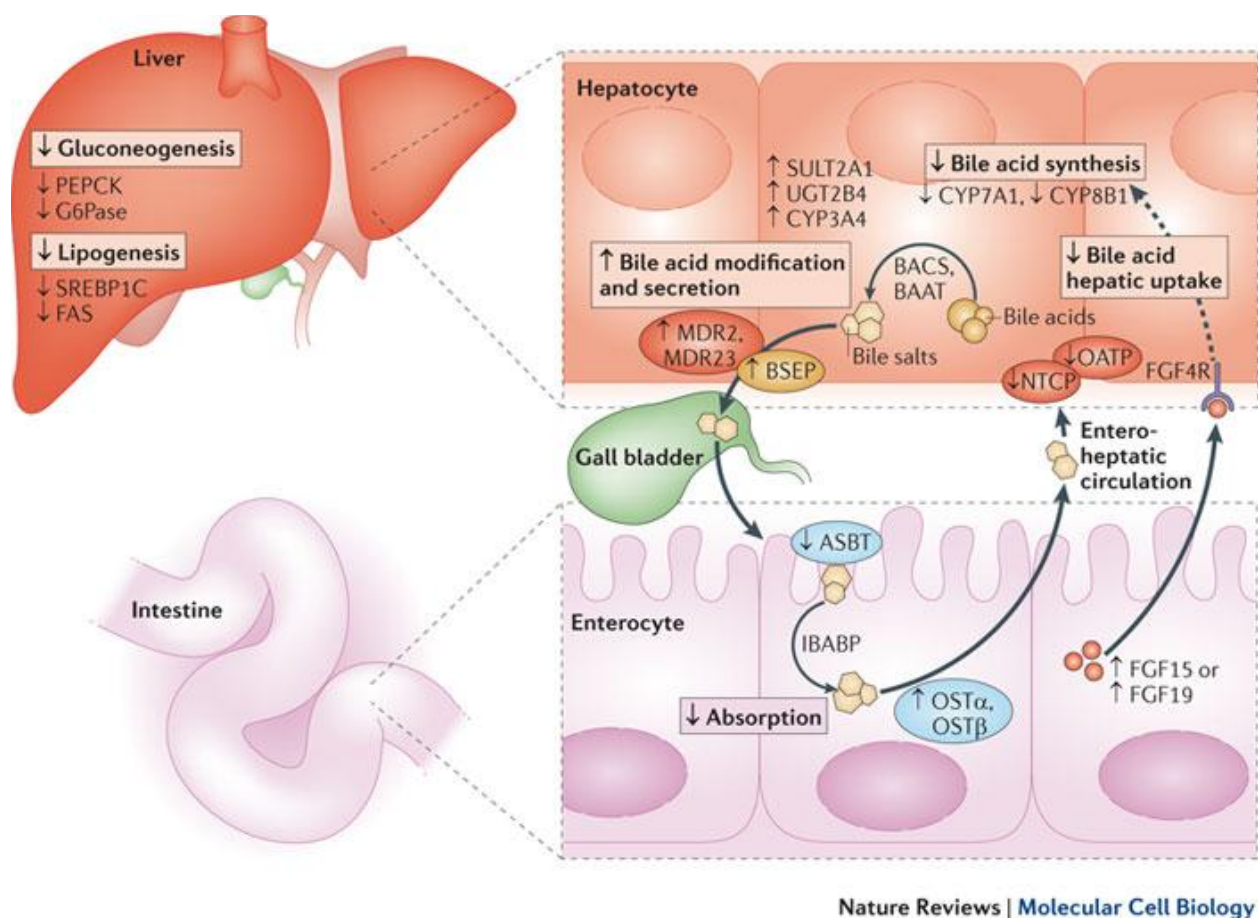


Figure 1.1 Schematic representation of FXR action.

Upwards arrow indicates upregulation and downwards arrow indicates downregulation. Copied from [5].

Farnesoid X receptor (FXR); cytochrome P450 7A1 (CYP7A1) and CYP8B1; bile acid-modifying enzymes sulphotransferase 2A1 (SULT2A1), UDP-glucuronosyltransferase 2B4 (UGT2B4) and CYP3A4; bile acid CoA synthase (BACS) and bile acid CoA–amino acid N-acetyltransferase (BAAT); bile salt export pump (BSEP); multidrug resistance protein 2 (MDR2) and MDR3; the apical sodium-dependent bile acid transporter (ASBT); ileal bile acid binding-protein (IBABP); organic solute transporter- $\alpha$  (OST $\alpha$ ) and OST $\beta$ ; organic anion transporting polypeptide (OATP); sodium taurocholate cotransporting polypeptide (NTCP); fibroblast growth factor 15 (FGF15) in mice or FGF19 in humans; FGF4 receptor (FGF4R); phosphoenolpyruvate carboxykinase (PEPCK) and glucose-6-phosphatase (G6Pase); sterol-regulatory element-binding protein 1C (SREBP1C) and fatty acid synthase (FAS).

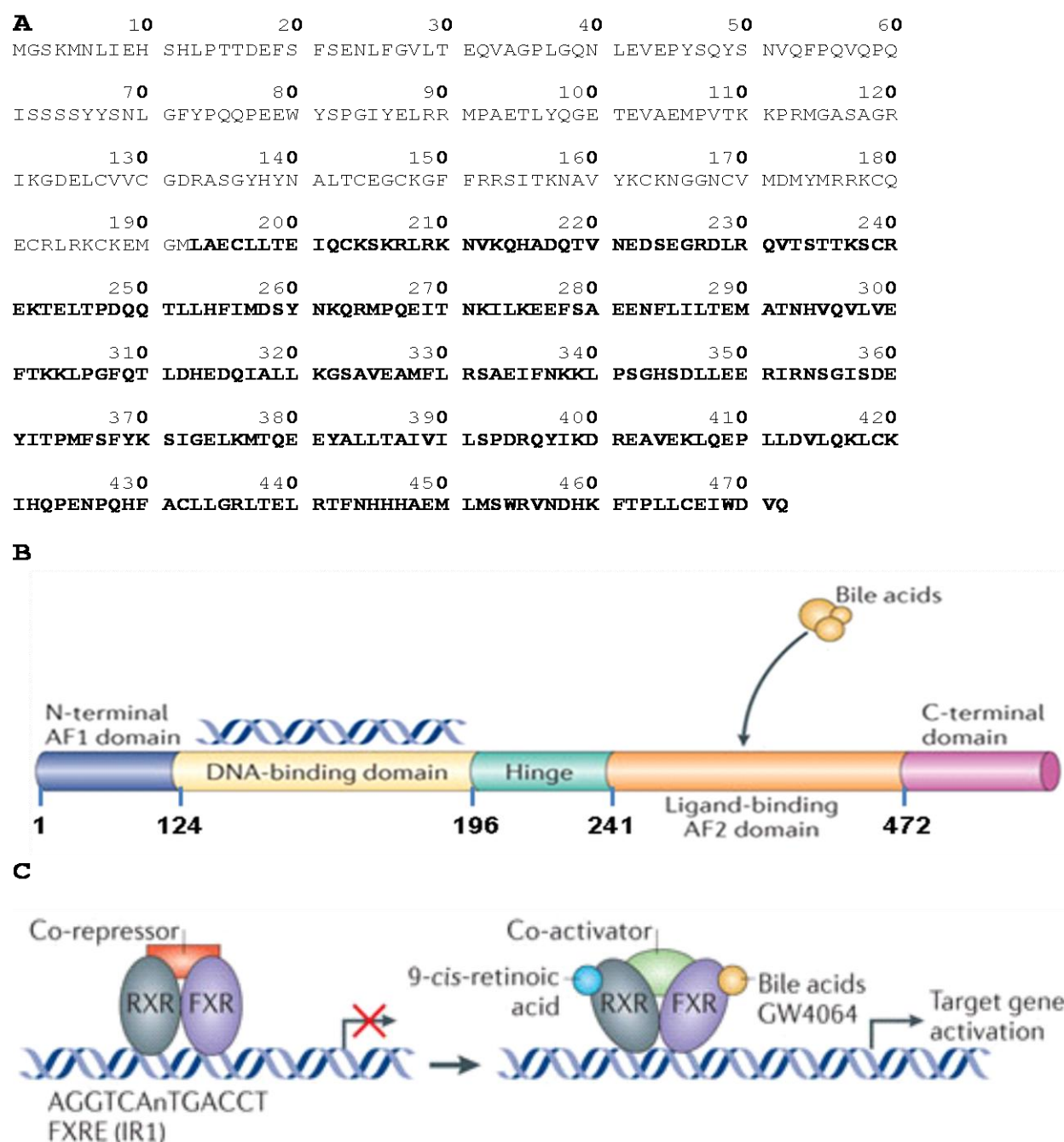
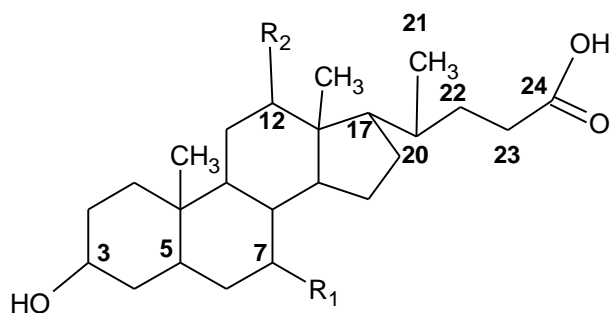


Figure 1.2 The amino acid sequence and classical modular architecture of the FXR

(A) The full length amino acid sequence of human FXT (hFXR). The highlighted sequence corresponds to the amino acid sequence of the FXR-LBD construct used in this dissertation.

(B) The basic structure of a ligand-activated nuclear receptor. The five functional domains are highlighted. The AF2 domain encompasses the ligand binding domain. This thesis focuses on the

partial sequence 241 – 472 of the AF2 domain of human FXR. (C) The farnesoid X receptor (FXR) forms a heterodimer with RXR and binds to the FXR response element (FXRE), which is typically an inverse repeat spaced by one nucleotide (IR1), in its target genes to induce gene expression. AF domain, activation function domain; C-terminal, carboxy-terminal; N-terminal, amino-terminal. Adapted from [5].



	R1	R2
Cholic acid (CA)	OH ( $\alpha$ )	OH
Chenodeoxycholic acid (CDCA)	OH ( $\alpha$ )	H
Deoxycholic acid (DA)	H	OH
Lithocholic acid (LA)	H	H
Ursodeoxycholic acid (UDCA)	OH ( $\beta$ )	H
Ursocholic acid (UCA)	OH ( $\beta$ )	OH

Figure 1.3 Chemical structures of bile acids

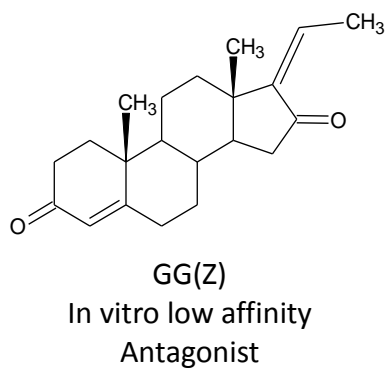


Figure 1.4 Chemical structure of the GG

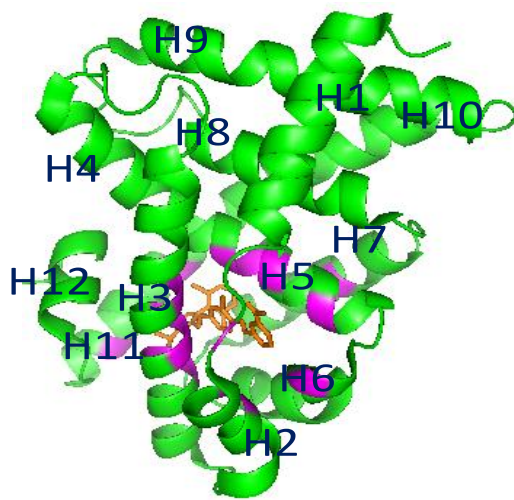


Figure 1.5 Crystal structure of FXR-LBD with GW4064 (PDB ID 3DCT)

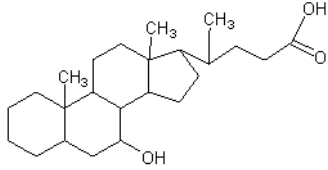
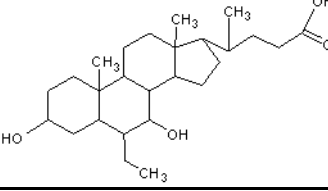
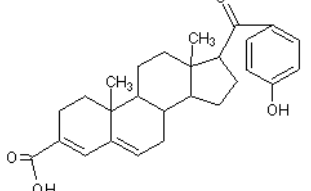
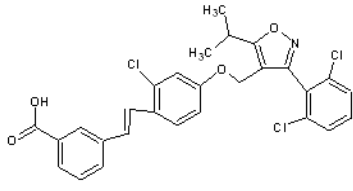
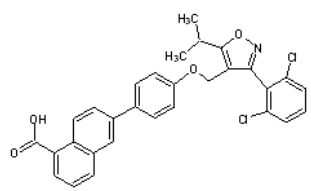
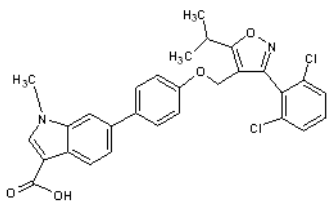
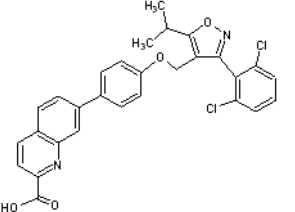
The crystal structure exemplifies the classical ligand activated nuclear receptor fold: Twelve (12) helices that are arranged in an alpha helical sandwich fold formed by three anti-parallel alpha helices that are flanked by two alpha helices on one side and three on the other side. The ligand binding cavity is within the interior of the LBD. The contact residues between the FXR-LBD and GW4064 are shown in magenta

Table 1.1 List of marine natural compounds that act as in vitro antagonists of FXR

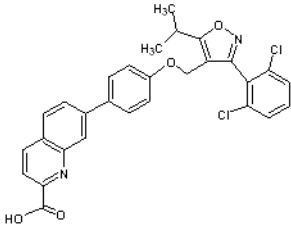
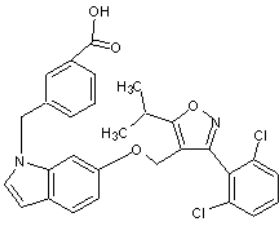
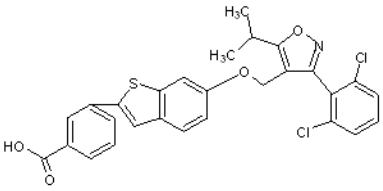
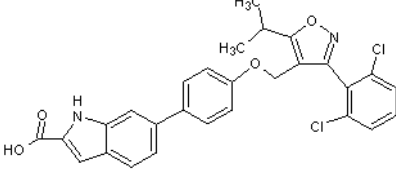
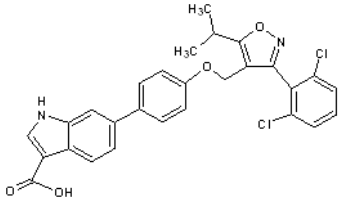
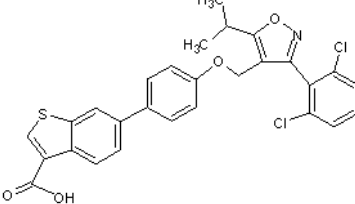
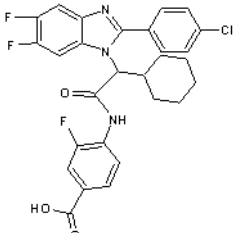
( adapted from [104])

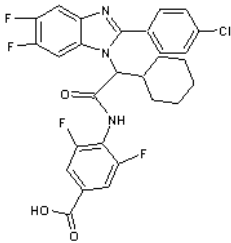
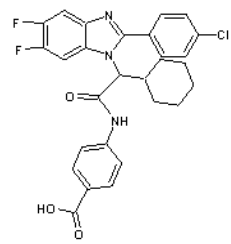
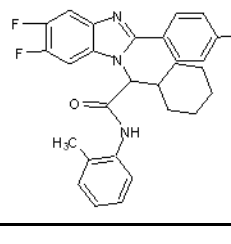
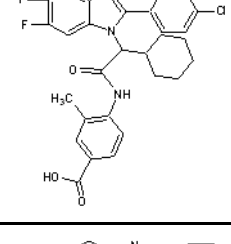
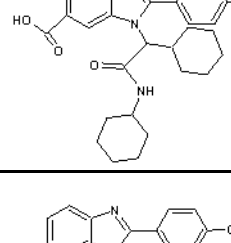
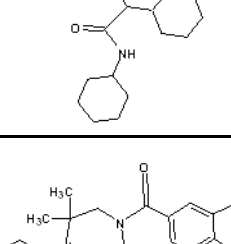
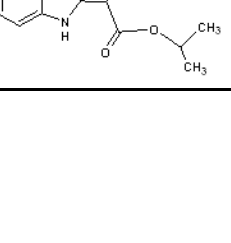
Compounds	Origin	Reference
Tuberatolide A	Korean marine tunicate <i>Botryllus tuberatus</i>	[38]
tuberatolide B	Korean marine tunicate <i>Botryllus tuberatus</i>	[38]
2'-epi-tuberatolide B	Korean marine tunicate <i>Botryllus tuberatus</i>	[38]
yezoquinolide	Korean marine tunicate <i>Botryllus tuberatus</i>	[38]
sagachromenol	Korean marine tunicate <i>Botryllus tuberatus</i>	[38]
Compounds 1-5	marine sponge <i>Spongia Sp.</i>	[105]
4-methylenesterols	marine sponge <i>Theonellaswinhoei</i>	[36]
Suvanine	marine sponge	[106]
Sulfated sterol	marine invertebrates	[37]
theonellasterol	marine sponge <i>Theonellaswinhoei</i>	[107]
Compound 1	soft coral <i>Dendronephthya gigantea</i>	[108]

Table 1.2 Published crystal structures of FXR-ligand complexes  
(as of 12/2013)

Chemotypes	Ligand - Chemical Structures	PDB ID	Reference
steroid type		1OT7	[24]
		1OSV	[24]
		3BEJ	[39]
GW4064 and derivatives		3DCT	[42]
		3DCU	[49]
		3FXV	[48]
		3P89	[49]



		3P88	[49]
		3HC6	[51]
		3HC5	[51]
		3RVF	[49]
		3RUU	[49]
		3RUT	[49]
Benzimidazole		3OMM	[46]

		30OK	[46]
		30OF	[46]
		30MK	[46]
		30LF	[46]
		30KH	[45]
		30KI	[45]
Azepino Indole		3FLI	[53]

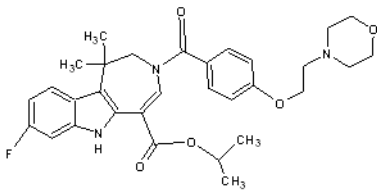
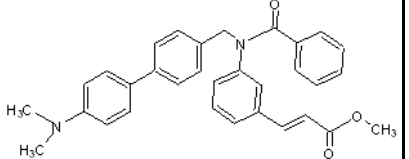
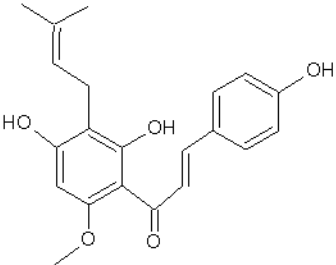
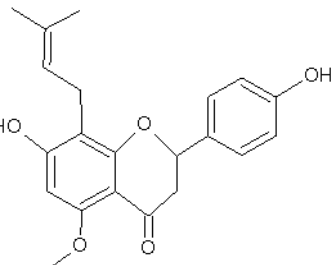
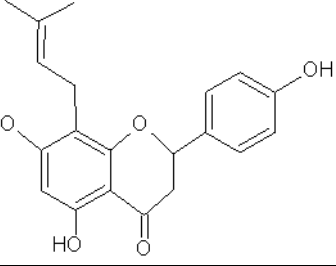
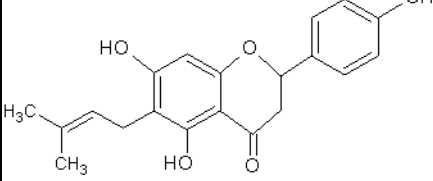
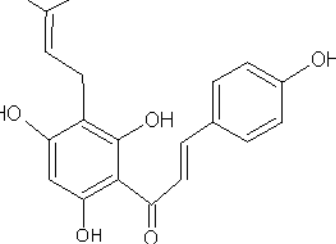
	 <chem>CC(C)OC(=O)c1c2c(c3cc(F)ccc3n1)nc(C)(C)c4cc(=O)cc(OCN5CCOCC5)cc4</chem>	3L1B	[54]
Fexaramine	 <chem>CCN(C)c1ccc(cc1)-c2ccc(cc2)CN(C(=O)c3ccccc3)/C=C/C(=O)OC</chem>	1OSH	[44]

Table 1.3 In vitro biological activities of prenylflavonoids

(Adapted from [109])

Prenylflavonoids	Chemical Structures	Biological Activities	Reference
xanthohumol (XN)		Antiproliferative activity	[60] [65, 66]
		Induction of QR activity	[110, 111]
		Antioxidant and antiperoxidant	[75, 112]
		Inhibit procarcinogens activation	[110]
		Inhibit cyclooxygenase enzymes	[110]
		Inhibit nitric oxide synthase	[110]
		Inhibit angiogenesis	[113]
		Induction of apoptosis	[63, 114, 115]
isoxanthohumol (IX)		Antiproliferative activity	[60, 65, 66]
		Induction of QR activity	[110]
		Inhibit procarcinogens activation	[110]
		Inhibit nitric oxide synthase	[110]
		Inhibit angiogenesis	[116]
8-prenylnaringenin (8PN)		Antiproliferative activity	[65, 66]
		Induction of QR activity	[111]
		Inhibit procarcinogens activation	[110]
		Inhibit cyclooxygenase enzymes	[110]
		Inhibit angiogenesis	[117]
		Estrogenic activity	[70, 71]
6-prenylnaringenin (6PN)		Antiproliferative activity	[65, 66]
		Induction of QR activity	[111]
		Inhibit procarcinogens activation	[110]
		Estrogenic activity	[70, 71]
Desmethylxanthohumol (DX)		Antiproliferative activity	[65, 66]
		Antioxidant and antiperoxidant	[75, 112]

QR, quinone reductase

## 1.4 Reference

- [1] B. Goodwin, S.A. Jones, R.R. Price, M.A. Watson, D.D. McKee, L.B. Moore, C. Galardi, J.G. Wilson, M.C. Lewis, M.E. Roth, P.R. Maloney, T.M. Willson, S.A. Kliewer, A regulatory cascade of the nuclear receptors FXR, SHP-1, and LRH-1 represses bile acid biosynthesis, *Mol Cell*, 6 (2000) 517-526.
- [2] K. Ma, P.K. Saha, L. Chan, D.D. Moore, Farnesoid X receptor is essential for normal glucose homeostasis, *J Clin Invest*, 116 (2006) 1102-1109.
- [3] L.B. Moore, D.J. Parks, S.A. Jones, R.K. Bledsoe, T.G. Consler, J.B. Stimmel, B. Goodwin, C. Liddle, S.G. Blanchard, T.M. Willson, J.L. Collins, S.A. Kliewer, Orphan nuclear receptors constitutive androstane receptor and pregnane X receptor share xenobiotic and steroid ligands, *J Biol Chem*, 275 (2000) 15122-15127.
- [4] S. Westin, R.A. Heyman, R. Martin, FXR, a therapeutic target for bile acid and lipid disorders, *Mini Rev Med Chem*, 5 (2005) 719-727.
- [5] A.C. Calkin, P. Tontonoz, Transcriptional integration of metabolism by the nuclear sterol-activated receptors LXR and FXR, *Nat Rev Mol Cell Biol*, 13 (2012) 213-224.
- [6] L.A. Denson, E. Sturm, W. Echevarria, T.L. Zimmerman, M. Makishima, D.J. Mangelsdorf, S.J. Karpen, The orphan nuclear receptor, shp, mediates bile acid-induced inhibition of the rat bile acid transporter, ntcp, *Gastroenterology*, 121 (2001) 140-147.
- [7] T. Kanda, L. Foucand, Y. Nakamura, I. Niot, P. Besnard, M. Fujita, Y. Sakai, K. Hatakeyama, T. Ono, H. Fujii, Regulation of expression of human intestinal bile acid-binding protein in Caco-2 cells, *Biochem J*, 330 ( Pt 1) (1998) 261-265.
- [8] Y. Zhang, H.R. Kast-Woelbern, P.A. Edwards, Natural structural variants of the nuclear receptor farnesoid X receptor affect transcriptional activation, *J Biol Chem*, 278 (2003) 104-110.
- [9] A.I. Shulman, C. Larson, D.J. Mangelsdorf, R. Ranganathan, Structural determinants of allosteric ligand activation in RXR heterodimers, *Cell*, 116 (2004) 417-429.
- [10] A. Kassam, B. Miao, P.R. Young, R. Mukherjee, Retinoid X receptor (RXR) agonist-induced antagonism of farnesoid X receptor (FXR) activity due to absence of coactivator recruitment and decreased DNA binding, *J Biol Chem*, 278 (2003) 10028-10032.
- [11] S. Fiorucci, G. Rizzo, A. Donini, E. Distrutti, L. Santucci, Targeting farnesoid X receptor for liver and metabolic disorders, *Trends Mol Med*, 13 (2007) 298-309.
- [12] C. Soldani, M.G. Bottone, C. Pellicciari, A.I. Scovassi, Nucleolus disassembly in mitosis and apoptosis: dynamic redistribution of phosphorylated-c-Myc, fibrillarin and Ki-67, *Eur J Histochem*, 50 (2006) 273-280.

- [13] M.L. Crawley, Farnesoid X receptor modulators: a patent review, *Expert Opin Ther Pat*, 20 (2010) 1047-1057.
- [14] R. Pellicciari, R.C. Rizzo, G. Costantino, M. Marinozzi, L. Amori, P. Guidetti, H.Q. Wu, R. Schwarcz, Modulators of the kynurenine pathway of tryptophan metabolism: synthesis and preliminary biological evaluation of (S)-4-(ethylsulfonyl)benzoylalanine, a potent and selective kynurenine aminotransferase II (KAT II) inhibitor, *ChemMedChem*, 1 (2006) 528-531.
- [15] D. Merk, D. Steinhilber, M. Schubert-Zsilavecz, Medicinal chemistry of farnesoid X receptor ligands: from agonists and antagonists to modulators, *Future Med Chem*, 4 (2012) 1015-1036.
- [16] H. Wang, J. Chen, K. Hollister, L.C. Sowers, B.M. Forman, Endogenous bile acids are ligands for the nuclear receptor FXR/BAR, *Mol Cell*, 3 (1999) 543-553.
- [17] M. Makishima, A.Y. Okamoto, J.J. Repa, H. Tu, R.M. Learned, A. Luk, M.V. Hull, K.D. Lustig, D.J. Mangelsdorf, B. Shan, Identification of a nuclear receptor for bile acids, *Science*, 284 (1999) 1362-1365.
- [18] D.J. Parks, S.G. Blanchard, R.K. Bledsoe, G. Chandra, T.G. Consler, S.A. Kliewer, J.B. Stimmel, T.M. Willson, A.M. Zavacki, D.D. Moore, J.M. Lehmann, Bile acids: natural ligands for an orphan nuclear receptor, *Science*, 284 (1999) 1365-1368.
- [19] A. Lanzini, M.G. De Taroni, B. Panarotto, S. Scalia, A. Mora, F. Benini, O. Baisini, F. Lanzarotto, Intestinal absorption of the bile acid analogue Se-75-homocholic acid-aurine is increased in primary biliary cirrhosis, and reverts to normal during ursodeoxycholic acid administration, *Gut*, 52 (2003) 1371-1375.
- [20] C.J. Sinal, M. Tohkin, M. Miyata, J.M. Ward, G. Lambert, F.J. Gonzalez, Targeted disruption of the nuclear receptor FXR/BAR impairs bile acid and lipid homeostasis, *Cell*, 102 (2000) 731-744.
- [21] G.L. Guo, S. Santamarina-Fojo, T.E. Akiyama, M.J.A. Amar, B.J. Paigen, B. Brewer, F.J. Gonzalez, Effects of FXR in foam-cell formation and atherosclerosis development, *Bba-Mol Cell Biol L*, 1761 (2006) 1401-1409.
- [22] E.A. Hanniman, G. Lambert, T.C. McCarthy, C.J. Sinal, Loss of functional farnesoid X receptor increases atherosclerotic lesions in apolipoprotein E-deficient mice, *Journal of Lipid Research*, 46 (2005) 2595-2604.
- [23] Y.Q. Zhang, X.P. Wang, C. Vales, F.Y. Lee, H. Lee, A.J. Lusis, P.A. Edwards, FXR deficiency causes reduced atherosclerosis in *Ldlr*(-/-) mice, *Arterioscl Throm Vas*, 26 (2006) 2316-2321.
- [24] L.Z. Mi, S. Devarakonda, J.M. Harp, Q. Han, R. Pellicciari, T.M. Willson, S. Khorasanizadeh, F. Rastinejad, Structural basis for bile acid binding and activation of the nuclear receptor FXR, *Mol Cell*, 11 (2003) 1093-1100.

- [25] A. Zhao, J. Yu, J.L. Lew, L. Huang, S.D. Wright, J. Cui, Polyunsaturated fatty acids are FXR ligands and differentially regulate expression of FXR targets, *DNA Cell Biol*, 23 (2004) 519-526.
- [26] C.J. Sinal, F.J. Gonzalez, Guggulsterone: an old approach to a new problem, *Trends Endocrinol Metab*, 13 (2002) 275-276.
- [27] J. Wu, C. Xia, J. Meier, S. Li, X. Hu, D.S. Lala, The hypolipidemic natural product guggulsterone acts as an antagonist of the bile acid receptor, *Mol Endocrinol*, 16 (2002) 1590-1597.
- [28] N.L. Urizar, D.D. Moore, GUGULIPID: a natural cholesterol-lowering agent, *Annu Rev Nutr*, 23 (2003) 303-313.
- [29] N.L. Urizar, A.B. Liverman, D.T. Dodds, F.V. Silva, P. Ordentlich, Y. Yan, F.J. Gonzalez, R.A. Heyman, D.J. Mangelsdorf, D.D. Moore, A natural product that lowers cholesterol as an antagonist ligand for FXR, *Science*, 296 (2002) 1703-1706.
- [30] R.B. Singh, M.A. Niaz, S. Ghosh, Hypolipidemic and antioxidant effects of *Commiphora mukul* as an adjunct to dietary therapy in patients with hypercholesterolemia, *Cardiovasc Drugs Ther*, 8 (1994) 659-664.
- [31] C. Ulbricht, E. Basch, P. Szapary, P. Hammerness, S. Axentsev, H. Boon, D. Kroll, L. Garraway, M. Vora, J. Woods, Guggul for hyperlipidemia: a review by the Natural Standard Research Collaboration, *Complement Ther Med*, 13 (2005) 279-290.
- [32] S. Rayalam, J.Y. Yang, M.A. Della-Fera, H.J. Park, S. Ambati, C.A. Baile, Anti-obesity effects of xanthohumol plus guggulsterone in 3T3-L1 adipocytes, *J Med Food*, 12 (2009) 846-853.
- [33] R. Deng, Therapeutic effects of guggul and its constituent guggulsterone: cardiovascular benefits, *Cardiovasc Drug Rev*, 25 (2007) 375-390.
- [34] B.Z. Yu, R. Kaimal, S. Bai, K.A. El Sayed, S.A. Tatulian, R.J. Apitz, M.K. Jain, R. Deng, O.G. Berg, Effect of guggulsterone and cembranoids of *Commiphora mukul* on pancreatic phospholipase A(2): role in hypocholesterolemia, *J Nat Prod*, 72 (2009) 24-28.
- [35] H. Nozawa, Xanthohumol, the chalcone from beer hops (*Humulus lupulus* L.), is the ligand for farnesoid X receptor and ameliorates lipid and glucose metabolism in KK-A(y) mice, *Biochem Biophys Res Commun*, 336 (2005) 754-761.
- [36] S. De Marino, R. Ummarino, M.V. D'Auria, M.G. Chini, G. Bifulco, B. Renga, C. D'Amore, S. Fiorucci, C. Debitus, A. Zampella, Theonellasterols and conicasterols from *Theonella swinhoei*. Novel marine natural ligands for human nuclear receptors, *J Med Chem*, 54 (2011) 3065-3075.

- [37] V. Sepe, G. Bifulco, B. Renga, C. D'Amore, S. Fiorucci, A. Zampella, Discovery of sulfated sterols from marine invertebrates as a new class of marine natural antagonists of farnesoid-X-receptor, *J Med Chem*, 54 (2011) 1314-1320.
- [38] H. Choi, H. Hwang, J. Chin, E. Kim, J. Lee, S.J. Nam, B.C. Lee, B.J. Rho, H. Kang, Tuberatolides, potent FXR antagonists from the Korean marine tunicate *Botryllus tuberatus*, *J Nat Prod*, 74 (2011) 90-94.
- [39] S.M. Soisson, G. Parthasarathy, A.D. Adams, S. Sahoo, A. Sitlani, C. Sparrow, J. Cui, J.W. Becker, Identification of a potent synthetic FXR agonist with an unexpected mode of binding and activation, *Proc Natl Acad Sci U S A*, 105 (2008) 5337-5342.
- [40] T.P. Charles, R.; Pruzanski, M.; Auwxr, J.; Schoonjans, K. , Targeting bile-acid signalling for metabolic diseases, *Nat Rev Drug Discovery*, 7 (2008) 678.
- [41] J.D. Love, J.T. Gooch, S. Benko, C. Li, L. Nagy, V.K. Chatterjee, R.M. Evans, J.W. Schwabe, The structural basis for the specificity of retinoid-X receptor-selective agonists: new insights into the role of helix H12, *J Biol Chem*, 277 (2002) 11385-11391.
- [42] A. Akwabi-Ameyaw, J.Y. Bass, R.D. Caldwell, J.A. Caravella, L. Chen, K.L. Creech, D.N. Deaton, S.A. Jones, I. Kaldor, Y. Liu, K.P. Madauss, H.B. Marr, R.B. McFadyen, A.B. Miller, F.N. Iii, D.J. Parks, P.K. Spearing, D. Todd, S.P. Williams, G.B. Wisely, Conformationally constrained farnesoid X receptor (FXR) agonists: Naphthoic acid-based analogs of GW 4064, *Bioorg Med Chem Lett*, 18 (2008) 4339-4343.
- [43] B. Flatt, R. Martin, T.L. Wang, P. Mahaney, B. Murphy, X.H. Gu, P. Foster, J. Li, P. Pircher, M. Petrowski, I. Schulman, S. Westin, J. Wrobel, G. Yan, E. Bischoff, C. Daige, R. Mohan, Discovery of XL335 (WAY-362450), a highly potent, selective, and orally active agonist of the farnesoid X receptor (FXR), *J Med Chem*, 52 (2009) 904-907.
- [44] M. Downes, M.A. Verdecia, A.J. Roecker, R. Hughes, J.B. Hogenesch, H.R. Kast-Woelbern, M.E. Bowman, J.L. Ferrer, A.M. Anisfeld, P.A. Edwards, J.M. Rosenfeld, J.G. Alvarez, J.P. Noel, K.C. Nicolaou, R.M. Evans, A chemical, genetic, and structural analysis of the nuclear bile acid receptor FXR, *Mol Cell*, 11 (2003) 1079-1092.
- [45] H.G.F. Richter, G.M. Benson, D. Blum, E. Chaput, S. Feng, C. Gardes, U. Grether, P. Hartman, B. Kuhn, R.E. Martin, J.M. Plancher, M.G. Rudolph, F. Schuler, S. Taylor, K.H. Bleicher, Discovery of novel and orally active FXR agonists for the potential treatment of dyslipidemia & diabetes, *Bioorganic & Medicinal Chemistry Letters*, 21 (2011) 191-194.
- [46] H.G.F. Richter, G.M. Benson, K.H. Bleicher, D. Blum, E. Chaput, N. Clemann, S. Feng, C. Gardes, U. Grether, P. Hartman, B. Kuhn, R.E. Martin, J.M. Plancher, M.G. Rudolph, F. Schuler, S. Taylor, Optimization of a novel class of benzimidazole-based farnesoid X receptor (FXR) agonists to improve physicochemical and ADME properties, *Bioorganic & Medicinal Chemistry Letters*, 21 (2011) 1134-1140.
- [47] J.Y. Bass, R.D. Caldwell, J.A. Caravella, L. Chen, K.L. Creech, D.N. Deaton, K.P. Madauss, H.B. Marr, R.B. McFadyen, A.B. Miller, D.J. Parks, D. Todd, S.P. Williams, G.B.



Wisely, Substituted isoxazole analogs of farnesoid X receptor (FXR) agonist GW4064, *Bioorg Med Chem Lett*, 19 (2009) 2969-2973.

[48] S. Feng, M. Yang, Z. Zhang, Z. Wang, D. Hong, H. Richter, G.M. Benson, K. Bleicher, U. Grether, R.E. Martin, J.M. Plancher, B. Kuhn, M.G. Rudolph, L. Chen, Identification of an N-oxide pyridine GW4064 analog as a potent FXR agonist, *Bioorg Med Chem Lett*, 19 (2009) 2595-2598.

[49] A. Akwabi-Ameyaw, J.A. Caravella, L.H. Chen, K.L. Creech, D.N. Deaton, K.P. Madauss, H.B. Marr, A.B. Miller, F. Navas, D.J. Parks, P.K. Spearing, D. Todd, S.P. Williams, B. Wisely, Conformationally constrained farnesoid X receptor (FXR) agonists: Alternative replacements of the stilbene, *Bioorganic & Medicinal Chemistry Letters*, 21 (2011) 6154-6160.

[50] J.Y. Bass, J.A. Caravella, L.H. Chen, K.L. Creech, D.N. Deaton, K.P. Madauss, H.B. Marr, R.B. McFadyen, A.B. Miller, W.Y. Mills, F. Navas, D.J. Parks, T.L. Smalley, P.K. Spearing, D. Todd, S.P. Williams, G.B. Wisely, Conformationally constrained farnesoid X receptor (FXR) agonists: Heteroaryl replacements of the naphthalene, *Bioorganic & Medicinal Chemistry Letters*, 21 (2011) 1206-1213.

[51] A. Akwabi-Ameyaw, J.Y. Bass, R.D. Caldwell, J.A. Caravella, L.H. Chen, K.L. Creech, D.N. Deaton, K.P. Madauss, H.B. Marr, R.B. McFadyen, A.B. Miller, F. Navas, D.J. Parks, P.K. Spearing, D. Todd, S.P. Williams, G.B. Wisely, FXR agonist activity of conformationally constrained analogs of GW 4064, *Bioorganic & Medicinal Chemistry Letters*, 19 (2009) 4733-4739.

[52] J.Y. Bass, R.D. Caldwell, J.A. Caravella, L.H. Chen, K.L. Creech, D.N. Deaton, K.P. Madauss, H.B. Marr, R.B. McFadyen, A.B. Miller, D.J. Parks, D. Todd, S.P. Williams, G.B. Wisely, Substituted isoxazole analogs of farnesoid X receptor (FXR) agonist GW4064, *Bioorganic & Medicinal Chemistry Letters*, 19 (2009) 2969-2973.

[53] B. Flatt, R. Martin, T.L. Wang, P. Mahaney, B. Murphy, X.H. Gu, P. Foster, J.L. Li, P. Pircher, M. Petrowski, I. Schulman, S. Westin, J. Wrobel, G. Yan, E. Bischoff, C. Daige, R. Mohan, Discovery of XL335 (WAY-362450), a Highly Potent, Selective, and Orally Active Agonist of the Farnesoid X Receptor (FXR), *Journal of Medicinal Chemistry*, 52 (2009) 904-907.

[54] J.T. Lundquist, D.C. Harnish, C.Y. Kim, J.F. Mehlmann, R.J. Unwalla, K.M. Phipps, M.L. Crawley, T. Commons, D.M. Green, W.X. Xu, W.T. Hum, J.E. Eta, I. Feingold, V. Patel, M.J. Evans, K. Lai, L. Borges-Marcucci, P.E. Mahaney, J.E. Wrobel, Improvement of Physiochemical Properties of the Tetrahydroazepinoindole Series of Farnesoid X Receptor (FXR) Agonists: Beneficial Modulation of Lipids in Primates, *Journal of Medicinal Chemistry*, 53 (2010) 1774-1787.

[55] J.F. Stevens, A.W. Taylor, M.L. Deinzer, Quantitative analysis of xanthohumol and related prenylflavonoids in hops and beer by liquid chromatography-tandem mass spectrometry, *J Chromatogr A*, 832 (1999) 97-107.

- [56] M. Blumenthal, The complete german commission E monograph: therapeutic guide to herbal medicines., Amercan botanical council, (1998) 147.
- [57] L.G. Carr, Westey, C., , Surviving folktales and herbal lore among the shinnecock Indians., *Journal of American Folklore*, 58 (1945) 113-123.
- [58] C.R. Karnick, *Pharmacopoeial Standards of Herbal Plants*; Srisatgure Publications, Delhi, Vol. 1, Vol. 2 (1994) 183-184, 167.
- [59] M. Blumenthal, Goldberg, A., Brinckmann J., , *Herbal Medicine: Expanded Commission E Monographs.* , Intergrative Medicine Communications, Newton, MA, (2000) 297-103.
- [60] C.L. Miranda, J.F. Stevens, A. Helmrich, M.C. Henderson, R.J. Rodriguez, Y.H. Yang, M.L. Deinzer, D.W. Barnes, D.R. Buhler, Antiproliferative and cytotoxic effects of prenylated flavonoids from hops (*Humulus lupulus*) in human cancer cell lines, *Food Chem Toxicol*, 37 (1999) 271-285.
- [61] J.F. Stevens, J.E. Page, Xanthohumol and related prenylflavonoids from hops and beer: to your good health!, *Phytochemistry*, 65 (2004) 1317-1330.
- [62] C. Gerhauser, Beer constituents as potential cancer chemopreventive agents, *Eur J Cancer*, 41 (2005) 1941-1954.
- [63] E.C. Colgate, C.L. Miranda, J.F. Stevens, T.M. Bray, E. Ho, Xanthohumol, a prenylflavonoid derived from hops induces apoptosis and inhibits NF-kappaB activation in prostate epithelial cells, *Cancer Lett*, 246 (2007) 201-209.
- [64] J.F. Stevens, Miranda, C.L., Buhler, D.R., Deinzer, M.L., *Chemistry and Biology of Hop Flavonoids*, *Journal of the American Society of Brewing Chemists*, 56 (1998) 136-145.
- [65] L. Delmulle, A. Bellahcene, W. Dhooge, F. Comhaire, F. Roelens, K. Huvaere, A. Heyerick, V. Castronovo, D. De Keukeleire, Anti-proliferative properties of prenylated flavonoids from hops (*Humulus lupulus* L.) in human prostate cancer cell lines, *Phytomedicine*, 13 (2006) 732-734.
- [66] L. Delmulle, T. Vanden Berghe, D.D. Keukeleire, P. Vandenabeele, Treatment of PC-3 and DU145 prostate cancer cells by prenylflavonoids from hop (*Humulus lupulus* L.) induces a caspase-independent form of cell death, *Phytother Res*, 22 (2008) 197-203.
- [67] R. Costa, R. Negrao, I. Valente, A. Castela, D. Duarte, L. Guardao, P.J. Magalhaes, J.A. Rodrigues, J.T. Guimaraes, P. Gomes, R. Soares, Xanthohumol modulates inflammation, oxidative stress, and angiogenesis in type 1 diabetic rat skin wound healing, *J Nat Prod*, 76 (2013) 2047-2053.
- [68] M. Festa, M. Caputo, C. Cipolla, C. D'Acunto, A. Rossi, M. Tecce, A. Capasso, The involvement of xanthohumol in the expression of annexin in human malignant glioblastoma cells, *Open Biochem J*, 7 (2013) 1-10.

- [69] M. Festa, A. Capasso, C.W. D'Acunto, M. Masullo, A.G. Rossi, C. Pizza, S. Piacente, Xanthohumol induces apoptosis in human malignant glioblastoma cells by increasing reactive oxygen species and activating MAPK pathways, *J Nat Prod*, 74 (2011) 2505-2513.
- [70] S.R. Milligan, J.C. Kalita, A. Heyerick, H. Rong, L. De Cooman, D. De Keukeleire, Identification of a potent phytoestrogen in hops (*Humulus lupulus* L.) and beer, *J Clin Endocrinol Metab*, 84 (1999) 2249-2252.
- [71] O. Schaefer, M. Humpel, K.H. Fritzemeier, R. Bohlmann, W.D. Schleuning, 8-Prenyl naringenin is a potent ERalpha selective phytoestrogen present in hops and beer, *J Steroid Biochem Mol Biol*, 84 (2003) 359-360.
- [72] A. Heyerick, S. Vervarcke, H. Depypere, M. Bracke, D. De Keukeleire, A first prospective, randomized, double-blind, placebo-controlled study on the use of a standardized hop extract to alleviate menopausal discomforts, *Maturitas*, 54 (2006) 164-175.
- [73] J. Bowe, X.F. Li, J. Kinsey-Jones, A. Heyerick, S. Brain, S. Milligan, K. O'Byrne, The hop phytoestrogen, 8-prenylnaringenin, reverses the ovariectomy-induced rise in skin temperature in an animal model of menopausal hot flushes, *J Endocrinol*, 191 (2006) 399-405.
- [74] M. Rad, M. Humpel, O. Schaefer, R.C. Schoemaker, W.D. Schleuning, A.F. Cohen, J. Burggraaf, Pharmacokinetics and systemic endocrine effects of the phyto-oestrogen 8-prenylnaringenin after single oral doses to postmenopausal women, *Br J Clin Pharmacol*, 62 (2006) 288-296.
- [75] C.L. Miranda, J.F. Stevens, V. Ivanov, M. McCall, B. Frei, M.L. Deinzer, D.R. Buhler, Antioxidant and prooxidant actions of prenylated and nonprenyated chalcones and flavanones in vitro, *J Agric Food Chem*, 48 (2000) 3876-3884.
- [76] C. Gerhauser, Broad spectrum anti-infective potential of xanthohumol from hop (*Humulus lupulus* L.) in comparison with activities of other hop constituents and xanthohumol metabolites, *Mol Nutr Food Res*, 49 (2005) 827-831.
- [77] Y.M. Lee, K.H. Hsieh, W.J. Lu, H.C. Chou, D.S. Chou, L.M. Lien, J.R. Sheu, K.H. Lin, Xanthohumol, a Prenylated Flavonoid from Hops (*Humulus lupulus*), Prevents Platelet Activation in Human Platelets, *Evid Based Complement Alternat Med*, 2012 (2012) 852362.
- [78] L. Legette, C. Karnpracha, R.L. Reed, J. Choi, G. Bobe, J.M. Christensen, R. Rodriguez-Proteau, J.Q. Purnell, J.F. Stevens, Human pharmacokinetics of xanthohumol, an antihyperglycemic flavonoid from hops, *Mol Nutr Food Res*, 58 (2014) 248-255.
- [79] L.L. Legette, A.Y. Luna, R.L. Reed, C.L. Miranda, G. Bobe, R.R. Proteau, J.F. Stevens, Xanthohumol lowers body weight and fasting plasma glucose in obese male Zucker fa/fa rats, *Phytochemistry*, 91 (2013) 236-241.
- [80] J.S. Kirkwood, L.L. Legette, C.L. Miranda, Y. Jiang, J.F. Stevens, A metabolomics-driven elucidation of the anti-obesity mechanisms of xanthohumol, *J Biol Chem*, 288 (2013) 19000-19013.

- [81] N. Tabata, M. Ito, H. Tomoda, S. Omura, Xanthohumols, diacylglycerol acyltransferase inhibitors, from *Humulus lupulus*, *Phytochemistry*, 46 (1997) 683-687.
- [82] A. Casaschi, G.K. Maiyoh, B.K. Rubio, R.W. Li, K. Adeli, A.G. Theriault, The chalcone xanthohumol inhibits triglyceride and apolipoprotein B secretion in HepG2 cells, *J Nutr*, 134 (2004) 1340-1346.
- [83] J.Y. Yang, M.A. Della-Fera, S. Rayalam, C.A. Baile, Effect of xanthohumol and isoxanthohumol on 3T3-L1 cell apoptosis and adipogenesis, *Apoptosis*, 12 (2007) 1953-1963.
- [84] Y. Campbell, The effect of dietary compounds on human cathelicidin antimicrobial peptide gene expression mediated through farnesoid X receptor and its potential role in gastrointestinal health.
- [85] K.C. Nicolaou, R.M. Evans, A.J. Roecker, R. Hughes, M. Downes, J.A. Pfefferkorn, Discovery and optimization of non-steroidal FXR agonists from natural product-like libraries, *Org Biomol Chem*, 1 (2003) 908-920.
- [86] C.S. Maier, M.L. Deinzer, Protein conformations, interactions, and H/D exchange, *Methods Enzymol*, 402 (2005) 312-360.
- [87] C.S. Maier, O.H. Kim, M.L. Deinzer, Conformational properties of the A-state of cytochrome c studied by hydrogen/deuterium exchange and electrospray mass spectrometry, *Anal Biochem*, 252 (1997) 127-135.
- [88] C.S. Maier, M.I. Schimerlik, M.L. Deinzer, Thermal denaturation of *Escherichia coli* thioredoxin studied by hydrogen/deuterium exchange and electrospray ionization mass spectrometry: monitoring a two-state protein unfolding transition, *Biochemistry*, 38 (1999) 1136-1143.
- [89] T.E. Wales, J.R. Engen, Hydrogen exchange mass spectrometry for the analysis of protein dynamics, *Mass Spectrom Rev*, 25 (2006) 158-170.
- [90] X. Yan, C.S. Maier, Hydrogen/deuterium exchange mass spectrometry, *Methods Mol Biol*, 492 (2009) 255-271.
- [91] Y. Hamuro, S.J. Coales, J.A. Morrow, K.S. Molnar, S.J. Tuske, M.R. Southern, P.R. Griffin, Hydrogen/deuterium-exchange (H/D-Ex) of PPARgamma LBD in the presence of various modulators, *Protein Sci*, 15 (2006) 1883-1892.
- [92] X. Yan, M.L. Deinzer, M.I. Schimerlik, D. Broderick, M.E. Leid, M.I. Dawson, Investigation of ligand interactions with human RXRalpha by hydrogen/deuterium exchange and mass spectrometry, *J Am Soc Mass Spectrom*, 17 (2006) 1510-1517.
- [93] S.Y. Dai, T.P. Burris, J.A. Dodge, C. Montrose-Rafizadeh, Y. Wang, B.D. Pascal, M.J. Chalmers, P.R. Griffin, Unique ligand binding patterns between estrogen receptor alpha and beta revealed by hydrogen-deuterium exchange, *Biochemistry*, 48 (2009) 9668-9676.

- [94] J. Zhang, M.J. Chalmers, K.R. Stayrook, L.L. Burris, R.D. Garcia-Ordonez, B.D. Pascal, T.P. Burris, J.A. Dodge, P.R. Griffin, Hydrogen/deuterium exchange reveals distinct agonist/partial agonist receptor dynamics within vitamin D receptor/retinoid X receptor heterodimer, *Structure*, 18 (2010) 1332-1341.
- [95] M.J. Chalmers, B.D. Pascal, S. Willis, J. Zhang, S.J. Iturria, J.A. Dodge, P.R. Griffin, Methods for the Analysis of High Precision Differential Hydrogen Deuterium Exchange Data, *Int J Mass Spectrom*, 302 (2011) 59-68.
- [96] S.Y. Dai, M.J. Chalmers, J. Bruning, K.S. Bramlett, H.E. Osborne, C. Montrose-Rafizadeh, R.J. Barr, Y. Wang, M. Wang, T.P. Burris, J.A. Dodge, P.R. Griffin, Prediction of the tissue-specificity of selective estrogen receptor modulators by using a single biochemical method, *Proc Natl Acad Sci U S A*, 105 (2008) 7171-7176.
- [97] J.R. Lakowicz, SpringerLink (Online service), Principles of Fluorescence Spectroscopy, in, Springer Science+Business Media, LLC, Boston, MA, 2006.
- [98] J.A. Lupisella, J.E. Driscoll, W.J. Metzler, P.R. Reczek, The ligand binding domain of the human retinoic acid receptor gamma is predominantly alpha-helical with a Trp residue in the ligand binding site, *J Biol Chem*, 270 (1995) 24884-24890.
- [99] D. Silva, C.M. Cortez, J. Cunha-Bastos, S.R. Louro, Methyl parathion interaction with human and bovine serum albumin, *Toxicol Lett*, 147 (2004) 53-61.
- [100] S. Bakkialakshmi, D. Chandrakala, A spectroscopic investigations of anticancer drugs binding to bovine serum albumin, *Spectrochim Acta A Mol Biomol Spectrosc*, 88 (2012) 2-9.
- [101] P.W. Chao, C.S. Chow, Monitoring aminoglycoside-induced conformational changes in 16S rRNA through acrylamide quenching, *Bioorg Med Chem*, 15 (2007) 3825-3831.
- [102] V. Guixe, P.H. Rodriguez, J. Babul, Ligand-induced conformational transitions in Escherichia coli phosphofructokinase 2: evidence for an allosteric site for MgATP<sub>2</sub>, *Biochemistry*, 37 (1998) 13269-13275.
- [103] H.M. Rawel, S.K. Frey, K. Meidtnier, J. Kroll, F.J. Schweigert, Determining the binding affinities of phenolic compounds to proteins by quenching of the intrinsic tryptophan fluorescence, *Mol Nutr Food Res*, 50 (2006) 705-713.
- [104] C. Yang, Q. Li, Y. Li, Targeting nuclear receptors with marine natural products, *Mar Drugs*, 12 (2014) 601-635.
- [105] S.J. Nam, H. Ko, M. Shin, J. Ham, J. Chin, Y. Kim, H. Kim, K. Shin, H. Choi, H. Kang, Farnesoid X-activated receptor antagonists from a marine sponge *Spongia* sp, *Bioorg Med Chem Lett*, 16 (2006) 5398-5402.
- [106] F.S. Di Leva, C. Festa, C. D'Amore, S. De Marino, B. Renga, M.V. D'Auria, E. Novellino, V. Limongelli, A. Zampella, S. Fiorucci, Binding mechanism of the farnesoid X receptor marine

antagonist suvanine reveals a strategy to forestall drug modulation on nuclear receptors. Design, synthesis, and biological evaluation of novel ligands, *J Med Chem*, 56 (2013) 4701-4717.

[107] V. Sepe, R. Ummarino, M.V. D'Auria, O. Tagliatela-Scafati, S.D. Marino, C. D'Amore, B. Renga, M.G. Chini, G. Bifulco, Y. Nakao, N. Fusetani, S. Fiorucci, A. Zampella, Preliminary structure-activity relationship on theonellasterol, a new chemotype of FXR antagonist, from the marine sponge *Theonella swinhoei*, *Mar Drugs*, 10 (2012) 2448-2466.

[108] K. Shin, J. Chin, D. Hahn, J. Lee, H. Hwang, D.H. Won, J. Ham, H. Choi, E. Kang, H. Kim, M.K. Ju, S.J. Nam, H. Kang, Sterols from a soft coral, *Dendronephthya gigantea* as farnesoid X-activated receptor antagonists, *Steroids*, 77 (2012) 355-359.

[109] P. Zanolli, M. Zavatti, Pharmacognostic and pharmacological profile of *Humulus lupulus* L, *J Ethnopharmacol*, 116 (2008) 383-396.

[110] c. Gerhauser, Alt, A.P., Klimo, K., Knauf, J., Frank, N., Becker, H., Isolation and potential cancer chemopreventive activities of phenolic compounds of beer, *Phytochemistry Reviews*, 1 (2002) 369-377.

[111] C.L. Miranda, G.L. Aponso, J.F. Stevens, M.L. Deinzer, D.R. Buhler, Prenylated chalcones and flavanones as inducers of quinone reductase in mouse Hepa 1c1c7 cells, *Cancer Lett*, 149 (2000) 21-29.

[112] R.J. Rodriguez, C.L. Miranda, J.F. Stevens, M.L. Deinzer, D.R. Buhler, Influence of prenylated and non-prenylated flavonoids on liver microsomal lipid peroxidation and oxidative injury in rat hepatocytes, *Food Chem Toxicol*, 39 (2001) 437-445.

[113] A. Zhao, J.L. Lew, L. Huang, J. Yu, T. Zhang, Y. Hrywna, J.R. Thompson, N. de Pedro, R.A. Blevins, F. Pelaez, S.D. Wright, J. Cui, Human kininogen gene is transactivated by the farnesoid X receptor, *J Biol Chem*, 278 (2003) 28765-28770.

[114] L. Pan, H. Becker, C. Gerhauser, Xanthohumol induces apoptosis in cultured 40-16 human colon cancer cells by activation of the death receptor- and mitochondrial pathway, *Mol Nutr Food Res*, 49 (2005) 837-843.

[115] B. Vanhoecke, L. Derycke, V. Van Marck, H. Depypere, D. De Keukeleire, M. Bracke, Antiinvasive effect of xanthohumol, a prenylated chalcone present in hops (*Humulus lupulus* L.) and beer, *Int J Cancer*, 117 (2005) 889-895.

[116] E. Bertl, klimo, K., Heiss, E., Klenke, F., Peschke, P., Becker, H., Eicher, T., Herhaus, C., Kapadia, G., Bartsch, H., Gerhauser, C., Identification of novel inhibitors of angiogenesis using a human in vitro anti-angiogenic assay, *International Journal of Cancer Prevention*, 1 (2004) 47-61.

[117] M.S. Pepper, S.J. Hazel, M. Humpel, W.D. Schleuning, 8-prenylnaringenin, a novel phytoestrogen, inhibits angiogenesis in vitro and in vivo, *J Cell Physiol*, 199 (2004) 98-107.

## **Chapter 2**

### **Methods**

## **2.1 HDX-MS method**

### **2.1.1 The theory and mechanisms of HDX**

The solution-phase HDX method in conjunction with mass spectrometry is based on subjecting a protein to deuterium oxide ( $D_2O$ ) for different times. During incubation solvent-accessible amide hydrogens will exchange for deuterium. For subsequent mass spectrometric analysis, the protein samples are quenched at specific time points and subjected to peptidolysis under conditions that retard exchange and maintain the deuterium labeling information. The level of deuterium uptake is quantitatively determined for each peptides. The number of amide deuterons serves as readout for solvent accessibility and conformational dynamics. In this thesis HDX perturbation experiments were designed that allow the differential evaluation of deuterium levels in FXR LBD in presence of diverse small molecule ligands making this assay sensitive for evaluating perturbation of solvent accessibility and conformational dynamics due to ligand interactions.

The fundamental concept of HDX is that backbone amide hydrogens in proteins will show slower exchange kinetics due to hydrogen bonding networks and limited solvent accessibilities. Reduced solvent accessibilities are of particular relevance if amide hydrogens are located in interaction interfaces, where they are often involved in hydrogen bonding and/or electrostatic contact networks or buried in the protein core [1-3]. In the regions without hydrogen bonding or on the protein surface, backbone amide hydrogen exchange with deuterium will be less retarded [1-3]. Generally, the deuterium uptake level of backbone amide hydrogen will provide valuable information relating to the conformational dynamics of the protein, because their exchange rates are critically dependent on protein structure and stability. For other hydrogens in the protein, they either exchange too fast to be determined (such as in S-H and O-H

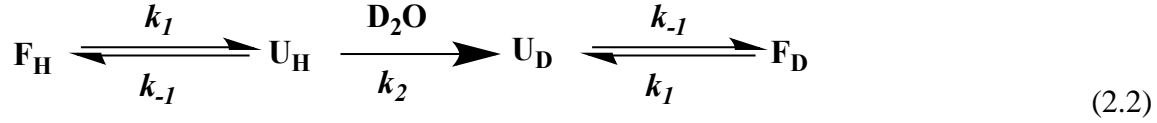


functional groups) or are unable to be exchanged with deuterium due to their strong chemical bonding (like alkyl hydrogens).

The amide hydrogen exchange rate is both pH and temperature dependent. When the pH during exchange decreases from 7 to ~2.5, the exchange rate will lessen  $10^3 - 10^4$  fold [4]. Additionally, the exchange rate will decrease by a factor of approximately ten following temperature reductions from 25 °C to 0 °C [5]. Under pH 2.5 and temperature 0 °C (i.e. quench conditions), the half-life of amide HDX is about 30-90 min which allows the sample to be analyzed by LC-MS [5]. Therefore, HDX reactions are often initiated under the physiological pH (pH 7-8), and room temperature 25 °C i.e. conditions that promote the native structure of the protein and then exchange is retarded under quench conditions at different exchange time points. Labeled protein samples are analyzed either intact or peptides produced by pepsin digestion.

To evaluate HDX data and determine which exchange behavior is observed, a dual pathway kinetic model [6, 7] is most often considered where F and U are the folded and unfolded state, respectively (Equation 2.1 and Equation 2.2). In this model, the first pathway (Equation 2.1) characterizes exchange directly from the folding state of a protein, where  $k_f$  is the exchange rate constant. Amide hydrogens located at or near the protein surface or within close proximity to solvent channels most likely undergo this pathway. In the second pathway (Equation 2.2), the breakage of hydrogen bonding is followed by isotopic exchange under transient reversible unfolding reactions. The exchange rate constant ( $k_u$ ) depends on the exchange rate constant in an unfolding state ( $k_2$ ) and the unfolding and refolding rate constant of the transient opening reaction ( $k_1$  and  $k_{-1}$ ).





The overall exchange rate constant ( $k_{ex}$ ) for a specific amide hydrogen can be stated as a sum of the contribution of exchange from both pathways (Equation 2.3) [8]. Under the second pathway, if  $k_2 \gg k_{-I}$  (EX1 kinetics mechanism), then  $k_u$  is directly related to  $k_I$ , which is the protein unfolding rate constant (Equation 2.4). A natural protein rarely undergoes the EX1 mechanism, however, addition of a denaturant [9] and pH increase [10] can induce a protein to demonstrate EX1 kinetics. On the other hand, if  $k_{-I} \gg k_2$  (EX2 kinetics mechanism),  $k_u$  is given by equation 2.5. The EX2 mechanism is observed for nearly all protein under physiological conditions or neutral pH in the absence of denaturants.

$$k_{ex} = k_f + k_u \quad (2.3)$$

$$k_u = k_I \quad (2.4)$$

$$k_u = k_2 k_I / k_{-I} \quad (2.5)$$

EX1 and EX2 exchange behaviors can be distinguished by mass spectrometry [11]. Under the EX1 behavior, the mass spectrum of a labeled protein will exhibit two populations. The fully exchanged form will express a high mass peak, and the fully protected form will express a low mass peak. The area under the two peaks instead of their mass will change as the exchange time increases. The unfolding rate constant,  $k_I$ , can be determined from the rate of the increase of area for the high mass peak [12]. Under the EX2 behavior, only one population is observed in the mass spectrum, and the mass of protein will increase over exchange time. For EX2, the rate constant can be calculated from the increase in deuterium as a function of time [13].

### 2.1.2 Mass spectrometry (MS)

MS is a powerful and useful analytical technique used to determine the molecular mass of an analyte. Depending on the resolving power on the instrument the molecular mass can be used for deriving the element composition of an analyte. Tandem mass spectrometry can be used for elucidating the chemical structure of an unknown compound by producing and detecting fragments. In proteomics, MS is applied to identify proteins and quantitatively determine protein concentrations in various biological samples including cells, tissues, and organisms. One main characteristic of all ions is that their kinetic energy and location in space can be regulated by using electric and magnetic fields. MS takes full advantage of this characteristic to separate and detect ions according to their mass-to-charge ratio ( $m/z$ ). The separation of ions must be performed under a high vacuum environment to avoid analyte ions from colliding with any other forms of matter, e.g., all ions must be in a gaseous phase.

Generally, a mass spectrometer contains three devices: ion source,  $m/z$  analyzer, and detector. A sample is ionized in an ion source to produce charged ions. The  $m/z$  analyzer operates under a very low pressure to help all ions efficiently move from the ion source to the detector. During the development of ion sources, two pioneering breakthroughs for large molecule ionization techniques occurred in the 1980s that rapidly expanded the application of MS for protein analysis. Electrospray ionization (ESI), as a soft ionization technique, is applied to ionize large biomolecules [14] and biopolymers [15]; and Matrix-Assisted Laser Desorption/Ionization (MALDI) is a desorption technique which is suitable for the analysis of protein molecules [16] and large organic molecules [17]. In ESI, a liquid sample is dispersed in a strong electric field (normally 3-6 kV) by electrospray to accumulate charged ions at the liquid surface that induce the formation of highly charged droplets. The droplets will be compressed

due to solvent evaporation until they break and generate desolvated ions (gas state ions). In MALDI ionization, proteins/peptides to be analyzed are dissolved in a solution containing small organic molecules with very strong absorption for the laser wavelength. Before MS analysis, all liquid solvent must be removed to produce cocrystallized analytes/matrix samples. Analyte ions will be released from the surface of the matrix by a laser pulse into the MS.

The most important device of a mass spectrometer is its analyzer, which includes Quadrupole (Q), Quadrupole ion trap (QIT), Time-of-Flight (ToF), Ion-mobility (IM) Orbitrap, and Fourier-transform ion cyclotron resonance (FTICR) analyzers. A combination of the above analyzers is realized in modern hybrid mass spectrometers. In this research, the ESI technique was applied to all protein/peptide ionizations, and a hybrid instrument was used that combines three analyzers, Q, IM, and TOF analyzers.

The Q analyzer separates ions of different  $m/z$  ratios in the radio frequency (RF) field by regulating the stability of their trajectories [18]. A typical Q analyzer consists of four hyperbolically shaped rod electrodes, and a RF voltage is utilized on the pairs of opposite rods with a direct voltage (DC) imposed on it. Like a mass filter, Q analyzer can let the selected  $m/z$  ions transmit by adjusting RF and DC but keep their ratio unchanged. This operation mode, i.e. RF/DC mode, often is applied to select precursor ion with specific  $m/z$  in a tandem mass spectrometer. Q also can be operated in a RF-only mode as an ion guide where ions within a broad  $m/z$  range will be transmitted.

The TOF analyzer separates ions with different  $m/z$  according to their flight time in a free-field region called the flight tube [19]. The flight time of an ion is proportional to the square root of the mass-to-charge ratio ( $m$ ) and is described as:  $t = [L (m/z)^{1/2}] / (2eU_s)^{1/2}$  where  $L$  is the length of the flight tube,  $U_s$  is the potential of the accelerating electric field. The broadening of

ion signal is caused by the kinetic energy distribution of the same  $m/z$  ions and can be reduced by applying an electrostatic reflectron [20] where the ions with higher kinetic energy will penetrate deeper in the reflectron than ions with low kinetic energy, resulting in a correction of flight time for all ions and ensuring that ions with the same  $m/z$  value reach the detector at the same time.

The IM analyzer separates ions on the basis of their size, shape (collision cross section area) and charge. In a traditional IM analyzer, the drift tube includes an electric field with constant electric strength and drift gas which has opposite direction compared with the ion's pathway. IM coupled with MS has great promise for gas-phase separations of complex peptide mixtures [21, 22]. Moreover, IM-MS separations are achieved after ionization, therefore they can be conveniently combined with other separation technologies such as liquid chromatography to provide additional separation space and/or data information (i.e. collisional cross sections). In 2004 [23], a new IM spectrometry (IMS) technique, traveling wave ion mobility (TWIM), was implemented in a quadrupole ToF hybrid instrument and commercialized in 2006 by Waters Corp. as Synapt High Definition Mass Spectrometry (HDMS) system [24]. Unlike the traditional IM analyzer in which a constant electric field is applied, in TWIM spectrometry a traveling electric field moves ions through the gas-filled stacked-ring RF ion guide which allows applying a repeating sequence of transient voltages to the ring electrodes. Ions with high mobility travel with the traveling waves and transverse the device more quickly compared to ions with low mobility that frequently crest over the waves and therefore need more time to pass through the device. In the context of the described HDX-MS studies, TWIM was used as an gas phase ion separation technology providing an additional dimension of separation for ions (besides the mass to charge ratio) and which is nested within the chromatographic timescale [25].

For the current HDX-MS experiments, a hybrid Q-TWIM-TOF mass spectrometer (Waters Synapt G1 HDMS instrument, depicted in Figure 2.1) was used for analyzing all samples [26]. The ions are produced in the ESI source and transmitted to the MS by regulating two cone voltages, sampling cone and extraction cone. Following a Z-shape travel pathway, the ions are guided into the first travelling wave ion guide and then reach a quadrupole device. The quadrupole device is operated in the RF-only mode to eliminate the effect of ion loss due to ion diffusion and to increase the efficiency of ion transmission. The ions then enter a tri-wave device consisting of a trap T-wave cell, a T-wave IM separation cell, and a transfer T-wave cell. In the MS mode the Triwave region is operated as ion guide to ensure efficient transmission of the ions into the ToF analyzer. In the MS/MS mode fragment ions can be generated in the trap or transfer T-wave cell by operating these devices in the higher energy regime to induce collision induced dissociation (CID). Under our experimental conditions, CID occurs in the transfer T-wave device in which precursor ions collide with Ar atoms resulting in some conversion of kinetic energy into internal energy which leads to formation of fragments [27, 28]. Finally, the precursor ions and product ions are analyzed by an orthogonal acceleration (oa) TOF analyzer before they reach the microchannel plate detector (MCD).

The traditional data acquisition mode for acquiring MS/MS data is the data dependent mode (DDA) in which survey scans and MS/MS scans are used sequentially. The selection of the precursor ion will determine from which precursor ion MS/MS data will be acquired. DDA acquisitions typically suffer from the irreproducibility of precursor ion selection and under-sampling if sample complexity increases. In addition, under conditions of constant instrument duty cycle times if the number of selected parent ions will need to be increased with the increase of sample complexity then the MS/MS acquisition time will need to be decreased, resulting in

decrease of quality of MS/MS data and consequently sequence coverage in the protein identification process [29]. Data-independent acquisition (DIA) techniques attempt to overcome at least some of these drawbacks. The DIA mode (also referred as  $MS^E$  mode) is supported by the Synapt HDMS instrument. In the  $MS^E$  mode alternating collision energy is applied to the transfer T-wave device (Figure 2.1.), i.e. alternating between low and elevated energy. Therefore, the information of precursor and product ions is collected in one cycle providing accurate mass information for the precursor ions as well as for the associated product ions. In this work, the  $MS^E$  mode was used for MS/MS data generation.

### **2.1.3 HDX-MS analysis**

#### **2.1.3.1 Protein expression and purification**

The pET 15B vector containing hFXR-LBD, residues 193-472 was transformed into *Escherichia coli* BL21 (DE3) pLysS and grown on LB agar plates. A single colony was used to inoculate 100 mL of 2XYT medium with antibiotics (Carbenicillin 100 µg/mL and Chloramphenicol 35 µg/mL) and grown overnight at 37°C. The overnight culture was centrifuged for 10 min at room temperature and then the pellet was resuspended in 6 mL of fresh 2XYT medium. Each liter of fresh 2XYT medium with antibiotics (ampicillin 150 µg/mL and Chloramphenicol 35 µg/mL) was inoculated with 1 mL of the resuspended cells (total six liter) and grown at 37°C to  $A_{600}=0.6$ . Protein expression was induced with 0.8 mM IPTG (isopropyl- $\beta$ -D-thiogalactopyranoside) and the cells were allowed to continue growing for 4 hours at 20°C. The cell pellets were harvested by centrifugation (4000 RPM, 25 min, 4°C), resuspended in cell wash solution (150 mM NaCl, 50 mM Tris and 10% w/v sucrose), centrifuged again and frozen at -80°C.

The frozen cell pellets were resuspended in buffer solution (50 mM sodium phosphate, 0.5 M NaCl, 0.5 mM CHAPS, 15 mM imidazole, 0.5 M sucrose, pH 7.3) and centrifuged. The His<sub>6</sub>-tagged FXR-LBD was mixed with Clonotech Talon Co<sup>2+</sup> polyhistidine affinity resin (equilibrated with the above buffer) at 4°C for 45 min. The proteins were eluted into a solution containing 50 mM sodium phosphate, 0.5 M NaCl, 0.5 mM CHAPS, 200 mM imidazole, 0.5 M sucrose, pH 7.3. The His tag was removed by thrombin digestion at 4°C (48 hours) followed by purification on a column packed with Co<sup>2+</sup> resin to yield purified human FXR-LBD monomer which was used for all experiments. The protein concentration was determined spectrophotometrically at 280 nm, and the purity (over 95%) was judged by sodium dodecyl sulfate –acrylamide gel electrophoresis (SDS-PAGE) and MS.

#### **2.1.3.2 HDX MS workflow**

The HDX workflow is shown in Figure 2.2. The purified FXR-LBD protein (15 µL, 98 µM, in 50 mM sodium phosphate, 0.5 M NaCl, 0.5 mM CHAPS, 1 mM TCEP, 0.5 M sucrose and 10% glycerol, pH=7.4) was equilibrated for 30 min in the presence of the respective DMSO solution (0.5 µL, ±10 mM ligand). The ligand/monomeric protein molar ratio was 3.2:1. The small amount of DMSO (3.3% v/v) did not affect protein binding as indicated by fluorescence titration data as well as by intact protein HDX data. The D<sub>2</sub>O buffer (50 mM sodium phosphate, 0.5 M NaCl, 0.5 mM CHAPS, 1 mM TCEP, 0.5 M sucrose and 10% glycerol, pH 7.3) was equilibrated for 30 min in the presence of the same percentage of DMSO. The exchange reaction was initiated by adding 10-times D<sub>2</sub>O buffer (150 µL). At different reaction time points, 0.5, 1, 2, 5, 10, 30 and 60 min, aliquots (15 µL) were added to pre-chilled vials containing the same volume of quenching solution (15 µL, 0.42% phosphoric acid, pH 2.5). The quenched sample



was immediately frozen in liquid nitrogen for subsequent LC-ESI-MS analysis. Experiments were performed in triplicate.

The experimental conditions for the ligand binding studies in combination with the HDX approach were chosen to ascertain that both the FXR-LBD protein and the respective low affinity ligand retained solubility throughout the period of labeling. Even in presence of structure promoting and stabilizing additives (CHAPS, sucrose, glycerol), the FXR-LBD protein showed a high tendency to precipitation in presence of low affinity ligands. This limited our flexibility in using large excess of low affinity ligands. We believe that the absence of X-ray structures of FXR-LBD in complex with low affinity ligands is at least in part caused by this shortcoming. For the three well known ligands described in the chapter 3, the reported dissociation constant/binding affinity values are 0.06  $\mu\text{M}$  [30], 10  $\mu\text{M}$  [31] for GW4064 and CDCA, respectively and for GG > 5  $\mu\text{M}$  [32]. The bound fraction of FXR-LBD in each ligand binding study before initiation of the HDX reaction is ~100% as estimated by applying equation 2.1 [33]:

$$F_p = \frac{(L_T + P_T + K_d) - \sqrt{(L_T + P_T + K_d)^2 - 4L_T P_T}}{2P_T} \quad (2.1)$$

where  $F_p$  is fraction of protein bound,  $L_T$  and  $P_T$  are the total ligand concentration and protein concentration used, respectively, and  $K_d$  is dissociation constant. In the present experimental protocol we kept the mole ratio between protein and ligand constant (being 3.2:1) during the time course of labeling. We also estimated the bound fraction of the FXR-LBD in prenylflavonoid-ligand bound system (~100%) based on their  $K_d$  values determined by fluorescence titration quenching technique in chapter 5. Moreover, for all FXR-LBD-ligand binding systems studied in this dissertation, the mass spectrums of each peptide at different exchange time points are checked manually. The evaluation of the mass isotope distributions and

elution time features of all peptides indicated that no mixed populations were detected in accordance with that the fraction of 'protein bound' is the predominant population present in solution.

#### **2.1.3.3 Mass spectrometry setup used for intact protein analysis**

For intact protein HDX-MS, the protein was eluted through a Micro Trap<sup>TM</sup> C4 column (1×8 mm) with a steep 10-90% (v/v) B gradient within 10 min (mobile phase A: 0.1% HCOOH in H<sub>2</sub>O, mobile phase B: 0.1% HCOOH in CH<sub>3</sub>CN, flow rate 40 µL/min) and eluted into a Waters LCT ESI-ToF mass spectrometer.

#### **2.1.3.4 HDX-MS data generation**

HDX information at the peptide level was obtained by employing a nanoUPLC system equipped with a Waters "chilled" LC module, and coupled to a Waters Synapt HDMS instrument. Protein was digested by an online Poroszyme® immobilized pepsin column (2.1×30 mm) with a 100 µL/min solvent (0.05% HCOOH in H<sub>2</sub>O). The proteolytic products were captured on a Acquity BEH C18 VanGuard Pre-column (1.7 µm, 2.1 x 5 mm), eluted and separated on an Acquity UPLC® BEH C18 column (1.7 µm, 1.0×100 mm) using the following elution program: B from 8 to 40% during 6 minutes, hold at 40% for 1 minute, then from 40 to 85% in 0.5 minute, hold at 85% for 1 minute, finally from 85% to 8% in 0.5 minute, hold B at 8% for 3 minutes, total 12 minutes (same LC solvents as described above for the intact protein analysis). In order to minimize contamination of the mass spectrometer with detergents a Rheodyne MX Series II 6-port valve was installed between the nanoAcquity UPLC and the ESI source. All solvents were immersed in an ice bath.

A Waters Synapt G1 mass spectrometer equipped with a Z-spray ESI source was used to acquire all mass spectral data sets in the positive-ion mode. The voltages of capillary, sampling

cone, and extraction cone are 3000 V, 35 V, and 4.0 V respectively. The source and desolvation temperatures are 90 °C and 180 °C. The desolvation gas flow is 100 L/hour. For determining deuterium incorporation levels in peptides LC-MS analysis was performed using the following conditions: trap and transfer collision energy was set to 6.0 eV and 4.0 eV, respectively; gas flow (N<sub>2</sub>) in the trap and IMS device was set to 1.5 mL/min and 24 mL/min respectively.

For peptide identifications, LC-MS/MS data was collected in an alternating low energy and elevated energy mode of acquisition which is defined as DIA mode, namely MS<sup>E</sup> mode. The mass range was set to m/z 50 to 1900. For each scan, the low collision energy (10 eV) mode surveys all precursor ions almost without fragmentation and the high collision energy (a ramp from 10 eV to 25 eV) mode surveys both parent and product ions. Lockmass correction scans of Glu-fibrinopeptide (GFP) (m/z = 785.8421) were collected every 30 sec during each dataset acquisition (12 min).

## **2.1.4 HDX data processing and analysis**

### **2.1.4.1 Peptide identification**

HDX data analysis pipeline is showed in Figure 2.3. The first step is the identification of pepsin-generated peptides. Mass spectral datasets were acquired on a Synapt HDMS system equipped with a ESI source and operated in the MS<sup>E</sup> mode [34], an approach which can collect both precursor and fragment ion information in one analytical run. The MS<sup>E</sup> dataset is input to the ProteinLynx Global Server (PLGS) 2.4 software program (Waters) for searching against an “in house” protein database to which the human FXR-LBD sequence was added. Specifically, three RAW data files corresponding to the three runs of the control sample are processed in PLGS by two algorithms: apex 3D peak detection and ion accounting identification. The databank search query settings were as followed: minimum fragment ion matches per peptide,

3; minimum fragment ion matches per protein, 7; minimum peptide matches per protein, 3; maximum protein mass, 250,000; primary digest reagent, non specific; missed cleavages, 1. The PLGS processing parameters were set as followed: lock mass window, 0.25 Da; low energy threshold, 200 counts; elevated energy threshold, 75 counts; intensity threshold, 1500 counts. An ion accounting (IA) file containing an identified peptides list is generated by PLGS in CSV format. The IA file provides valuable information relating to protein and peptides, such as the number of matched product ions and peptides for protein, protein sequence coverage, each peptide sequence, the number of matched product ions for a specific peptide, the charge number and m/z value of every precursor ion.

#### **2.1.4.2 The determination of deuterium uptake levels**

The deuterium incorporation levels for protein or peptic peptides are directly derived from the observed mass difference between the deuterated and nondeuterated proteins/peptides without back exchange correction. The back-exchange correction is omitted due to the comparative nature of the present study [7, 35-38]. The intact protein molecular mass at each exchange time point was obtained by MaxEnt1 algorithm in MassLynx 4.0 and the deuterium uptake level at each time point was manually calculated by subtracting the molecular mass of the nondeuterated protein from that of the deuterated protein.

The centroid mass of each peptide at each time point was obtained using Waters' HDX Browser software in combination with the HX express program described by Weis et al [39]. In detail, the IA file with all identified peptides generated by PLGS was loaded into the HDX Browser and then all RAW files for each exchange time point (0, 0.5, 1, 2, 5, 15, 30, 60 min) were also loaded as the sequence of time increased. The HDX Browser generates a peptide list as well as the mass spectra for each peptide under different time point. The peptic peptides with

poor quality were filtered by setting the thresholds for the following parameters: precursor ion intensity, matched products, consecutive matched products, sequence length, and peptide score. In addition, for a set of data (8 RAW files from 0 min to 60 min), some peptides were excluded under three situations: any peptides that did not appear in at least the given number; any peptides where the relative standard error of intensity exceeded a threshold; any peptides where the absolute distribution of retention times exceeded the threshold. All peptides complying with filtering rules were kept in the list. Subsequently, the mass spectra of each peptide under every time point were checked manually to ensure peptides with high quality to be analyzed as well as to get maximum amino acid sequence coverage. The HDX Browser imports the overlaid mass spectra (all labeled time points) for each peptide as a CSV file with m/z versus intensity list for HX express processing. All CSV files were processed by HX express software to calculate centroid mass and peak width values for all mass spectra and further provided a summary of the absolute deuterium uptake level at each exchange time point.

#### **2.1.4.3 The determination of HDX rate constants**

Under our experimental condition, the deuterium volume percentage is over 90% and the pH and temperature is kept constant at 7.3 and 25 °C, respectively. The total D content in a specific peptide can be described by the equation 2.2 because HDX will follow a first-order kinetics [40].

$$D = N - \sum_i^n \exp(-k_i t) \quad (2.2)$$

Where  $D$  is the deuterium content in a peptide containing  $N$  amide hydrogens,  $k_i$  is the rate constant for each exchangeable amide hydrogen,  $t$  is the exchange reaction time. The rate constant can be calculated by statistical software until the best curve fit is obtained [41, 42].

A fixed-rate-constant binning model was chosen to fit all peptide HDX data by minimizing the sum of square error in R statistical software. In this model, deuterium uptake can be plotted according to equation 2.3 derived by equation 2.2, where  $A_i$  is the amplitude which means the number of amide hydrogen in a specific bin and  $k_i$  is the rate constant in the  $i$ -th kinetic phase which is fixed to six different bins ( 10, 1, 0.1, 0.01, 0.001, 0.0001 min<sup>-1</sup> ).

$$D = \sum_i^n A_i [1 - \exp(-k_i t)] \quad (2.3)$$

The HDX data of three replicates for each sample was fitted together and the best fitted curve was presented with average value of three trials and  $\pm$  standard deviation as error bar for each exchange time point.

#### 2.1.4.4 The normalization of deuterium up-take level

Peptides produced by pepsin digestion usually have different amino acid numbers. To compare the flexibility and dynamics among different regions in protein, the deuterium number in each peptide need to be normalized by the following equation:

$$D\% = \left( \frac{m - m_0}{N} \right) \times 100\% \quad (2.4)$$

Where  $D\%$  is the percentage of deuterium in a peptide;  $m$  is the deuterated peptide mass;  $m_0$  is the undeuterated peptide mass;  $N$  is the total number of exchangeable amide hydrogen in a peptide. No back exchange correction was made for all HDX data because only a relative comparison in specific peptides was considered in the present study.

## 2.2 Fluorescence method

### 2.2.1 The theory of fluorescence

The fluorescence is a phenomenon that the molecules absorb light energy at an appropriate wavelength and subsequently emit light at longer wavelength. The basic concept of fluorescence is described in the Figure 2.4. The electrons of molecules are excited by a light source and elevated to a higher energy state (S1) from a ground state (S0). The energy loss happens within a few nanoseconds resulting in the fluorescent light at longer wavelength when the electrons fall back to the ground energy state (S0) undergoing a radiation transition. The average period of time electrons stay in the excited state is typically around  $10^{-8}$  second which is termed as the fluorescence lifetime.

Any process that decreases the fluorescence intensity of a sample is called fluorescence quenching which is extensively applied to obtain the information in biochemical system. The quenching can result from various molecular interactions including excited-state reactions, molecular rearrangements, energy transfer, ground-state complex formation (static quenching), and collisional quenching (dynamic quenching) [43]. In this thesis, we focus on the quenching resulting from static quenching where a complex without fluorescence (often protein-ligand complexes) is produced and dynamic quenching where the quencher collides with the fluorophore (often tryptophan in proteins). The contact between quencher and protein is a requirement for both static and dynamic quenching. The tryptophan often is considered as the main source to contribute to protein fluorescence which is very sensitive to the environment polarity [44]. The protein conformational dynamics, subunit dissociation/association, ligand binding, and denaturation can affect the environmental surrounding of the tryptophan residue in solution and further change its the emission spectrum.

### 2.2.2 Fluorescence analysis

A LS 50 luminescence spectrometer (Perkin Elmer) was used to measure steady state fluorescence. The spectral bandwidths for excitation and emission were both set to 3.5 nm. The protein sample was excited at 295 nm to minimize the fluorescence contribution of tyrosine residues and the emission spectra were acquired from 305 nm to 480 nm after each time increasing ligand concentration was added to protein and were incubated for 3 minutes. The ligand-hFXR-LBD interactions were studied by an intrinsic fluorescence titration method where 10  $\mu$ M proteins (50 mM sodium phosphate, 0.5 M NaCl, 0.5 mM CHAPS, 1 mM TCEP, 0.5 M sucrose and 10% glycerol, pH=7.4, 400  $\mu$ L) was titrated with 1000  $\mu$ M ligands until the ligand/protein ratio reached 5 to 1 (Figure 2.5). Before analysis of the binding and quenching data, fluorescence spectra were corrected ( $F_{cor}$ ) for background fluorescence of the specific ligand  $F_B$ , instrument-dependent monochromator and photomultiplier response emission correction factor  $F_S$  and dilution factor  $A$ :  $F_{cor} = (F_0 - F_B) \times 100 \times A / F_S$  where  $F_0$  is the measured fluorescence intensity. All measurements were performed at 25°C and repeated three times.

### 2.2.3 Fluorescence data analysis

For ligand binding studies, quenching data were analyzed according to the Stern-Volmer equation [43] which described the quenching process between protein and quenchers:

$$\frac{F_0}{F} = 1 + K_{sv}[Q] \quad (2.5)$$

where  $F_0$  and  $F$  are the fluorescence intensities in the absence and presence of quenchers (ligands), respectively;  $[Q]$  is the concentration of quencher.  $K_{sv}$  is the Stern-Volmer constant, which is related to the bimolecular quenching constant  $k_q$  and  $\tau_0$  the lifetime of the fluorophore in the absence of quencher.  $K_{sv}$  is given by:



$$K_{SV} = k_q \tau_0 \quad (2.6)$$

A linear Stern-Volmer plot of  $\frac{F_0}{F}$  versus  $[Q]$  usually indicates that all the tryptophan residues in the protein are equally accessible to the quencher.

The Stern-Volmer plots with downward curvature and concave towards the x-axis indicate that the fraction of the tryptophan residues is accessible to the quencher, were analyzed by using the Lehrer model [45], i.e. the modified Stern-Volmer equation:

$$\frac{F_0}{F_0 - F} = \frac{1}{f_a [Q] K_{SV}} + \frac{1}{f_a} \quad (2.7)$$

where  $f_a$  is the fraction of the initial tryptophan residues accessible to the quencher.

The Stern-Volmer plots with upward curvature and concave towards the y-axis, indicating a combination of static and dynamic quenching, were analyzed by the following equation [43]:

$$\frac{F_0}{F} = (1 + K_D [Q])(1 + K_S [Q]) \quad (2.8)$$

where  $K_D$  is the dynamic quenching constant;  $K_S$  is the static quenching constant.

For binding equilibrium analyses, binding data were analyzed by fitting a curve to the Hill equation [46] and the Scatchard plot (Annals of the New York Academy of Sciences Volume 51, Molecular Interaction pages 660–672, May 1949).

$$\frac{F_0 - F}{F_0} = \frac{[L]^n}{K_d + [L]^n} \quad (2.9)$$

$K_d$  is the apparent dissociation constant, a parameter describing affinity between protein and ligand;  $n$ , called the Hill coefficient  $n_H$ , is used to explain the cooperativity of ligands binding independently of multiple equivalent binding sites in a protein.

All data fittings, linear regression and non-linear regression, were performed with the GraphPad Prism software program and gave correlation coefficient (R) values exceeding 0.99.

## Figures

Figure 2.1 Schematic of a Synapt G1 HDMS mass spectrometry instrument

Figure 2.2 The experimental workflow used for the HDX-MS analyses of FXR LBD in presence of diverse ligands.

Figure 2.3 Pipeline of HDX data analysis

Figure 2.4 Basic theory of fluorescence

Figure 2.5 Workflow of fluorescence quenching experiment

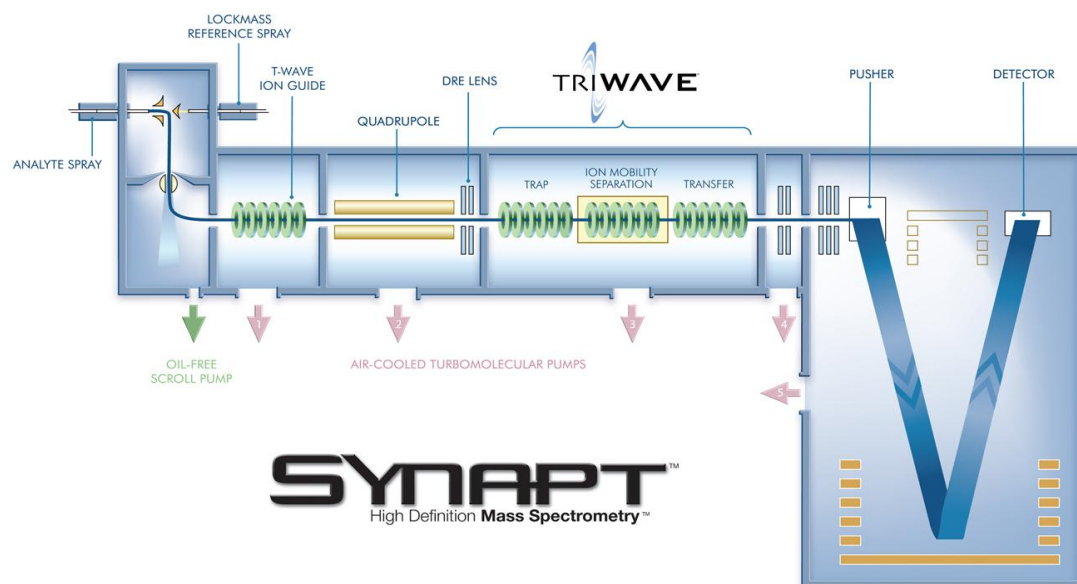


Figure 2.1 Schematic of a Synapt G1 HDMS mass spectrometry instrument

This type of accurate mass high resolution ToF instrument was predominately used for the HDX-MS analyses of FXR LBD in presence of different ligands.

Copied from: <http://www.waters.com>

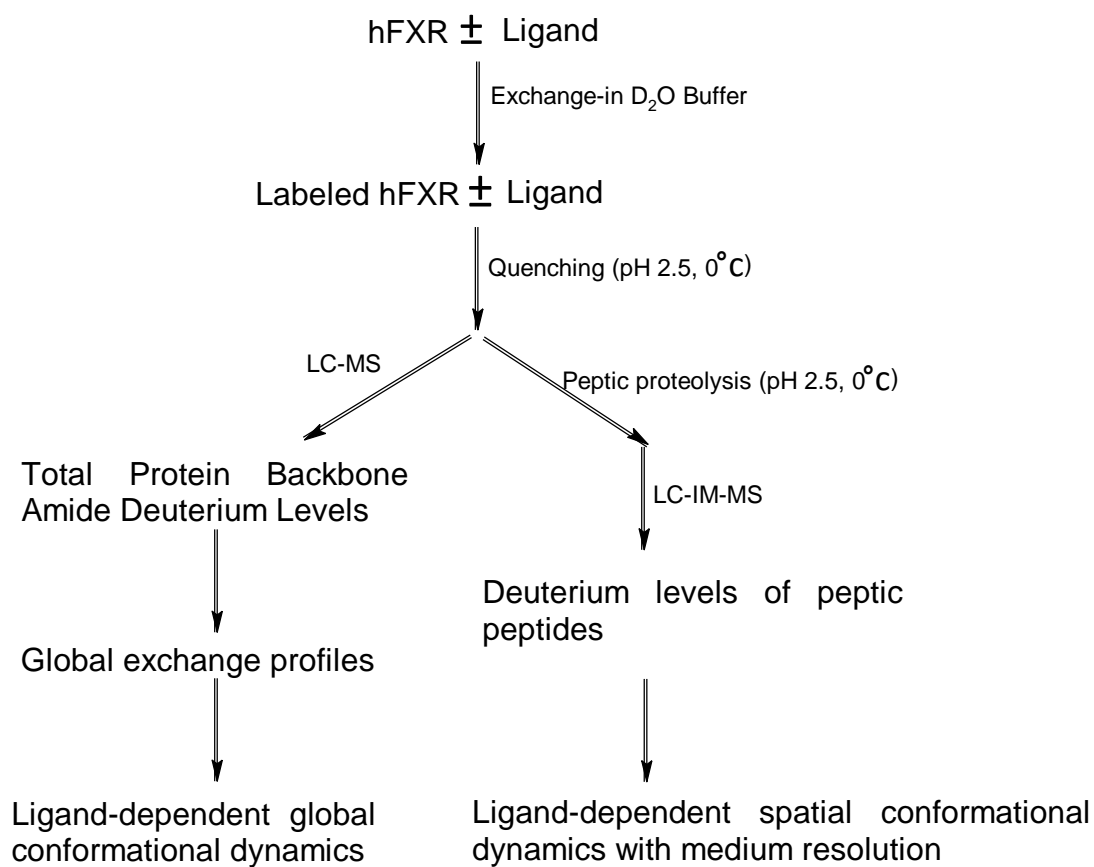


Figure 2.2 Experimental workflow used for the HDX-MS analyses of FXR LBD in presence of diverse ligands

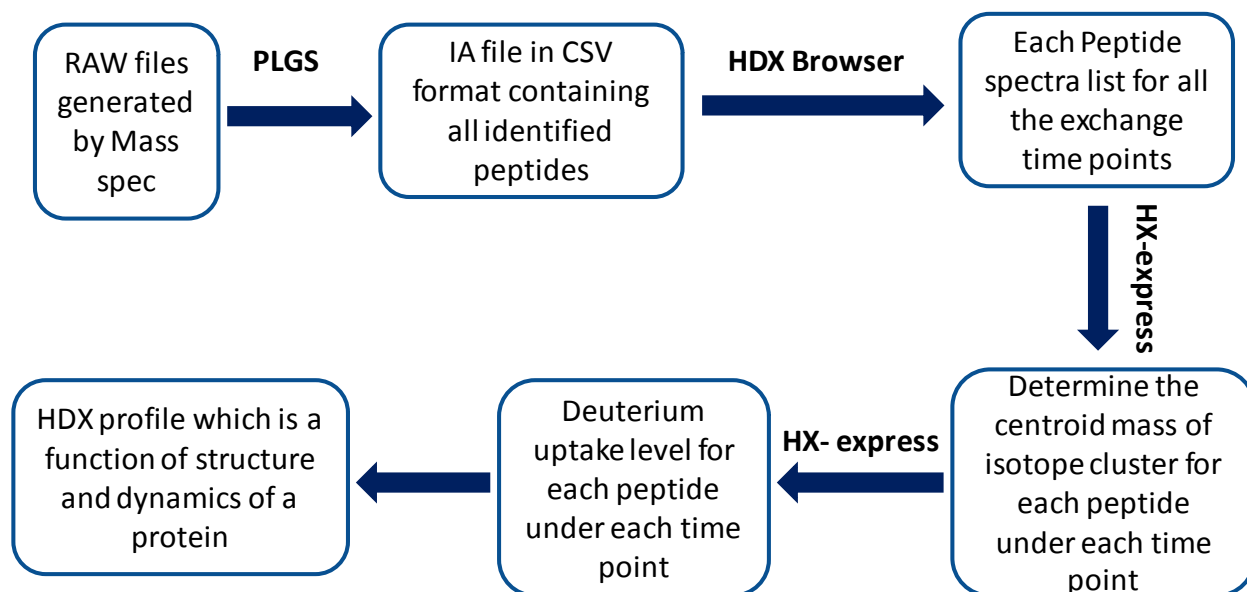


Figure 2.3 Pipeline of HDX data analysis

## Theory of Fluorescence

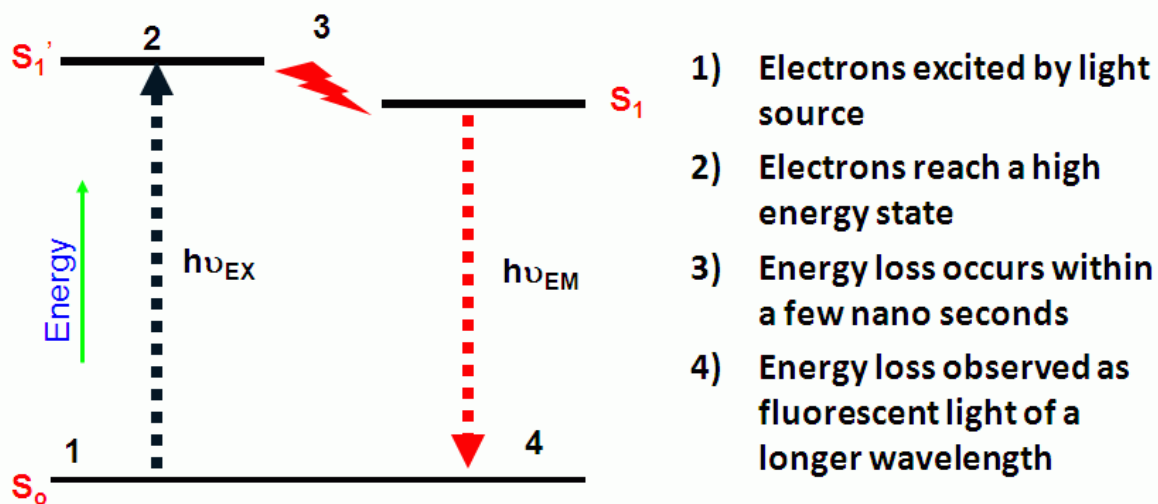


Figure 2.4 Basic theory of fluorescence

<http://www.icms.qmul.ac.uk/flowcytometry/flowcytometry/principles/index.html>

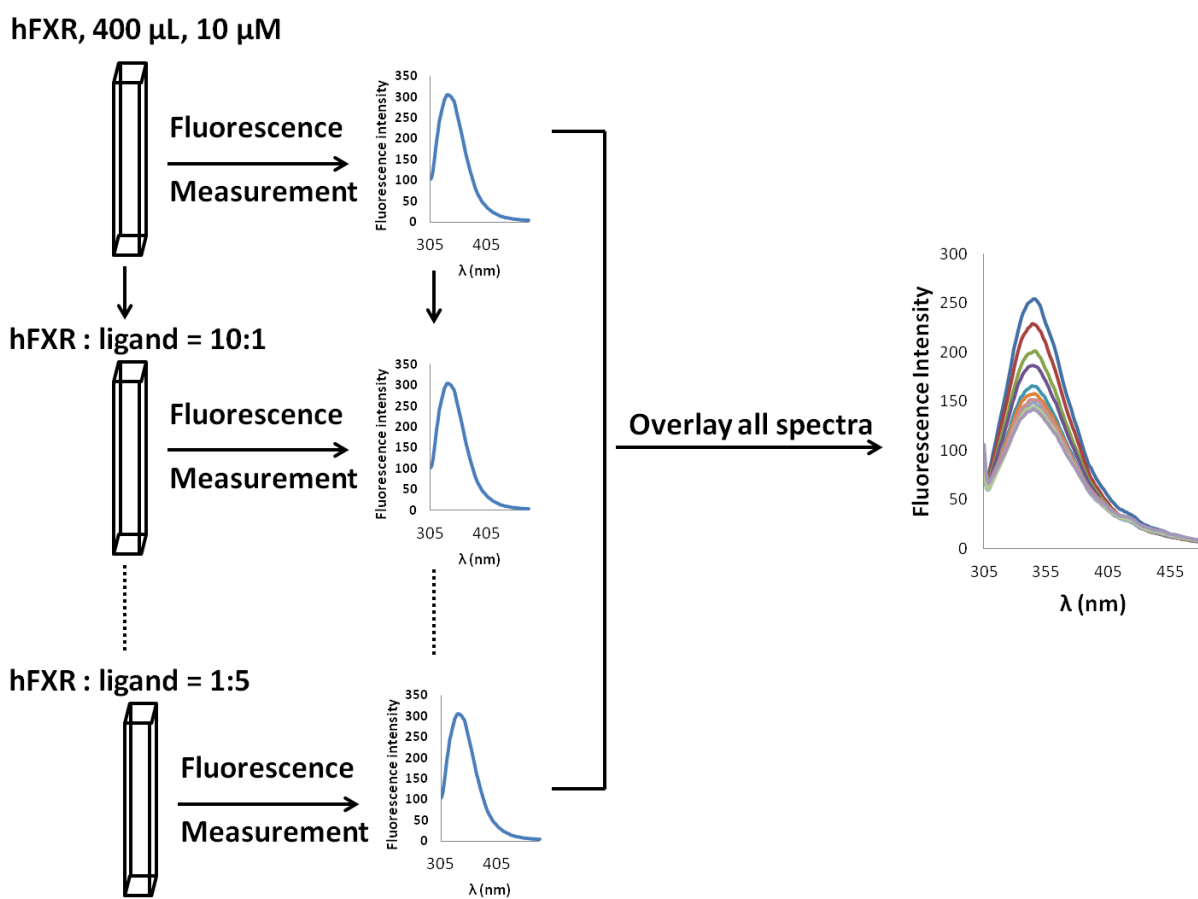


Figure 2.5 Workflow of fluorescence quenching experiment



## 2.3 Reference

- [1] S.W. Englander, T.R. Sosnick, J.J. Englander, L. Mayne, Mechanisms and uses of hydrogen exchange, *Curr Opin Struct Biol*, 6 (1996) 18-23.
- [2] C.A. Hughes, J.G. Mandell, G.S. Anand, A.M. Stock, E.A. Komives, Phosphorylation causes subtle changes in solvent accessibility at the interdomain interface of methylesterase CheB, *J Mol Biol*, 307 (2001) 967-976.
- [3] J.G. Mandell, A. Baerga-Ortiz, S. Akashi, K. Takio, E.A. Komives, Solvent accessibility of the thrombin-thrombomodulin interface, *J Mol Biol*, 306 (2001) 575-589.
- [4] M.A. Eriksson, T. Hard, L. Nilsson, On the pH dependence of amide proton exchange rates in proteins, *Biophys J*, 69 (1995) 329-339.
- [5] Y. Bai, J.S. Milne, L. Mayne, S.W. Englander, Primary structure effects on peptide group hydrogen exchange, *Proteins*, 17 (1993) 75-86.
- [6] X. Yan, C.S. Maier, Hydrogen/deuterium exchange mass spectrometry, *Methods Mol Biol*, 492 (2009) 255-271.
- [7] T.E. Wales, J.R. Engen, Hydrogen exchange mass spectrometry for the analysis of protein dynamics, *Mass Spectrom Rev*, 25 (2006) 158-170.
- [8] K.S. Kim, C. Woodward, Protein internal flexibility and global stability: effect of urea on hydrogen exchange rates of bovine pancreatic trypsin inhibitor, *Biochemistry*, 32 (1993) 9609-9613.
- [9] Y. Deng, D.L. Smith, Identification of unfolding domains in large proteins by their unfolding rates, *Biochemistry*, 37 (1998) 6256-6262.
- [10] L. Swint-Kruse, A.D. Robertson, Temperature and pH dependences of hydrogen exchange and global stability for ovomucoid third domain, *Biochemistry*, 35 (1996) 171-180.
- [11] A. Miranker, C.V. Robinson, S.E. Radford, R.T. Aplin, C.M. Dobson, Detection of transient protein folding populations by mass spectrometry, *Science*, 262 (1993) 896-900.
- [12] C.S. Maier, M.I. Schimerlik, M.L. Deinzer, Thermal denaturation of Escherichia coli thioredoxin studied by hydrogen/deuterium exchange and electrospray ionization mass spectrometry: monitoring a two-state protein unfolding transition, *Biochemistry*, 38 (1999) 1136-1143.
- [13] Z. Zhang, D.L. Smith, Thermal-induced unfolding domains in aldolase identified by amide hydrogen exchange and mass spectrometry, *Protein Sci*, 5 (1996) 1282-1289.
- [14] M. Yamashita, Fenn, J.B., Electrospray ion source. Another variation on the freejet theme., *J Phys Chem*, 88 (1984) 4451-4459.

- [15] J.B. Fenn, M. Mann, C.K. Meng, S.F. Wong, C.M. Whitehouse, Electrospray ionization for mass spectrometry of large biomolecules, *Science*, 246 (1989) 64-71.
- [16] K. Tanaka, Waki, H., Ido, Y., Akita, s., Yoshida, Y., Yoshida, T., , Protein and polymer analyses up to  $m/z$  100 000 by laser ionization time-of-flight mass spectrometry., *Rapid Commun Mass Spectrom*, 2 (1988) 151-153.
- [17] M. Karas, Bachmann, D., Hillenkamp, F., Influence of the wavelength in high irradiance ultraviolet laser desorption mass spectrometry of organic molecules, *Anal Chem*, 57 (1985) 2935-2939.
- [18] P.H. Dawson, *Quadrupole Mass Spectrometry and Its Applications.*, in, Springer, New York, 1995.
- [19] C. Weickhardt, Moritz, F., Grotemeyer, J. , Time-of-flight mass spectrometry: State-of-the-art in chemical analysis and molecular science, *Mass Spectrom Rev*, 15 (1996) 139-162.
- [20] B.A. Mamyrin, Karataev, V. I., Shmikk, D. V., Zagulin, V. A., The mass reflectron, a new nonmagnetic time-of-flight mass spectrometer with high resolution, *Soviet Phy JETP*, 37 (1973) 45-48.
- [21] A.B. Kanu, P. Dwivedi, M. Tam, L. Matz, H.H. Hill, Jr., Ion mobility-mass spectrometry, *J Mass Spectrom*, 43 (2008) 1-22.
- [22] L.S. Fenn, J.A. McLean, Biomolecular structural separations by ion mobility-mass spectrometry, *Anal Bioanal Chem*, 391 (2008) 905-909.
- [23] M. Giles, C. McClenahan, E. Cairns, J. Mallet, An application of the Theory of Planned Behaviour to blood donation: the importance of self-efficacy, *Health Educ Res*, 19 (2004) 380-391.
- [24] S.D.G. Pringle, K.; Wildgoose, J. L.; Williams, J. P.; Slade, S. E.; Thalassinou, K.; Bateman, R. H.; Bowers, M. T.; Scrivens,, An investigation of the mobility separation of some peptide and protein ions using a new hybrid quadrupole/travelling wave IMS/oa-ToF instrument, *International journal of mass spectrometry*, 261 (2007).
- [25] K.G. Steven D. Pringle, Jason L. Wildgoose, Jonathan P. Williams, Susan E. Slade, Konstantinos Thalassinos, Rober H. Bateman, Michael T. Bowers, James H. Scrivens, An investigation of the mobility separation of some peptide and protein ions using a new hybrid quadrupole/travelling wave IMS/oa-TOF instrument, *International journal of mass spectrometry*, 261 (2006) 1-12.
- [26] C. Eckers, A.M. Laurs, K. Giles, H. Major, S. Pringle, Evaluating the utility of ion mobility separation in combination with high-pressure liquid chromatography/mass spectrometry to facilitate detection of trace impurities in formulated drug products, *Rapid Commun Mass Spectrom*, 21 (2007) 1255-1263.

- [27] A.K. Shukla, J.H. Futrell, Tandem mass spectrometry: dissociation of ions by collisional activation, *J Mass Spectrom*, 35 (2000) 1069-1090.
- [28] R.N. Hayes, M.L. Gross, Collision-induced dissociation, *Methods Enzymol*, 193 (1990) 237-263.
- [29] S.J. Geromanos, J.P. Vissers, J.C. Silva, C.A. Dorschel, G.Z. Li, M.V. Gorenstein, R.H. Bateman, J.I. Langridge, The detection, correlation, and comparison of peptide precursor and product ions from data independent LC-MS with data dependant LC-MS/MS, *Proteomics*, 9 (2009) 1683-1695.
- [30] R. Pellicciari, S. Fiorucci, E. Camaioni, C. Clerici, G. Costantino, P.R. Maloney, A. Morelli, D.J. Parks, T.M. Willson, 6alpha-ethyl-chenodeoxycholic acid (6-ECDCA), a potent and selective FXR agonist endowed with anticholestatic activity, *J Med Chem*, 45 (2002) 3569-3572.
- [31] J.L. Lew, A. Zhao, J. Yu, L. Huang, N. De Pedro, F. Pelaez, S.D. Wright, J. Cui, The farnesoid X receptor controls gene expression in a ligand- and promoter-selective fashion, *J Biol Chem*, 279 (2004) 8856-8861.
- [32] T.P. Burris, C. Montrose, K.A. Houck, H.E. Osborne, W.P. Bocchinfuso, B.C. Yaden, C.C. Cheng, R.W. Zink, R.J. Barr, C.D. Hepler, V. Krishnan, H.A. Bullock, L.L. Burris, R.J. Galvin, K. Bramlett, K.R. Stayrook, The hypolipidemic natural product guggulsterone is a promiscuous steroid receptor ligand, *Molecular Pharmacology*, 67 (2005) 948-954.
- [33] S. Titolo, E. Welchner, P.W. White, J. Archambault, Characterization of the DNA-binding properties of the origin-binding domain of simian virus 40 large T antigen by fluorescence anisotropy, *J Virol*, 77 (2003) 5512-5518.
- [34] R.S. Plumb, K.A. Johnson, P. Rainville, B.W. Smith, I.D. Wilson, J.M. Castro-Perez, J.K. Nicholson, UPLC/MSE; a new approach for generating molecular fragment information for biomarker structure elucidation (vol 20, pg 1989, 2006), *Rapid Commun Mass Sp*, 20 (2006) 2234-2234.
- [35] J.B. Sperry, R.Y. Huang, M.M. Zhu, D.L. Rempel, M.L. Gross, Hydrophobic Peptides Affect Binding of Calmodulin and Ca as Explored by H/D Amide Exchange and Mass Spectrometry, *Int J Mass Spectrom*, 302 (2011) 85-92.
- [36] R.Y. Huang, D.L. Rempel, M.L. Gross, HD exchange and PLIMSTEX determine the affinities and order of binding of Ca<sup>2+</sup> with troponin C, *Biochemistry*, 50 (2011) 5426-5435.
- [37] R.Y. Huang, J. Wen, R.E. Blankenship, M.L. Gross, Hydrogen-deuterium exchange mass spectrometry reveals the interaction of Fenna-Matthews-Olson protein and chlorosome CsmA protein, *Biochemistry*, 51 (2012) 187-193.
- [38] C.H. Parker, C.R. Morgan, K.D. Rand, J.R. Engen, J.W. Jorgenson, D.W. Stafford, A Conformational Investigation of Propeptide Binding to the Integral Membrane Protein gamma-Glutamyl Carboxylase Using Nanodisc Hydrogen Exchange Mass Spectrometry, *Biochemistry*, 53 (2014) 1511-1520.

- [39] D.D. Weis, J.R. Engen, I.J. Kass, Semi-automated data processing of hydrogen exchange mass spectra using HX-Express, *J Am Soc Mass Spectrom*, 17 (2006) 1700-1703.
- [40] S.W. Englander, N.R. Kallenbach, Hydrogen exchange and structural dynamics of proteins and nucleic acids, *Q Rev Biophys*, 16 (1983) 521-655.
- [41] X. Yan, H. Zhang, J. Watson, M.I. Schimerlik, M.L. Deinzer, Hydrogen/deuterium exchange and mass spectrometric analysis of a protein containing multiple disulfide bonds: Solution structure of recombinant macrophage colony stimulating factor-beta (rhM-CSFbeta), *Protein Sci*, 11 (2002) 2113-2124.
- [42] Z. Zhang, C.B. Post, D.L. Smith, Amide hydrogen exchange determined by mass spectrometry: application to rabbit muscle aldolase, *Biochemistry*, 35 (1996) 779-791.
- [43] J.R. Lakowicz, SpringerLink (Online service), Principles of Fluorescence Spectroscopy, in, Springer Science+Business Media, LLC, Boston, MA, 2006.
- [44] M. Moller, A. Denicola, Protein tryptophan accessibility studied by fluorescence quenching, *Biochem Mol Biol Edu*, 30 (2002) 175-178.
- [45] S.S. Lehrer, Solute perturbation of protein fluorescence. The quenching of the tryptophyl fluorescence of model compounds and of lysozyme by iodide ion, *Biochemistry*, 10 (1971) 3254-3263.
- [46] A.V. Hill, The Combinations of Haemoglobin with Oxygen and with Carbon Monoxide. I, *Biochem J*, 7 (1913) 471-480.

### Chapter 3

#### **Conformational dynamics of human FXR-LBD ligand interactions studied by hydrogen/deuterium exchange mass spectrometry: Insights into the antagonism of the hypolipidemic agent Z-guggulsterone**

Liping Yang<sup>1</sup>, David Broderick<sup>1</sup>, Yuan Jiang<sup>2</sup>, Victor Hsu<sup>3</sup> and Claudia S. Maier<sup>1</sup>

Departments of Chemistry<sup>1</sup>, Department of Statistics<sup>2</sup>, and Biochemistry and Biophysics<sup>3</sup>,  
Oregon State University, Corvallis, Oregon 97331

**Running Title:** Ligand-dependent HDX-MS analysis of FXR LBD

Corresponding author: Dr. Claudia S. Maier

Email: [claudia.maier@oregonstate.edu](mailto:claudia.maier@oregonstate.edu)

Phone: +1-541-737-9533

Fax: +1-541-737-2062

**Key Words**

Farnesoid X receptor, hydrogen/deuterium exchange, mass spectrometry, conformation, dynamics, ligand interaction, guggulsterone

**Abbreviations**

HDX, hydrogen/deuterium exchange; LC-ESI-MS, liquid chromatography electrospray ionization mass spectrometry; FXR-LBD, farnesoid X receptor ligand binding domain; ligand binding cavity, LBC; CDCA, chenodeoxycholic acid; GG, Z-guggulsterone; 6ECDCA, 6-ethylchenodeoxycholic acid; UDCA, ursodeoxycholic acid; DMSO, dimethylsulfoxide; TCEP, Tris (2-carboxyethyl) phosphine hydrochloride; TOF, time of flight; PPAR $\gamma$ , peroxisome proliferator-activated receptor; RXR, retinoid X receptor, THR, thyroid hormone receptor; ER, estrogen receptor; VDR, vitamin D receptor; GR, glucocorticoid receptor.

### 3.1 Abstract

Farnesoid X Receptor (FXR) is a member of the nuclear receptor superfamily of transcription factors that plays a key role in the regulation of bile acids, lipid and glucose metabolisms. The regulative function of FXR is governed by conformational changes of the ligand binding domain (LBD) upon ligand binding. Although FXR is a highly researched potential therapeutic target, only a limited number of FXR-agonist complexes have been successfully crystallized and subsequently yielded high resolution structures. There is currently no structural information of any FXR-antagonist complexes publically available. We therefore explored the use of amide hydrogen/deuterium exchange (HDX) coupled with mass spectrometry for characterizing conformational changes in the FXR-LBD upon ligand binding. Ligand-specific deuterium incorporation profiles were obtained for three FXR ligand chemotypes: GW4064, a synthetic non-steroidal high affinity agonist; the bile acid chenodeoxycholic acid (CDCA), the endogenous low affinity agonist of FXR; and Z-guggulsterone (GG), an *in vitro* antagonist of the steroid chemotype. Comparison of the HDX profiles of their ligand-bound FXR-LBD complexes revealed a unique mode of interaction for GG. The conformational features of the FXR-LBD-antagonist interaction are discussed.

### 3.2 Introduction

The farnesoid X receptor (FXR) is a therapeutic target with the potential to modulate metabolic pathways associated with diverse liver and metabolic disorders. FXR's prominence stems from its role as a key regulator of bile acid homeostasis, and glucose and lipoprotein metabolisms [1, 2]. FXR has been identified as a bile acid sensor and is expressed mainly in the liver, intestine, and kidney. Many reviews have discussed the physiologically relevant role of FXR regulation and the potential of FXR as a target for synthetic ligands to prevent, manage or treat metabolic diseases, such as hyperlipidemia and type 2 diabetes [3-5].

FXR is a member of the nuclear receptor (NR) superfamily and a ligand-activated transcription factor. Since chenodeoxycholic acid (CDCA) was identified as the endogenous agonist of FXR that modulates the expression of target genes related to bile acid metabolism, FXR activation rapidly became the objective of intense research efforts. Synthetic FXR agonists have been developed with the potential to treat cholestatic liver diseases, including primary biliary cirrhosis, and metabolic disorders [6]. For instance, FXR agonists have been identified that improve myocardial fatty acid metabolism in obese (fa/fa) Zucker rats, and to counteract pro-atherogenic lipoprotein profiles and thereby confer protection against aortic plaque formation in (ApoE<sup>-/-</sup>) mice, a model of accelerated atherosclerosis [7-10]. Ursodeoxycholic acid (UDCA), an isomer of CDCA, was the first FXR-targeting drug approved by the FDA to treat primary biliary cirrhosis [11].

The X-ray structures of agonist-bound FXR complexes show the classical NR fold, consisting of 12 helices that form a three-layer sandwich harboring the LBC. Ligand binding is primarily facilitated by interactions with residues located in helices 3, 5, 6, 7, and 11. Ligand binding changes the position of the AF-12 helix and facilitates recruitment of co-activator



proteins. Despite FXR's importance as a potentially therapeutically relevant receptor, only a limited number of X-ray structures of the FXR-LBD bound to high affinity synthetic ligands are available that may guide structure-activity relationship (SAR) studies. The published X-ray crystal structures of FXR-ligand complexes illustrate binding modes of five different ligand chemotypes: three steroid-like agonists [12, 13], ten stilben-based agonists (GW4064 and derivatives) [14-18], seven benzimidazole-based agonists [19, 20], two azepino [4,5-b] indole agonists (XL335 and FXR 450) [21, 22], and one fexaramide y-shaped ligand [23]. To date, there are no published crystal structures available for antagonist-bound FXR-LBD complexes or the apo-protein. The conformational plasticity of FXR's LBD has been discussed as one of the possible reasons for the limited success of X-ray structural analyses of FXR-LBD ligand complexes [12].

HDX-MS has been previously used successfully for studying the conformational properties of diverse nuclear receptors and their conformational changes upon binding to diverse ligands [24-27]. In the current study, we used HDX-MS for studying conformational changes of the FXR-LBD upon binding to different classes of ligands: (1) CDCA, a primary bile acid ligand and a low affinity agonist; (2) GW4064, a synthetic non-steroidal stilben-based high affinity agonist; and (3) Z-guggulsterone (GG), a natural steroidal FXR ligand and one of the few ligands described as an *in vitro* FXR antagonist ( $K_d > 5\mu\text{M}$ ) [28]. Comparison of the deuterium incorporation profiles obtained in absence and presence of the chemically diverse ligands enabled the identification of distinct regions of the FXR-LBD that exhibit ligand-specific exchange behaviors. Insights into the ligand-dependent modulation of the conformational properties within the LBD may aid the development of selective bile acid receptor modulators

(SBARMs) which show promise to manipulate FXR's pleiotropic regulation of metabolic networks.

### **3.3 Materials and Methods**

#### **3.3.1. Materials**

Deuterium oxide (D<sub>2</sub>O, 99.9% deuterium) was from Sigma-Aldrich Chemical Co. (St. Louis, MO). GG was purchased from ChromaDex<sup>TM</sup> Corporate (Irvine, CA). GW4064 and CDCA were obtained from Tocris (Ellisville, MO). All ligands were prepared as 10 mM stock solution in dimethylsulfoxide (DMSO). All other materials were obtained from standard commercial sources.

#### **3.3.2. Protein expression and purification**

The pET 15B vector containing hFXR-LBD, residues 193-472 was transformed into *Escherichia coli* BL21 (DE3) pLysS and grown on LB agar plates. A single colony was used to inoculate 100 mL of 2XYT medium with antibiotics (Carbenicillin 100 µg/mL and Chloramphenicol 35 µg/mL) and grown overnight at 37°C. The overnight culture was centrifuged for 10 min at room temperature and then the pellet was resuspended in 6 mL of fresh 2XYT medium. Each liter of fresh 2XYT medium with antibiotics (ampicillin 150 µg/mL and Chloramphenicol 35 µg/mL) was inoculated with 1 mL of the resuspended cells (total six liter) and grown at 37°C to A<sub>600</sub>=0.6. Protein expression was induced with 0.8 mM IPTG (isopropyl-β-D-thiogalactopyranoside) and the cells were allowed to continue growing for 4 hours at 20°C. The cell pellets were harvested by centrifugation (4000 RPM, 25 min, 4°C), resuspended in cell wash solution (150 mM NaCl, 50 mM Tris and 10% w/v sucrose), centrifuged again and frozen at -80°C.

The frozen cell pellets were resuspended in buffer solution (50 mM sodium phosphate, 0.5 M NaCl, 0.5 mM CHAPS, 15 mM imidazole, 0.5 M sucrose, pH 7.3) and centrifuged. The His<sub>6</sub>-tagged FXR-LBD was mixed with Clontech Talon Co<sup>2+</sup> polyhistidine affinity resin (equilibrated with the above buffer) at 4°C for 45 min. The proteins were eluted into a solution containing 50 mM sodium phosphate, 0.5 M NaCl, 0.5 mM CHAPS, 200 mM imidazole, 0.5 M sucrose, pH 7.3. The His tag was removed by thrombin digestion at 4°C (48 hours) followed by purification on a column packed with Co<sup>2+</sup> resin to yield purified human FXR-LBD monomer which was used for all experiments. The protein concentration was determined spectrophotometrically at 280 nm, and the purity (over 95%) was judged by sodium dodecyl sulfate –acrylamide gel electrophoresis (SDS-PAGE) and mass spectrometry (Fig. S3.1).

### 3.3.3 Fluorescence titration experiment

Steady state fluorescence measurements were performed with a Perkin Elmer LS 50 luminescence spectrophotometer. The protein sample was excited at 295 nm, and the sample temperature was maintained at 25°C. The ligand solutions ( $1 \times 10^{-3}$  M) were titrated into a fixed volume (400  $\mu$ l) of FXR-LBD ( $1 \times 10^{-5}$  M) until the ligand/protein ratio reached 5 to 1. The fluorescence intensity was measured over a wavelength range of 305-480 nm. The fluorescence spectra were corrected ( $F_{cor}$ ) for background fluorescence, instrument-dependent monochromator and photomultiplier response emission and dilution factor effects:  $F_{cor} = (F_0 - F_B) \times 100 \times A / F_S$ , where  $F_0$  is the measured fluorescence intensity,  $F_B$  is the background fluorescence of the specific ligand,  $A$  is the dilution factor of the protein sample, and  $F_S$  is the emission correction factor. Based on the FXR-LBD-GG binding data, the dissociation constant (Kd) of GG was derived by fitting a curve to the Hill equation [29] using the GraphPad Prism software program.

### 3.3.4 HDX-MS analysis

The purified FXR-LBD protein (15  $\mu$ L, 98  $\mu$ M, in 50 mM sodium phosphate, 0.5 M NaCl, 0.5 mM CHAPS, 1 mM TCEP, 0.5 M sucrose and 10% glycerol, pH=7.4) was equilibrated for 30 min in the presence of the respective DMSO solution (0.5  $\mu$ L,  $\pm$ 10 mM ligand). The ligand/monomeric protein molar ratio was 3.2:1. The small amount of DMSO (3.3% v/v) did not affect protein binding as indicated by fluorescence titration data as well as by intact protein HDX data. The D<sub>2</sub>O buffer (50 mM sodium phosphate, 0.5 M NaCl, 0.5 mM CHAPS, 1 mM TCEP, 0.5 M sucrose and 10% glycerol, pH 7.3) was equilibrated for 30 min in the presence of the same percentage of DMSO. The exchange reaction was initiated by adding 10-times D<sub>2</sub>O buffer (150  $\mu$ L). At different reaction time points, 0.5, 1, 2, 5, 10, 30 and 60 min, aliquots (15  $\mu$ L) were added to pre-chilled vials containing the same volume of quenching solution (15  $\mu$ L, 0.42% phosphoric acid, pH 2.5). The quenched sample was immediately frozen in liquid nitrogen for subsequent LC-ESI-MS analysis. Experiments were performed in triplicate.

The experimental conditions for the ligand binding studies in combination with the HDX approach were chosen to ascertain that both the FXR-LBD protein and the respective low affinity ligand retained solubility throughout the period of labeling. Even in presence of structure promoting and stabilizing additives (CHAPS, sucrose, glycerol, DMSO) the FXR-LBD protein showed a high tendency to precipitation in presence of low affinity ligands. This limited our flexibility in using large excess of low affinity ligands. We believe that the absence of X-ray structures of FXR-LBD in complex with low affinity ligands is at least in part caused by this shortcoming. The reported dissociation constant/binding affinity values for GW4064, CDCA, and GG are 0.06  $\mu$ M [30], 10  $\mu$ M [31], and GG > 5  $\mu$ M [28], respectively. The bound fraction of

FXR-LBD in each ligand binding study before initiation of the HDX reaction is ~100% as estimated by applying equation 3.1 [32]:

$$F_P = \frac{(L_T + P_T + K_d) - \sqrt{(L_T + P_T + K_d)^2 - 4L_T P_T}}{2P_T} \quad (3.1)$$

where  $F_P$  is fraction of protein bound,  $L_T$  and  $P_T$  are the total ligand concentration and protein concentration used, respectively, and  $K_d$  is the dissociation constant. In the present experimental protocol we kept the mole ratio between protein and ligand constant (being 3.2:1) during the time course of labeling. The evaluation of the mass isotope distributions and elution time features of all peptides evaluated indicated that no mixed populations were detected in accordance with that the fraction of ‘protein bound’ was the predominant population present in solution (Fig. S3.5).

For intact protein HDX-MS, the protein was eluted through a Micro Trap<sup>TM</sup> C4 column (1×8 mm) with a steep 10-90% (v/v) B gradient within 10 min (mobile phase A: 0.1% HCOOH in H<sub>2</sub>O, mobile phase B: 0.1% HCOOH in CH<sub>3</sub>CN, flow rate 40 µL/min) and eluted into a Waters LCT ESI-ToF mass spectrometer. HDX information at the peptide level was obtained by employing a nanoUPLC system equipped with a Waters “chilled” LC module, and coupled to a Waters Synapt HDMS instrument. Protein was digested by an online Poroszyme immobilized pepsin column (2.1×30 mm) with a 100 µL/min solvent (0.05% HCOOH in H<sub>2</sub>O). The proteolytic products were captured on a Acquity BEH C18 VanGuard Pre-column (1.7 µm, 2.1 x 5 mm), eluted and separated on an Acquity UPLC BEH C18 column (1.7 µm, 1.0×100 mm) using the following elution program: solvent B, increase from 8 to 40% within 6 minutes, hold at 40% for 1 minute, then increase from 40 to 85% in 0.5 minute, hold at 85% for 1 minute, then decrease from 85% to 8% in 0.5 minute, hold solvent B at 8% for 3 minutes. The elution protocol was completed in 12 minutes. In order to minimize contamination of the mass spectrometer with additives and detergents a Rheodyne MX Series II 6-port valve was installed

between the nanoAcquity UPLC and the ESI source. The details of the UPLC setup used in this study are provided in the supplementary materials (Fig. S3.3). All solvents were immersed in an ice bath.

### 3.3.5 Mass spectral data analysis

The deuterium incorporation levels for protein or peptic peptides were directly derived from the observed mass difference between the deuterated and nondeuterated proteins/peptides without back exchange correction. The back-exchange correction was omitted due to the comparative nature of the present study [33-38]. The intact protein molecular mass and the centroid mass of each peptide, respectively, were obtained using Waters' MassLynx 4.0 and HDX Browser software in combination with the HX express program described by Weis et al [39].

To identify pepsin-generated peptides, mass spectral data were acquired on a Synapt HDMS system equipped with a ESI source and operated in the MS<sup>E</sup> mode [40]. The MS<sup>E</sup> dataset was input to the ProteinLynx Global Server 2.4 software program (Waters) for searching against an "in house" protein database to which the human FXR-LBD sequence was added. The sequence of the current construct and the peptic map of FXR-LBD are depicted in Fig. S3.4.

### 3.3.6 HDX kinetics

Under our experimental conditions, the deuterium volume percentage is over 90%. In the applied protocol pH and temperature were kept constant at 7.3 and 25 °C, respectively. The total D content in a specific peptide can be described by the equation 3.2 because HDX will follow a first-order kinetics [41].

$$D = N - \sum_i^n \exp(-k_i t) \quad (3.2)$$

where  $D$  is the deuterium content in a peptide containing  $N$  amide hydrogens,  $k_i$  is the rate constant for each exchangeable amide hydrogen, and  $t$  is the exchange reaction time. The rate constant  $k_i$  can be determined by applying a curve fitting software [42, 43]. In the present study, we applied a fixed-rate-constant binning model for fitting the deuterium incorporation curves of all peptides by minimizing the sum of square error in R statistical software. In this model, deuterium uptake can be plotted according to equation 3.3 derived by equation 3.2, where  $A_i$  is the amplitude which means the number of amide hydrogen located in a specific bin and  $k_i$  is the rate constant in the  $i$ -th kinetic phase which is fixed to six different bins (10, 1, 0.1, 0.01, 0.001, 0.0001  $\text{min}^{-1}$ ).

$$D = \sum_i^n A_i [1 - \exp(-k_i t)] \quad (3.3)$$

The HDX data of three replicates for each sample was fitted together. The best fitted curve was plotted using as data points the average  $D$  value of the three trials including  $\pm$  standard deviation as error bar for each exchange time point (Fig. S3.6).

### 3.4 Results

#### 3.4.1. Ligand binding studies by intrinsic protein fluorescence measurements

The X-ray crystal structure of the FXR-LBD-GW4064 complex (PDB: 3DCT) showed that the two tryptophan residues in FXR-LBD, W454 and W469, located in helix 11 and helix 12, respectively, are in proximity to GW4064. Therefore, we chose intrinsic fluorescence titration experiments to test if the ligands interact and bind to our FXR-LBD construct under the current experimental conditions used. We monitored intensity changes in protein fluorescence emission (Fig. 3.1) using an excitation wavelength of  $\lambda_{\text{exc}} = 295$  nm to minimize fluorescence contributions of the six tyrosine residues present in the FXR-LBD construct. The fluorescence

spectra of apo FXR-LBD showed a strong fluorescence emission with a maximum at 343 nm. Binding of the GW4064 to FXR-LBD caused a red-shift in the emission spectrum confirming that under the solution conditions used the mode of binding of GW4064 is consistent with the binding interactions that were observed in the crystal structure of the FXR-LBD-GW4064 complex [18]. Only a slight change ( $\pm 3\%$ ) of the FXR-LBD fluorescence intensity in presence of CDCA was observed, suggesting that CDCA binding induces rather subtle changes within the microenvironment of the two tryptophan residues. These results were consistent with recent studies by Han et al [44], who reported that the fluorescence spectra of FXR-LBD showed little increase of intensity at a molar ratio of CDCA to FXR-LBD of 100:1. The *in vitro* antagonist GG [45] caused a concentration-dependent quenching of FXR-LBD fluorescence with no changes in either the maximum emission wavelength or shape of the spectra. The ligand-specific differences observed in the fluorescence titration experiment suggested that each ligand, GG, CDCA and GW4064, adopted distinct modes of binding. From the titration curve of GG (Fig. S3.2) a dissociation constant of  $5.9 \pm 0.3 \mu\text{M}$  was determined implying that GG is a low affinity ligand in accord with previous reports by Burris et al [28].

### **3.4.2. Global HDX profiles of FXR-LBD.**

To investigate to what extent interaction of the different ligands affect the global conformational plasticity of the FXR-LBD, we compared the deuterium incorporation profile of apo FXR-LBD with the exchange profiles of the FXR-LBD in the presence of the diverse ligands. Fig. 3.2 shows the overall deuterium levels of intact FXR-LBD in absence and presence of the ligands at different exchange-in periods ranging from 0.5, 1, 2, 5, 10, 30 to 60 min. Comparison of the global exchange profiles observed for the ligand-bound FXR-LBD revealed that exchange was significantly more retarded for the complex with the high affinity agonist



GW4064 compared to the protein complexes formed with the two low affinity binders, CDCA and GG. The FXR-LBD contains a total of 274 exchangeable backbone amide hydrogens. The reduced deuterium incorporation levels observed for the protein-ligand complexes suggested that ligand binding resulted in increased structural compactness, loss of conformational flexibility and/or decreased overall solvent accessibility. HDX-MS analysis of the apo FXR-LBD after 60 min incubation indicated that 144 backbone amide hydrogens were exchanged with deuterium. In contrast, exchange-in deuterium incorporation levels for the ligand-bound FXR-LBD were 108, 132 and 136 ( $\pm <10\%$  RSD) in presence of the respective ligand, GW4064, CDCA and GG (323  $\mu$ M ligand and ligand/protein ratio  $> 3$ ). Overall conformational stabilization upon ligand binding was also reported for other nuclear receptor LBDs [25, 26].

### **3.4.3 Peptide-level HDX-MS analysis.**

Forty peptides covering 91% of the FXR-LBD sequence were generated under the current experimental conditions (Fig. S3.4). A subset of 20 peptides was selected for which mass spectral data was consistently of high enough quality to allow determining the time-dependent isotopic compositions and deuterium incorporation levels for the different protein systems (Fig. S3.5). For all deuterium-labeled peptides evaluated, the observed mass spectral isotope patterns at all time points were consisted with EX2 kinetics (Fig. S3.5).

#### **3.4.3.1 HDX-MS of the apo FXR-LBD.**

Fig. S3.7 summarizes the HDX-MS data for apo-FXR-LBD. Both, the composite plot of the deuterium levels determined for peptide after different incubation times (Fig. S3.7A) and the derived heat map presentation (Fig. S3.7B), let us to postulate that large parts of the apo-FXR-LBD show exchange behaviors commonly associated with solvent exposed, disordered and/or conformationally flexible regions. For instance, the N-terminal regions, 201-241 (peptides 201-

222 and 229-241) and 256-278 (peptides 256-269 and 269-278), and the C-terminal peptide covering residues 454-465, showed high deuterium levels with little time dependency. This type of exchange behaviors is usually observed for highly solvent exposed and/or disordered regions which render little protection against exchange. The peptides encompassing the partial sequences 288-298, 320-328, 328-336, 348-360, 361-367, 368-375 showed exchange profiles that are were indicative of gradual exchange over time in concurrence with exchange properties associated with conformationally flexible regions that undergo multiple partial folding and unfolding reactions and variable solvent exposure which collectively result in some level of exchange retardation. A similar time dependency of the deuterium levels was observed for the peptides encompassing the residues 386-396, 406-412, 419-433 and 434-440. The peptide covering the partial sequence 440-451 was detected with the lowest deuterium levels and little variation of time; after 30 min exposure to D<sub>2</sub>O deuterium levels barely reached 20%. Overall, these HDX-MS results led us to speculate that apo FXR LBD adopts a state of considerable conformational flexibility and openness. FXR's plasticity was discussed by Soisson et al. and put forward as possible reason that allows the FXR-LBD to bind structurally diverse ligands but also severely hampers attempts to obtain crystal structural information of the apo protein and FXR-LBD complexes with low affinity ligands [12].

#### **3.4.3.2 Peptide-level HDX profiles of FXR-LBD in presence of different ligands**

To dissect the impact of the different ligands on the conformational dynamics of FXR-LBD, we performed HDX-MS studies of the ligand-bound FXR-LBD complexes. HDX-MS analysis at the peptide level provides an approach to determine the regions in the FXR-LBD that experience conformational changes induced by ligand binding. Fig. 3.3 compiles heat map presentations of the deuterium uptake for each of three ligand-bound forms of the FXR-LBD. In

the heatmaps, regions that show high levels of deuterium incorporation are colored red and regions that showed low levels of deuterium incorporation are colored blue. The comparative presentations of the heatmaps of the deuterium incorporation levels observed for the FXR-LBD in presence of the different ligands allowed us to visualize regions that show disparate deuterium level characteristics dependent on the ligand present. The most pronounced ligand-dependent differences in deuterium uptake were observed for the following peptides: 288-298, 320-328, 328-336, 348-360, 361-367, and 368-375.

To further evaluate how the interactions of the ligands affect the conformational properties of the FXR LBD we evaluated the deuterium incorporation dynamics at the peptide level by applying a six-fixed-rate-constant binning model as described in the method section. The results of the fits for each peptide exchange-in curve are compiled in Table S3.2. The curve fitting plots for the peptide that displayed disparate exchange-in levels dependent on the ligand present are depicted in Figure 4A. In Figure 4B we used the X-ray structure of GW4064-bound FXR LBD to visualize that the peptide that showed the ligand-dependent exchange-in characteristics, i.e. peptides encompassing the partial sequences 288-298, 320-328, 328-326, 348-360, 361-367, and 368-375, are partaking in forming the LBC in the FXR LBD. For instance, the peptide 288-298 with 10 exchangeable amide hydrogens displayed the highest retardation against exchange-in in each protein-ligand system studied. The applied binning model revealed that this peptide has 4, 2, and 4 exchangeable sites in the apo FXR-LBD conforming to category I (fast exchanging sites,  $k = 10$  or  $1 \text{ min}^{-1}$ ), category II (medium exchanging sites,  $k = 0.1$  or  $0.01 \text{ min}^{-1}$ ), and category III (slow exchanging sites,  $k = 0.001$  or  $0.0001 \text{ min}^{-1}$ ), respectively. In presence of the ligand the distribution of the amide hydrogens conforming to the category II and category III increased. For GW4064 the deuterium

incorporation profiles showed that the exchanging sites in category I were reduced to 1, whereas 3 and 6 sites conformed to category II and III, respectively. For the low affinity ligand CDCA the distribution of exchanging sites conforming to category I, II and III was 3, 2, and 5, respectively. For GG, the binning modeling resulted in 3, 1 and 6 sites that met the requirements for the exchange characteristics grouped under category I, II and III, respectively. Similar changes in the distribution of sites within each category dependent on the ligand present were observed for the other LBC peptides as well: the number of sites that conform to category I decreased while the number of sites in category II and III increased upon ligand interaction. The retardation of the exchange-in dynamics of these six peptides is consistent with that ligand interactions stabilize the LBC and reduces the dynamical flexibility of the regions that are involved in forming the LBC compared to the respective regions in the apo FXR-LBD. The disparate exchange-in behavior observed for these six peptides also suggests that despite that the ligands studied have different chemotypes all seem to interact and stabilize the same region of the FXR-LBD but each ligand interaction causes a ligand-specific modulation of the conformational properties of the regions forming the cavity.

Differential HDX-MS analysis was used to spatially resolve the impact of the diverse chemotypes on the conformational dynamics of the FXR-LBD. The average differences in percentage of deuterium exchange-in for the three ligand-bound FXR complexes relative to the apo-protein were computed. Peptides showing statistically significant differential deuterium level ( $p < 0.001$ ) were colored and overlaid on the X-ray crystal structure of the FXR-LBD bound to GW4064 and 6-ECDCA, respectively (Fig. 3.5, data compiled in Table S3.1). Comparison of the HDX-MS results for the GW4064-bound protein with the crystallographic data of the FXR-LBD-GW4064 complex (PDB ID 3DCT) revealed that regions containing the contact residues

and forming the LBC displayed reduced HDX rates, which included the peptides representing the helices H3 (288-298), H4-H5 (320-328), H5 (328-326), H6 (348-360), and H7 (361-367 and 368-375). As observed in the active conformation of the FXR-LBD GW4064 complex, the carboxylic acid group of GW4064 forms a hydrogen bond with Arg-331 (helix 5), while the stilbenoid moiety interacts with Leu-287 (helix 3), Met-290 (helix 3), Met-328 (helix 5), Ile-335 (helix 5), and Leu-348 (helix 6), and the dichlorophenyl group occupies a hydrophobic core formed by residues Phe-329 (helix 5), Ile-352 (helix 6), Ile-357 (helix 6), Met-365 (helix 7), and Tyr-369 (helix 7) [18]. The hydrogen bonding and hydrophobic interaction network between GW4064 and the LBC of the FXR-LBD resulted in significant exchange protection in these regions. Remarkably, the peptides 299-316 (helix 3-loop-helix 4), 388-405 (helix 9), 406-412 (helix 9) and 434-440 (helix 10), which all encompass regions not involved in GW4064 binding, exhibited reduced exchange-in rates as well. No changes in exchange-in kinetics upon GW4064 binding were observed for the peptides 256-268 (helix 1-helix 2), 269-278 (helix 2), 337-347 (helix 5-helix 6) and 454-465 (helix 11-helix 12).

To rationalize our current HDX MS data on CDCA binding to FXR in solution we used the crystal structure of FXR-LBD bound to a close synthetic high affinity analog of CDCA, 6-ethylchenodeoxycholic acid (6ECDCA) (PDB ID 1OSV) [13]. We hypothesized that both steroidal ligands may share similar binding sites within the FXR-LBD, except for those hydrophobic interactions between the 6ECDCA 6 $\alpha$ -ethyl group and residues Ile-362 (helix 7), Phe-366 (helix 7) and Tyr-369 (helix 7), which collectively contribute to the much higher affinity of 6ECDCA ( $EC_{50}$  99 nM) [46] compared to CDCA ( $EC_{50}$  10  $\mu$ M) [30]. Peptides encompassing the contact residues, including partial sequences 288-298 (helix 3), 320-328 (helix 4-helix 5), 328-336 (helix 5), 348-360 (helix 6) and 361-367 (helix 7), showed reduced levels of

exchange-in compared to the corresponding peptides derived from the apo-protein (Fig. 5). Regions remote from the LBC, such as residues 256-268 (helix 1-helix 2), 406-412 (helix 9), and 434-440 (helix 10), exhibited only slight protection against deuterium exchange-in (Fig. 3.5).

GG is a low affinity in vitro antagonist of FXR [47] and the co-incubation of GG and FXR-LBD resulted in HDX data that indicated exchange-in protection in regions encompassing the LBC (Fig. 3.4) suggesting that the interaction sites of GG coincide with the recognition sites of typical FXR agonists. The most intriguing feature of this HDX dataset is however one region that exhibited slightly higher extent of protection in presence of GG compared to the other two agonists probed. This region is the most N-terminal region of FXR-LBD, corresponding to the partial sequence 201-278 encompassing helix 1 - loop - helix 2 (256-268). In addition, the region 388-396 was also found as being protected against exchange-in in presence of GG. Interestingly, these two protected regions coincide with a noncanonical binding site that was predicted by docking studies by Meyer et al [48]. In their model, GG's noncanonical interaction involves Tyr-260 (helix 1), the partial sequence Lys-262 to Met-265 (helix 1 - helix 2 loop), Thr-386 (helix 8) and Ile-390 (helix 8) [48].

### 3.5 Discussion

We conducted a comparative HDX-MS study of the FXR-LBD in presence of structurally diverse ligands to advance our understanding of the conformational requirements that are potentially relevant to the molecular mechanisms that culminate in the regulation of the FXR activity. We initially conducted HDX-MS studies of the FXR-LBD in presence of the known high affinity non-steroid agonist GW4064. We evaluated our HDX-MS peptide level data using the B-factors associated with the crystal structure of the GW4064-bound FXR LBD (PDB ID 3DCT) (Fig. S3.10). Structurally flexible regions with high B-factors showed high average

deuterium levels. Regions that showed low average deuterium levels aligned well with regions that have low B-factors ( $< 40$ ), and these regions coincided with ligand binding recognition sites. For four FXR-LBD peptides, namely 299-316 (helix 3 – loop - helix 4), 397-405 (helix 9), 406-412 (helix 9) and 434-440 (helix 10), deuterium levels were observed that were much lower in GW4064-bound protein compared to the apo protein (Figures S3.9 and S3.10) and, interestingly, these regions did not contain ligand interaction sites in the crystal structure of GW4064-bound FXR LBD. The extent of protection observed for these regions suggested that ligand binding resulted in reduced solvent accessibility of the backbone amide hydrogens and/or had a stabilizing effect on the conformational dynamics of these regions distant from the GW4064-binding cavity (purple colored regions in Figure 3.5D).

A comparison of the HDX-MS datasets obtained for the FXR-LBD in the presence of GW4064 and CDCA, respectively, highlights differences in the impact of the chemotype on the conformational dynamics between the synthetic stilben-like agonist GW4064 and the bile acid CDCA (Fig. 3.6C). The most striking differences in protection between these two ligands were detected for the regions encompassing the helices 3 and 5, both of which are part of the LBC. In addition, disparate response to ligand binding was detected for regions distant to the LBC, namely for regions encompassing helix 9 and helix 10; both showed more extensive exchange-in protection for the GW4064-bound state. We may further speculate that the observed differences in HDX kinetics for the FXR-LBD in presence of a stilben- and a steroid-based agonist, respectively, may reflect distinct conformational states that may translate to the ligand-specific recruitment of coregulator proteins and expression of FXR-target genes. Distinct gene expression profiles have been reported for GW4064 and CDCA [23].

Next, we evaluated the HDX profile obtained for the interaction of FXR-LBD with CDCA. Initially, we used the crystal structure of 6ECDCA-bound FXR-LBD as a template (Fig. 3.5). This allowed us to study the impact of a low affinity ligand interaction on the conformational properties of the FXR-LBD. Compared to the high affinity interaction with GW4064, the amide hydrogen exchange protection was generally less pronounced. The interaction of CDCA with the LBD was evident by the reduced deuterium incorporation levels that were observed for the peptides 288-298, 320-336, 348-375 indicating stabilization of these regions. Mapping onto the 6ECDCA-bound FXR-LBD structure these stabilized regions marked the cognate binding cavity and included helix 3, the small transition segment helix 4-helix 5 and the regions encompassing the helices 5, 6 and 7.

GG was originally identified as a FXR antagonist *in vitro* [47], but later was classified as a selective bile acid receptor modulator (SBARM) based on the following findings: (1) GG inhibited activation of FXR-LBD *in vitro*, but only in presence of CDCA in a dose-dependent manner [45]; and (2) GG acted to enhance transcription of the bile salt export pump (BSEP) in a dose-dependent manner *in vivo* [47]. Although GG has a steroidal scaffold, it has an *all trans* and quasi planar ABCD ring system in contrast to bile acids in which ring A and B are conjugated in a *cis* configuration [48]. In the absence of a co-crystal structure of FXR-LBD in complex with GG, the current HDX-MS results advance our understanding of the molecular determinants that govern the interaction of GG with the FXR-LBD. The differential HDX-MS profiles presented in Fig. 3.6A and B reveal that the N-terminal regions of the FXR-LBD (residues 201-278) showed slightly higher protection against exchange-in in the GG-bound state compared to conformational states induced by the two agonists studied. Interestingly, recent molecular modeling studies have predicted a novel noncanonical binding site for GG near the loop region



located between helix 1 and helix 2 [48] with Gln267 playing a key role in binding of the unusual second coactivator peptide which is visible in the 6ECDCA-bound FXR-LBD crystal structure (PDB ID 1OSV). The observed protection against exchange-in in the N-terminal region in presence of GG is consistent with the prediction of a non-canonical ligand binding site in that region of the LBD [48]. The C-terminal fraction of helix 8 and part of the helix 8 - helix 9 loop, corresponding to the partial sequence 388-396, exhibited protection upon binding of GG (Fig. 3.5). As such, the HDX-MS data is in accord to the docking study of GG with the FXR-LBD that predicted that helix 8 is involved in the stabilization of GG and flanks the non-canonical GG binding site.

Helix 12 is a highly conserved feature in ligand-activated nuclear receptors and acts as a molecular switch to activate or repress receptor functions upon binding of appropriate ligands [49]. Therefore we expected to observe difference in HDX kinetics between the apoprotein and the agonist-bound LBD. However, the HDX-MS data obtained for the C-terminal fraction of the LBD (peptides 440-451 and 454-465) showed only minimal differences in deuterium incorporation levels for the apo protein and the holo systems studied. The lack of disparity in the HDX-MS data for the sequence encompassing the C-terminal fraction of the FXR-LBD upon ligand binding was surprising because a molecular dynamics simulation predicted that the C-terminal region of the protein should experience a gain in conformational motility upon removal of 6ECDCA [50]. The current observation is however consistent with previous HDX-MS studies of some nuclear receptor LBDs. For instance, a lack of change in HDX kinetics of helix 12 upon ligand binding was also observed for the human apo RXR $\alpha$  LBD [25, 51] and for both isoforms of the ER LBD, the ER $\alpha$  and ER $\beta$  protein [26]. For other nuclear receptor, including PPAR $\gamma$ , THR, and GR, higher solvent protections was observed for the helices helix 11 and helix 12 with

agonists relative to antagonists [24, 52, 53]. Griffin et al. observed that the helices 11 and 12 of the VDR LBD showed less solvent exposure with agonists compared to the apo VDR-LBD [27]. In view of these diverse observations we propose that binding of a coactivator peptide may govern the exchange properties of helix 12. This hypothesis is based on previous findings that showed that inclusion of a coactivator peptide resulted in a decrease of deuterium uptake for the RXR $\alpha$  helix 12 and GR helix 12 in the presence or absence of different ligands [53, 54].

### 3.6 Conclusion

The current work demonstrates that HDX experiments in conjunction with mass spectrometry are capable of providing structural dynamics information for studying FXR ligand interactions. The observed differences in HDX kinetics reflect on the disparate modes of conformational modulation elicited by ligands endowed with structurally distinct scaffolds. The protection against deuterium uptake observed for the partial sequences 201-278 and 388-396, which cover the H1-H2 loop and parts of helix H8 including the H8-H9 loop, respectively, supports a model in which *in vitro* antagonism and modulation of FXR by GG may indeed involve a noncanonical binding site as predicted previously by Meyer et al [48].

## Acknowledgement

This research was supported in part by Grants S10RR025628 and P30ES000210 from the National Institutes of Health.

## Supporting Data

Supplementary data to this article can be found online and includes: SDS-PAGE image and ESI-MS spectrum of the purified hFXR-LBD (Fig. S3.1); plot depicting the binding curve of GG (Z) to FXR-LBD (Fig. S3.2); nanoAcquity UPLC setup with switching valve to divert buffer constituents and CHAPS to waste (Fig. S3.3); peptide coverage map (Fig. S3.4); HDX mass spectra of each peptide (Fig. S3.5); kinetic plots (deuterium level as a function of labeling time) for each peptide for all four systems studied (Fig. S3.6); compilation of the HDX-MS data for the apo protein (Fig. S3.7); compiled deuterium level profiles for the FXR-LBD in presence of GW4064, CDCA and GG(Z) (Fig. S3.8); ligand-dependent deuterium exchange protection plots (Fig. S3.9); plot depicting the overlay of the B-values extracted from the crystal structure of FXR with GW4064 bound (PDB ID 3DCT) with the deuterium levels of each peptide observed in the presence of GW4064 (Fig. S3.10); tabular compilation of the HDX data used for the differential HDX analyses (Table S3.1); tabular compilation of the kinetic results derived by our kinetic model (Table S3.2).

### 3.7 References

- [1] B. Goodwin, S.A. Jones, R.R. Price, M.A. Watson, D.D. McKee, L.B. Moore, C. Galardi, J.G. Wilson, M.C. Lewis, M.E. Roth, P.R. Maloney, T.M. Willson, S.A. Kliewer, A regulatory cascade of the nuclear receptors FXR, SHP-1, and LRH-1 represses bile acid biosynthesis, *Mol Cell*, 6 (2000) 517-526.
- [2] K. Ma, P.K. Saha, L. Chan, D.D. Moore, Farnesoid X receptor is essential for normal glucose homeostasis, *J Clin Invest*, 116 (2006) 1102-1109.
- [3] S. Fiorucci, G. Rizzo, A. Donini, E. Distrutti, L. Santucci, Targeting farnesoid X receptor for liver and metabolic disorders, *Trends Mol Med*, 13 (2007) 298-309.
- [4] C. Soldani, M.G. Bottone, C. Pellicciari, A.I. Scovassi, Nucleolus disassembly in mitosis and apoptosis: dynamic redistribution of phosphorylated-c-Myc, fibrillarin and Ki-67, *Eur J Histochem*, 50 (2006) 273-280.
- [5] S. Westin, R.A. Heyman, R. Martin, FXR, a therapeutic target for bile acid and lipid disorders, *Mini Rev Med Chem*, 5 (2005) 719-727.
- [6] A. Lanzini, M.G. De Taronatti, B. Panarotto, S. Scalia, A. Mora, F. Benini, O. Baisini, F. Lanzarotto, Intestinal absorption of the bile acid analogue Se-75-homocholic acid-taurine is increased in primary biliary cirrhosis, and reverts to normal during ursodeoxycholic acid administration, *Gut*, 52 (2003) 1371-1375.
- [7] C.J. Sinal, M. Tohkin, M. Miyata, J.M. Ward, G. Lambert, F.J. Gonzalez, Targeted disruption of the nuclear receptor FXR/BAR impairs bile acid and lipid homeostasis, *Cell*, 102 (2000) 731-744.
- [8] G.L. Guo, S. Santamarina-Fojo, T.E. Akiyama, M.J.A. Amar, B.J. Paigen, B. Brewer, F.J. Gonzalez, Effects of FXR in foam-cell formation and atherosclerosis development, *Bba-Mol Cell Biol L*, 1761 (2006) 1401-1409.
- [9] E.A. Hanniman, G. Lambert, T.C. McCarthy, C.J. Sinal, Loss of functional farnesoid X receptor increases atherosclerotic lesions in apolipoprotein E-deficient mice, *Journal of Lipid Research*, 46 (2005) 2595-2604.
- [10] Y.Q. Zhang, X.P. Wang, C. Vales, F.Y. Lee, H. Lee, A.J. Lusis, P.A. Edwards, FXR deficiency causes reduced atherosclerosis in *Ldlr*(-/-) mice, *Arterioscl Throm Vas*, 26 (2006) 2316-2321.
- [11] G. Paumgartner, U. Beuers, Ursodeoxycholic acid in cholestatic liver disease: mechanisms of action and therapeutic use revisited, *Hepatology*, 36 (2002) 525-531.
- [12] S.M. Soisson, G. Parthasarathy, A.D. Adams, S. Sahoo, A. Sitlani, C. Sparrow, J. Cui, J.W. Becker, Identification of a potent synthetic FXR agonist with an unexpected mode of binding and activation, *Proc Natl Acad Sci U S A*, 105 (2008) 5337-5342.

- [13] L.Z. Mi, S. Devarakonda, J.M. Harp, Q. Han, R. Pellicciari, T.M. Willson, S. Khorasanizadeh, F. Rastinejad, Structural basis for bile acid binding and activation of the nuclear receptor FXR, *Mol Cell*, 11 (2003) 1093-1100.
- [14] A. Akwabi-Ameyaw, J.A. Caravella, L.H. Chen, K.L. Creech, D.N. Deaton, K.P. Madauss, H.B. Marr, A.B. Miller, F. Navas, D.J. Parks, P.K. Spearing, D. Todd, S.P. Williams, B. Wisely, Conformationally constrained farnesoid X receptor (FXR) agonists: Alternative replacements of the stilbene, *Bioorganic & Medicinal Chemistry Letters*, 21 (2011) 6154-6160.
- [15] J.Y. Bass, J.A. Caravella, L.H. Chen, K.L. Creech, D.N. Deaton, K.P. Madauss, H.B. Marr, R.B. McFadyen, A.B. Miller, W.Y. Mills, F. Navas, D.J. Parks, T.L. Smalley, P.K. Spearing, D. Todd, S.P. Williams, G.B. Wisely, Conformationally constrained farnesoid X receptor (FXR) agonists: Heteroaryl replacements of the naphthalene, *Bioorganic & Medicinal Chemistry Letters*, 21 (2011) 1206-1213.
- [16] A. Akwabi-Ameyaw, J.Y. Bass, R.D. Caldwell, J.A. Caravella, L.H. Chen, K.L. Creech, D.N. Deaton, K.P. Madauss, H.B. Marr, R.B. McFadyen, A.B. Miller, F. Navas, D.J. Parks, P.K. Spearing, D. Todd, S.P. Williams, G.B. Wisely, FXR agonist activity of conformationally constrained analogs of GW 4064, *Bioorganic & Medicinal Chemistry Letters*, 19 (2009) 4733-4739.
- [17] J.Y. Bass, R.D. Caldwell, J.A. Caravella, L.H. Chen, K.L. Creech, D.N. Deaton, K.P. Madauss, H.B. Marr, R.B. McFadyen, A.B. Miller, D.J. Parks, D. Todd, S.P. Williams, G.B. Wisely, Substituted isoxazole analogs of farnesoid X receptor (FXR) agonist GW4064, *Bioorganic & Medicinal Chemistry Letters*, 19 (2009) 2969-2973.
- [18] A. Akwabi-Ameyaw, J.Y. Bass, R.D. Caldwell, J.A. Caravella, L. Chen, K.L. Creech, D.N. Deaton, S.A. Jones, I. Kaldor, Y. Liu, K.P. Madauss, H.B. Marr, R.B. McFadyen, A.B. Miller, F.N. Iii, D.J. Parks, P.K. Spearing, D. Todd, S.P. Williams, G.B. Wisely, Conformationally constrained farnesoid X receptor (FXR) agonists: Naphthoic acid-based analogs of GW 4064, *Bioorg Med Chem Lett*, 18 (2008) 4339-4343.
- [19] H.G.F. Richter, G.M. Benson, D. Blum, E. Chaput, S. Feng, C. Gardes, U. Grether, P. Hartman, B. Kuhn, R.E. Martin, J.M. Plancher, M.G. Rudolph, F. Schuler, S. Taylor, K.H. Bleicher, Discovery of novel and orally active FXR agonists for the potential treatment of dyslipidemia & diabetes, *Bioorganic & Medicinal Chemistry Letters*, 21 (2011) 191-194.
- [20] H.G.F. Richter, G.M. Benson, K.H. Bleicher, D. Blum, E. Chaput, N. Clemann, S. Feng, C. Gardes, U. Grether, P. Hartman, B. Kuhn, R.E. Martin, J.M. Plancher, M.G. Rudolph, F. Schuler, S. Taylor, Optimization of a novel class of benzimidazole-based farnesoid X receptor (FXR) agonists to improve physicochemical and ADME properties, *Bioorganic & Medicinal Chemistry Letters*, 21 (2011) 1134-1140.
- [21] B. Flatt, R. Martin, T.L. Wang, P. Mahaney, B. Murphy, X.H. Gu, P. Foster, J.L. Li, P. Pircher, M. Petrowski, I. Schulman, S. Westin, J. Wrobel, G. Yan, E. Bischoff, C. Daige, R. Mohan, Discovery of XL335 (WAY-362450), a Highly Potent, Selective, and Orally Active Agonist of the Farnesoid X Receptor (FXR), *Journal of Medicinal Chemistry*, 52 (2009) 904-907.

- [22] J.T. Lundquist, D.C. Harnish, C.Y. Kim, J.F. Mehlmann, R.J. Unwalla, K.M. Phipps, M.L. Crawley, T. Commons, D.M. Green, W.X. Xu, W.T. Hum, J.E. Eta, I. Feingold, V. Patel, M.J. Evans, K. Lai, L. Borges-Marcucci, P.E. Mahaney, J.E. Wrobel, Improvement of Physiochemical Properties of the Tetrahydroazepinoindole Series of Farnesoid X Receptor (FXR) Agonists: Beneficial Modulation of Lipids in Primates, *Journal of Medicinal Chemistry*, 53 (2010) 1774-1787.
- [23] M. Downes, M.A. Verdecia, A.J. Roecker, R. Hughes, J.B. Hogenesch, H.R. Kast-Woelbern, M.E. Bowman, J.L. Ferrer, A.M. Anisfeld, P.A. Edwards, J.M. Rosenfeld, J.G. Alvarez, J.P. Noel, K.C. Nicolaou, R.M. Evans, A chemical, genetic, and structural analysis of the nuclear bile acid receptor FXR, *Mol Cell*, 11 (2003) 1079-1092.
- [24] Y. Hamuro, S.J. Coales, J.A. Morrow, K.S. Molnar, S.J. Tuske, M.R. Southern, P.R. Griffin, Hydrogen/deuterium-exchange (H/D-Ex) of PPARgamma LBD in the presence of various modulators, *Protein Sci*, 15 (2006) 1883-1892.
- [25] X. Yan, M.L. Deinzer, M.I. Schimerlik, D. Broderick, M.E. Leid, M.I. Dawson, Investigation of ligand interactions with human RXRalpha by hydrogen/deuterium exchange and mass spectrometry, *J Am Soc Mass Spectrom*, 17 (2006) 1510-1517.
- [26] S.Y. Dai, T.P. Burris, J.A. Dodge, C. Montrose-Rafizadeh, Y. Wang, B.D. Pascal, M.J. Chalmers, P.R. Griffin, Unique ligand binding patterns between estrogen receptor alpha and beta revealed by hydrogen-deuterium exchange, *Biochemistry*, 48 (2009) 9668-9676.
- [27] J. Zhang, M.J. Chalmers, K.R. Stayrook, L.L. Burris, R.D. Garcia-Ordenez, B.D. Pascal, T.P. Burris, J.A. Dodge, P.R. Griffin, Hydrogen/deuterium exchange reveals distinct agonist/partial agonist receptor dynamics within vitamin D receptor/retinoid X receptor heterodimer, *Structure*, 18 (2010) 1332-1341.
- [28] T.P. Burris, C. Montrose, K.A. Houck, H.E. Osborne, W.P. Bocchinfuso, B.C. Yaden, C.C. Cheng, R.W. Zink, R.J. Barr, C.D. Hepler, V. Krishnan, H.A. Bullock, L.L. Burris, R.J. Galvin, K. Bramlett, K.R. Stayrook, The hypolipidemic natural product guggulsterone is a promiscuous steroid receptor ligand, *Molecular Pharmacology*, 67 (2005) 948-954.
- [29] A.V. Hill, The Combinations of Haemoglobin with Oxygen and with Carbon Monoxide. I, *Biochem J*, 7 (1913) 471-480.
- [30] R. Pellicciari, S. Fiorucci, E. Camaioni, C. Clerici, G. Costantino, P.R. Maloney, A. Morelli, D.J. Parks, T.M. Willson, 6alpha-ethyl-chenodeoxycholic acid (6-ECDCA), a potent and selective FXR agonist endowed with anticholestatic activity, *J Med Chem*, 45 (2002) 3569-3572.
- [31] J.L. Lew, A. Zhao, J. Yu, L. Huang, N. De Pedro, F. Pelaez, S.D. Wright, J. Cui, The farnesoid X receptor controls gene expression in a ligand- and promoter-selective fashion, *J Biol Chem*, 279 (2004) 8856-8861.
- [32] M.D. Shortridge, D.S. Hage, G.S. Harbison, R. Powers, Estimating protein-ligand binding affinity using high-throughput screening by NMR, *J Comb Chem*, 10 (2008) 948-958.

- [33] T.E. Wales, J.R. Engen, Hydrogen exchange mass spectrometry for the analysis of protein dynamics, *Mass Spectrom Rev*, 25 (2006) 158-170.
- [34] J.B. Sperry, R.Y. Huang, M.M. Zhu, D.L. Rempel, M.L. Gross, Hydrophobic Peptides Affect Binding of Calmodulin and Ca as Explored by H/D Amide Exchange and Mass Spectrometry, *Int J Mass Spectrom*, 302 (2011) 85-92.
- [35] R.Y. Huang, D.L. Rempel, M.L. Gross, HD exchange and PLIMSTEX determine the affinities and order of binding of Ca<sup>2+</sup> with troponin C, *Biochemistry*, 50 (2011) 5426-5435.
- [36] R.Y. Huang, J. Wen, R.E. Blankenship, M.L. Gross, Hydrogen-deuterium exchange mass spectrometry reveals the interaction of Fenna-Matthews-Olson protein and chlorosome CsmA protein, *Biochemistry*, 51 (2012) 187-193.
- [37] C.H. Parker, C.R. Morgan, K.D. Rand, J.R. Engen, J.W. Jorgenson, D.W. Stafford, A Conformational Investigation of Propeptide Binding to the Integral Membrane Protein gamma-Glutamyl Carboxylase Using Nanodisc Hydrogen Exchange Mass Spectrometry, *Biochemistry*, 53 (2014) 1511-1520.
- [38] Z. Zhang, D.L. Smith, Determination of amide hydrogen exchange by mass spectrometry: a new tool for protein structure elucidation, *Protein Sci*, 2 (1993) 522-531.
- [39] D.D. Weis, J.R. Engen, I.J. Kass, Semi-automated data processing of hydrogen exchange mass spectra using HX-Express, *J Am Soc Mass Spectrom*, 17 (2006) 1700-1703.
- [40] R.S. Plumb, K.A. Johnson, P. Rainville, B.W. Smith, I.D. Wilson, J.M. Castro-Perez, J.K. Nicholson, UPLC/MSE; a new approach for generating molecular fragment information for biomarker structure elucidation (vol 20, pg 1989, 2006), *Rapid Commun Mass Sp*, 20 (2006) 2234-2234.
- [41] S.W. Englander, N.R. Kallenbach, Hydrogen exchange and structural dynamics of proteins and nucleic acids, *Q Rev Biophys*, 16 (1983) 521-655.
- [42] X. Yan, H. Zhang, J. Watson, M.I. Schimerlik, M.L. Deinzer, Hydrogen/deuterium exchange and mass spectrometric analysis of a protein containing multiple disulfide bonds: Solution structure of recombinant macrophage colony stimulating factor-beta (rhM-CSFbeta), *Protein Sci*, 11 (2002) 2113-2124.
- [43] Z. Zhang, C.B. Post, D.L. Smith, Amide hydrogen exchange determined by mass spectrometry: application to rabbit muscle aldolase, *Biochemistry*, 35 (1996) 779-791.
- [44] K.C. Han, J.H. Kim, K.H. Kim, E.E. Kim, J.H. Seo, E.G. Yang, Identification of farnesoid X receptor modulators by a fluorescence polarization-based interaction assay, *Anal Biochem*, 398 (2010) 185-190.
- [45] N.L. Urizar, A.B. Liverman, D.T. Dodds, F.V. Silva, P. Ordentlich, Y. Yan, F.J. Gonzalez, R.A. Heyman, D.J. Mangelsdorf, D.D. Moore, A natural product that lowers cholesterol as an antagonist ligand for FXR, *Science*, 296 (2002) 1703-1706.

- [46] M. Makishima, A.Y. Okamoto, J.J. Repa, H. Tu, R.M. Learned, A. Luk, M.V. Hull, K.D. Lustig, D.J. Mangelsdorf, B. Shan, Identification of a nuclear receptor for bile acids, *Science*, 284 (1999) 1362-1365.
- [47] J. Cui, L. Huang, A. Zhao, J.L. Lew, J. Yu, S. Sahoo, P.T. Meinke, I. Royo, F. Pelaez, S.D. Wright, Guggulsterone is a farnesoid X receptor antagonist in coactivator association assays but acts to enhance transcription of bile salt export pump, *J Biol Chem*, 278 (2003) 10214-10220.
- [48] U. Meyer, G. Costantino, A. Macchiarulo, R. Pellicciari, Is antagonism of E/Z-guggulsterone at the farnesoid X receptor mediated by a noncanonical binding site? A molecular modeling study, *J Med Chem*, 48 (2005) 6948-6955.
- [49] N. Novac, T. Heinzel, Nuclear receptors: overview and classification, *Curr Drug Targets Inflamm Allergy*, 3 (2004) 335-346.
- [50] G. Costantino, A. Entrena-Guadix, A. Macchiarulo, A. Gioiello, R. Pellicciari, Molecular dynamics simulation of the ligand binding domain of farnesoid X receptor. Insights into helix-12 stability and coactivator peptide stabilization in response to agonist binding, *J Med Chem*, 48 (2005) 3251-3259.
- [51] X. Yan, E. Perez, M. Leid, M.I. Schimerlik, A.R. de Lera, M.L. Deinzer, Deuterium exchange and mass spectrometry reveal the interaction differences of two synthetic modulators of RXRalpha LBD, *Protein Sci*, 16 (2007) 2491-2501.
- [52] A.C. Figueira, D.M. Saidenberg, P.C. Souza, L. Martinez, T.S. Scanlan, J.D. Baxter, M.S. Skaf, M.S. Palma, P. Webb, I. Polikarpov, Analysis of agonist and antagonist effects on thyroid hormone receptor conformation by hydrogen/deuterium exchange, *Mol Endocrinol*, 25 (2011) 15-31.
- [53] L. Frego, W. Davidson, Conformational changes of the glucocorticoid receptor ligand binding domain induced by ligand and cofactor binding, and the location of cofactor binding sites determined by hydrogen/deuterium exchange mass spectrometry, *Protein Sci*, 15 (2006) 722-730.
- [54] G. Xia, L.J. Boerma, B.D. Cox, C. Qiu, S. Kang, C.D. Smith, M.B. Renfrow, D.D. Muccio, Structure, Energetics, and Dynamics of Binding Coactivator Peptide to the Human Retinoid X Receptor alpha Ligand Binding Domain Complex with 9-cis-Retinoic Acid, *Biochemistry*, (2010).



## Figure Legends

**Figure 3.1** Fluorescence spectra of FXR-LBD with structures of the ligands used in the current study: GW4064, CDCA, and GG (Z)

**Figure 3.2** Deuterium levels observed for the FXR-LBD with and without ligands after the following incubation periods: 0.5, 1, 2, 5, 10, 30, 60min.

**Figure 3.3** Comparative presentation of the HDX heat maps of FXR-LBD in the presence of ligands. Each horizontal color block represents an analyzed peptic peptide, and each block contains seven time points (from top: 0.5, 1, 2, 5, 10, 30, 60 min).

**Figure 3.4** Exchange-in plots of peptides that showed disparate exchange-in characteristics. (A) Exchange-in kinetics: apo-FXR-LBD, red line; GW4064, blue line; CDCA, green line; GG, yellow line. (B) X-ray structure of FXR-LBD (green) bound to GW4064 (orange) (PDB ID 3DCT); peptides that showed disparate exchange-in characteristics in presence of the diverse ligands are colored blue.

**Figure 3.5** Average differences in deuterium levels (in %) of FXR-LBD with or without ligand overlaid onto crystallographic structures. The N-terminal region which is covered by the peptides 201-222 and 229-241 is not visible in the crystal structures.

Top row: Co-crystal structure of FXR-LBD ligand complex, PDB ID 3DCT for (A) and PDB ID 1OSV for (B) and (C). Contact residues between ligand and protein are colored in pink. The ligand itself is colored in orange.

Bottom row: Average differences in deuterium levels (D%) of seven time points (0.5, 1, 2, 5, 10, 30, and 60 min) are mapped onto the crystal structure of FXR-LBD-ligand complex, PDB ID 3DCT for (D) and PDB ID 1OSV for (E) and (F). Regions that were not covered by the current experiments are depicted in grey. NS, “not significant”.

**Figure 3.6** Differential HDX data of FXR-LBD-agonist and FXR-LBD-antagonist.

Left: Deuterium level differences in percentage (D %) from one complex to another are shown at different time points (0.5, 1, 2, 5, 10, 30, and 60 min, from left to right) for each peptide.

Right: Average differences in deuterium percentage (D %) of seven time points (0.5, 1, 2, 5, 10, 30, and 60 min) were overlaid onto the crystallographic structure, PDB ID 3DCT for (A) and (B), PDB ID 1OSV for (C). Positive numbers indicate higher deuterium levels and thus less protection in the FXR-LBD-GG relative to the FXR-LBD-GW4064. Negative numbers indicate lower deuterium levels and thus more protection in the FXR-LBD-GG relative to the FXR-LBD-GW4064.

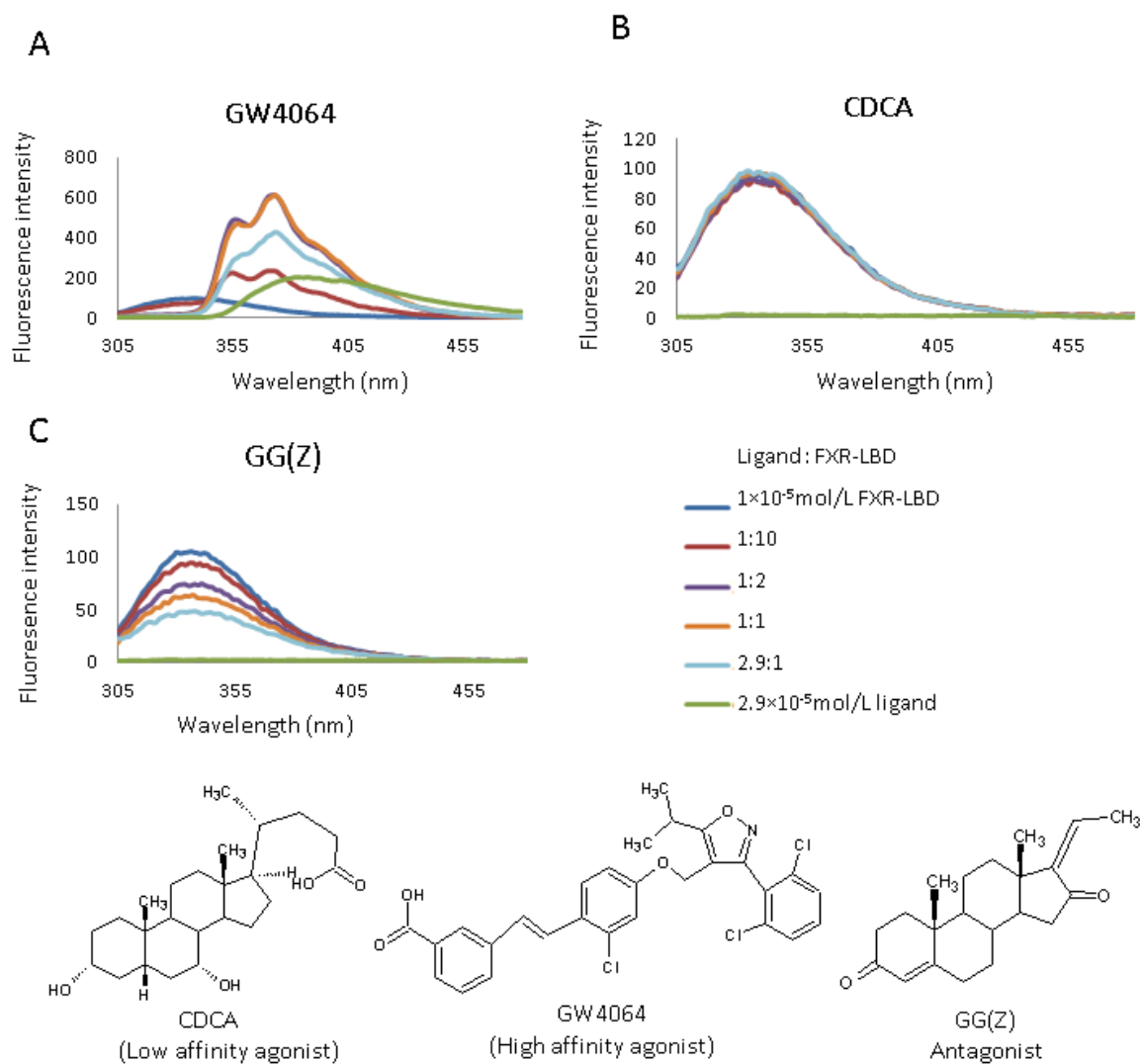
**Figure 3.1**

Figure 3.1 Fluorescence spectra of FXR-LBD with structures of the ligands used in the current study: GW4064, CDCA, and GG (Z)

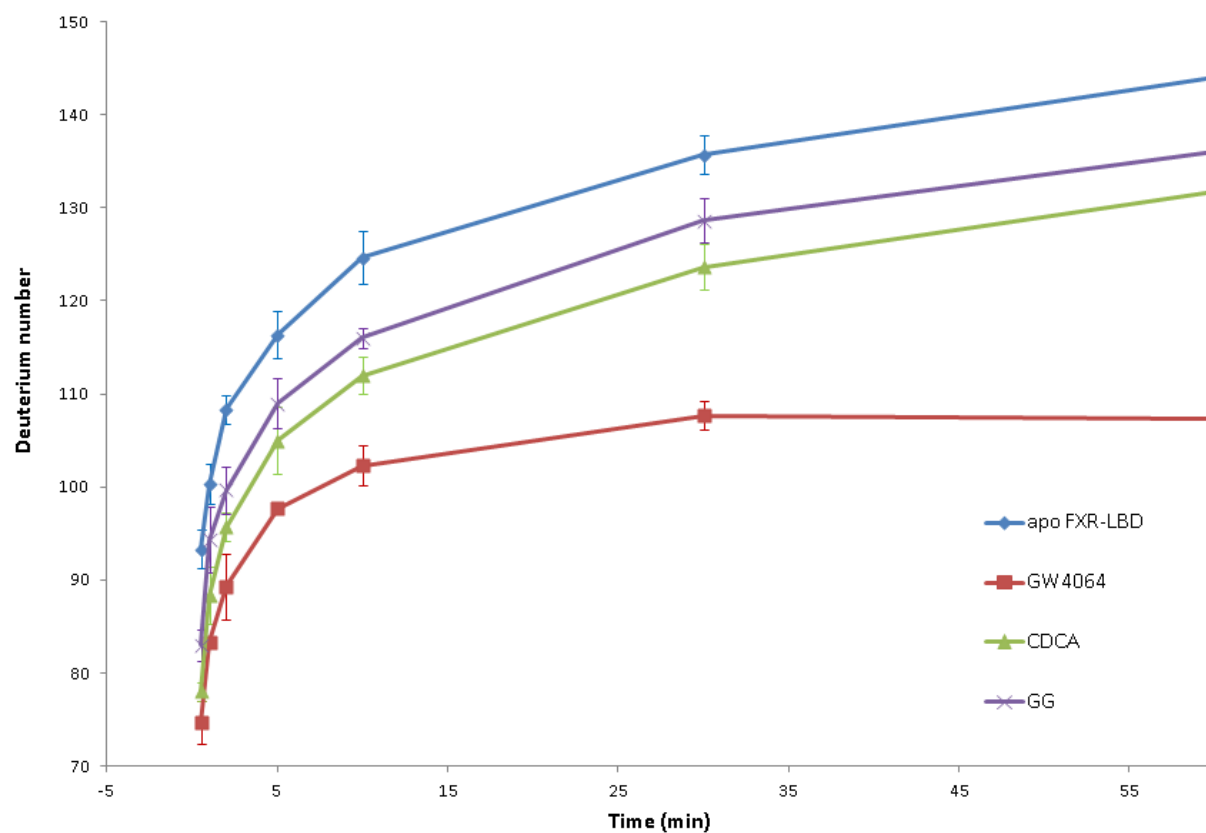
**Figure 3.2**

Figure 3.2 Deuterium levels observed for the FXR-LBD with and without ligands after the following incubation periods: 0.5, 1, 2, 5, 10, 30, 60min

Figure 3.3

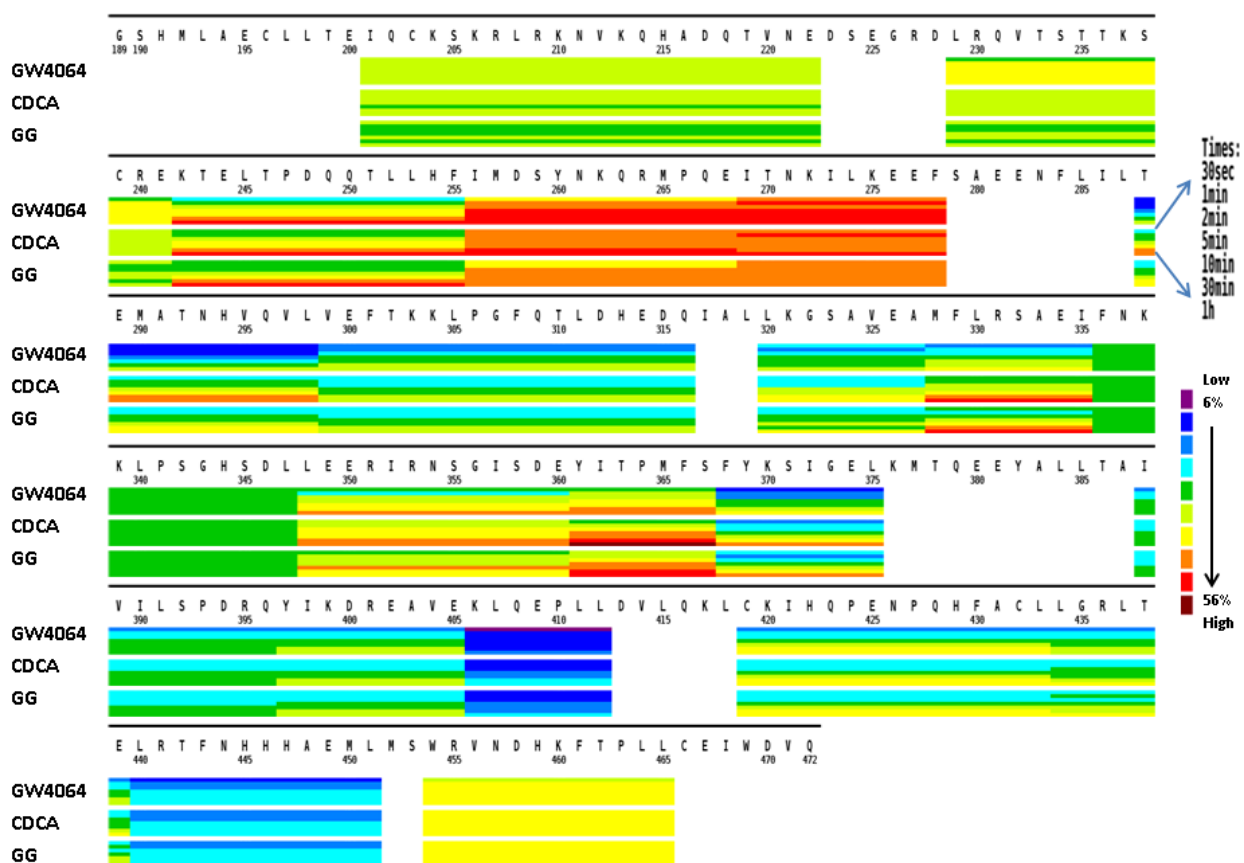


Figure 3.3 Comparative presentation of the HDX heat maps of FXR-LBD in the presence of ligands

Each horizontal color block represents an analyzed peptic peptide, and each block contains seven time points (from top: 0.5, 1, 2, 5, 10, 30, 60 min).

Figure 3.4

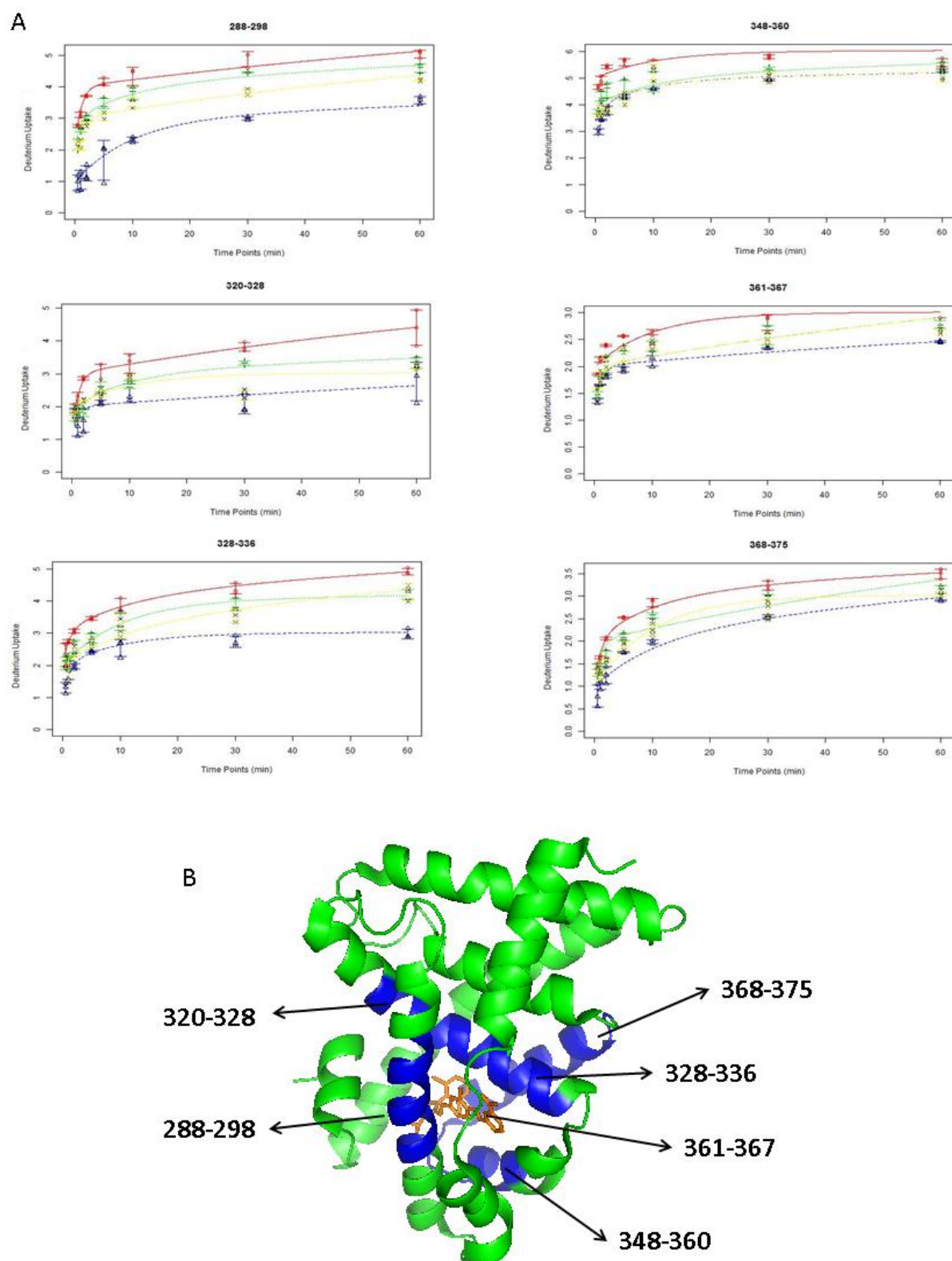


Figure 3.4 Exchange-in plots of peptides that showed disparate exchange characteristics  
(A) Kinetic plots: apo-FXR-LBD, red line; GW4064, blue line; CDCA, green line; GG, yellow line. (B) X-ray structure of FXR-LBD (green) bound to GW4064 (orange) (PDB ID 3DCT); peptides that showed disparate exchange characteristics in presence of the diverse ligands are colored blue.

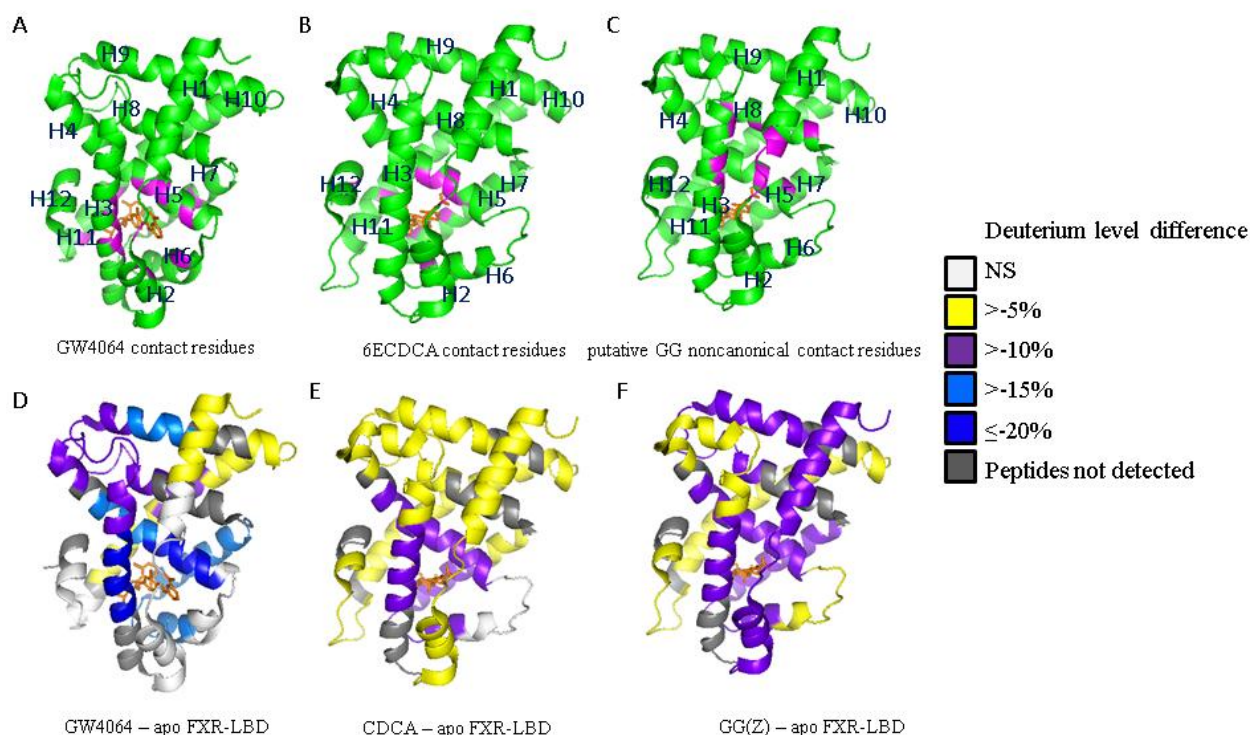
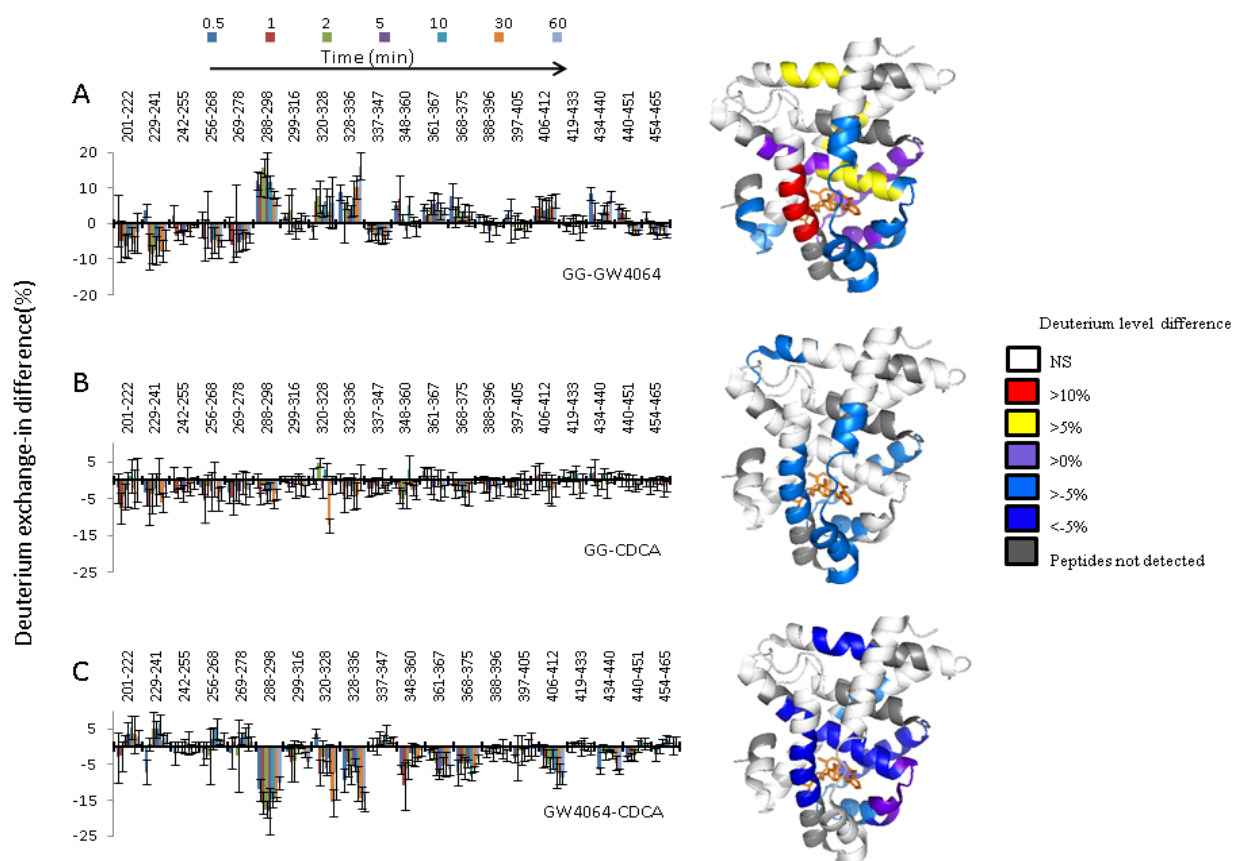
**Figure 3.5**

Figure 3.5 Average differences in deuterium uptake (in %) of FXR-LBD with or without ligand overlaid onto crystallographic structures

The N-terminal region which is covered by the peptides 201-222 and 229-241 is not visible in the crystal structures.

Top row: Co-crystal structure of FXR-LBD ligand complex, PDB ID 3DCT for (A) and PDB ID 1OSV for (B) and (C). Contact residues between ligand and protein are colored in pink. The ligand itself is colored in orange.

Bottom row: Average differences in deuterium levels expressed as percentage (D%) of the seven incubation periods used in this study (0.5, 1, 2, 5, 10, 30, and 60 min) are mapped onto the crystal structure of FXR-LBD-ligand complex, PDB ID 3DCT for (D) and PDB ID 1OSV for (E) and (F). Regions that were not covered by the current experiments are depicted in grey. NS, not significant.

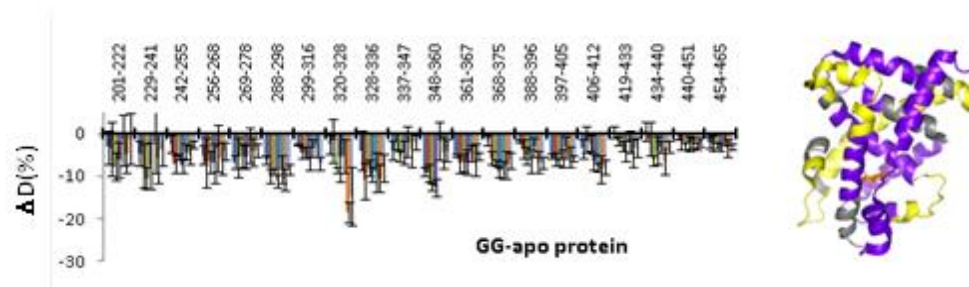
**Figure 3.6****Figure 3.6 Differential HDX data of FXR-LBD-agonist and FXR-LBD-antagonist**

Left: Deuterium differences in percentage (D%) from one complex to another are shown at different time points (0.5, 1, 2, 5, 10, 30, and 60 min, from left to right) for each peptide.

Right: Average differences in deuterium levels expressed as percentage (D%) of the seven time points (0.5, 1, 2, 5, 10, 30, and 60 min) were overlaid onto the crystallographic structure, PDB ID 3DCT for (A) and (B), PDB ID 1OSV for (C). Positive numbers indicate higher deuterium exchange levels and thus less protection in the FXR-LBD-GG relative to the FXR-LBD-GW4064. Negative numbers indicate lower deuterium exchange levels and thus more protection in the FXR-LBD-GG relative to the FXR-LBD-GW4064.



## Graphical Abstract



## Highlights

- Solution-phase conformational dynamics of FXR-LBD by HDX-MS
- HDX dynamics of FXR-LBD interactions with low affinity ligands
- Differential HDX-MS analysis reveals ligand-specific exchange-in kinetics
- HDX-MS analysis confirms noncanonical interaction site for (*Z*) guggelsterone

## 3.8 Supplementary data

**Conformational dynamics of human FXR-LBD ligand interactions studied by  
hydrogen/deuterium exchange mass spectrometry: Insights into the  
antagonism of the hypolipidemic agent Z-guggulsterone**

Liping Yang<sup>1</sup>, David Broderick<sup>1</sup>, Yuan Jiang<sup>2</sup>, Victor Hsu<sup>3</sup> and Claudia S. Maier<sup>1</sup>

Departments of Chemistry<sup>1</sup>, Department of Statistics<sup>2</sup>, and Biochemistry and Biophysics<sup>3</sup>,  
Oregon State University, Corvallis, Oregon 97331

Corresponding author: Dr. Claudia S. Maier

Email: [claudia.maier@oregonstate.edu](mailto:claudia.maier@oregonstate.edu)

Phone: +1-541-737-9533

Fax: +1-541-737-2062

Figure S3.1 A SDS PAGE of purified hFXR-LBD; B, MS spectrum of purified hFXR-LBD

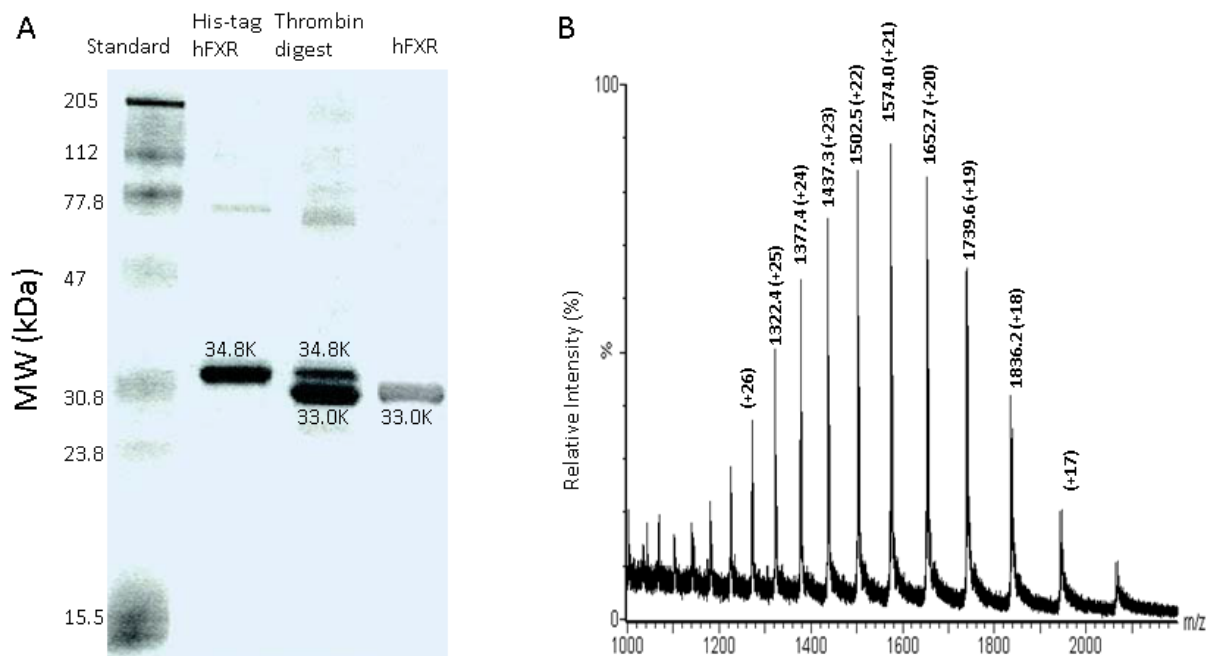


Figure S3.2 Binding of GG to FXR-LBD studied by intrinsic fluorescence titration

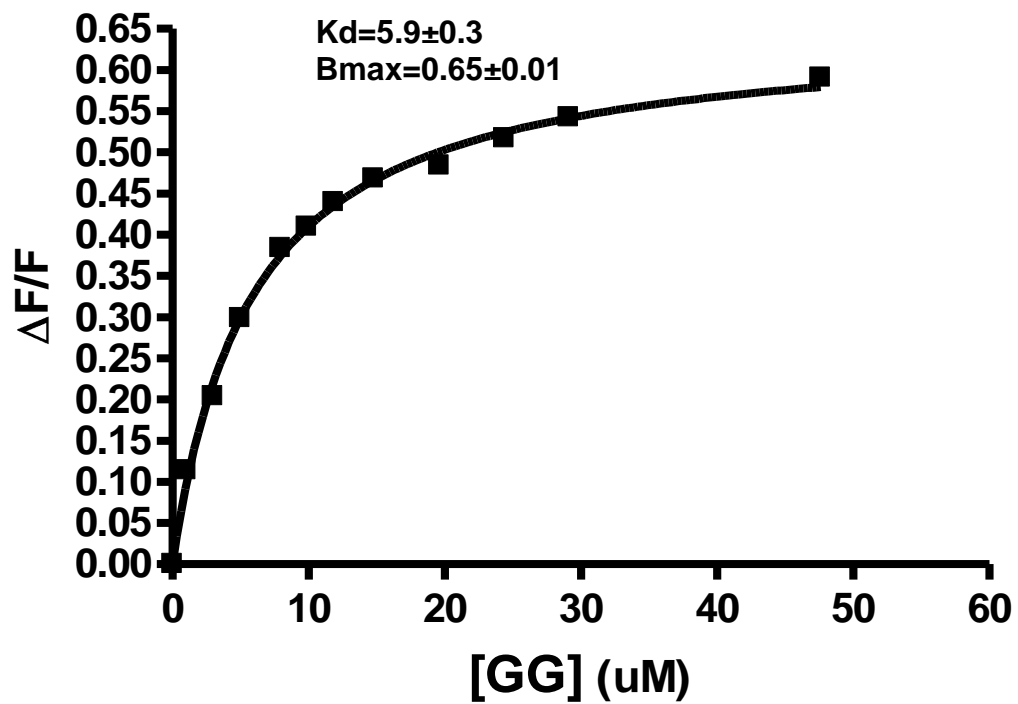


Figure S3.3 Design and schematic flow path diagrams of the UPLC system used in this study

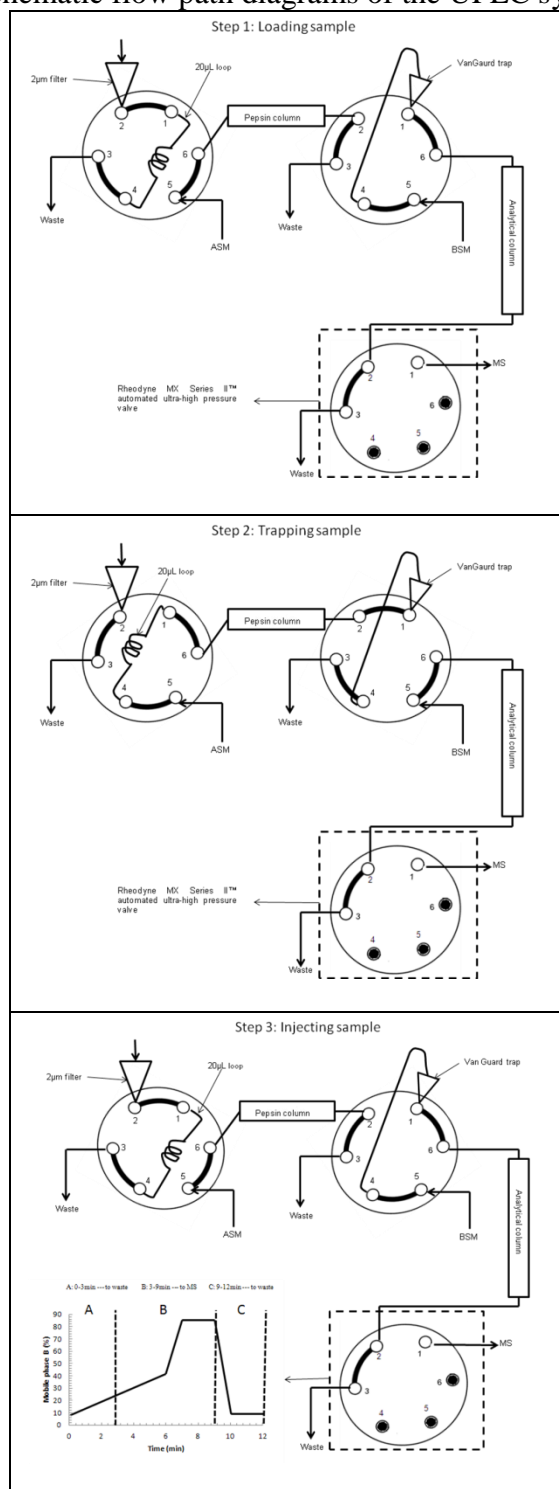


Figure S3.4 Peptide coverage map of FXR-LBD

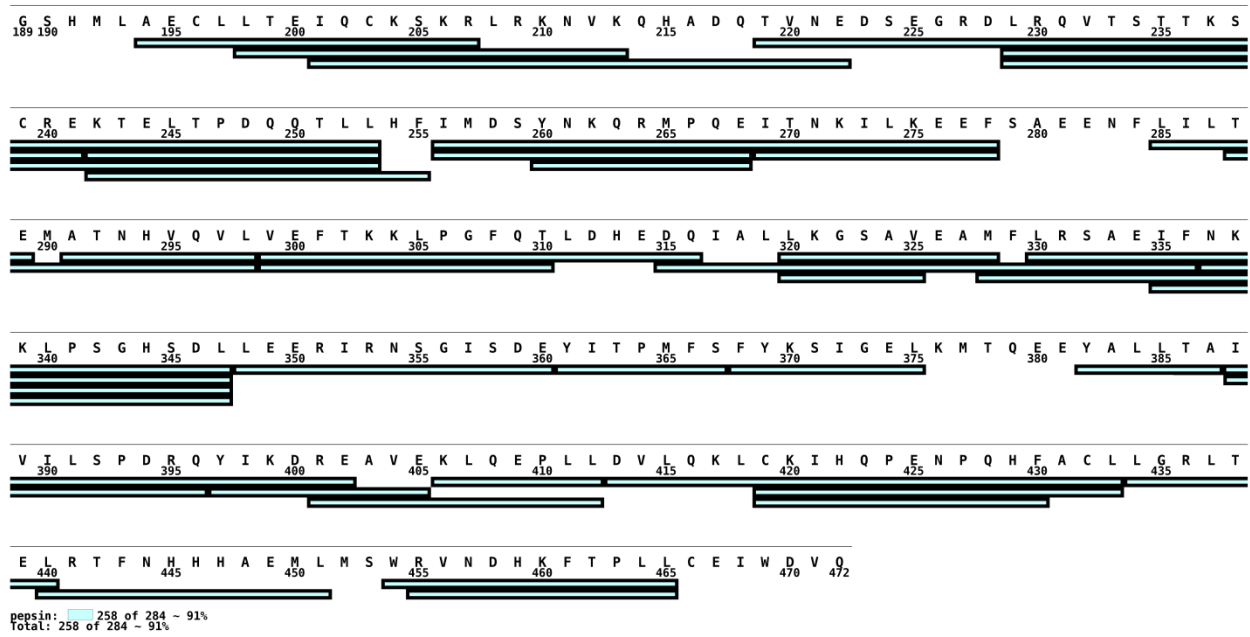
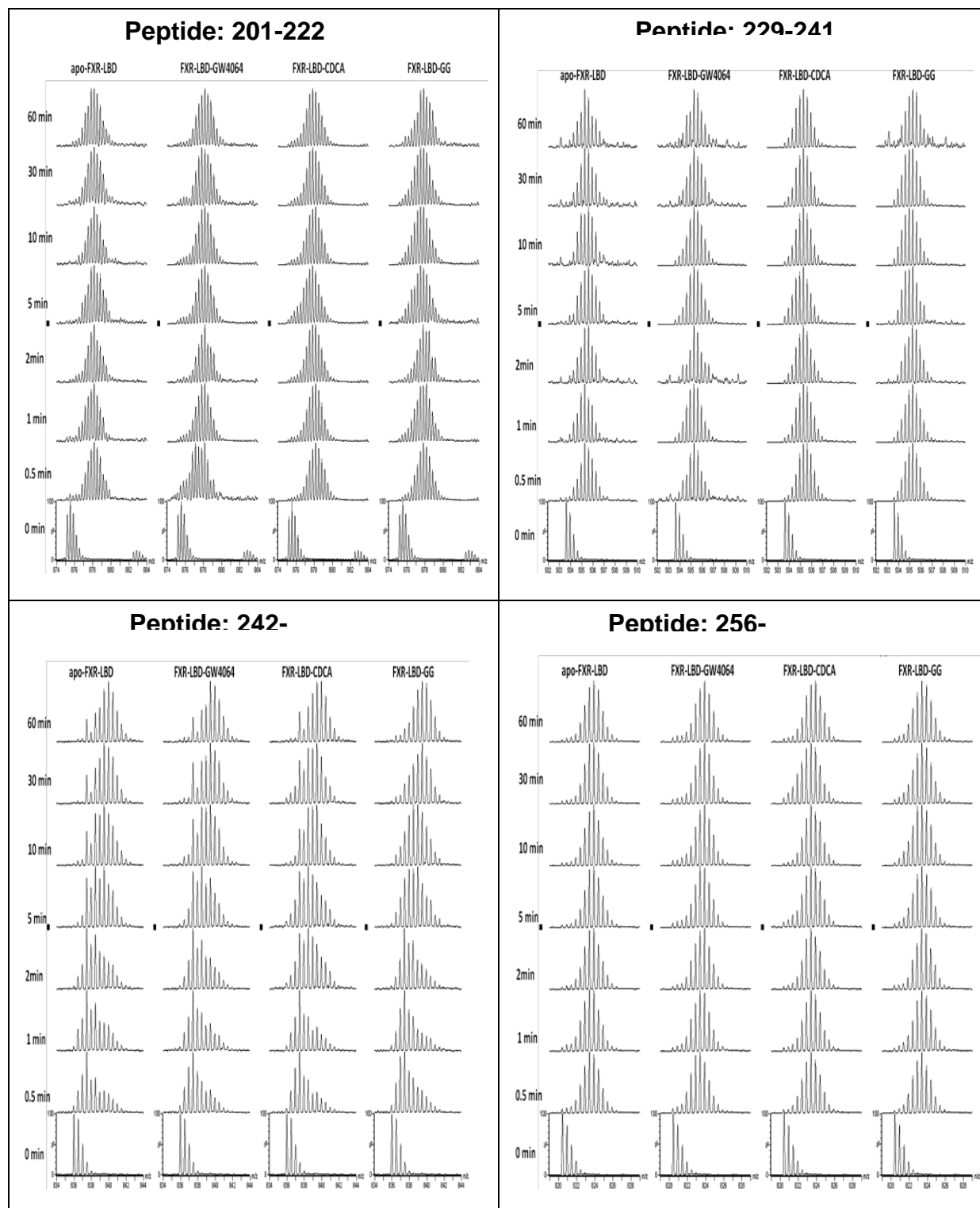
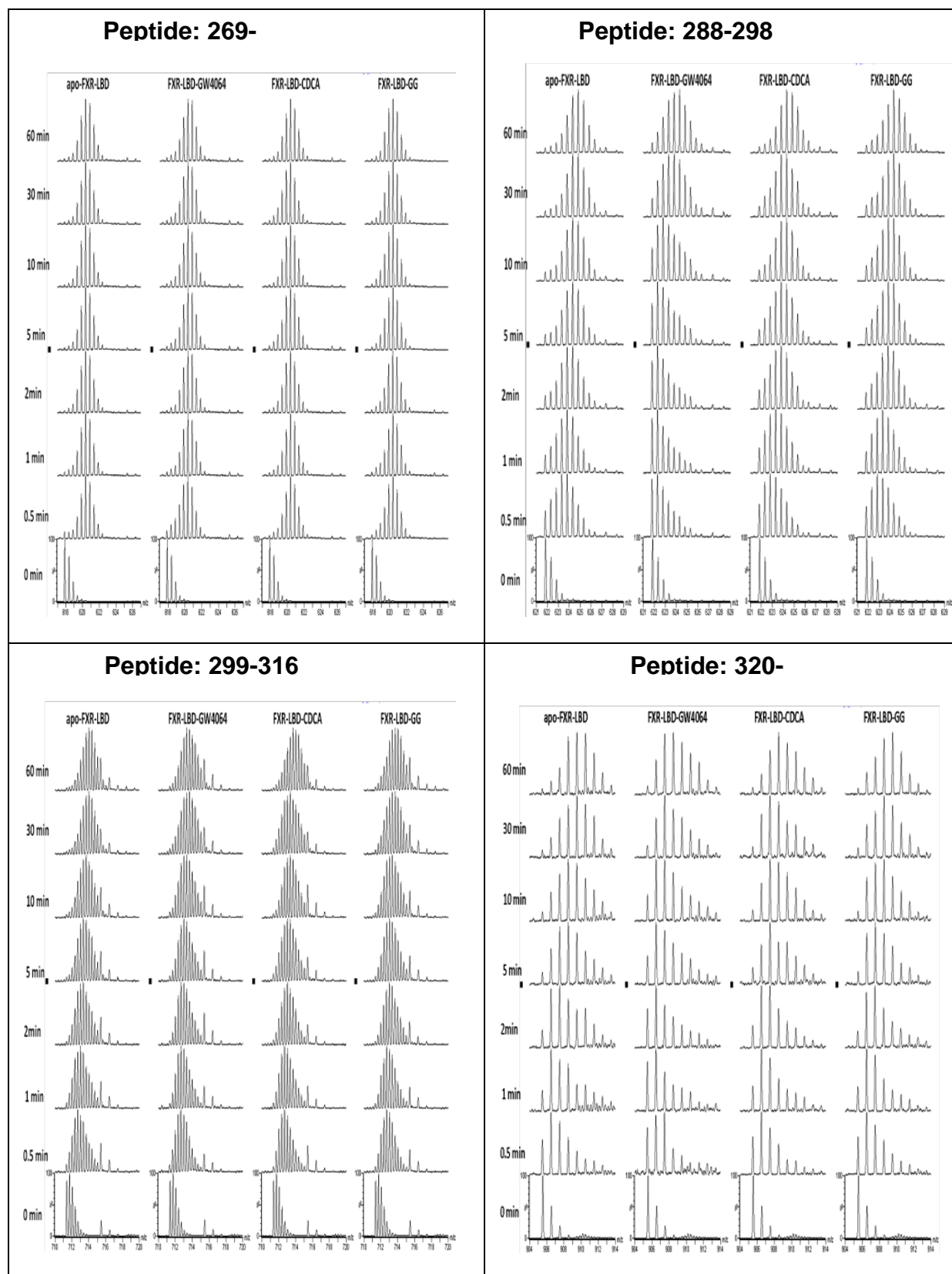


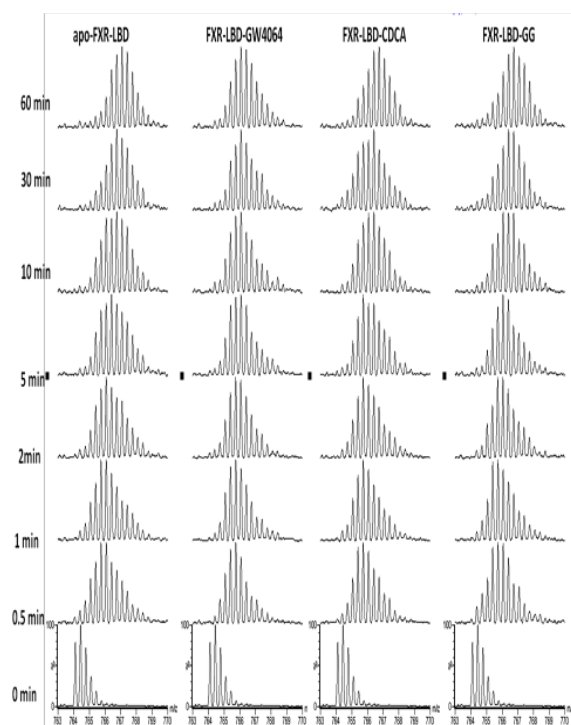
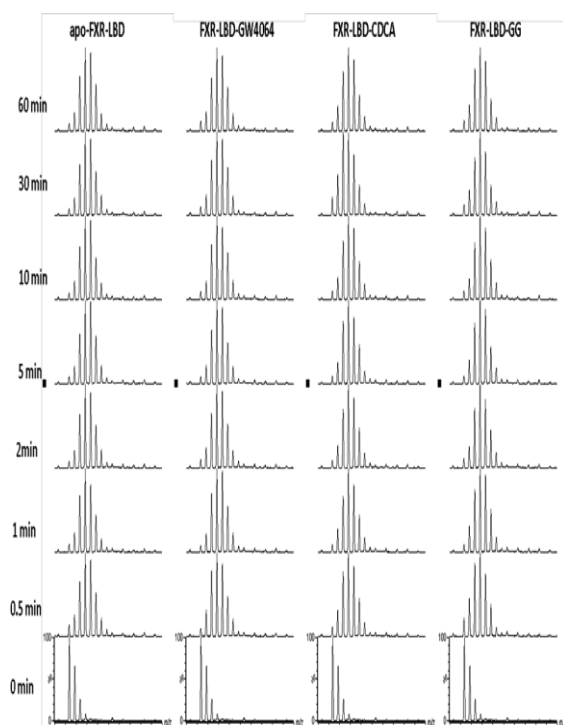
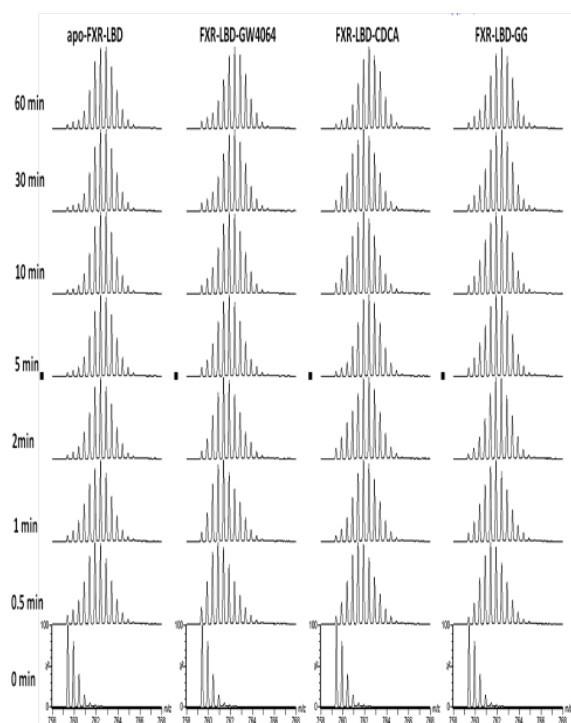
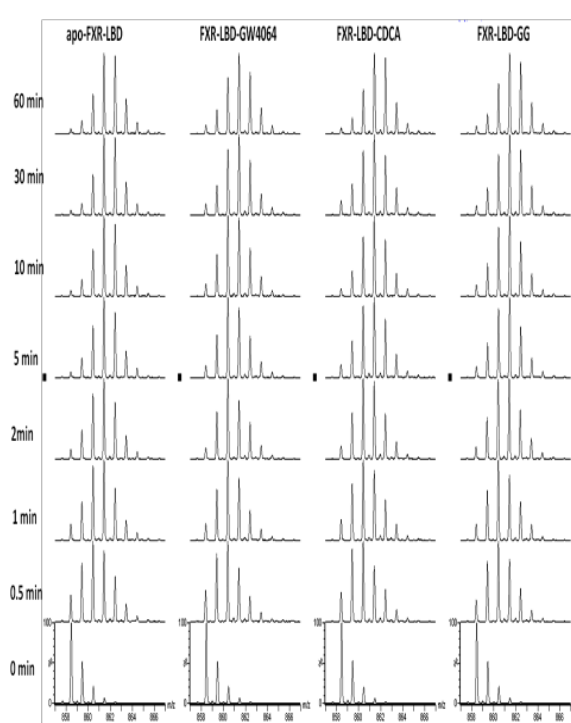
Figure S3.5 Mass spectra for peptides demonstrating evolution of deuterium incorporation into peptic peptides

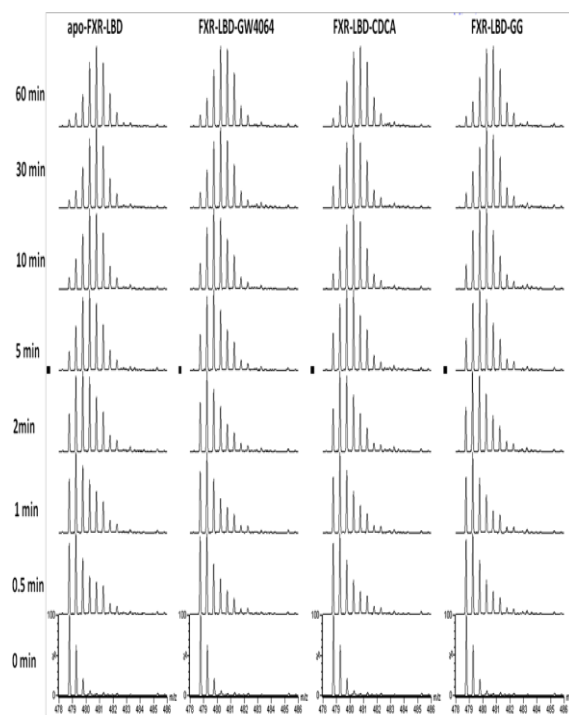
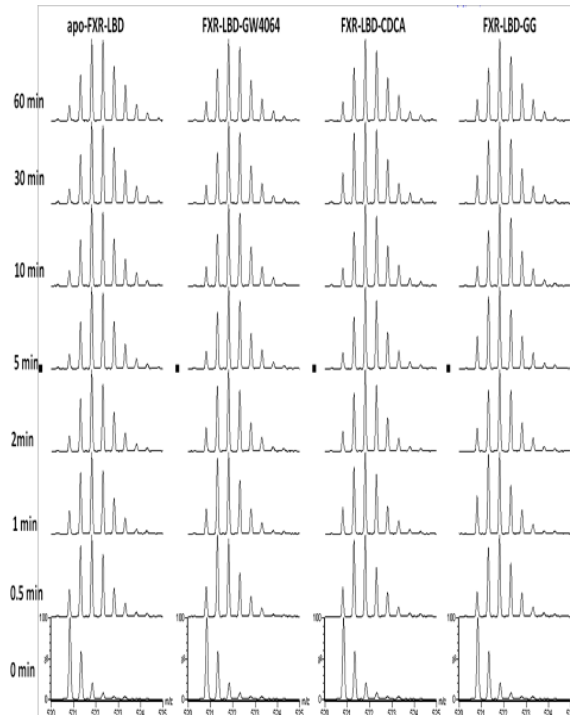
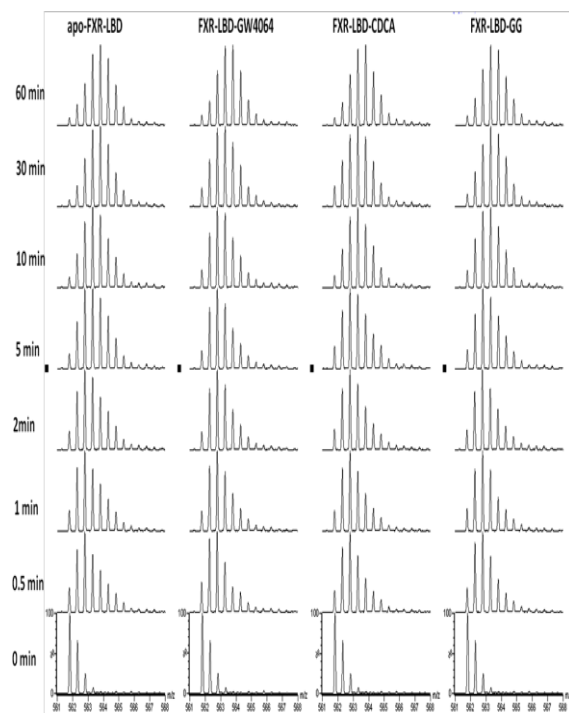
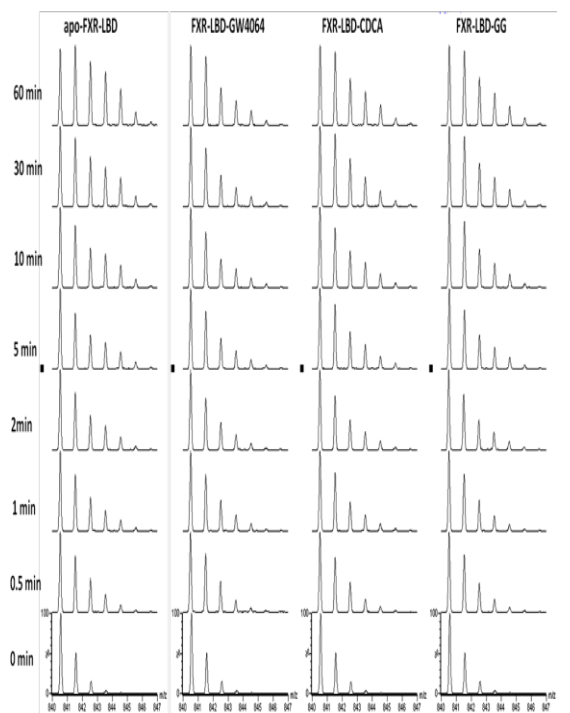
The partial sequence of each peptide is depicted at the top of each panel. Deuteration times (0, 0.5, 1, 2, 5, 15, 30, 60 min) are denoted in each panel.







**Peptide: 328-347****Peptide: 337-347****Peptide: 348-360****Peptide: 361-367**

**Peptide: 368-****Peptide: 388-396****Peptide: 397-****Peptide: 406-**

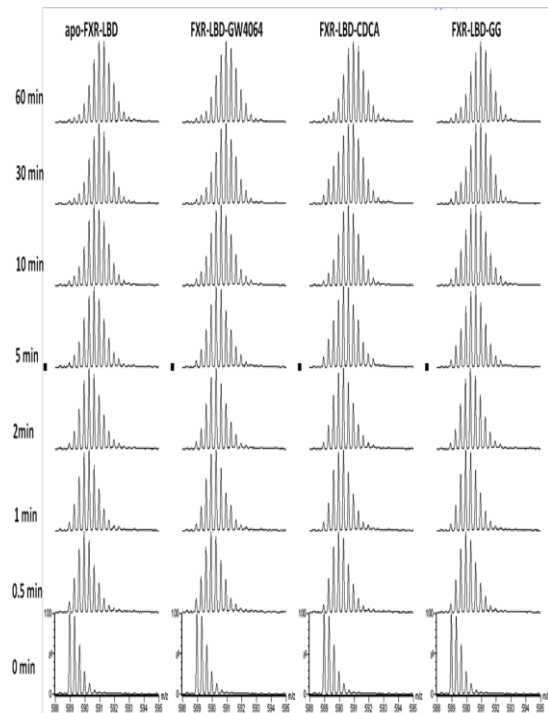
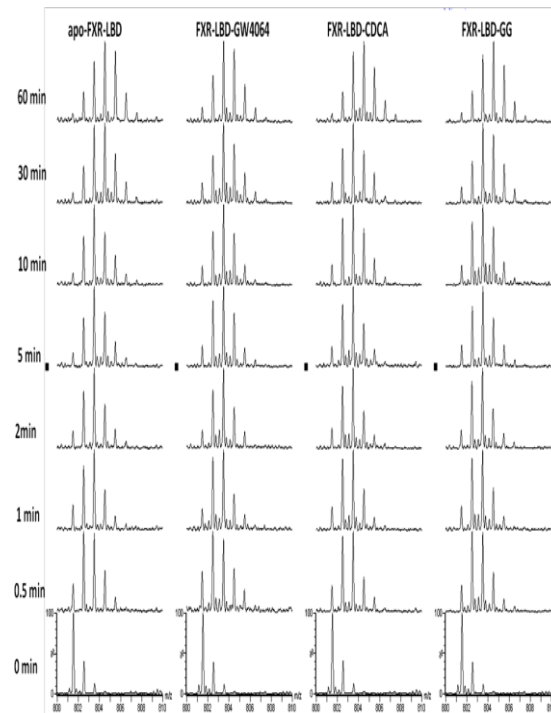
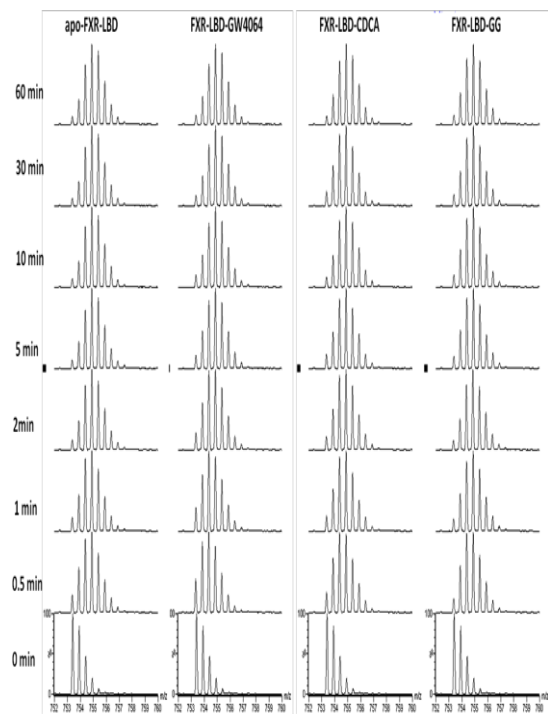
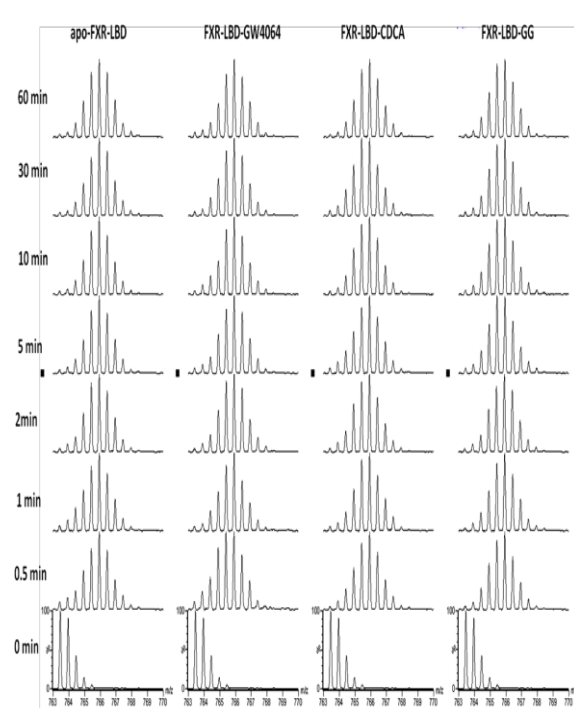
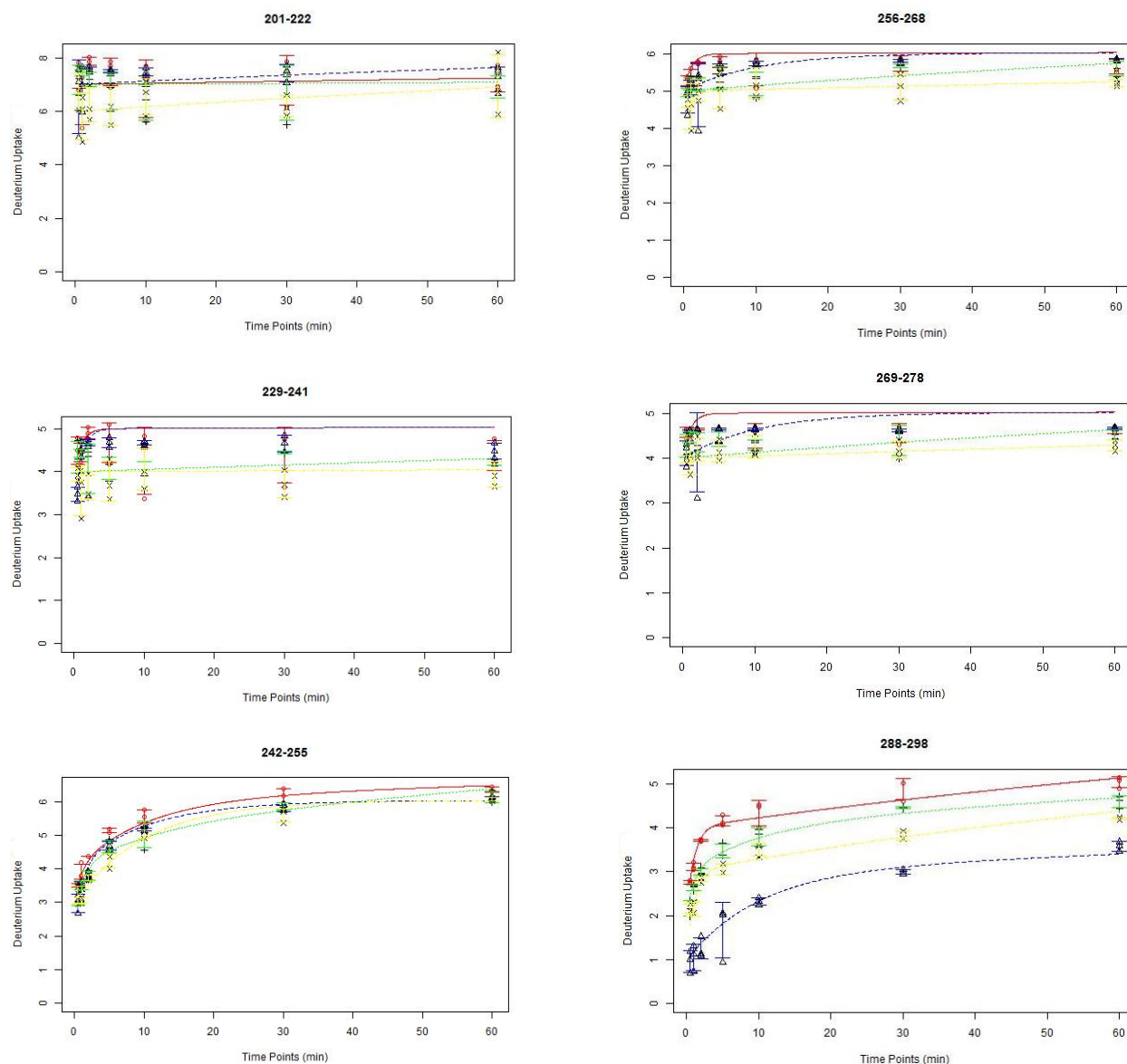
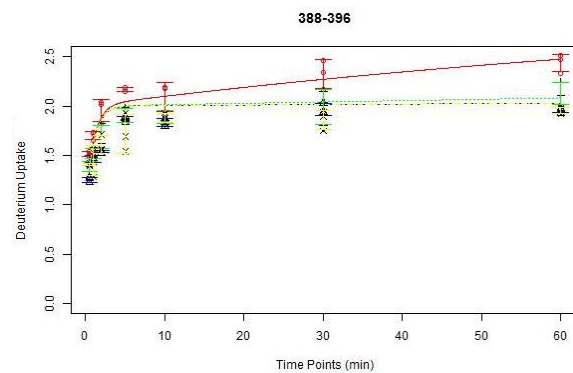
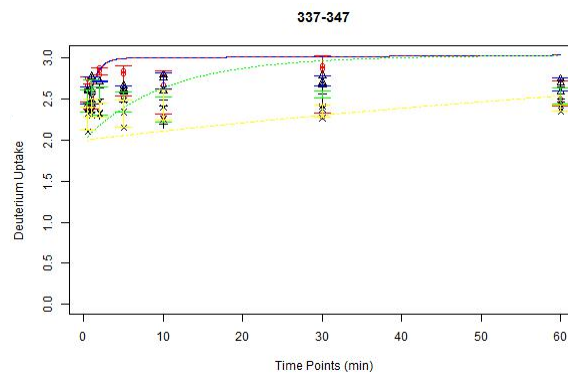
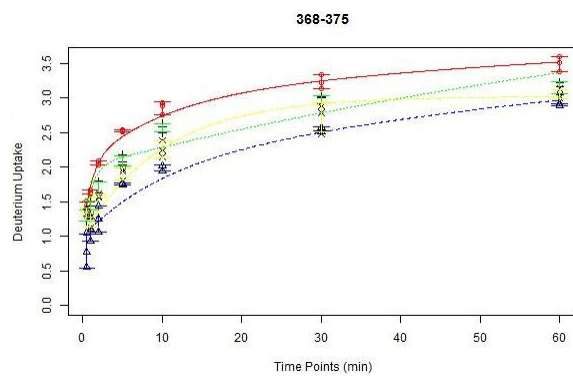
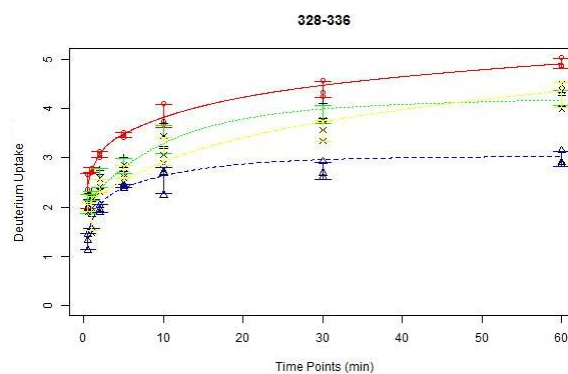
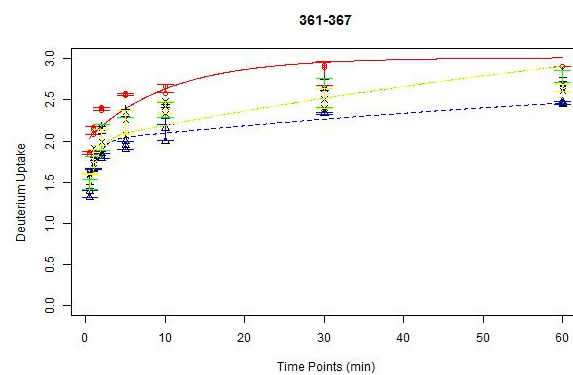
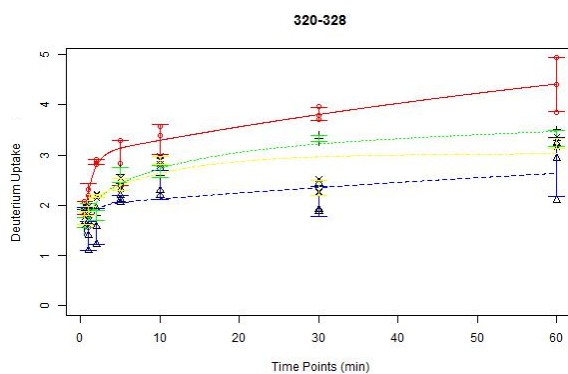
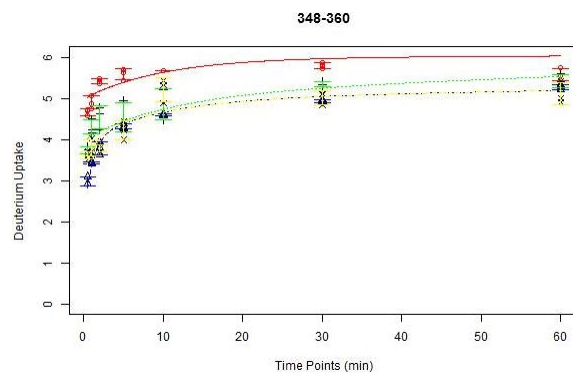
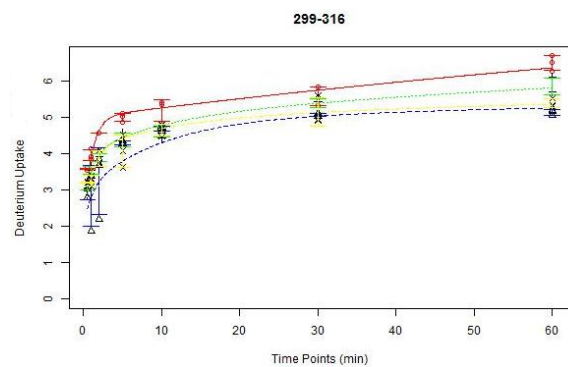
**Peptide: 419-****Peptide: 434-****Peptide: 440-****Peptide: 454-465**

Figure S3.6 Deuterium incorporation levels for each peptide at seven exchange-in time points. (0.5, 1, 2, 5, 10, 30, 60 min). The curves were fit with a six fixed exchange rate constants kinetic model ( $10, 1, 0.1, 0.01, 0.001, 0.0001 \text{ min}^{-1}$ ). The error bar for each data point is based on the three experimental replicates. Color code: apo-FXR-LBD, red line; GW4064, blue line; CDCA, green line; GG, yellow line.





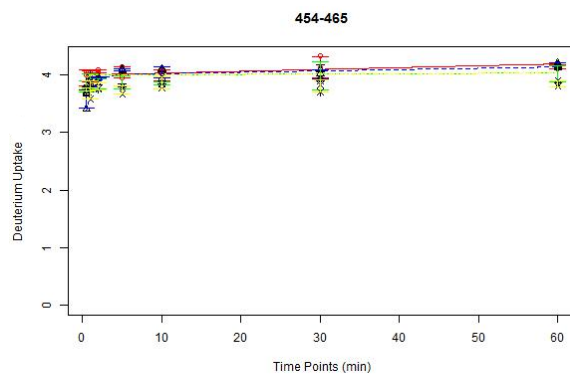
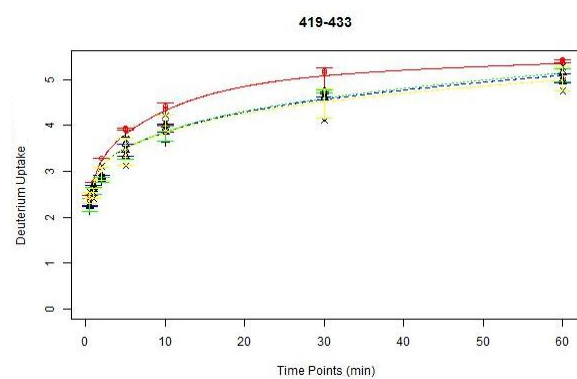
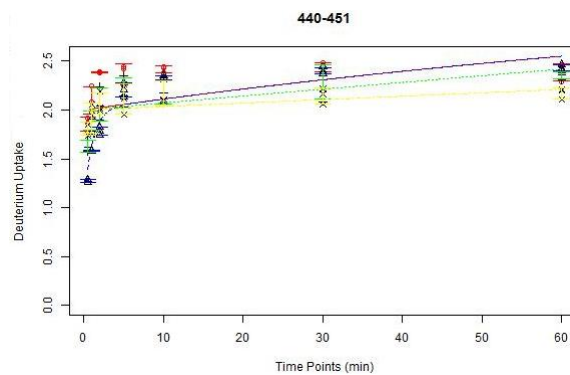
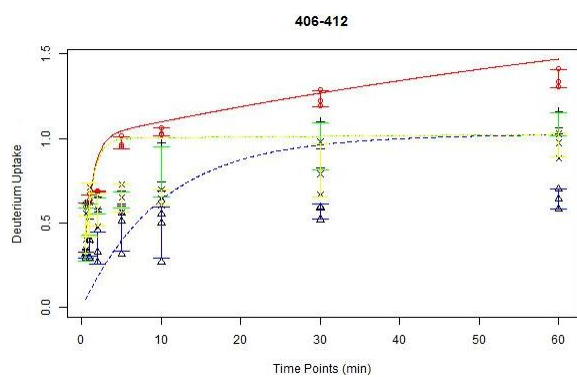
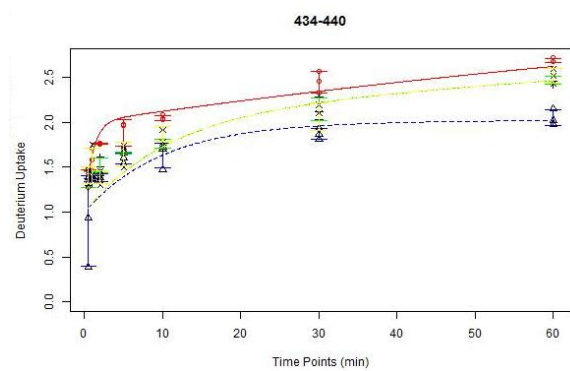
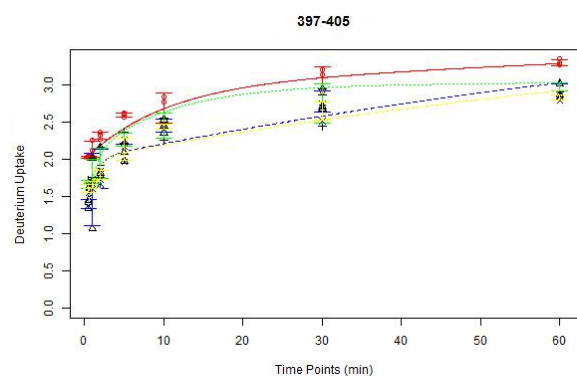




Figure S3.7 Deuterium exchange data for apo FXR-LBD

(A) Peptic peptides HDX profiles of apo FXR-LBD. Deuterium exchange levels for each peptide (in % based on the number of backbone amides present in the peptide) are shown at different reaction time points (0.5, 1, 2, 5, 10, 30, and 60 min, from left to right). (B) HDX heat map for apo FXR-LBD. Each horizontal color block represents an analyzed peptic peptide, and each block contains seven time points (from top: 0.5, 1, 2, 5, 10, 30, 60min). The secondary structure of holo-FXR with GW4064 is based on a three-dimensional crystallographic structure (PDB ID: 3DCT) and was added for reference purposes only.

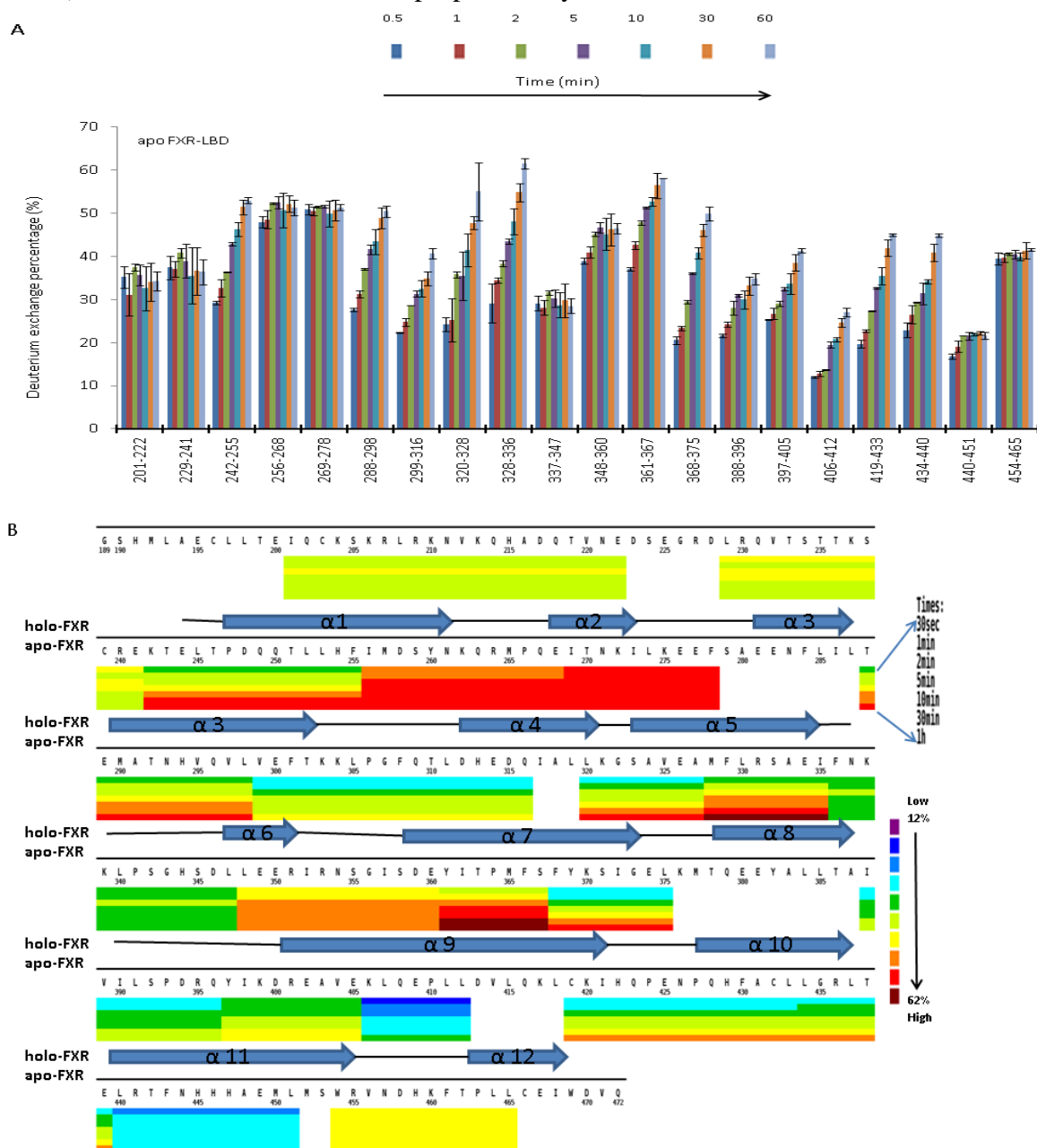




Figure S3.8 Peptide-level HDX profiles of FXR-LBD in the presence of GW4064, CDCA and GG(Z), respectively.

Deuterium exchange for each peptide (in % based on the number of backbone amide hydrogens present in the peptide) is shown at different reaction time points (0.5, 1, 2, 5, 10, 30, and 60 min, from left to right).

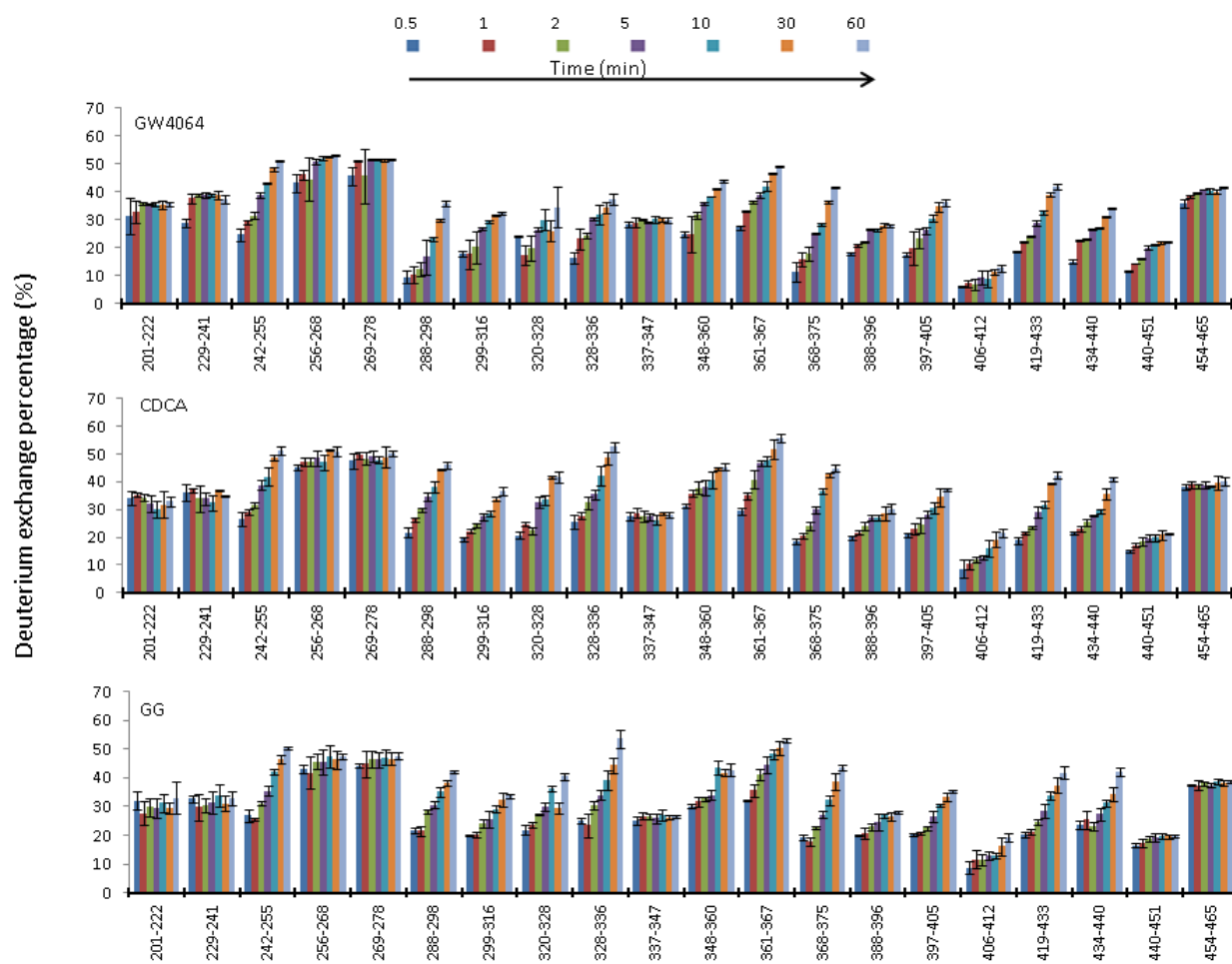


Figure S3.9 Ligand-dependent deuterium exchange protection plots at the peptide level. Ligand-specific deuterium exchange-in differences between ligand-free FXR-LBD and ligand-bound FXR-LBD is shown at different time points (0.5, 1, 2, 5, 10, 30, and 60 min, from left to right) for each peptide. Negative percentages indicate the increase of protection against deuterium exchange-in in a particular region of the FXR-LBD ligand complex relative to apo FXR.

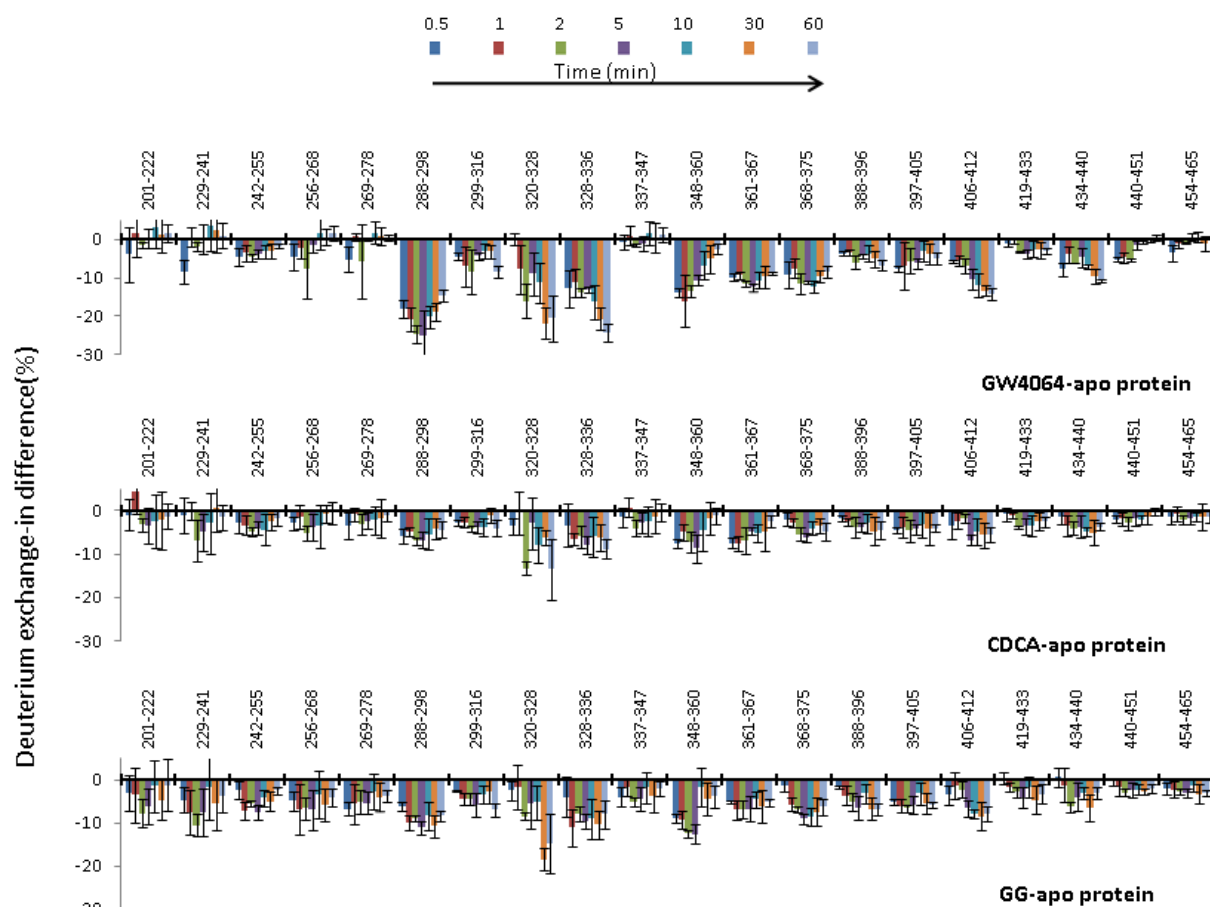


Figure S3.10 Overlay of the peptide deuterium levels of GW4064-bound hFXR-LBD and the B-factors of the backbone N atoms extracted from the crystal structure, PDB ID 3DCT.

Asterisks mark the following: \* regions containing direct interaction sites; \*\* regions that showed changes in exchange kinetics but showed no interacting residues in the crystal structure. For comparison the peptide deuterium levels of the apo protein are shown illustrating disparate retardation of exchange (reduced deuterium levels) in different region of the protein upon binding of the high affinity agonist GW4064.

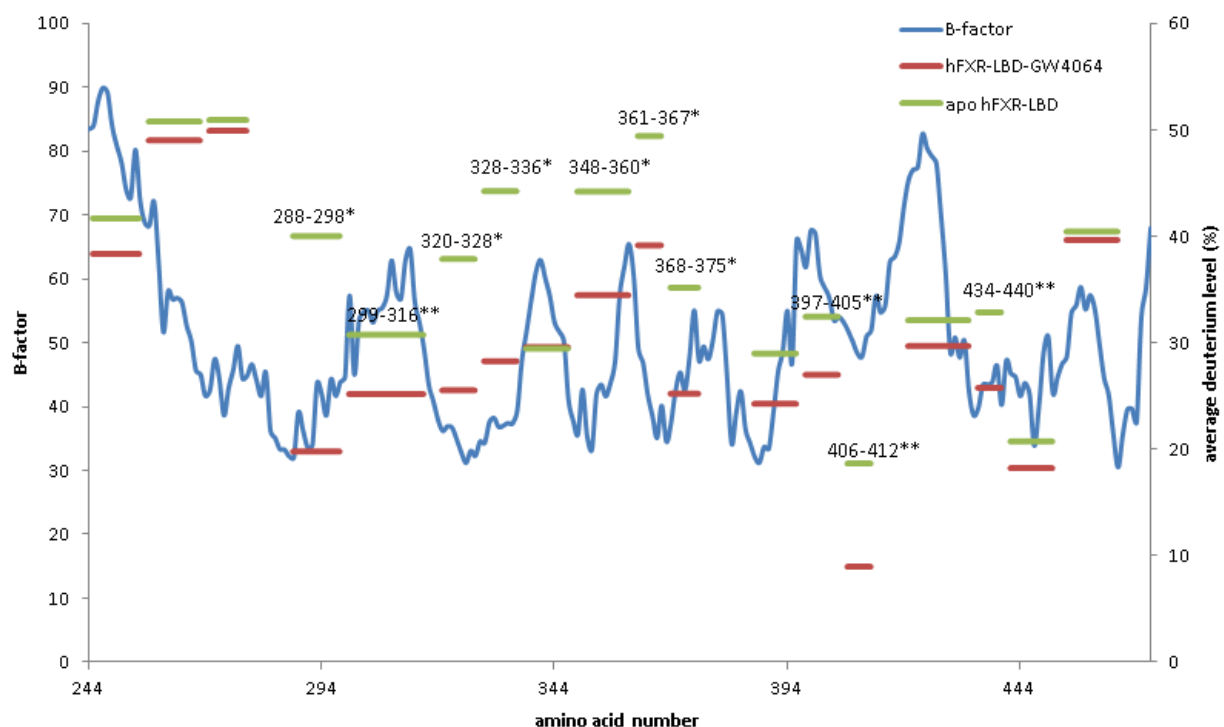


Table S3.1 Averaged differences in deuterium incorporation levels for each of the 20 peptides used in the current HDX-MS study

The values were obtained by averaging the differences in deuterium levels across the seven reaction time points (0.5, 1, 2, 5, 10, 30 to 60 min) used in the current time course study. A negative percentage indicates the increase of protection against deuterium exchange-in upon ligand binding and a positive number indicates less protection in a particular region of the FXR-LBD ligand complex.


Deuterium level differences of regions with  $p < 0.001$ , calculated by two-way ANOVA, are statistically significant.


Structure <sup>a</sup>	Residue <sup>b</sup>	Charge <sup>c</sup>	apo <sup>d</sup>	GW4064- apo <sup>e</sup>	P-value	CDCA-apo <sup>f</sup>	P-value	GG-apo <sup>g</sup>	P-value	GG- GW4064 <sup>h</sup>	P-value	GG-CDCA <sup>i</sup>	P-value	GW4064- CDCA <sup>j</sup>	P-value
H1(-)	201-222	3	34%	0%	0.789	-1%	0.178	-4%	<0.001	-4%	<0.001	-3%	0.014	2%	0.080
H1(-)	229-241	2	38%	0%	0.627	-2%	0.022	-6%	<0.001	-5%	<0.001	-3%	<0.001	2%	0.003
H1	242-255	2	42%	-4%	<0.001	-3%	<0.001	-5%	<0.001	-1%	0.002	-1%	0.007	0%	0.755
H1-H2	256-268	2	51%	-2%	0.040	-3%	<0.001	-5%	<0.001	-4%	<0.001	-3%	<0.001	1%	0.362
H2	269-278	2	51%	-1%	0.258	-2%	<0.001	-5%	<0.001	-4%	<0.001	-3%	<0.001	2%	0.280
H3	288-298	2	40%	-20%	<0.001	-6%	<0.001	-9%	<0.001	11%	<0.001	-3%	<0.001	-14%	<0.001
H3-H4	299-316	3	31%	-6%	<0.001	-3%	<0.001	-4%	<0.001	1%	0.086	-1%	0.017	-1%	0.002
H4-H5	320-328	1	38%	-12%	<0.001	-7%	<0.001	-8%	<0.001	4%	<0.001	-1%	0.012	-5%	<0.001
H5	328-336	2	44%	-16%	<0.001	-6%	<0.001	-9%	<0.001	7%	<0.001	-2%	0.012	-9%	<0.001
H5-H6	337-347	2	29%	0%	0.834	-2%	0.008	-3%	<0.001	-3%	<0.001	-2%	0.002	2%	<0.001
H6	348-360	2	44%	-10%	<0.001	-5%	<0.001	-8%	<0.001	2%	0.003	-2%	<0.001	-4%	<0.001
H7	361-367	1	49%	-10%	<0.001	-6%	<0.001	-6%	<0.001	4%	<0.001	0%	0.603	-5%	<0.001
H7	368-375	2	35%	-10%	<0.001	-4%	<0.001	-6%	<0.001	4%	<0.001	-2%	<0.001	-7%	<0.001
H8	388-396	2	29%	-5%	<0.001	-3%	<0.001	-5%	<0.001	0%	0.997	-1%	0.009	-1%	0.13
H9	397-405	2	32%	-5%	<0.001	-4%	<0.001	-5%	<0.001	0%	0.924	-1%	0.010	-1%	0.073
H9	406-412	1	19%	-10%	<0.001	-4%	<0.001	-5%	<0.001	4%	<0.001	-1%	0.129	-5%	<0.001
H10	419-433	3	32%	-2%	<0.001	-3%	<0.001	-3%	<0.001	0%	0.860	0%	0.916	0%	0.663
H10	434-440	1	33%	-7%	<0.001	-4%	<0.001	-3%	<0.001	4%	<0.001	0%	0.415	-3%	<0.001
H11	440-451	2	21%	-3%	<0.001	-2%	<0.001	-2%	<0.001	1%	0.043	0%	0.503	-1%	0.010
H11-H12	454-465	2	40%	-1%	0.009	-1%	0.023	-2%	<0.001	-2%	<0.001	-1%	0.009	1%	0.067


- a) The structure segment of each peptide based on the FXR-LBD-GW4064 X ray structure (PDB:3DCT) without contain the first two peptides (201-222, 229-241).
- b) Residue numbers for the full-length FXR-LBD (UniRef100\_B6ZGS9)
- c) Charge state of each peptide observed in the LC-MS experiment.
- d) Deuterium level of each peptide in apo FXR-LBD.
- e) Deuterium level difference percentage between GW4064 and apo FXR-LBD.
- f) Deuterium level difference percentage between CDCA and apo FXR-LBD.
- g) Deuterium level difference percentage between GG and apo FXR-LBD.
- h) Deuterium level difference percentage between GG and GW4064.
- i) Deuterium level difference percentage between GG and CDCA.
- j) Deuterium level difference percentage between GW4064 and CDCA.


Table S3.2 The amide hydrogen distribution of each peptide in the six-fixed-rate-constant binning model (10, 1, 0.1, 0.01, 0.001, and 0.0001 min<sup>-1</sup>). Although the six-bin model provided the best fits to the deuterium uptake plots (Figure S3.6) we reduced the model to three categories to simplify the discussion of the HDX data in terms of distributions of exchanging sites: category I (fast exchanging sites,  $k = 10$  or  $1$  min<sup>-1</sup>), category II (medium exchanging sites,  $k = 0.1$  or  $0.01$  min<sup>-1</sup>), and category III (slow exchanging sites,  $k = 0.001$  or  $0.0001$  min<sup>-1</sup>).

peptides		apo-FXR-LBD						GW4064						CDCA						GG					
		Category I		Category II		Category III		Category I		Category II		Category III		Category I		Category II		Category III		Category I		Category II		Category III	
from	to	10	1	0.1	0.01	0.001	0.0001	10	1	0.1	0.01	0.001	0.0001	10	1	0.1	0.01	0.001	0.0001	10	1	0.1	0.01	0.001	0.0001
201	222	7	0	0	1	0	13	7	0	0	1	2	11	7	0	0	0	0	14	6	0	0	1	0	14
229	241	4	1	0	0	0	7	3	2	0	0	0	7	4	0	0	0	6	2	4	0	0	0	0	8
242	255	3	1	2	1	0	5	2	2	2	0	0	6	2	2	1	3	0	4	3	0	3	0	0	6
256	268	5	1	0	0	0	5	5	0	1	0	0	5	5	0	0	1	5	0	5	0	0	0	4	2
269	278	4	1	0	0	0	4	4	1	0	0	0	4	4	0	0	1	3	1	4	0	0	0	5	0
288	298	2	2	0	2	4	0	1	0	2	1	0	6	2	1	1	1	4	1	1	2	1	0	4	2
299	316	2	3	0	2	8	1	2	2	1	0	2	9	2	2	1	1	6	4	2	2	1	0	6	5
320	328	1	2	0	4	0	1	2	0	0	1	5	0	1	1	1	1	0	4	2	0	1	0	0	5
328	336	2	1	1	2	0	2	1	1	1	0	0	5	2	0	2	0	3	1	2	0	1	3	0	2
337	347	2	1	0	0	0	6	2	1	0	0	0	6	2	0	1	0	0	6	2	0	0	1	1	5
348	360	5	0	1	0	0	6	2	2	1	0	3	4	4	0	1	1	1	5	3	1	1	0	3	4
361	367	2	0	1	0	0	2	1	1	0	1	0	2	1	1	0	2	0	1	1	1	0	2	0	1
368	375	1	1	1	1	1	2	1	0	1	2	1	2	1	1	0	3	0	2	1	0	2	0	0	4
388	396	1	1	0	1	0	4	1	1	0	0	0	5	1	1	0	0	1	4	1	1	0	0	0	5
397	405	2	0	1	0	5	0	1	1	0	2	2	2	1	1	1	0	0	5	1	1	0	2	0	4
406	412	0	1	0	1	0	3	0	0	1	0	0	4	0	1	0	0	0	4	0	1	0	0	0	4
419	433	2	1	2	0	6	1	2	1	1	2	3	3	2	1	1	2	4	2	2	1	1	2	1	5
434	440	1	1	0	1	3	0	1	0	1	0	0	4	1	0	1	1	0	3	1	0	1	1	0	3
440	451	2	0	0	1	1	7	1	1	0	1	1	7	2	0	0	0	7	2	2	0	0	0	3	6
454	465	4	0	0	0	3	3	3	1	0	0	2	4	4	0	0	0	0	6	4	0	0	0	0	6

  
Fast Slow  
exchanging amide hydrogens/peptide

  
Fast Slow  
exchanging amide hydrogens/peptide

  
Fast Slow  
exchanging amide hydrogens/peptide

  
Fast Slow  
exchanging amide hydrogens/peptide

## Chapter 4

### **Probing human FXR LBD – prenylflavonoid interactions by hydrogen/deuterium exchange mass spectrometry**

Liping Yang<sup>1</sup>, David Broderick<sup>1</sup>, Yan Campbell<sup>4,6</sup>, Adrian F. Gombart<sup>4,6</sup>, J. Fred Stevens<sup>4,5</sup>,  
Victor Hsu<sup>5</sup>, Yuan Jiang<sup>3</sup>, William H. Bisson<sup>2\*</sup> and Claudia S. Maier<sup>1\*</sup>

Department of Chemistry<sup>1</sup>, Oregon State University, Corvallis, OR 97331

Department of Environmental and Molecular Toxicology<sup>2</sup>, Oregon State University, Corvallis,  
OR 97331

Department of Statistics<sup>3</sup>, Oregon State University, Corvallis, OR 97331

Linus Pauling Institute<sup>4</sup>, Oregon State University, Corvallis, OR 97331

Department of Pharmaceutical Science<sup>5</sup>, Oregon State University, Corvallis, OR 97331

Department of Biochemistry and Biophysics<sup>6</sup>, Oregon State University, Corvallis, OR 97331

Corresponding authors:

Claudia S. Maier (HDX-MS)

Email: [claudia.maier@oregonstate.edu](mailto:claudia.maier@oregonstate.edu)

Phone: +1-541-737-9533; Fax: +1-541-737-2062

William Bisson (Computational Modeling)

Email: [William.bisson@oregonstate.edu](mailto:William.bisson@oregonstate.edu)

Phone: +1-541-737-5735

## 4.1 Abstract

Several recent studies revealed that prenylflavonoids, including xanthohumol (XN), isoxanthohumol (IX), and 8-prenylnaringenin (8-PN), are capable of modulating lipid metabolism possibly via modulating the farnesoid X receptor (FXR) activity. This finding enhanced our interest in studying the interaction between FXR-ligand binding domain (FXR-LBD) and prenylflavonoids by Hydrogen Deuterium Exchange (HDX) Mass Spectrometry (MS). Deuterium incorporation profiles were obtained for four prenylflavonoids: XN, IX, 8-PN, and one derivative of XN, tetrahydroxanthohumol (TX). Comparison of the HDX protection profiles of FXR-LBD in presence of the diverse prenylflavonoids indicated that modulation of the conformational dynamics of FXR LBD by prenylflavonoids. *In silico* molecular docking studies predicted that the series of prenylflavonoids tested are ligands of the FXR-LBD, in agreement with the HDX data. We reported the first systematic study of FXR LBD interactions by prenylflavonoids providing direct support to our hypothesis, that XN and related prenylflavonoids (IX, 8-PN, and TX) represent a new class of small molecule ligands that bind to FXR-LBD and affect its structural dynamics in ligand-specific manners.



## 4.2 Introduction

FXR has been considered as a highly promising therapeutic target [1] to manipulate diverse metabolic disorders because of its vital role in regulating expression of genes involved in bile acid, cholesterol and glucose homeostasis [2, 3]. Like other nuclear receptors, FXR shares the classical modular architecture of other nuclear receptors: a ligand-binding domain (LBD), a DNA-binding domain (DBD), and a connecting hinge region [4]. The LBD harbors the canonical ligand binding cavity. Ligand binding results in conformational changes that control release of the corepressor proteins and subsequent recruitment of the coactivator proteins. Since chenodeoxycholic acid (CDCA) was reported as the endogenous FXR agonist in 1999 [5-7], much research went into the discovery and synthesis of ligands that target FXR [8].

XN, the principal prenylflavonoid in hops (*Humulus lupulus L.*), has gained attention due to its “health promoting effects” [9] and research is ongoing in Dr. J. Fred Stevens’ group at Oregon State University since the 1990’s. Their work significantly contributed to the emergence of the prenylflavonoids as highly potent bio-active natural products [9]. Other research groups have reported that XN exhibits anti-inflammatory, anti-oxidant and anti-platelet activity [10-12]. Recent studies have reported that XN shows potential in modulating hyperlipidemia based on the following experimental observations: XN inhibits expression or activity of the diacylglycerol acyltransferase [13]; XN inhibits triglyceride synthesis and secretion in HepG2 cells [14]; XN functions as an FXR agonist in a transient transfection assay, and also determination of the hepatic gene expression in XN-fed mice suggests that XN acts as an selective bile acid receptor modulator [15]; XN and IX inhibit lipid accumulation in maturing preadipocytes, possibly partly by modulating FXR target genes [16].

A study recently completed by Dr. Adrian Gombart's group at Oregon State University showed that XN induced BSEP promoter activity, one of FXR target genes in transfected HEK293 cells (manuscript in preparation). This induction occurred at a similar level as observed for chenodeoxycholic acid (CDCA) and guggulsterone (GG) in the transfected cells. These findings prompted us to study FXR LBD – prenylflavonoid interactions at the molecular level by utilizing HDX-MS. Over the past two decades, HDX coupled with LC-ESI-MS has emerged as a powerful technology to probe conformational changes in proteins induced by interactions with other proteins and small molecule ligands. HDX-MS reports on changes of backbone amide hydrogen exchange rates which are highly sensitive to the protein structural changes relating to conformational flexibility, hydrogen bonding strength, and solvent accessibility of protein surfaces. [17]. In this study, HDX-MS and molecular docking methods were used to test the hypothesis that XN and related prenylflavonoids, IX, 8-PN, and TX bind to the FXR-LBD. Our studies provide for the first time structural information with respect to the molecular recognition of prenylflavonoids by the FXR-LBD and describe the modulation of the conformational dynamics of FXR LBD by prenylflavonoids. Our findings indicate that prenylflavonoids represent an emerging class of potential selective bile acid receptor modulators (SBAMs) that may provide a scientific basis for utility of XN and related prenylflavonoids as dietary supplements in prevention and treatment of metabolic disorders.

## **4.3 Materials and Methods**

### **4.3.1 Materials**

Deuterium oxide (D<sub>2</sub>O, 99.9% deuterium) was obtained from Sigma-Aldrich Chemical Co. (St. Louis, MO). GW4064 and Z-guggulsterone were purchased from Tocris Bioscience (Bristol, UK). CDCA was purchased from Sigma-Aldrich (St. Louis, MO). The extractions

and/or syntheses of XN and its derivatives were completed by Dr. Fred J. Stevens research group (College of Pharmacy in Oregon State University, Corvallis, OR). Briefly, XN crystals were obtained by recrystallizing HPLC-purified material from an aqueous acetonitrile solution. X-ray crystal diffraction intensity data were collected by a Bruker Smart Apex CCD diffractometer at 173K using Mo $\alpha$ -radiation (0.71073 Å). XN-derived compounds were synthesized from 99% pure XN. Chemical structures of all compounds are shown in Fig. 1. Each compound has over 99% HPLC purity and was prepared as 10 mM stock solution in dimethylsulfoxide (DMSO).

#### 4.3.2 Protein expression and purification

Protein was expressed in *Escherichia coli* BL 21 (DE23) pLysS with a pET 15B vector encompassing residues L193 to Q472 which were grown in 2XYT medium with antibiotics (Ampicillin 150  $\mu$ g/mL, Chloramphenicol 35  $\mu$ g/mL) at 37°C to A<sub>600</sub> reached 0.6-0.8. The cells were allowed to grow for another four hours at 20°C with 0.8 mM IPTG (isopropyl-beta-D-thiogalactopyranoside) induction to produce an N-terminal Histidine (His6) tagged hFXR LBD and then harvested by centrifugation, washed and frozen at -80°C.

Isolated protein was purified by affinity chromatography on Clontech Talon Co<sup>2+</sup> polyhistidine affinity resins which was equilibrated with pH 7.3 buffer containing 50 mM sodium phosphate, 0.5 M NaCl, 0.5 mM CHAPS, 15 mM imidazole, and 0.5 M sucrose. The His6-tagged protein was eluted with imidazole from the Co<sup>2+</sup> resin until A<sub>280</sub> was less than 0.03. The protein fractions were analyzed by sodium dodecyl sulfate–acrylamide gel electrophoresis (SDS-PAGE). The purest fractions were pooled and incubated with thrombin for 48 hours at 4°C to remove the His6-tag. Subsequently, the protein was additionally purified by a Co<sup>2+</sup> resin column with and without imidazole to remove uncut His-tagged protein and the free His6Tag.

Purified hFXR LBD was collected and concentrated, aliquoted, snap-frozen in liquid nitrogen and stored at -80°C.

#### 4.3.4 Hydrogen/deuterium exchange mass spectrometry

The recombinant human FXR-LBD (15  $\mu$ L, 98  $\mu$ M) was equilibrated for 30 min in H<sub>2</sub>O buffer (in 50 mM sodium phosphate, 0.5 M NaCl, 0.5 mM CHAPS, 1 mM TCEP, 0.5 M sucrose, and 10% glycerol, pH 7.4) at room temperature in absence and presence of each ligand (0.5  $\mu$ L,  $\pm$ 10 mM ligand). The ratio of ligand to protein was kept at 3.2 as previously described (Chapter 3). The mass spectra of each peptide at different exchange time points were checked manually, and then their mass isotope distributions and elution time features were evaluated. There was no evidence that indicated existence of mixed exchange population in our HDX binding studies (Figure S4.1). To initiate the exchange-in reaction, 10-fold D<sub>2</sub>O buffer with the same composition as the above described H<sub>2</sub>O buffer was added to equilibrate apo protein and holo protein solutions. Exchange was quenched (pH 2.5, 0 C°) by adding 15  $\mu$ L 0.42% chilled phosphoric acid at different reaction time points. Liquid nitrogen was used to flash freeze all quenched samples for subsequent MS analysis. Experiments were performed in triplicate.

The quenched intact protein were loaded onto a Micro Trap<sup>TM</sup> C4 column (1 mm  $\times$  8 mm) and eluted with a fast 10-90% (v/v) B gradient in 12 min (solvent A: 0.1% HCOOH in H<sub>2</sub>O, solvent B: 0.1% HCOOH in CH<sub>3</sub>CN, flow rate 40  $\mu$ L/min). Deuterium level for global protein was measured by using an LCT ESI-ToF mass spectrometer. HDX information of peptic peptides was obtained by using a Synapt HDMS instrument equipped with a Waters HDX module enabling online peptic digestion and “cold” LC separation. Briefly, a Poroszyme® immobilized pepsin column (2.1 $\times$ 30 mm) was connected with LC system to digest intact protein with a 100  $\mu$ L/min solvent (0.05% HCOOH in H<sub>2</sub>O). The peptides were loaded onto an Acquity

BEH C18 VanGuard Pre-column (1.7  $\mu\text{m}$ , 2.1 x 5 mm) and separated via an Acquity UPLC® BEH C18 column (1.7  $\mu\text{m}$ , 1.0x100 mm) using the following LC gradient: 8% B to 40% in 6 minutes, held at 40% B for 1 minute, 40% B to 85% B in 0.5 minute, held at 85% B for 1 minute, 85% to 8% in 0.5 minute, and held at 8% B for 3 minutes, resulting in a 12 minutes total run time (using the same LC solvents as described above for intact protein analysis).

#### 4.3.5 HDX data analysis

The deuterium numbers of the intact protein were directly obtained from the mass difference between deuterated and nondeuterated protein. Protein mass spectra were analyzed using MassLynx 4.0 program (Waters Corporation). For obtaining peptide identifications, the raw data of the undeuterated samples were analyzed in the  $\text{MS}^E$  mode. ProteinLynx Global Server (PLGS) 2.4 software (Waters) was used for searching against an “in house” protein database to which the human FXR-LBD sequence was added. After database searching, a peptide list covering specific protein regions was produced. Peptides that resulted in mass spectra of high spectral quality and protein sequence coverage were chosen for the subsequently conducted HDX-MS studies. The deuterium uptake for each peptide and time point was derived by calculating the differences between the centroid of the deuterated peptide isotope distribution and the centroid of the undeuterated peptide isotope distribution. This data analysis step was supported by HDX Browser software (Waters) in conjunction with HX-Express software [18].

The deuterium number of each peptide was normalized to account for differences in peptide length by applying the following equation 4.1:

$$D\% = \left( \frac{m - m_0}{N} \right) \times 100\% \quad (4.1)$$

Where  $D\%$  is percentage of the deuterium in a peptide;  $m$  is deuterated peptide mass;  $m_0$  is undeuterated peptide mass;  $N$  is total number of the exchangeable amide hydrogens in a peptide. Because of the high reproducibility of the online pepsin UPLC setup and the comparative nature of this study we omitted to apply back exchange corrections in accord to other HDX-MS studies [19-21].

#### 4.3.6 Kinetic Modeling

A six-bin-fixed-rate-constant kinetic model was built by using R software where the sum of the square error was minimized. The relationship between deuterium uptake and exchange time can be described by equation 4.2 because the HDX reaction follows first-order kinetics [22].

$$D = \sum_i^n A_i [1 - \exp(-k_i t)] \quad (4.2)$$

where  $D$  is deuterium uptake;  $k_i$  is rate constant of deuterium exchange which is fixed to six values (six bins) ( 10, 1, 0.1, 0.01, 0.001, and 0.0001 min<sup>-1</sup>);  $A_i$  is amide hydrogen number in a specific bin;  $t$  is incubation time. All peptide deuterium uptake plots were fit with the above model to obtain local HDX kinetic profiles for the FXR LBD in presence of different ligands (Figure S1).

#### 4.3.7 The Hierarchical clustering analysis

The main principle of hierarchical clustering is to iteratively identify two ligands (or ligand groups) with a highest similarity for their local HDX profile by comparing their deuterium exchange-in level on each peptide, and cluster them into a ligand group, until all ligands are clustered into a single group. Initially, each ligand is assigned to its own cluster and then the algorithm proceeds iteratively, at each stage joining the two most similar clusters, continuing

until there is just a single cluster. At each stage distances between clusters are recomputed using the complete linkage, i.e., the distance between those two elements (one in each cluster) that are farthest away from each other. A combination of a heat map with a dendrogram is used to illustrate the arrangement of the clusters produced by the hierarchical clustering.

#### **4.3.8 Molecular docking study**

The 3D-coordinates of the FXR-LBD in complex with 3-deoxy-CDCA were retrieved from PDB ID 1OT7 [23] and energetically minimized in the internal coordinate space with Molsoft [24]. For clarity, the numbers of the relevant amino acids in PDB ID 1OT7 file, Arg328, Ser329, and Tyr366, have been adjusted as Arg331, Ser332, and Tyr369 (UniRef100\_B6ZGS9). Molecular docking was run against the ligand binding pocket of the FXR-LBD as previously reported [24-27]. In the ICM-VLS (Molsoft ICM) screening procedure, the ligand scoring is optimized to obtain maximal separation between binders and non-binders. Each compound is assigned a score according to its fit within the receptor, and this score accounts for continuum and discreet electrostatics, hydrophobicity, and entropy parameters [28]. The docking protocol was initially validated by docking 3-deoxy-CDCA into the FXR-LBD. The agonist docked with a score of -26.63 reproducing the crystallographic binding pose involving interactions with residues Arg331, Ser332, and Tyr369 [23].

### **4.4 Results**

#### **4.4.1 HDX-MS analysis of intact protein provides indication of molecular recognition of prenylflavonoids by FXR LBD**

To determine the effects of bindings of the four prenylflavonoid compounds on the global structural dynamics of FXR-LBD, we performed HDX-MS studies of the FXR-LBD. The sum of

the exchangeable amide hydrogens in FXR-LBD construct used in this study is 274. Figure 4.2 depicts the global deuterium uptake plots for the apo protein and the FXR-LBD in presence of the prenylflavonoid ligands. Comparison of the global deuterium uptake between the apo protein and the protein in presence of the ligand indicated retardation of exchange of approximately 10 amide hydrogen. The observed exchange protection pointed to an increase in structural compactness, loss of conformational flexibility, and/or decrease of global solvent accessibility upon ligand interaction. This let us to speculate that the prenylflavonoids indeed directly interact with the FXR LBD, and thereby induce conformational stabilization.

#### **4.4.2 Peptide-level HDX protection profiles of FXR-LBD in presence of prenylflavonoid ligands**

Twenty peptides with high quality covering over 85% of the amino acid sequence were chosen for determining deuterium uptake levels in the different protein systems tested. Peptic peptides HDX profiles of holo FXR-LBD are presented in Figure 3. The peptides encompassing the amino acid residues 201-222, 229-241, 256-268, 269-278, 337-347, and 454-465 reached maximum deuterium uptake level of observable exchange in 30 seconds and deuterium uptake became relatively constant for the following time points. Regions that are highly solvent exposed, disordered and/or conformationally highly flexible without stabilizing hydrogen bonding networks commonly exhibit this type of deuterium exchange pattern. It is noteworthy that in the FXR-LBD-3-deoxy-CDCA complex crystal structure (PDB ID 1OT7) no secondary structure was assigned to the regions encompassing residues 264-266, 277-278, 339-341, 454-456, and 459-462. Our observations that the deuterium uptake level of these regions exhibited no differences in deuterium uptake levels when compared to that of the apo protein is in accord with the absence of these regions in the cocrystal structure of FXR-LBD-3-deoxy-CDCA complex



likely due to their conformational flexibilities (Figure 4.4). These results are consistent with the limitation of X-ray structural analysis technique that regions with high mobility in proteins often result in large errors during data collections so that it is not feasible to give an accuracy interpretation [29].

Comparison of peptide-level HDX protection profiles revealed that each tested prenylflavonoid induced statistically significant protection in the following regions: 288-298, 320-336 , and 361-375 (Figure 4) which is consistent with that these peptides are involved in forming the typical canonical ligand binding cavity in FXR-LBD. In presence of ligands, exchanges in those regions were retarded indicating stabilization of the conformational properties and/or reduced solvent accessibility caused by ligand interaction. The exchange protection upon ligand interaction was observed for peptide 288-298, which is part of helix 3 and involved in the coordination of ligands as shown in two crystal structures of FXR-LBD-ligand complexes (PDB ID 1OSH and 1OSV). Exchange protection was also observed for the region 348-360 in presence of 8-PN and TX (Figure 4.4). For the regions that displayed retarded exchange in presence of ligand, kinetic modeling results (Table S4.2) revealed that the distribution of the amide hydrogens in the six bins was rearranged in presence of the ligands. Compared to the apo protein, ligand binding decreased the number of the amide hydrogens in the ‘fast exchange rate’ bins ( $k = 10$  and  $1 \text{ min}^{-1}$ ) while the number of amide hydrogen that were grouped into the ‘medium’ ( $k = 0.1$  and  $0.01 \text{ min}^{-1}$ ) and the ‘low exchange rate’ bins ( $k = 0.001$  and  $0.0001 \text{ min}^{-1}$ ) increased (Table S4.2).

## 4.5 Discussion

Comparison of the HDX protection profile of XN and TX was used to decipher the possible effect caused by covalent modification of XN, an electrophile with the potential to

alkylate nucleophilic groups in FXR LBD (Figure 4.4). MS data analysis showed that multiple XN molecules can covalently bind with FXR-LBD (Figure S4.3), possibly by a Michael addition reaction involving the  $\alpha$ ,  $\beta$  unsaturated carbonyl group (C=O) of XN and SH functional groups cysteine residue. A comparison of the HDX protection profile (Figure 4.4) showed that the binding of XN and TX resulted in exchange protection in the following regions: 288-298 (helix 3), 320-328 (helix 6), 328-336 (helix 6), 348-360 (helix 7), 361-367 (helix 8), and 368-375 (helix 8); all are part of the ligand binding pocket in FXR-LBD.

Our molecular docking study demonstrated that XN and TX were able to dock into the ligand binding pocket of the FXR-LBD with similar scores (Table 4.1), and that both compounds revealed the same pattern of non-covalent interactions established by the agonist 3-deoxy-CDCA [23]. Both ligands, similar to 3-deoxy-CDCA, interact with the side chain of residues Arg331, Ser332, and Tyr369 involving their 4-hydroxyphenyl and 2-OH groups, respectively (Figure 4.6). Overall our data suggested that the covalent binding of XN with FXR-LBD has no effect on XN binding in FXR-LBD. Notably, this type of irreversible binding between nuclear receptor and ligand has been considered as an indispensable requirement for Peroxisome Proliferator-Activated Receptor  $\gamma$  (PPAR $\gamma$ ) activation by natural ligands [30, 31]. Further experiments should be completed to test whether covalent binding between XN and FXR-LBD plays a role in directly or indirectly regulating expression of FXR target genes.

To further evaluate how the interactions of the ligands affect the conformational properties of the FXR LBD, we attempted to find specific binding sites between prenylflavonoid molecules and the FXR-LBD by molecular docking studies. Data integration of HDX and docking is demonstrated in Figure 4.6. The average differences in percentage of deuterium level for the four ligand-bound FXR complexes relative to the apo-protein were overlaid on the X-ray

crystal structure of the FXR-LBD bound to 3-D-CDCA (PDB ID 1OT7) (Fig. 4.6F, G, H, and I, data compiled in Table S4.1). The HDX profiles of all prenylflavonoids indicated decreased deuterium incorporation in the following regions: 288-298 (helix 3), 320-336 (helix 6), and 361-375 (helix 8), which are all involved in forming of the FXR ligand binding cavity (Figure 4.4 and 4.6). The docking data suggested, similar to 3-D-CDCA, the 4-hydroxyphenyl and 2-OH groups in XN and TX could interact with the side chain of residues Arg331, Ser332, and Tyr369 via the hydrogen bonds (Figure 4.6B and C), and two amino acids Arg332 and Tyr369 also could form hydrogen bonding interactions with the carbonyl group (C=O) in IX and 8PN (Figure 4.6D and E). Additionally, each prenylflavonoid molecule docked with a favorable energy (negative scores in Table 4.1). These results suggested that prenylflavonoid-type compounds, like other FXR ligands, shared similar binding sites and were able to occupy the canonical ligand binding pocket of the FXR-LBD. XN has been described as a potential ligand of the FXR in 2005 [15], after that, no further experimental evidence was reported to further promote the role of XN as a natural ligand acting on FXR. The results reported here provided direct evidence that prenylflavonoid-type compounds could function as FXR ligands.

Interestingly, our cluster analysis showed that GG and CDCA induced very similar conformational changes for the FXR-LBD (Figure 4.5) with a major difference that only GG showed slightly but statistically significant protection for two regions: 201-222 and 229-241. While amino acid sequence 197-241 [32] in the FXR located in the hinge region between the DNA binding domain and the LBD has been claimed to involve heterodimer formation with retinoid X receptor (RXR), and/or interaction between FXR and its target genes [4, 33]. The regulative role of the hinge region in FXR's physiological function might be a reasonable

explanation why GG, as an *in vitro* antagonist of the FXR, has no antagonistic effects for FXR target genes *in vivo* [34].

#### 4.6 Conclusion

This study provides the first direct evidence that XN and related prenylflavonoids are FXR ligands and are endowed with a structural scaffold that allows targeting the classical FXR LBD. We reported the binding of four prenylflavonoid-type compounds (XN, IX, 8-PN, and TX) to the FXR-LBD by means of HDX-MS and molecular docking. In addition, the data suggest that it is possible, starting from the metabolically unstable compound (XN), to obtain a more stable derivative (TX) with the same binding properties. Cluster analysis based on ligand-induced HDX fingerprints was successfully applied to classify ligands into different groups and extended the list of HDX-enabled nuclear receptor ligand binding studies in which this approach was successfully applied [35, 36]. The current findings promote further research to explore the potential of prenylflavonoids as ligands of FXR. We foresee that prenylflavonoids and other dietary polyphenols [37, 38] may serve as future leads in the development of new synthetic FXR ligands for prevention and treatment of lipid disorders and metabolic syndrome.

## **ACKNOWLEDGEMENT**

This research was supported in part by Grants S10RR025628 and P30ES000210 from the National Institutes of Health.

## **Supporting Information Available**

The supporting information includes mass spectra for peptides demonstrating evolution of deuterium incorporation into peptic peptides (Figure S4.1); deuterium incorporation curves for each peptide for all system studied (Figure S4.2); the covalent modification of XN with the FXR-LBD (Figure S4.3); a tabular compilation of the HDX data used for the differential HDX analyses (Table S4.1), the kinetic results derived by our kinetic model (Table S4.2), and average deuterium exchange-in levels for each peptides (Table S4.3).

**Tables**

**Table 4.1.** ICM Docking score data into the ligand binding pocket of the human FXR-LBD.

## Figure Legend

**Figure 4.1.** Chemical structures of the prenylflavonoids used in the present study.

**Figure 4.2** Global HDX uptake plots for the apo FXR-LBD in comparison to the FXR-LBD in presence of ligands. For each ligand tested HDX-MS analysis was conducted in triplicate, and the error bars represent the standard deviation.

**Figure 4.3.** Peptic peptides HDX profiles of the holo FXR-LBD. Deuterium exchange-in percentage is shown at different reaction time points (0.5, 1, 2, 5, 10, 30, and 60 min, from left to right) for each peptide.

**Figure 4.4.** Comparison of the HDX protection profiles at the peptide level.

Deuterium exchange-in percentage difference between apo and holo FXR-LBD is shown at different reaction time points (0.5, 1, 2, 5, 10, 30, and 60 min, from left to right) for each peptide.

**Figure 4.5.** Cluster analysis of the HDX data for seven FXR-LBD-bound complexes.

The deuterium exchange-in level is from low to high and color-coded from red to green.

**Figure 4.6.** Top row: Detailed view of the hydrogen bonds formed between ligands and protein. Docking of (A) TX, (B) XN, (C) IX, and (D) 8PN in human FXR-LBD (PDB 1OT7, Molsoft ICM). Docked ligands are displayed as sticks and colored by atom type, with carbon atoms in magenta (XN), orange (TX), cyan (IX) and white (8PN); protein residues are displayed as stick with the carbon atoms colored in green. Secondary structure is displayed as ribbon. Protein-ligand hydrogen binding interactions are displayed as dashed black lines.

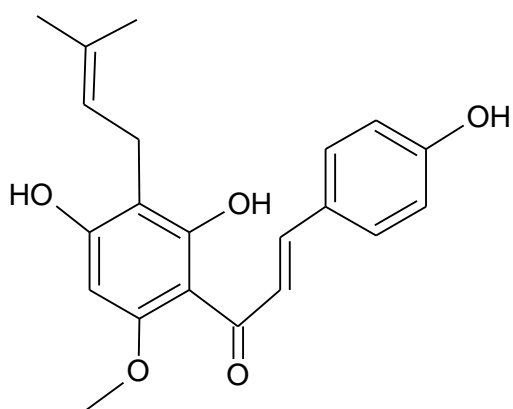
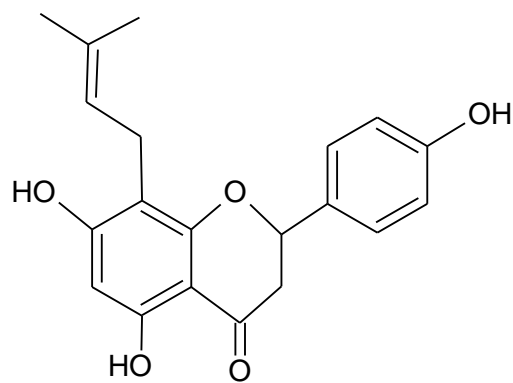
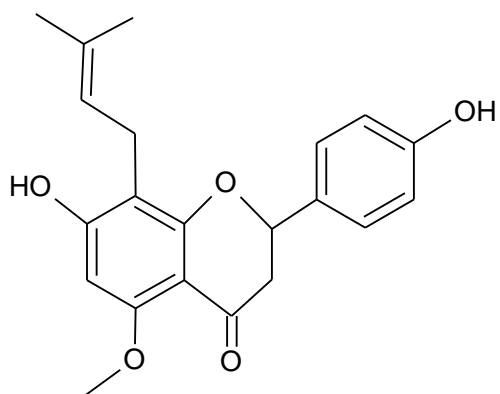
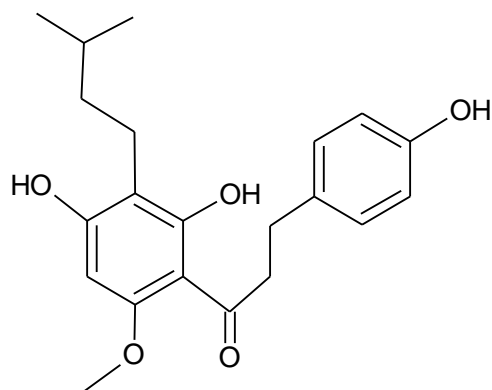
Bottom row: Average differences in deuterium percentage (D%) of seven time points (0.5, 1, 2, 5, 10, 30, and 60 min) are mapped onto the crystal structure of FXR-LBD-ligand complex, PDB ID 1OT7. Regions uncovered by the current experiments are depicted in grey. NS, “not significant”.

Table 4.1

Ligand	Docking Score
3-D-CDCA	-26.63
XN	-22.38
TX	-22.03
IX	-11.73
8-PN	-10.83

Table 4.1 ICM Docking score data into ligand binding pocket of the human FXR-LBD.



**Figure 4.1****Xanthohumol (XN)****8-Prenylnaringenin (8-PN)****Isoxanthohumol (IX)****Tetrahydroxanthohumol (TX)****Figure 4.1** Chemical structures of the prenylflavonoids used in the present study

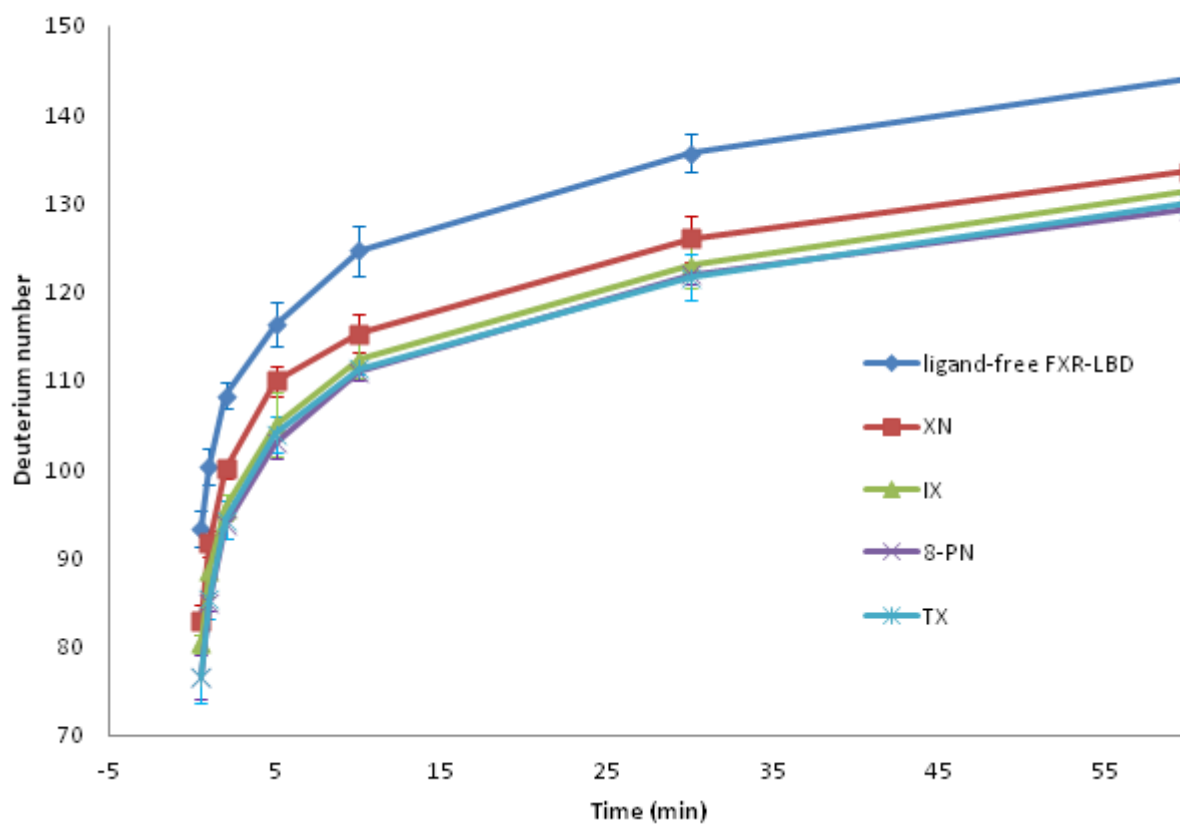
**Figure 4.2**

Figure 4.2 Global HDX uptake plots for the apo FXR-LBD in comparison to the FXR-LBD in presence of ligands.

Figure 4.3

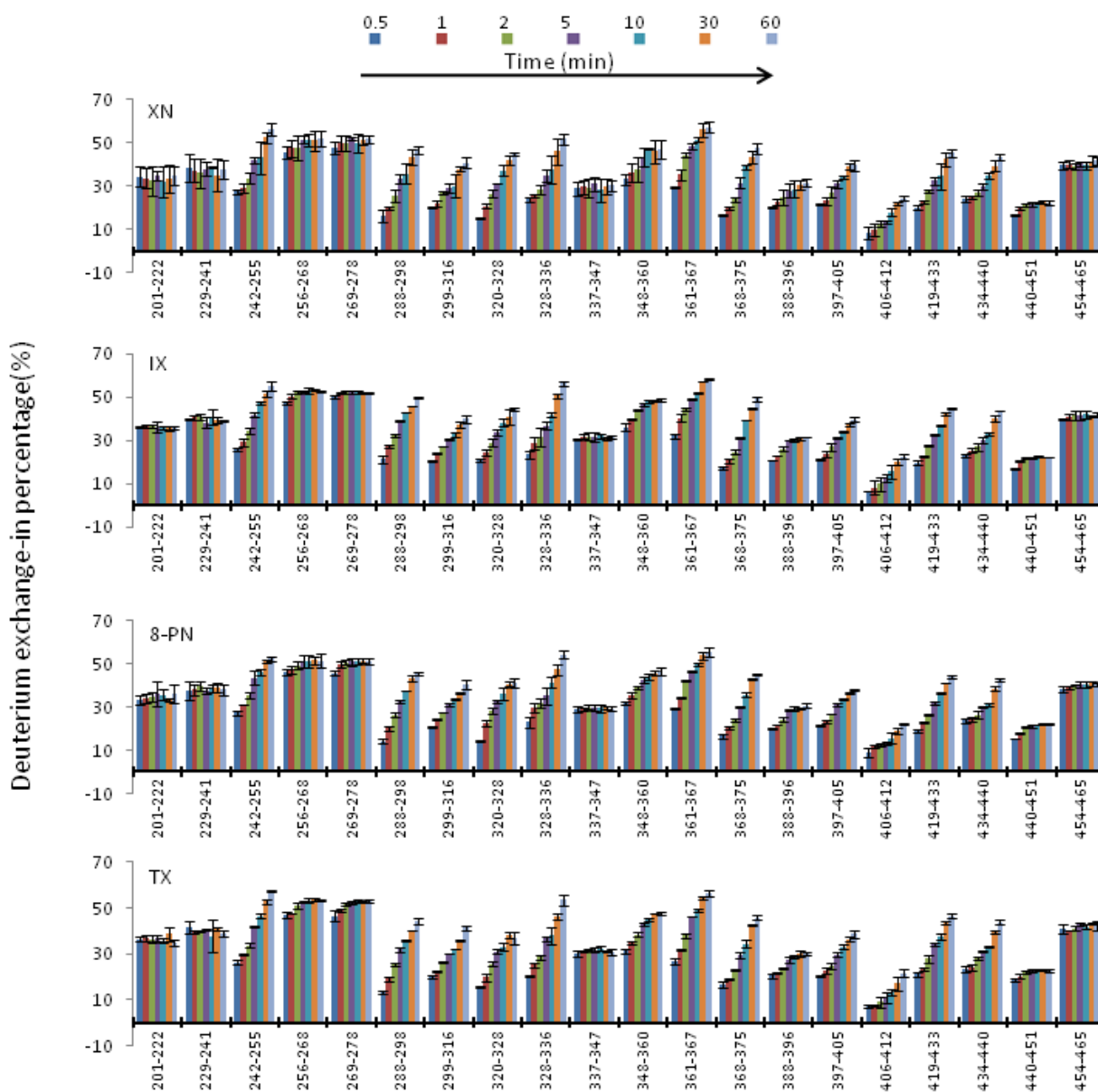


Figure 4.3 Peptic peptides HDX profiles of the holo FXR-LBD

Figure 4.4

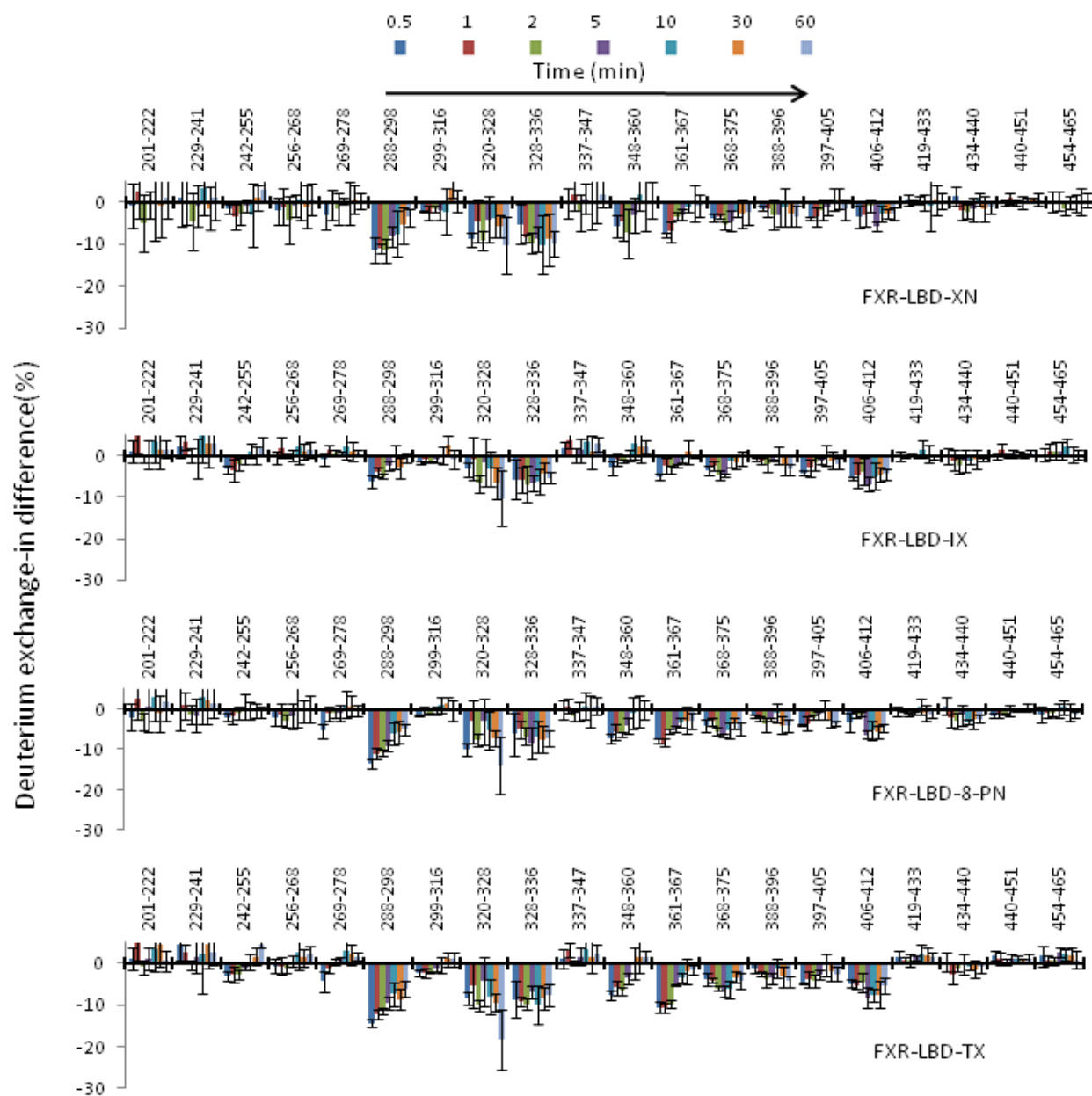


Figure 4.4 Comparison of the HDX protection profiles at the peptide level

Figure 4.5

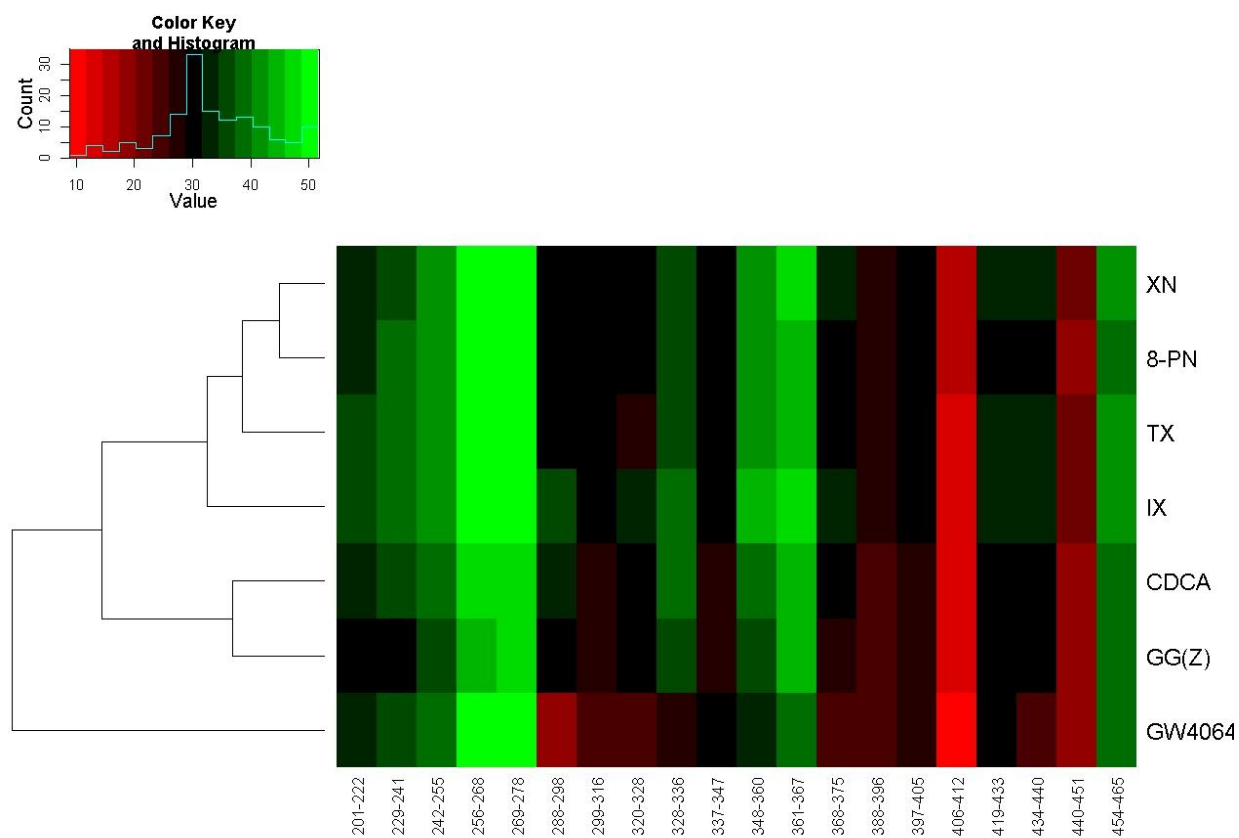


Figure 4.5 Cluster analysis of the HDX data for seven FXR-LBD-bound complexes

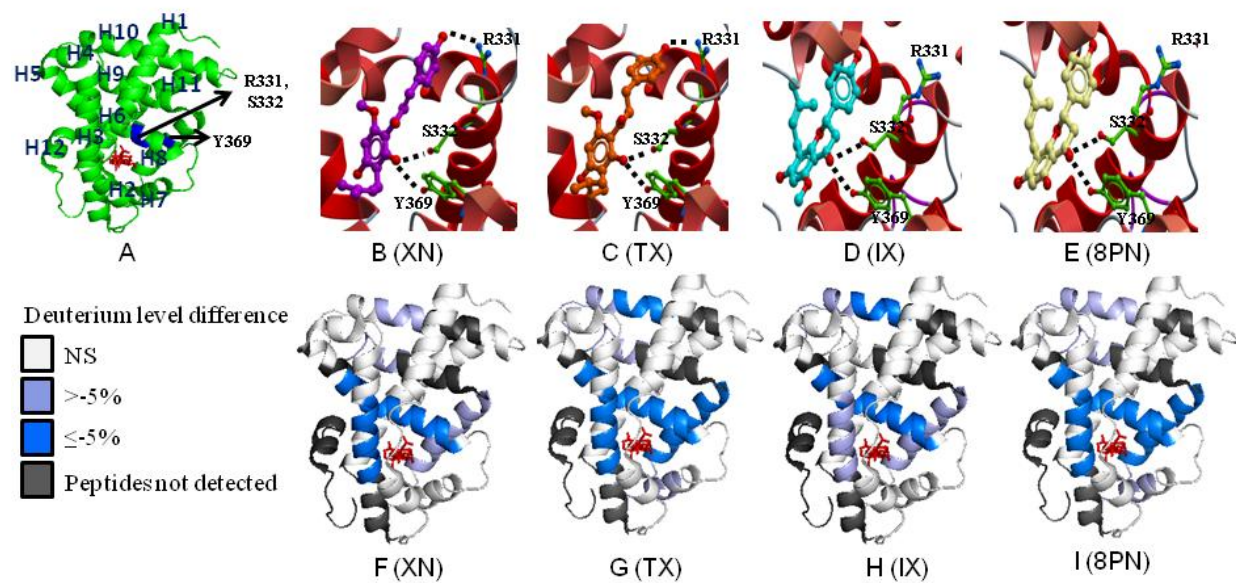
**Figure 4.6**

Figure 4.6 Top row: Detailed view of the hydrogen bonds formed between ligands and protein  
 Bottom row: Average differences in deuterium percentage (D%) of seven time points

## 4.7 Reference

- [1] A. Mencarelli, S. Fiorucci, FXR an emerging therapeutic target for the treatment of atherosclerosis, *J Cell Mol Med*, 14 (2010) 79-92.
- [2] B. Goodwin, S.A. Jones, R.R. Price, M.A. Watson, D.D. McKee, L.B. Moore, C. Galardi, J.G. Wilson, M.C. Lewis, M.E. Roth, P.R. Maloney, T.M. Willson, S.A. Kliewer, A regulatory cascade of the nuclear receptors FXR, SHP-1, and LRH-1 represses bile acid biosynthesis, *Mol Cell*, 6 (2000) 517-526.
- [3] K. Ma, P.K. Saha, L. Chan, D.D. Moore, Farnesoid X receptor is essential for normal glucose homeostasis, *J Clin Invest*, 116 (2006) 1102-1109.
- [4] Y. Zhang, H.R. Kast-Woelbern, P.A. Edwards, Natural structural variants of the nuclear receptor farnesoid X receptor affect transcriptional activation, *J Biol Chem*, 278 (2003) 104-110.
- [5] H. Wang, J. Chen, K. Hollister, L.C. Sowers, B.M. Forman, Endogenous bile acids are ligands for the nuclear receptor FXR/BAR, *Mol Cell*, 3 (1999) 543-553.
- [6] M. Makishima, A.Y. Okamoto, J.J. Repa, H. Tu, R.M. Learned, A. Luk, M.V. Hull, K.D. Lustig, D.J. Mangelsdorf, B. Shan, Identification of a nuclear receptor for bile acids, *Science*, 284 (1999) 1362-1365.
- [7] D.J. Parks, S.G. Blanchard, R.K. Bledsoe, G. Chandra, T.G. Consler, S.A. Kliewer, J.B. Stimmel, T.M. Willson, A.M. Zavacki, D.D. Moore, J.M. Lehmann, Bile acids: natural ligands for an orphan nuclear receptor, *Science*, 284 (1999) 1365-1368.
- [8] D. Merk, D. Steinhilber, M. Schubert-Zsilavecz, Medicinal chemistry of farnesoid X receptor ligands: from agonists and antagonists to modulators, *Future Med Chem*, 4 (2012) 1015-1036.
- [9] J.F. Stevens, J.E. Page, Xanthohumol and related prenylflavonoids from hops and beer: to your good health!, *Phytochemistry*, 65 (2004) 1317-1330.
- [10] C. Gerhauser, A. Alt, E. Heiss, A. Gamal-Eldeen, K. Klimo, J. Knauft, I. Neumann, H.R. Scherf, N. Frank, H. Bartsch, H. Becker, Cancer chemopreventive activity of Xanthohumol, a natural product derived from hop, *Mol Cancer Ther*, 1 (2002) 959-969.
- [11] A. Hartkorn, F. Hoffmann, H. Ajamieh, S. Vogel, J. Heilmann, A.L. Gerbes, A.M. Vollmar, S. Zahler, Antioxidant effects of xanthohumol and functional impact on hepatic ischemia-reperfusion injury, *J Nat Prod*, 72 (2009) 1741-1747.
- [12] Y.M. Lee, K.H. Hsieh, W.J. Lu, H.C. Chou, D.S. Chou, L.M. Lien, J.R. Sheu, K.H. Lin, Xanthohumol, a Prenylated Flavonoid from Hops (*Humulus lupulus*), Prevents Platelet Activation in Human Platelets, *Evid Based Complement Alternat Med*, 2012 (2012) 852362.

- [13] N. Tabata, M. Ito, H. Tomoda, S. Omura, Xanthohumols, diacylglycerol acyltransferase inhibitors, from *Humulus lupulus*, *Phytochemistry*, 46 (1997) 683-687.
- [14] A. Casaschi, G.K. Maiyoh, B.K. Rubio, R.W. Li, K. Adeli, A.G. Theriault, The chalcone xanthohumol inhibits triglyceride and apolipoprotein B secretion in HepG2 cells, *J Nutr*, 134 (2004) 1340-1346.
- [15] H. Nozawa, Xanthohumol, the chalcone from beer hops (*Humulus lupulus* L.), is the ligand for farnesoid X receptor and ameliorates lipid and glucose metabolism in KK-A(y) mice, *Biochem Biophys Res Commun*, 336 (2005) 754-761.
- [16] J.Y. Yang, M.A. Della-Fera, S. Rayalam, C.A. Baile, Effect of xanthohumol and isoxanthohumol on 3T3-L1 cell apoptosis and adipogenesis, *Apoptosis*, 12 (2007) 1953-1963.
- [17] X. Yan, C.S. Maier, Hydrogen/deuterium exchange mass spectrometry, *Methods Mol Biol*, 492 (2009) 255-271.
- [18] D.D. Weis, J.R. Engen, I.J. Kass, Semi-automated data processing of hydrogen exchange mass spectra using HX-Express, *J Am Soc Mass Spectrom*, 17 (2006) 1700-1703.
- [19] J.B. Sperry, R.Y. Huang, M.M. Zhu, D.L. Rempel, M.L. Gross, Hydrophobic Peptides Affect Binding of Calmodulin and Ca as Explored by H/D Amide Exchange and Mass Spectrometry, *Int J Mass Spectrom*, 302 (2011) 85-92.
- [20] C.H. Parker, C.R. Morgan, K.D. Rand, J.R. Engen, J.W. Jorgenson, D.W. Stafford, A Conformational Investigation of Propeptide Binding to the Integral Membrane Protein gamma-Glutamyl Carboxylase Using Nanodisc Hydrogen Exchange Mass Spectrometry, *Biochemistry*, 53 (2014) 1511-1520.
- [21] R.Y. Huang, J. Wen, R.E. Blankenship, M.L. Gross, Hydrogen-deuterium exchange mass spectrometry reveals the interaction of Fenna-Matthews-Olson protein and chlorosome CsmA protein, *Biochemistry*, 51 (2012) 187-193.
- [22] S.W. Englander, N.R. Kallenbach, Hydrogen exchange and structural dynamics of proteins and nucleic acids, *Q Rev Biophys*, 16 (1983) 521-655.
- [23] L.Z. Mi, S. Devarakonda, J.M. Harp, Q. Han, R. Pellicciari, T.M. Willson, S. Khorasanizadeh, F. Rastinejad, Structural basis for bile acid binding and activation of the nuclear receptor FXR, *Mol Cell*, 11 (2003) 1093-1100.
- [24] P. Rajendran, A.I. Kidane, T.W. Yu, W.M. Dashwood, W.H. Bisson, C.V. Lohr, E. Ho, D.E. Williams, R.H. Dashwood, HDAC turnover, CtIP acetylation and dysregulated DNA damage signaling in colon cancer cells treated with sulforaphane and related dietary isothiocyanates, *Epigenetics*, 8 (2013) 612-623.



- [25] M.A. Neves, M. Totrov, R. Abagyan, Docking and scoring with ICM: the benchmarking results and strategies for improvement, *J Comput Aided Mol Des*, 26 (2012) 675-686.
- [26] R. Abagyan, M. Totrov, Biased probability Monte Carlo conformational searches and electrostatic calculations for peptides and proteins, *J Mol Biol*, 235 (1994) 983-1002.
- [27] R. Abagyan, M. Totrov, and D. Kuznetsov. , ICM - A new method for protein modeling and design: applications to docking and structure prediction from the distorted native conformation, *J Comput Chem*, 15 (1994) 488-506.
- [28] M. Totrov, Abagyan, R., Derivation of sensitive discrimination potential for virtual ligand screening proceedings of RECOMB99  
in: ACM, Lyon, France, 1999, pp. 312-320.
- [29] K.R. Acharya, the advantages and limitations of protein crystal structure, *Trends in pharmacological sciences*, 26 (2005) 10-14.
- [30] T. Waku, T. Shiraki, T. Oyama, Y. Fujimoto, K. Maebara, N. Kamiya, H. Jingami, K. Morikawa, Structural insight into PPARgamma activation through covalent modification with endogenous fatty acids, *J Mol Biol*, 385 (2009) 188-199.
- [31] T. Shiraki, N. Kamiya, S. Shiki, T.S. Kodama, A. Kakizuka, H. Jingami, Alpha,beta-unsaturated ketone is a core moiety of natural ligands for covalent binding to peroxisome proliferator-activated receptor gamma, *J Biol Chem*, 280 (2005) 14145-14153.
- [32] S. Caron, C. Huaman Samanez, H. Dehondt, M. Ploton, O. Briand, F. Lien, E. Dorchies, J. Dumont, C. Postic, B. Cariou, P. Lefebvre, B. Staels, Farnesoid X receptor inhibits the transcriptional activity of carbohydrate response element binding protein in human hepatocytes, *Mol Cell Biol*, 33 (2013) 2202-2211.
- [33] A.Q. Sun, Y. Luo, D.S. Backos, S. Xu, N. Balasubramaniyan, P. Reigan, F.J. Suchy, Identification of functionally relevant lysine residues that modulate human farnesoid X receptor activation, *Mol Pharmacol*, 83 (2013) 1078-1086.
- [34] R. Deng, D. Yang, A. Radke, J. Yang, B. Yan, The hypolipidemic agent guggulsterone regulates the expression of human bile salt export pump: dominance of transactivation over farsenoid X receptor-mediated antagonism, *J Pharmacol Exp Ther*, 320 (2007) 1153-1162.
- [35] S.Y. Dai, T.P. Burris, J.A. Dodge, C. Montrose-Rafizadeh, Y. Wang, B.D. Pascal, M.J. Chalmers, P.R. Griffin, Unique ligand binding patterns between estrogen receptor alpha and beta revealed by hydrogen-deuterium exchange, *Biochemistry*, 48 (2009) 9668-9676.
- [36] S.Y. Dai, M.J. Chalmers, J. Bruning, K.S. Bramlett, H.E. Osborne, C. Montrose-Rafizadeh, R.J. Barr, Y. Wang, M. Wang, T.P. Burris, J.A. Dodge, P.R. Griffin,

Prediction of the tissue-specificity of selective estrogen receptor modulators by using a single biochemical method, *Proc Natl Acad Sci U S A*, 105 (2008) 7171-7176.

[37] Josep Maria Del Bas<sup>1</sup>, Marie-Louise Ricketts<sup>2</sup>, Montserrat Vaqué<sup>1</sup>, Esther Sala<sup>1</sup>, Helena Quesada<sup>1</sup>, Anna Ardevol<sup>1</sup>, M. Josepa Salvadó<sup>1</sup>, Mayte Blay<sup>1</sup>, Lluís Arola<sup>1</sup>, David D. Moore<sup>2</sup>, Gerard Pujadas<sup>1</sup>, J.F.-L. and, C. Bladé<sup>1</sup>, Dietary procyanidins enhance transcriptional activity of bile acid-activated FXR in vitro and reduce triglyceridemia in vivo in a FXR-dependent manner, *Molecular Nutrition & Food Research*, 53 (2009) 805-814.

[38] G. Li, W. Lin, J.J. Araya, T. Chen, B.N. Timmermann, G.L. Guo, A tea catechin, epigallocatechin-3-gallate, is a unique modulator of the farnesoid X receptor, *Toxicol Appl Pharmacol*, 258 (2012) 268-274.

#### 4.8 Supplementary data

##### **Probing human FXR LBD – prenylflavonoid interactions by hydrogen/deuterium exchange mass spectrometry**

Liping Yang<sup>1</sup>, David Broderick<sup>1</sup>, Yan Campbell<sup>4,6</sup>, Adrian F. Gombart<sup>4,6</sup>, J. Fred Stevens<sup>4,5</sup>, Victor Hsu<sup>5</sup>, Yuan Jiang<sup>3</sup>, William H. Bisson<sup>2\*</sup> and Claudia S. Maier<sup>1\*</sup>

Department of Chemistry<sup>1</sup>, Oregon State University, Corvallis, OR 97331

Department of Environmental and Molecular Toxicology<sup>2</sup>, Oregon State University,  
Corvallis, OR 97331

Department of Statistics<sup>3</sup>, Oregon State University, Corvallis, OR 97331

Linus Pauling Institute<sup>4</sup>, Oregon State University, Corvallis, OR 97331

Department of Pharmaceutical Science<sup>5</sup>, Oregon State University, Corvallis, OR 97331

Department of Biochemistry and Biophysics<sup>6</sup>, Oregon State University, Corvallis, OR  
97331

Corresponding authors:

Claudia S. Maier (HDX-MS)

Email: [claudia.maier@oregonstate.edu](mailto:claudia.maier@oregonstate.edu)

Phone: +1-541-737-9533; Fax: +1-541-737-2062

William Bisson (Computational Modeling)

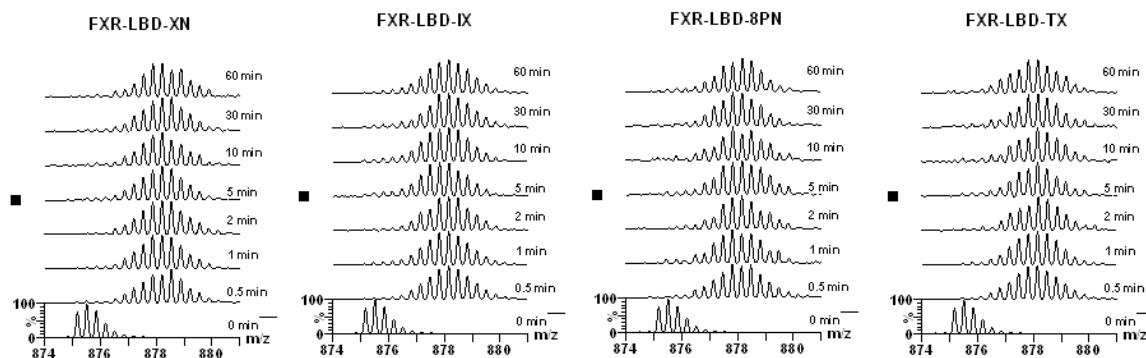
Email: [William.bisson@oregonstate.edu](mailto:William.bisson@oregonstate.edu)

Phone: +1-541-737-5735

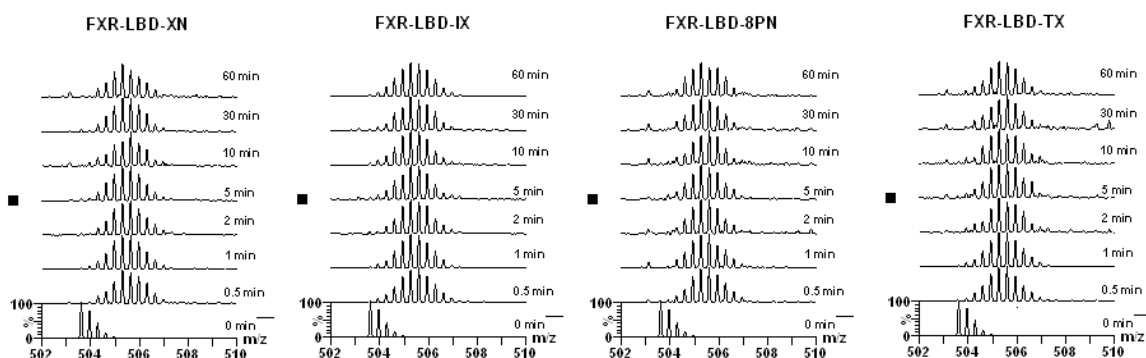
Figure S4.1 Mass spectra for peptides demonstrating evolution of deuterium incorporation into peptic peptides.

The partial sequence of each peptide is depicted at the top of each panel. Deuteration times (0, 0.5, 1, 2, 5, 10, 30, 60 mins) are denoted in each panel.

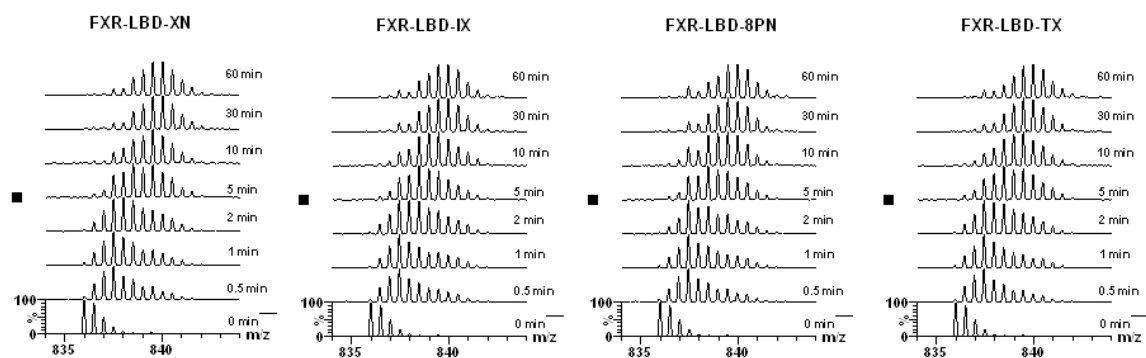
201-222



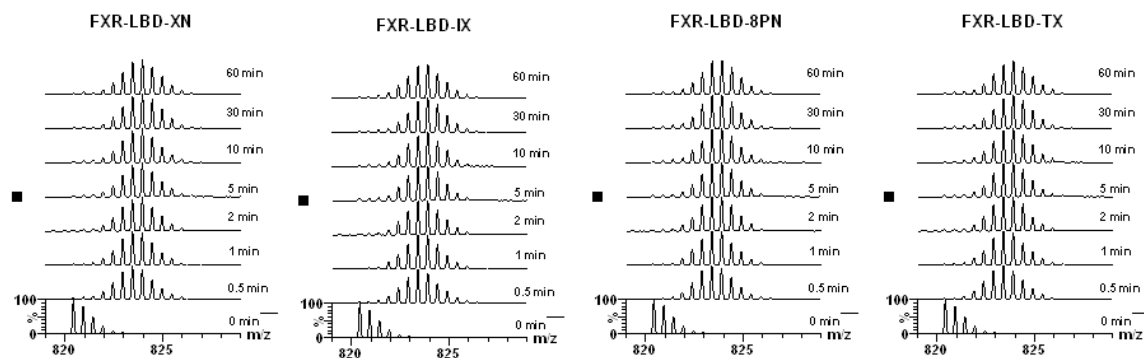
229-241



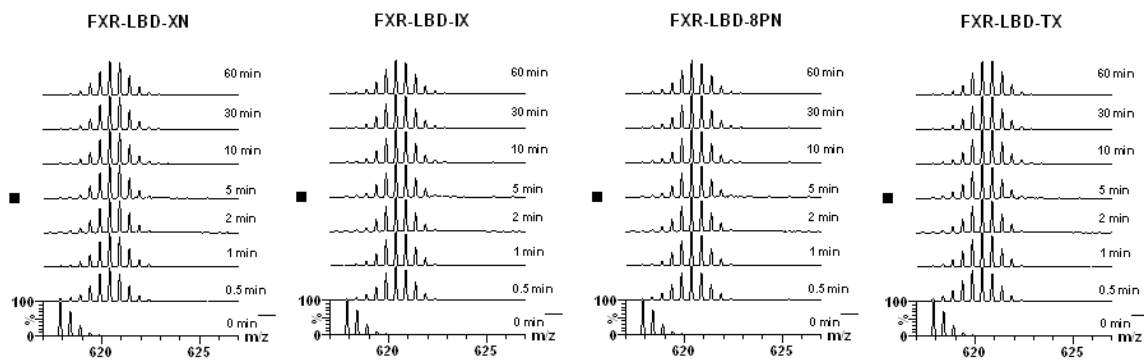
242-255



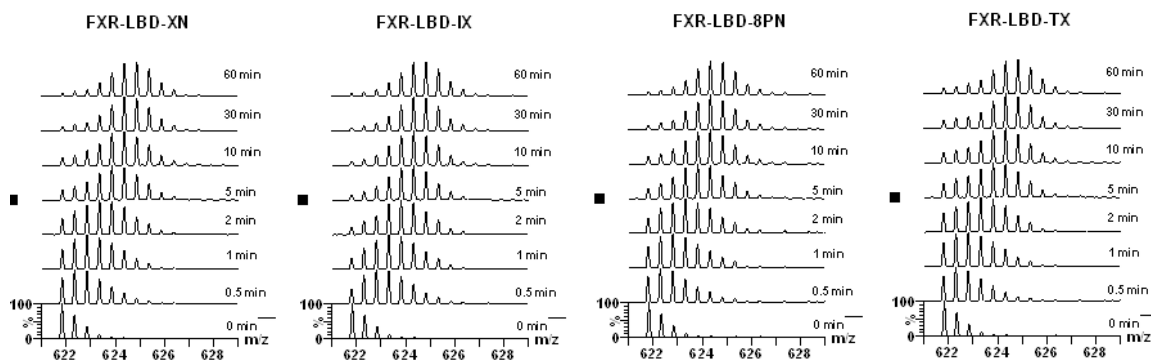
256-268



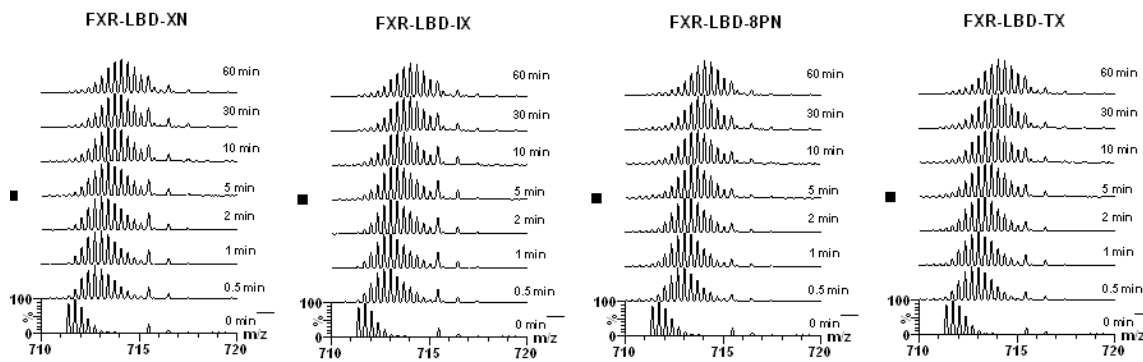
269-278



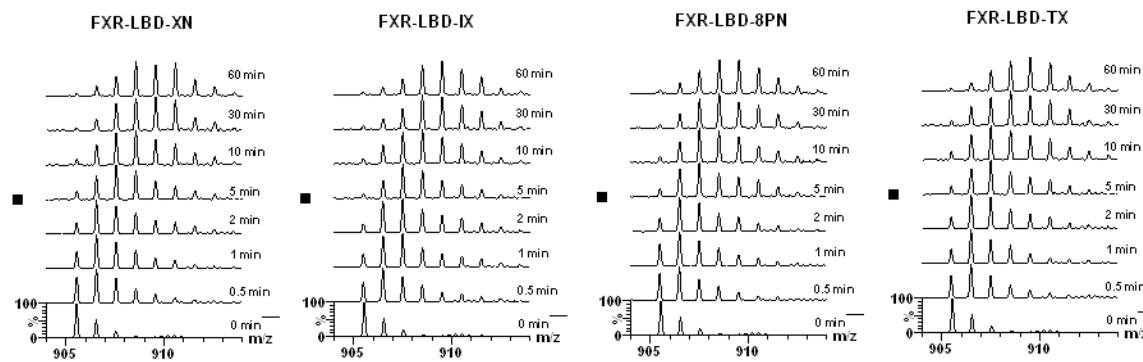
288-298



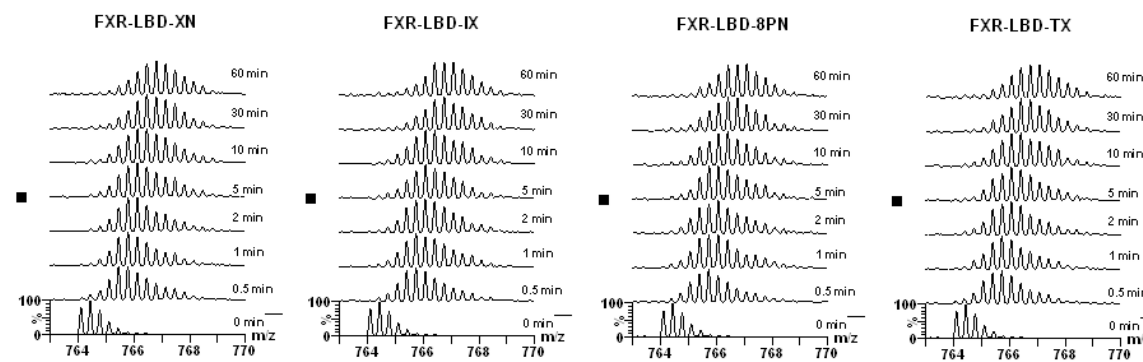
299-316



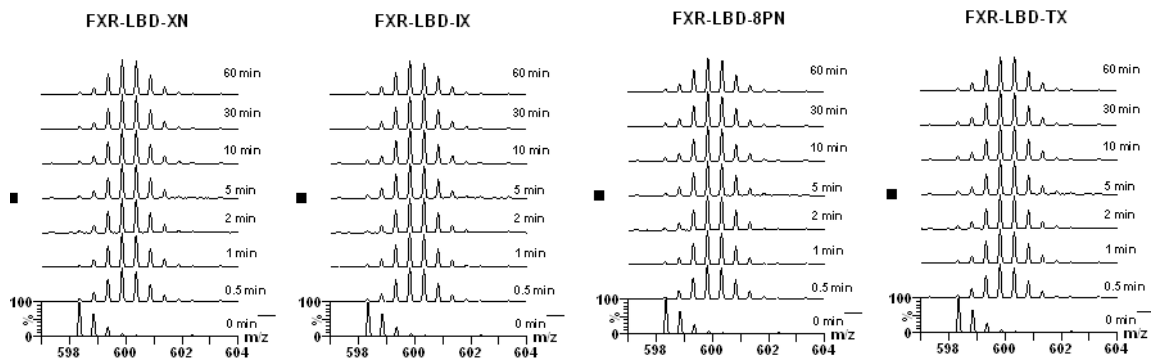
320-328



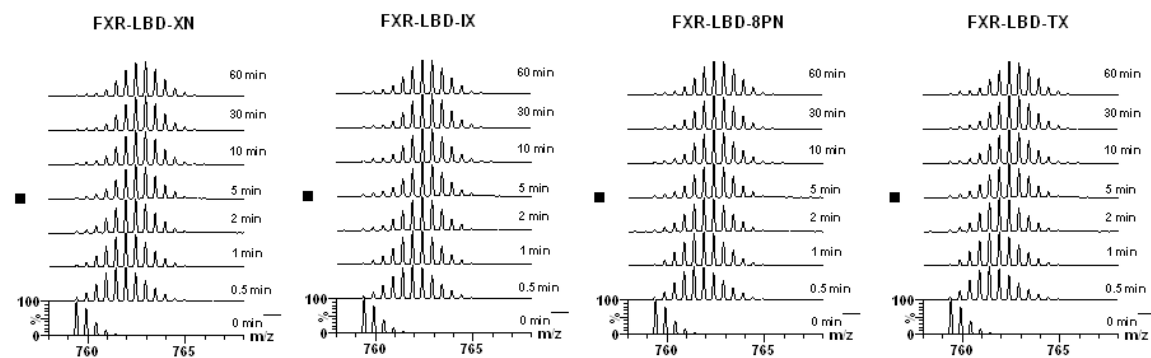
328-347



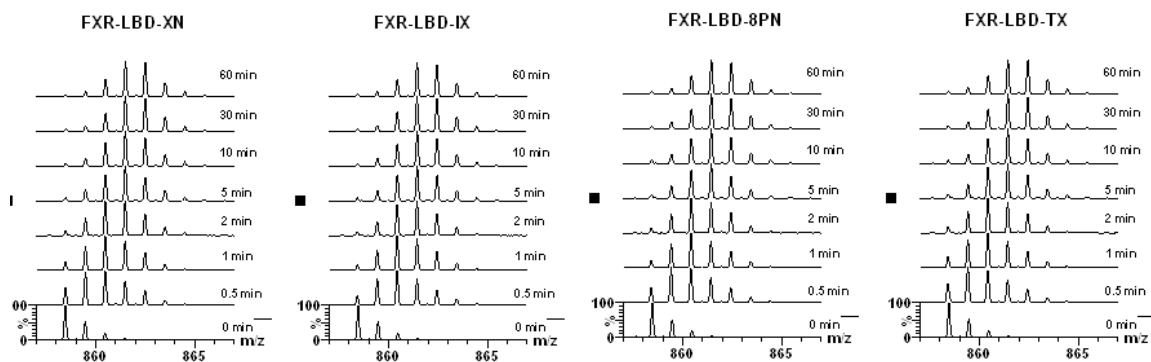
337-347



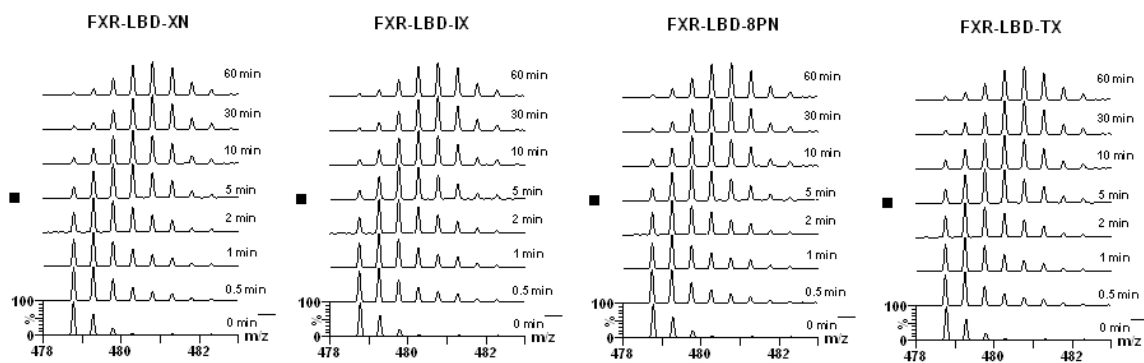
348-360



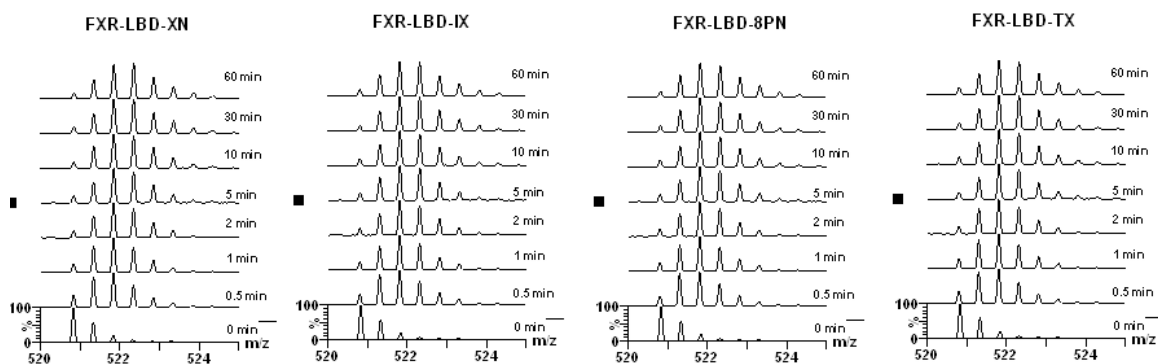
361-367



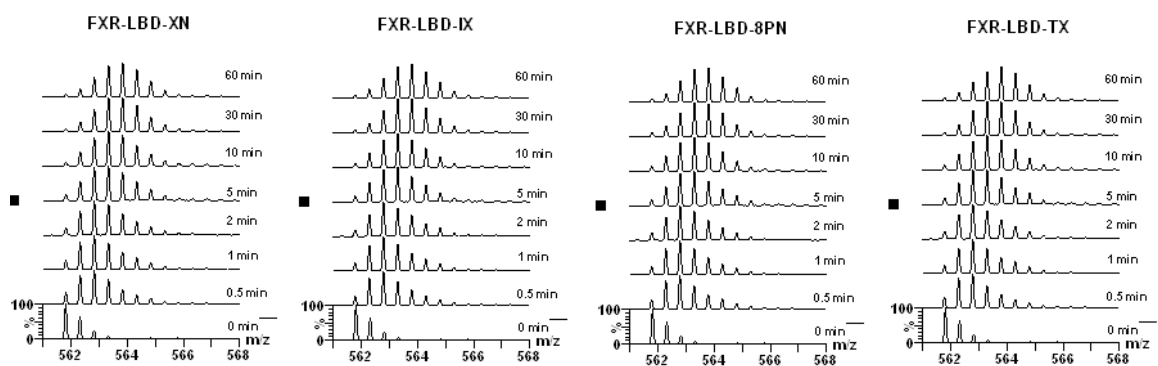
368-375



388-396

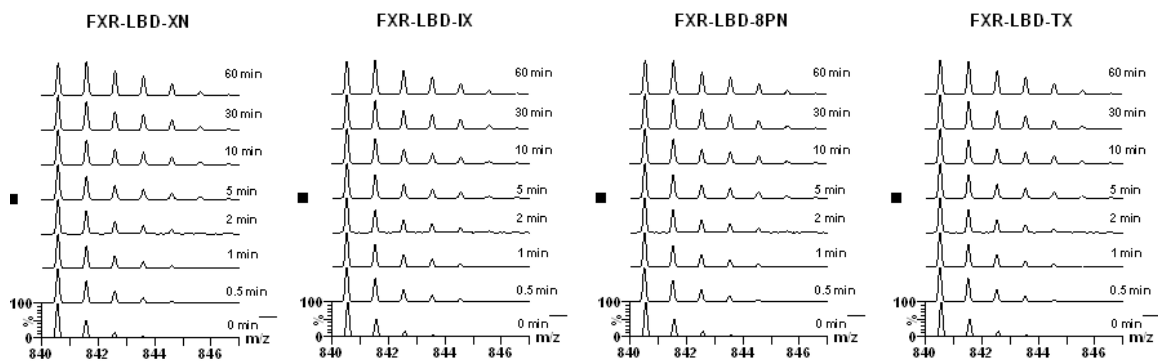


397-405

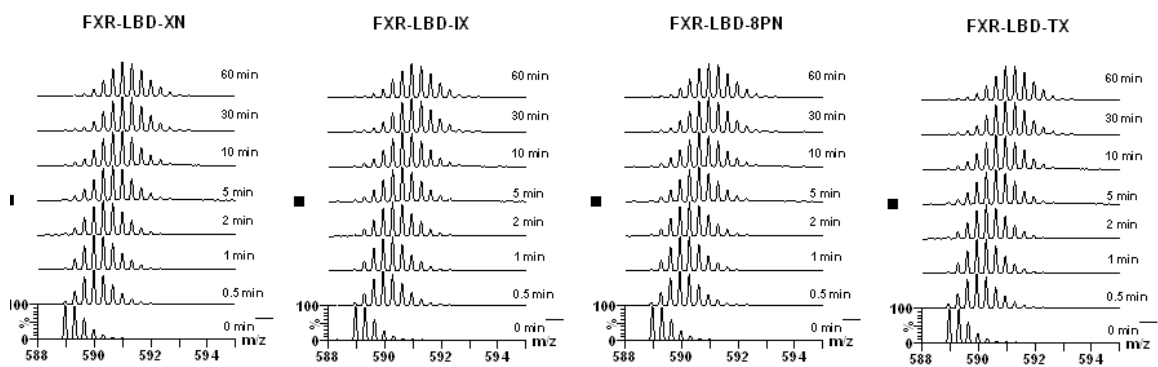


406-412

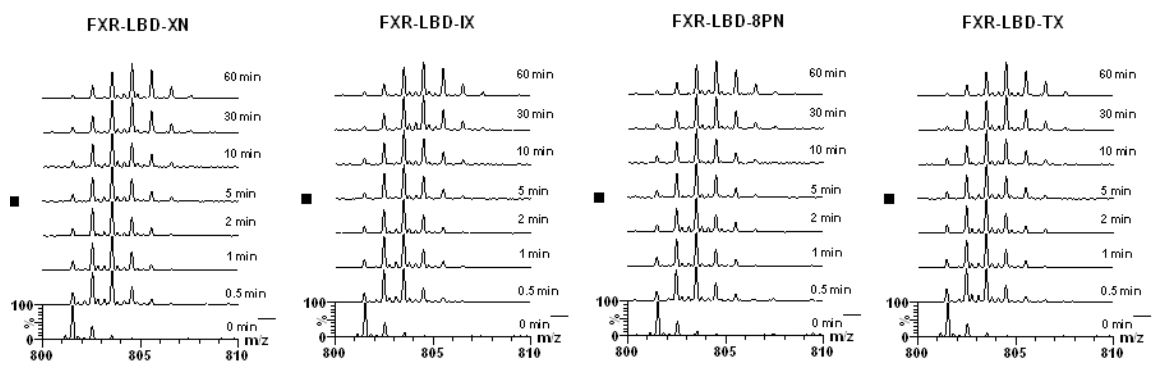




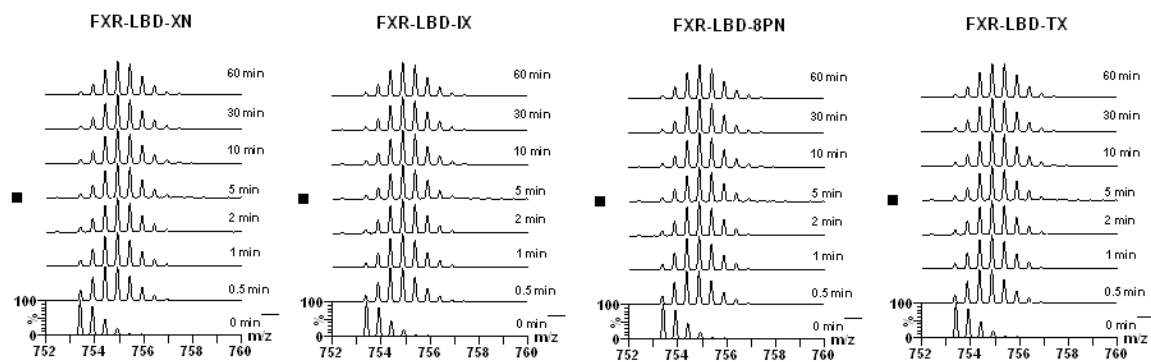
419-433



434-440



440-451



454-465

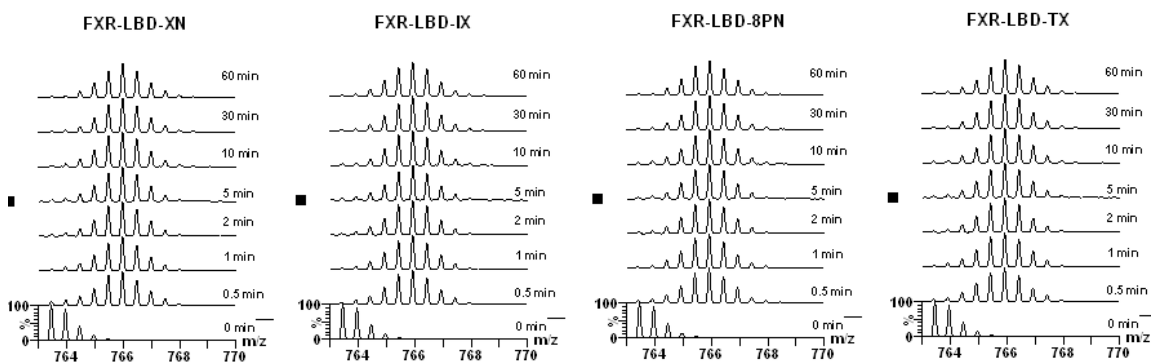
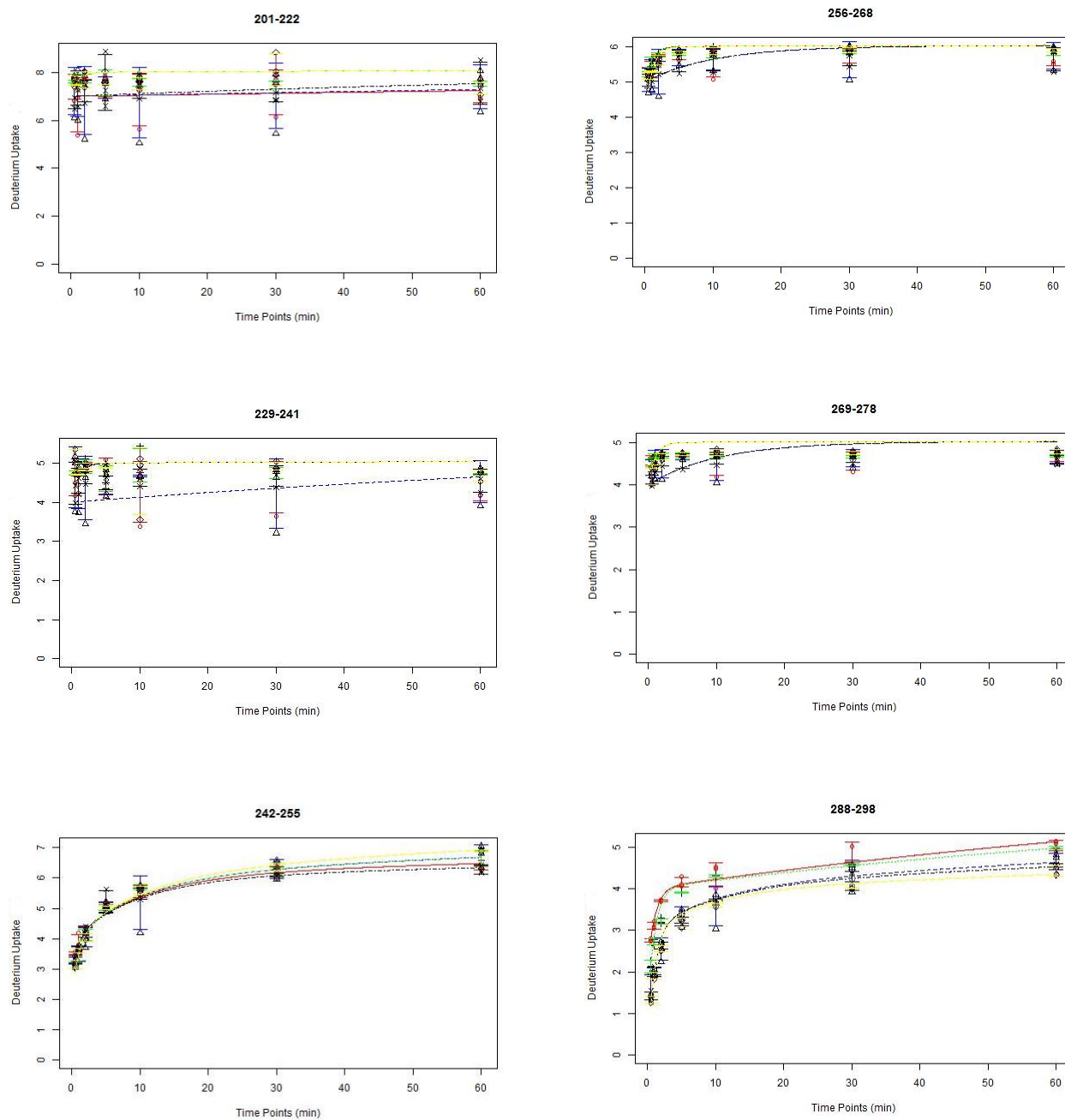
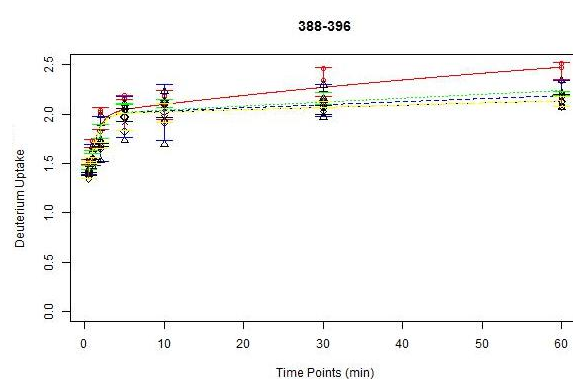
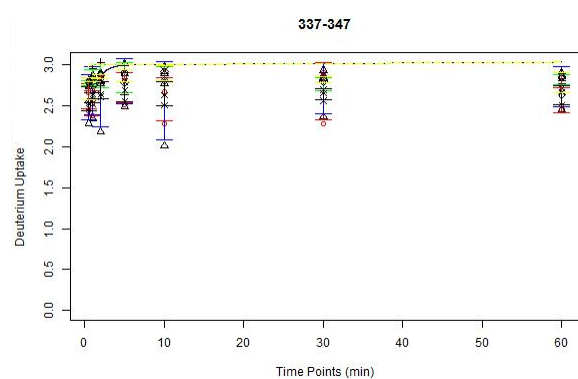
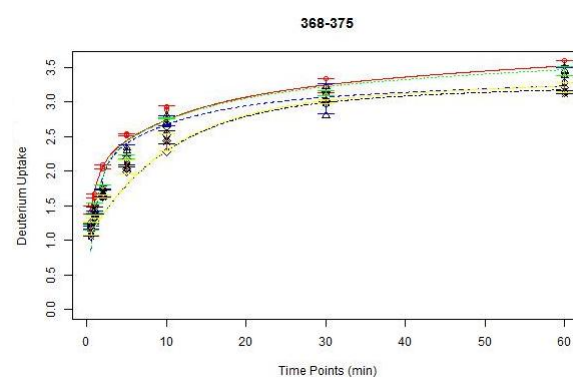
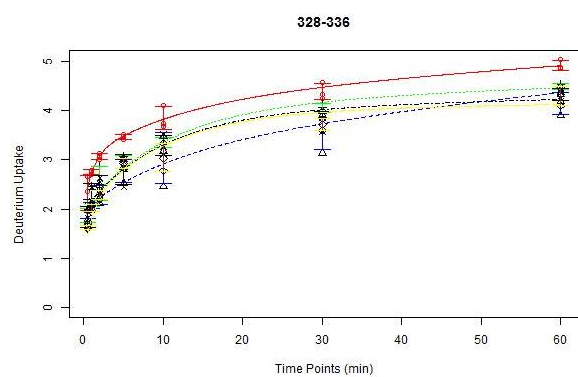
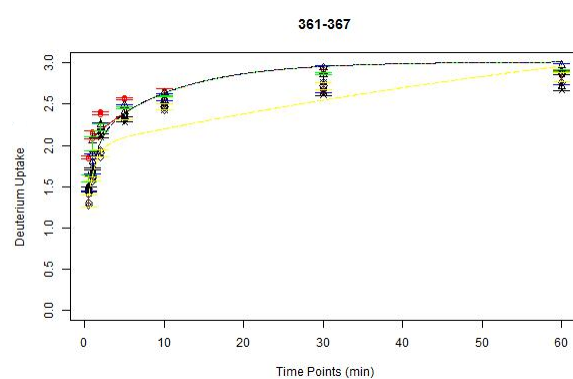
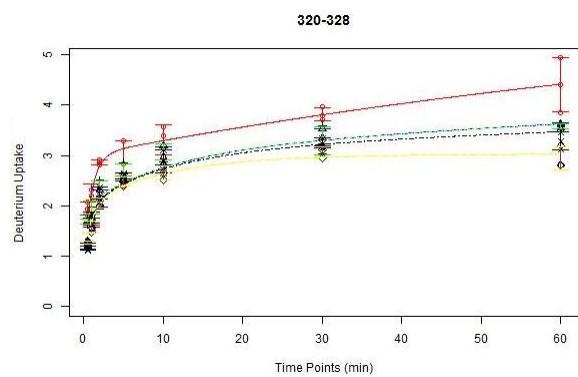
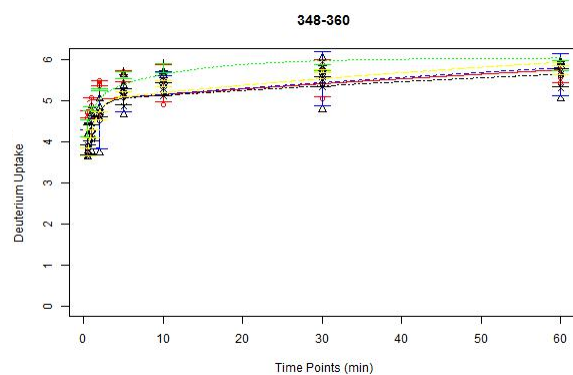
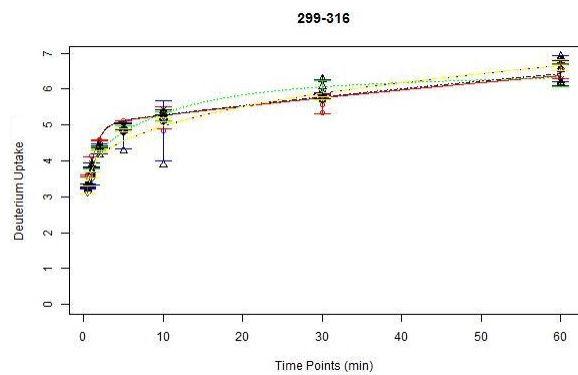


Figure S4.2 Deuterium incorporation level for each peptide at seven exchange-in time points

(0.5, 1, 2, 5, 10, 30, 60 min). Each data point shows the error bar based on the three experimental replicates. Color code: apo-FXR-LBD, red; XN, blue; IX, green; 8-PN, black; TX, yellow.





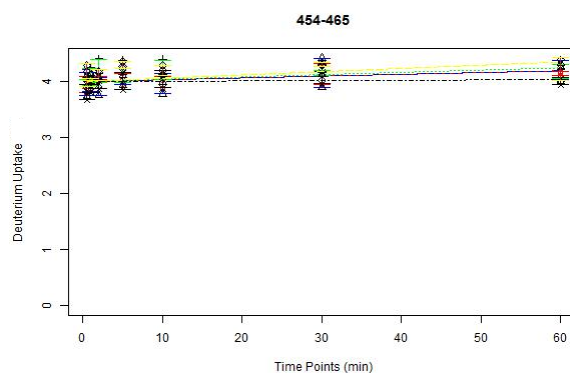
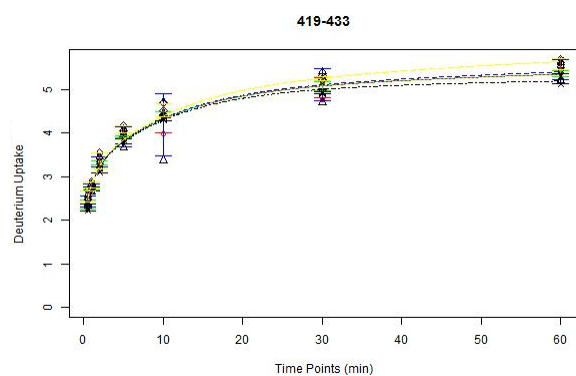
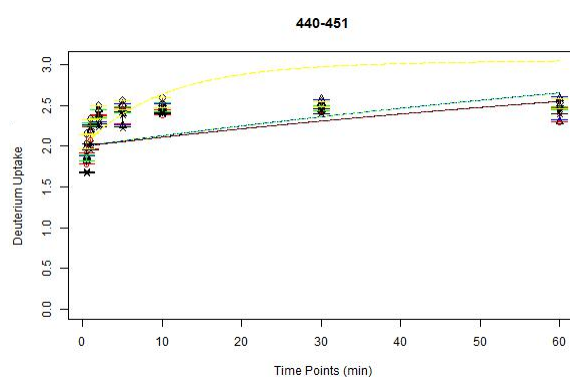
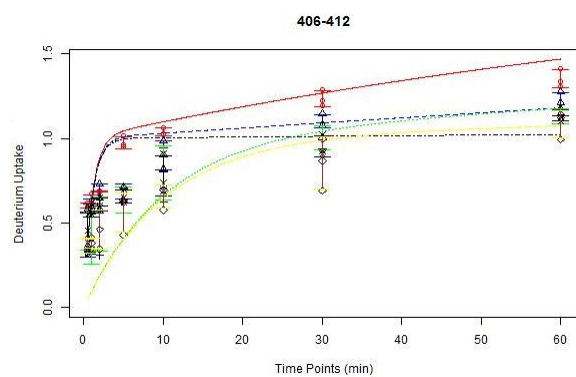
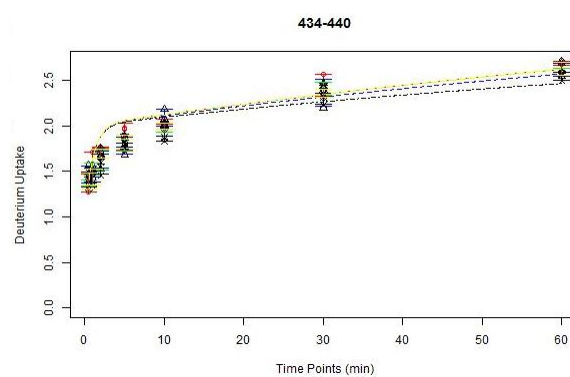
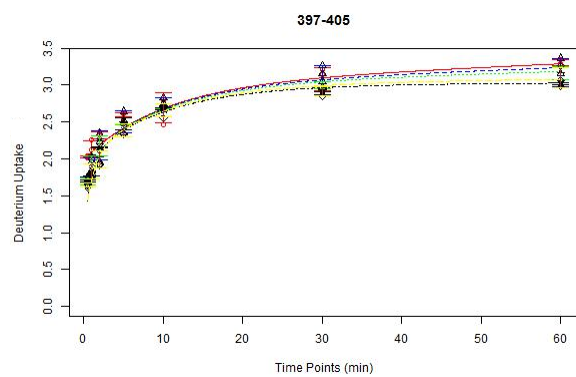
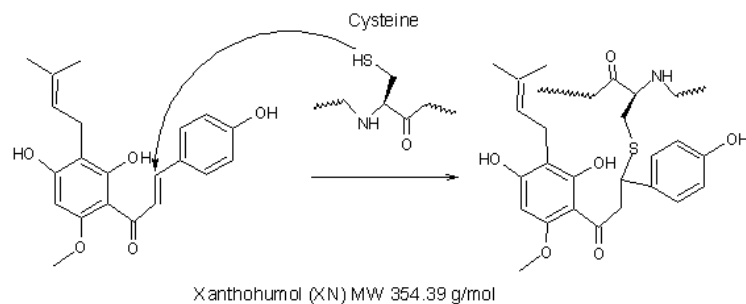


Figure S4.3 The covalent modification of XN with the FXR-LBD.

(A) The proposed Michael addition reaction between a  $\alpha, \beta$  unsaturated ketone group in XN and a SH functional group of a cysteine residue in the FXR-LBD.

(B) The mass spectra demonstrating multiple XN molecules covalently bind with FXR-LBD following the increase of reaction time.

A



B

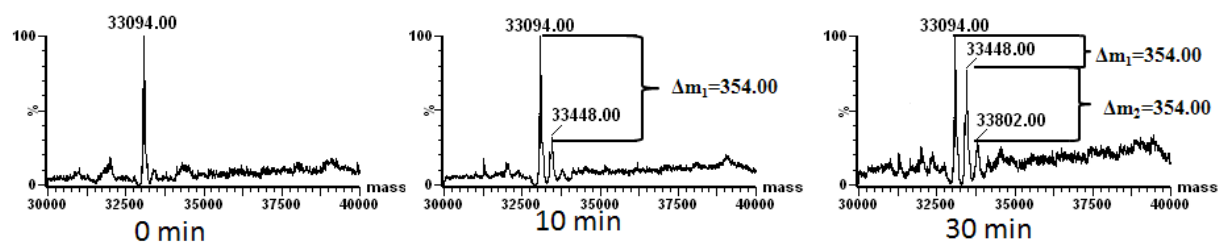


Table S4.1 Average differences in deuterium incorporation levels for each of the peptide used in the current HDX-MS study

The values were obtained by averaging the differences in deuterium levels across the seven reaction time points (0.5, 1, 2, 5, 10, 30 to 60 min) used in the current time course study. A negative percentage indicates the increase of protection against deuterium exchange upon ligand binding and a positive number indicates less protection in a particular region of the FXR-LBD ligand complex. Deuterium level differences of regions with  $p < 0.001$ , calculated by two-way ANOVA, are statistically significant.

Structure <sup>a</sup>	Residue <sup>b</sup>	Charge <sup>c</sup>	apo <sup>d</sup>	XN-apo <sup>e</sup>	P-value	IX-apo <sup>f</sup>	P-value	8PN-apo <sup>g</sup>	P-value	TX-apo <sup>h</sup>	P-value
H1(-)	201-222	3	34%	-1%	0.707	2%	0.028	0%	0.845	2%	0.012
H1(-)	229-241	2	38%	0%	0.945	2%	0.017	1%	0.523	3%	0.025
H1	242-255	2	42%	-1%	0.210	-1%	0.048	-1%	0.058	0%	0.208
H1-H2	256-268	2	51%	-1%	0.263	1%	0.078	-1%	0.075	1%	0.233
H2-H3	269-278	2	51%	-1%	0.459	1%	0.037	-1%	0.045	0%	0.397
H3	288-298	2	40%	-8%	<0.001	-3%	<0.001	-9%	<0.001	-10%	<0.001
H3-H6	299-316	3	31%	-1%	0.108	0%	0.306	0%	0.467	-1%	0.003
H6	320-328	1	38%	-7%	<0.001	-5%	<0.001	-7%	<0.001	-9%	<0.001
H6	328-336	2	44%	-9%	<0.001	-6%	<0.001	-7%	<0.001	-9%	<0.001
H6-H7	337-347	2	29%	0%	0.768	2%	0.002	0%	0.833	2%	0.013
H7	348-360	2	44%	-1%	0.017	0%	0.452	-4%	<0.001	-3%	<0.001
H8	361-367	1	49%	-3%	<0.001	-2%	<0.001	-5%	<0.001	-6%	<0.001
H8	368-375	2	35%	-3%	<0.001	-3%	<0.001	-5%	<0.001	-5%	<0.001
H9	388-396	2	29%	-2%	<0.001	-1%	0.005	-3%	<0.001	-3%	<0.001
H10	397-405	2	32%	-1%	0.005	-2%	<0.001	-2%	<0.001	-3%	<0.001
H10	406-412	1	19%	-3%	<0.001	-5%	<0.001	-4%	<0.001	-6%	<0.001
H11	419-433	3	32%	0%	0.711	0%	0.326	-1%	0.028	1%	0.014
H11	434-440	1	33%	-1%	0.083	-1%	0.021	-2%	0.011	-1%	0.028
H11	440-451	2	21%	0%	0.111	1%	0.004	-1%	0.004	1%	0.002
H11-H12	454-465	2	40%	0%	0.909	1%	0.030	-1%	0.033	1%	0.004

- a) The structure segment of each peptide based on the FXR-LBD-3-D-CDCA X ray structure (PDB:1OT7) without contain the first two peptides (201-222, 229-241).
- b) Residue numbers for the full-length FXR-LBD (UniRef100\_B6ZGS9)
- c) Charge state of each peptide observed in the LC-MS experiment.
- d) Deuterium level of each peptide in apo FXR-LBD.
- e) Deuterium level difference percentage between XN and apo FXR-LBD.
- f) Deuterium level difference percentage between IX and apo FXR-LBD.
- g) Deuterium level difference percentage between 8-PN and apo FXR-LBD.
- h) Deuterium level difference percentage between TX and apo FXR-LBD.





Table S4.3 Average deuterium exchange-in levels of each peptide for the FXR-LBD with presence and absence of ligands

The values were obtained by averaging deuterium exchange-in levels across seven reaction time points (0.5, 1, 2, 5, 10, 30 to 60 min) used in current time course study.

Peptide	apo-FXR-LBD	GW4064	CDCA	GG(Z)	XN	IX	8-PN	TX
201-222	34%	35%	33%	30%	34%	36%	35%	37%
229-241	38%	37%	35%	32%	37%	40%	38%	40%
242-255	42%	38%	38%	37%	41%	41%	41%	41%
256-268	51%	49%	48%	45%	50%	52%	50%	51%
269-278	51%	50%	49%	46%	50%	52%	50%	51%
288-298	40%	20%	34%	31%	32%	37%	31%	30%
299-316	31%	25%	27%	26%	30%	30%	31%	30%
320-328	38%	26%	31%	30%	31%	33%	31%	29%
328-336	44%	28%	38%	36%	36%	38%	37%	36%
337-347	29%	30%	28%	26%	30%	31%	29%	31%
348-360	44%	34%	39%	37%	42%	45%	41%	41%
361-367	49%	39%	44%	44%	46%	48%	44%	43%
368-375	35%	25%	31%	29%	32%	32%	30%	30%
388-396	29%	24%	26%	24%	27%	27%	26%	26%
397-405	32%	27%	28%	27%	31%	31%	30%	30%
406-412	19%	9%	14%	13%	16%	14%	15%	12%
419-433	32%	30%	30%	30%	32%	32%	31%	34%
434-440	33%	26%	29%	30%	32%	32%	31%	32%
440-451	21%	18%	19%	19%	21%	21%	20%	22%
454-465	40%	40%	39%	38%	40%	41%	40%	42%

## Chapter 5

### **Human Farnesoid X Receptor Ligand Binding Domain (hFXR-LBD)–prenylflavonoid Interaction Investigated by Intrinsic Fluorescence Quenching**

Liping Yang<sup>1</sup>, David Broderick<sup>1</sup>, Claudia S. Maier\*<sup>1</sup> and Victor Hsu\*<sup>2</sup>

Departments of Chemistry<sup>1</sup> and Biochemistry and Biophysics<sup>2</sup>, Oregon State University,  
Corvallis, Oregon 97331

\*Corresponding author: Victor Hsu

Email: [hsuv@science.oregonstate.edu](mailto:hsuv@science.oregonstate.edu)

Phone: 541-737-4398

Fax: 541-737-0481

\*Corresponding author: Claudia S. Maier

Email: [claudia.maier@oregonstate.edu](mailto:claudia.maier@oregonstate.edu)

Phone: 541-737-9533

Fax: 541-737-2062

## 5.1 Abstract

Xanthohumol (XN), one of the principal prenylflavonoids of the hop plant, has been reported to be a ligand of human farnesoid X receptor (hFXR) and to be involved in lipid metabolism. Therefore we hypothesized that the related prenylflavonoids, including isoxanthohumol (IX), 8-prenylnaringenin (8-PN), and tetrahydroxanthohumol (TX), are also ligands of hFXR. The interactions between these compounds and the hFXR ligand binding domain (LBD) have been studied by the intrinsic fluorescence quenching method that occurs upon complex formation. The analysis of quenching data showed that each compound strongly quenches the tryptophan fluorescence in the hFXR-LBD primarily through a static quenching mechanism. The apparent dissociate constants  $K_d$  for three prenylflavonoids XN, IX, and 8-PN with hFXR-LBD were  $2.7 \pm 0.1 \mu\text{M}$ ,  $5.9 \pm 0.3 \mu\text{M}$ , and  $2.2 \pm 0.0 \mu\text{M}$ , respectively, demonstrating low affinity interactions between these prenylflavonoids and the receptor protein. Scatchard plots and Hill plots analysis revealed that hFXR-LBD has more than one ligand binding site for IX and 8-PN. A comparison of the molecular volume between the currently studied compounds and eight well known typical FXR agonists suggested that hFXR-LBD has a tendency to exceed one-to-one ligand binding stoichiometry for compounds with a smaller volume ( $<350 \text{ \AA}^3$ ). Our results show that all of the tested prenylflavonoids are low affinity ligands of FXR. The findings obtained here may help us not only to explain some of the peculiar biological activities of prenylflavonoids, but also to design and develop new hFXR ligands which have already showed a potential ability to manipulate FXR's regulation of metabolic networks.

## 5.2 Introduction

FXR is a bile acid activated receptor and plays a vital role in the regulation of bile acid biosynthesis and transport, in cholesterol, lipid and glucose metabolism [1]. As a potential drug target, FXR ligands currently under preclinical investigation strongly suggests that they play a therapeutic role in the treatment of cholestasis, dyslipidemic disorders, and show a potential utility in the treatment of insulin resistance in patients with metabolic syndrome, type 2 diabetes and non-alcoholic steatohepatitis [2, 3]. Hence, the design and development of small molecules targeting FXR is a very promising approach to treat various metabolic diseases [4].

Xanthohumol (XN) (Figure 5.1) is the principal prenylflavonoid found in the hops (*Humulus lupulus L.*) which are added in beer for bitterness and flavor. XN is mostly converted into its isomer, isoxanthohumol (IX) (Figure 5.1) during wort boiling, which has distinctly better solubility [5], and is the primary reason why IX is the most abundant prenylflavonoid found in beer [6]. 8-prenylnaringenin (8-PN) (Figure 5.1), another prenylflavonoid found in the hops, has been identified as one of the most potent phytoestrogens to date [7]. The chemistry, biological activity and biotechnological aspects of these prenylflavonoids have been reviewed [8-10]. Interesting, studies suggest XN is a natural ligand for FXR and ameliorates lipid and glucose metabolism in mice [11]. Yang et al reported that both XN and IX inhibit lipid accumulation in maturing preadipocytes, and they proposed regulation of adipogenesis by XN might be at least partly mediated by modulating FXR target genes [12]. Another investigation showed that XN can inhibit triglyceride synthesis and secretion in HepG2 cells [13]. All these researches imply that XN is involved in lipid metabolism, possibly by interacting with FXR.

Guggulsterone (GG) (Figure 5.1) has been identified as the key active ingredient in the gum resin of the tree *Commiphora mukul* which has been used to treat hypolipidemia in India

since 1987 [14]. Subsequent studies have shown that GG is an *in vitro* antagonist of FXR and the FXR antagonism by GG has been proposed as a mechanism for its hypolipidemic effect and cholesterol-lowering activity [15-17]. A number of studies relating to the biological activity of GG, both in animal models and human clinical trials, have focused primarily on its effects on lipid metabolism [16, 18, 19]. In addition, the combination of GG and XN is more potent in exerting anti-obesity effects than the additive effects of the individual compounds [20]. Internationally, GG has received considerable attention, and as a result several other biological activities have been uncovered [21, 22].

Based on previous studies and the ability of FXR to bind various compounds not structurally related to bile acids because of the very high flexibility of hFXR-LBD, we hypothesized that the three prenylflavonoids (XN, IX and 8-PN) and a XN derivative (TX) (Figure 5.1) are all potential ligands of FXR. The hFXR-LBD contained two tryptophan residues, tryptophan 454 and tryptophan 469, located in the helix 11 and helix 12, respectively. Tryptophan fluorescence is highly sensitive to its local environment in solution and its emission spectra are often altered due to protein conformational transitions, subunit association, substrate binding, or denaturation [23]. Intrinsic fluorescence titration has been used for studying protein structure and dynamics, and is regularly used for investigating ligand/receptor interactions [24-26]. In this work, we used intrinsic fluorescence quenching methodology to investigate the interaction between these compounds and FXR, and we attempt to clarify the quenching mechanism, to determine their apparent dissociate constants, and to find out how the exposure and environment of tryptophan residues in FXR are impacted by their presences. We also used two well studied ligands of FXR - the *in vitro* antagonist GG and the endogenous agonist chenodeoxycholic acid (CDCA) - as comparative ligands.

## 5.3 Materials and methods

### 5.3.1 Materials

Deuterium oxide (D<sub>2</sub>O, 99.9% deuterium), CDCA and GG were purchased from Sigma-Aldrich Chemical Co. (St. Louis, MO, USA), Tocris (Ellisville, MO, USA), and ChromaDex<sup>TM</sup> Corporate (Irvine, CA, USA), respectively. XN and related prenylfalvonoids were kindly provided by Dr. F.J. Stevens (College of Pharmacy in Oregon State University, Corvallis, OR). Each compound has over 99% pure (as determined by HPLC) and was dissolved in dimethylsulfoxide (DMSO) and prepared as 10 mM stock solution. All other materials were available from standard commercial sources.

### 5.3.2 Cell growth and purification of hFXR LBD

*Escherichia coli* BL 21 (DE23) pLysS with a pET 15B vector containing hFXR LBD (residues from L193 to Q472) were grown in 2XYT medium with antibiotics (Ampicillin 150 µg/ml, Chloremphenicol 35 µg/ml) at 37°C until A<sub>600</sub> reached 0.6-0.8 and were then induced at 20°C with 0.8 mM IPTG (isopropyl-beta-D-thiogalactopyranoside) for four hours to produce a N-terminal Histidine (His6) tagged hFXR LBD. The centrifuged pellets were resuspended in cell wash buffer (50 mM Tris pH 7.0, 150 mM NaCl, 10% sucrose), recentrifuged, and frozen at -80°C. The frozen pellet was resuspended in 50 mM sodium phosphate, pH 7.3, 0.5 M NaCl, 0.5 mM CHAPS, 15 mM imidazole, and 0.5 M sucrose (buffer A) and then was sonicated, centrifuged and the supernatant saved. Clontech Talon Co<sup>2+</sup> polyhistidine affinity resin was equilibrated with buffer A (1.5 mL resin/liter of culture medium). After samples for gel electrophoresis analysis were removed, the remaining supernatant was mixed with the affinity resin and shaken at 4°C for 45 minutes to bind the His6 tagged proteins. A column was packed with the protein-bound resin and washed with 10-15 column volumes of buffer A until A<sub>280</sub> is less than 0.03. The proteins were eluted with buffer A with 200 mM imidazole and the fractions

were run on the sodium dodecyl sulfate–acrylamide gel electrophoresis (SDS-PAGE) and the purest fractions were pooled.

The hFXR-LBD His6-Tag was removed slowly and incompletely (85-90%) by incubation for 48 hours at 4°C in the presence of thrombin. The uncut His6-Tagged hFXR LBD and the free His6-Tag were removed by diluting the sample 10 fold with buffer A without imidazole and binding to the reequilibrated Histidine Co<sup>++</sup> resin again. The flow-through was collected, concentrated to 3.23 mg/mL (98µM) with an Amicon Ultra centrifugal filter, made to 10% with glycerol and 1 mM TCEP, aliquotted, frozen with liquid nitrogen and stored at -80°C. The protein purity (over 95%) was judged by SDS-PAGE.

### 5.3.3 Fluorescence quenching experiments

A LS 50 luminescence spectrometer (Perkin Elmer) was used to measure steady state fluorescence. The monochromator slitwidths for excitation and emission were both set to 3.5 nm. For the fluorescence titrations, the protein sample was allowed to equilibrate for three minutes after each addition of ligand, and was excited at 295 nm to minimize the fluorescence contribution of tyrosine residues and the emission spectra were acquired from 305 nm to 480 nm. The ligand-hFXR-LBD interactions were studied by an intrinsic fluorescence titration method where 10 µM proteins (50 mM sodium phosphate, 0.5 M NaCl, 0.5 mM CHAPS, 1 mM TCEP, 0.5 M sucrose and 10% glycerol, pH=7.4, 400 µL) was titrated with 1000 µM ligands until the ligand/protein ratio reached 5 to 1. Before analysis of the binding and quenching data, fluorescence spectra were corrected ( $F_{cor}$ ) for the background fluorescence of the specific ligand  $F_B$ , the instrument-dependent monochromator and photomultiplier response emission correction factor  $F_S$ , and dilution factor A:  $F_{cor} = (F_0 - F_B) \times 100 \times A / F_S$  where  $F_0$  is the measured fluorescence intensity. All measurements were performed at 25°C and repeated three times.



### 5.3.4 Data analysis

For binding property studies, quenching data were analyzed according to the well-known Stern-Volmer equation [23] which described quenching process between protein and quenchers:

$$\frac{F_0}{F} = 1 + K_{sv}[Q] \quad (5.1)$$

where  $F_0$  and  $F$  are the fluorescence intensities in the absence and presence of quenchers (ligands), respectively;  $[Q]$  is the concentration of quencher.  $K_{sv}$  is the Stern-Volmer constant, which is related to the bimolecular quenching constant  $k_q$ , and  $\tau_0$  is the lifetime of the fluorophore in the absence of quencher.  $K_{sv}$  is given by:

$$K_{sv} = k_q \tau_0 \quad (5.2)$$

A linear Stern-Volmer plot of  $\frac{F_0}{F}$  versus  $[Q]$  usually indicates that all the tryptophan residues in the protein are equally accessible to the quencher.

The Stern-Volmer plots with downward curvature and concave towards the x-axis is an indicative that only the fraction of the tryptophan residues are accessible to the quencher, and can be analyzed by using the Lehrer model [27], i.e. the modified Stern-Volmer equation:

$$\frac{F_0}{F_0 - F} = \frac{1}{f_a [Q] K_{sv}} + \frac{1}{f_a} \quad (5.3)$$

where  $f_a$  is the fraction of the total tryptophan residues accessible to quencher.

Non-linear Stern-Volmer plots with upward curvature and concave towards the y-axis are characteristic of a combination of static and dynamic quenching, and can be analyzed by the following equation [23]:

$$\frac{F_0}{F} = (1 + K_D[Q])(1 + K_S[Q]) \quad (5.4)$$

where  $K_D$  is the dynamic quenching constant and  $K_S$  is the static quenching constant.

For binding equilibrium analysis, binding data were analyzed by fitting the curve to the Hill equation [28]

$$\frac{F_0 - F}{F_0} = \frac{[L]^n}{K_d + [L]^n} \quad (5.5)$$

where  $K_d$  is the apparent dissociation constant, a parameter describing affinity between protein and ligand;  $n$ , the Hill coefficient, describes the cooperativity of independent ligands binding to multiple equivalent binding sites on protein.

All data fits, linear regression and non-linear regression, were performed with the GraphPad Prism software program and gave correlation coefficient (R) values exceeding 0.99.

## 5.4 Results

### 5.4.1 Intrinsic Fluorescence of apo hFXR-LBD and holo hFXR-LBD

To investigate whether our hFXR-LBD construct would bind and interact with ligands under the desired experimental conditions, we firstly added GG and CDCA, two well known ligands of hFXR, individually to the protein sample and measured the changes of tryptophan fluorescence intensities under the emission  $\lambda_{\max}$ . When excited at 295 nm, apo hFXR-LBD exhibited significant intrinsic fluorescence in the range 305-480 nm with maximum emission

wavelength at 343 nm (Figure 5.2). GG titration of hFXR-LBD showed a concentration-dependent quenching without any changes in the emission  $\lambda_{\text{max}}$  and spectra's shape (Figure 5.2), which suggests a direct hFXR-LBD-GG interaction with the tryptophan residues involved the binding. On the other hand, only subtle fluorescence intensity changes ( $\pm 3\%$ ) were observed during CDCA titration of hFXR-LBD, suggesting the microenvironment of tryptophan residues in the hFXR-LBD was either unchanged or only slightly changed, as consistent with a recently study [29].

Under the same experimental conditions, there was a distinct decrease in the fluorescence intensity at 343 nm when hFXR-LBD was titrated with XN and its derivatives (Figure 5.2). When the molar ratio of compound and hFXR-LBD was 1:1, hFXR-LBD fluorescence was quenched by 78%, 51%, 68%, and 72% in the presence of XN, IX, 8-PN, and TX respectively, suggesting the quenching ability of these compounds is  $\text{XN} > \text{TX} > 8\text{-PN} > \text{IX}$ . Blue shifting of the emission  $\lambda_{\text{max}}$ , 343 nm  $\rightarrow$  330 nm for XN and 343 nm  $\rightarrow$  338 nm for TX, were observed with the presence of XN and TX (Figure 5.2) suggesting that upon ligand binding the tryptophan residues were placed in a more hydrophobic microenvironment possibly caused by exclusion of solvent at the binding sites of XN and TX. In addition, the addition of IX and 8-PN caused obvious red shifts from 343 nm to 364 nm and from 343 nm to 368 nm respectively (Figure 5.2), even exceeding the emission  $\lambda_{\text{max}}$  (350 nm) of the free tryptophan residue [30], suggesting one or more tryptophan residues in hFXR-LBD were exposed to solvent to a higher degree. Moreover, the existence of an isosbestic point in the spectra from the IX titration at 405 nm might suggest that IX was present at equilibrium in both the bound and unbound form.

### 5.4.2 Binding mechanism of ligand to the hFXR-LBD

In fluorescence titration experiments probing ligand/receptor interaction, any observed fluorescence quenching might be due to dynamic quenching (diffusive collisions) and/or static quenching (the formation of a ground-state complex). To determine the quenching mechanism in the process of the ligand binding in the hFXR-LBD, the equation (5.1) was used to analyze the quenching data (Figure 5.3). Of the four ligand-hFXR-LBD complexes under study, the fluorescence quenching plots of IX and 8-PN were linear, indicating that the two tryptophan residues in hFXR-LBD were accessible to these two ligands equally [23] and just a single type of quenching occurred, either dynamic or static [24]. For XN, the Stern-Volmer plot exhibited a slightly upward curvature (Figure 5.3) which is a characteristic of a combination of both dynamic and static quenching [23]. The downward curving plot (Figure 5.3) obtained for GG titration suggested that a fraction of tryptophan residues (in this case one tryptophan residue) was shielded from GG [27]. By fitting the experimental quenching data from the GG titration to equation (5.3) (Figure 5.4), the  $f_a$  value 0.53 was obtained, indicating that just half of tryptophan residues in hFXR-LBD was accessible to GG, i.e. only one tryptophan residue was involved in the interaction between protein and ligand.

The magnitude of  $K_{SV}$  often can be used to differentiate between dynamic and static quenching [31-36] based on the fact that if the bimolecular quenching constant  $k_q$  is larger than the maximal diffusion-controlled quenching constant of  $1 \times 10^{10} \text{ M}^{-1}\text{S}^{-1}$  [23], a decrease in the fluorescence intensity is caused mainly by the formation of a non-fluorescence complex and/or the existence of a specific kind of binding interaction [23]. The  $k_q$  values (Table 5.1) were calculated by the equation (5.2), where the average lifetime  $\tau_0$  of the native tryptophan fluorescence of protein was taken to be three nanoseconds [37]. The bimolecular quenching

constants  $k_q$  (Table 5.1) of IX, 8-PN, and GG fluorescence titration experiments were three orders of magnitude larger than the maximal expected value of  $k_q$ , suggesting that dynamic quenching was not responsible for the reduction of fluorescence intensity. Interestingly, based on the dynamic quenching constant  $K_D$  derived by fitting the quenching data from the XN titration to the equation 5.4, calculated  $k_q$  was  $2 \times 10^{11} \text{ M}^{-1}$ , 20 times bigger than  $1 \times 10^{10} \text{ M}^{-1} \text{ s}^{-1}$  (Table 5.1) which suggests the presence of another specific binding site located near the tryptophans.

#### 5.4.3 Analysis of hFXR-LBD-ligand equilibrium binding data

The Scatchard plots of the hFXR-LBD-ligand equilibrium binding data were shown in Figure 5.5 and the equilibrium binding parameters were determined by the best fit to the Hill equation (5.5) (Figure 5.6, Table 5.2). For the titration of the hFXR-LBD-XN complex the Scatchard plot was linear and the Hill coefficient was determined to be 1.02, suggesting that there is just one independent type of binding sites or that no binding cooperativity in the case of multiple binding sites. However, for IX, 8-PN, and GG, the hFXR-LBD titrations exhibited concave-upward Scatchard plots and Hill coefficients of 0.86, 0.78, and 0.50, respectively, indicating the presence of multiple binding sites with different dissociate constant and negative cooperativity in terms of ligand binding [38].

$K_d$  is a parameter describing how tightly the ligand binds to its receptor. The magnitude of the apparent dissociation constant for each of these prenylflavonoid compounds is micromole, implying that they are low affinity binders of the hFXR-LBD, which is consistent with our hydrogen/deuterium exchange data (chapter 3). Additionally, the  $K_d$  of the GG-hFXR-LBD complex was determined to be 5.4  $\mu\text{M}$ , similar to the previously reported  $K_d$  that was determined by radioligand binding assays method [40].

## 5.5 Discussion

From the fluorescence spectra of each of the four ligand-protein studied, fluorescence quenching of hFXR-LBD was observed from the first addition of the compounds, indicating that a high affinity binding site in hFXR-LBD is located close to the two tryptophan residues in the receptor protein. These results are consistent with the hFXR-LBD-GW4064 crystal structure (PDB ID 3DCT) in which both tryptophans are involved in the formation of a hydrophobic binding cavity. As discussed above, the interaction between hFXR-LBD and compounds under study exhibited the characteristics of a static quenching mechanism. In this case, the Stern-Volmer constant  $K_{SV}$  could be represented by the binding constant, which is the reciprocal of the dissociate constant  $K_d$  [23].  $K_d$  values for each compound were determined from the Stern-Volmer equation (5.1) and the Hill equation (5.5), and listed in Table 5.2 for comparison. From these results, we found the apparent dissociation constants calculated by above two equations agreed well with each other, suggesting the  $K_d$  values determined here to be reliable.

The Stern-Volmer plot of hFXR-LBD interaction with XN revealed the existence of both dynamic and static quenching at high ligand concentrations, which were also previously observed in the interaction of flavonoid compounds with bovine serum albumin and bovine milk xanthine oxidase as well [35, 36]. In addition, Kaldas et al reported that the flavonoid quercetin can covalently bind with human serum albumin (HSA) [41]. The  $k_q$  value determined for XN in table 5.1 implied the presence of a specific binding site in close proximity to the tryptophan residues and a ground-state complex formation. The chemical structure of XN contains a  $\alpha,\beta$ -unsaturated ketone moiety which can potentially modify nucleophile sites – such as the sulfide group of cysteine residues in the hFXR-LBD. Importantly, the covalent binding of XN to cysteine residues in hFXR-LBD was confirmed by mass spectrometry (Figure 5.7). Therefore,

we propose that XN binds to Cys466, which is located in close proximity to Try469, and that this covalent interaction is responsible for the dynamic quenching observed in the XN- hFXR-LBD complex. Interesting, similar covalent interaction also were found in nuclear receptor peroxisome proliferator-activated receptor- $\gamma$  (PPAR $\gamma$ )-ligand interaction [42, 43].

Scatchard plots are used extensively to study the binding data of ligand-receptor interactions [44-46]. The results reported in this study suggested, in addition to the canonical ligand binding cavity in FXR, that there might be additional ligand binding sites in hFXR-LBD. It is worth noting that Meyer et al. identified a novel and potential binding pocket for GG in FXR in their molecular modeling study, and that this pocket encompassed part of Helix1, the loop region between Helix 1 and Helix 2, Helix 3, Helix 5 and Helix 8 [47], which is in good agreement with our mass spectrometry hydrogen/deuterium data (chapter 3). When our binding data of hFXR-LBD complex with IX, 8-PN, and GG were fit to a two binding sites model system, the values of  $K_d$  were found to be  $K_{d1}=1.4\ \mu\text{M}$  and  $K_{d2} = 18.3\ \mu\text{M}$  for IX,  $K_{d1}=1.7\ \mu\text{M}$  and  $K_{d2} = 40.3\ \mu\text{M}$  for 8-PN,  $K_{d1}=2.2\ \mu\text{M}$  and  $K_{d2} = 24.5\ \mu\text{M}$  for GG (correlation coefficients R in excess of 0.99). Evidences implying that GG can compete with CDCA for binding the FXR ligand binding domain and inhibit FXR activation in vitro has been reported[17], and the similar dissociation constant of GG (2.2  $\mu\text{M}$ ) and CDCA (3.57  $\mu\text{M}$ ) [39] gave a reasonable explanation for their competitive binding in solution. In addition, although exhibiting relatively weak affinity, the existence of a second binding site may explain some of the biological activities of prenylflavonoids on lipid metabolism as well as some of the distinctive characteristics of GG observed when acting on the FXR [48, 49].

The intrinsic volume of FXR ligands was determined via online calculation ([www.chemicalize.com](http://www.chemicalize.com)). The volumes of known FXR agonists are at least larger 40 Å<sup>3</sup> than that of each prenylflavonoid in current study (Table 5.3). At the level of molecular interaction, the volume of a molecule is considered as an important feature of the natural nuclear receptor ligands that has been conserved through evolution [50]. Mi et al. proposed a physical–shape discrimination mechanism employed by FXR, that the recognition of the FXR ligand binding pocket by bile acids depended on both their nonplanar shapes and amphipathic physiochemical properties [51]. The x-ray crystal structures of the FXR-LBD-high affinity synthetic ligands (Group B in Table 5.3) complexes demonstrate, despite the chemical structure diversity of the FXR ligands, that ligands are only tightly bound in the canonical ligand binding site in FXR. On the other hand, despite the lack of a published X-ray structure available for an endogenous agonist CDCA-bound FXR complex, the interaction between FXR and CDCA as investigated by the mass spectrometry hydrogen/deuterium exchange method suggested CDCA only binds in the canonical binding cavity in hFXR-LBD as well (chapter 3). In contrast to the classical concept for nuclear receptor antagonism requiring antagonists larger than the endogenous agonists [52, 53], the FXR antagonist GG has much smaller volume (312.8 Å<sup>3</sup>) compared with CDCA (404.6 Å<sup>3</sup>) (Table 5.3). As mentioned earlier, there is now evidence that there might be two ligand binding sites in hFXR-LBD, and their volumes are 1075 Å<sup>3</sup> for the canonical binding site and 650 Å<sup>3</sup> for the noncanonical binding site, respectively [47]. These results suggest that a compound with the smaller volume, possibly < 350 Å<sup>3</sup>, has the potential to occupy both ligand binding sites in hFXR-LBD. Taken together, we proposed that the actual physical volume of a ligand is an important aspect to take into consideration during the design and development of the FXR modulators which show promise to therapy or to prevent metabolic disorders and diseases.



Our results imply that the existence of the noncanonical binding site in the hFXR-LBD could explain the especial characteristics attributed to GG acting on gene selective modulation.

## 5.6 Conclusion

This work represents the first reports the interactions of the FXR-LBD with prenylflavonoids studied by intrinsic fluorescence quenching techniques. The fluorescence intensity changes in the tryptophan residues of the hFXR-LBD in the presence of XN, IX, 8-PN, TX, and GG, indicate one high affinity ligand binding site in close proximity to the tryptophan residues in the receptor protein. In addition, we determined that the quenching mechanism of XN, IX, 8-PN, and GG bound to the hFXR-LBD is mainly through static quenching and thus is evidence for the formation of ground state protein-ligand complexes. The quenching data analysis of XN binding with hFXR-LBD suggests the combination both static and dynamic quenching, and that the later is caused by covalent binding between XN and hFXR-LBD. The values of apparently dissociation constant  $K_d$  suggest that XN, IX, and 8-PN are the low affinity ligands for hFXR-LBD. Our equilibrium binding data analysis also reveals the actual ligand size is an important factor that affects the interaction between ligand and protein. The studies presented here provide novel insights into the molecular mechanism that occurs when ligands bind to FXR and may help in the design and development of new FXR modulators.

**ACKNOWLEDGEMENT**

This research was supported in part by Grants S10RR025628 and P30ES000210 from the National Institutes of Health.

## Figures

Figure 5.1 Chemical structure of the four ligands

Figure 5.2 Fluorescence emission spectra of hFXR-LBD in the presence of different ligands

Figure 5.3 The Stern-Volmer plots of hFXR-LBD quenching by the different ligands

Figure 5.4 Modified Stern-Volmer plots for GG and XN quenching of hFXR-LBD

Figure 5.5 Scatchard plots of the hFXR-LBD-molecule binding data

Figure 5.6 Hill plots of the hFXR-LBD-molecule binding data

.

Figure 5.7 Mass spectra of XN exhibiting covalently binding to hFXR-LBD

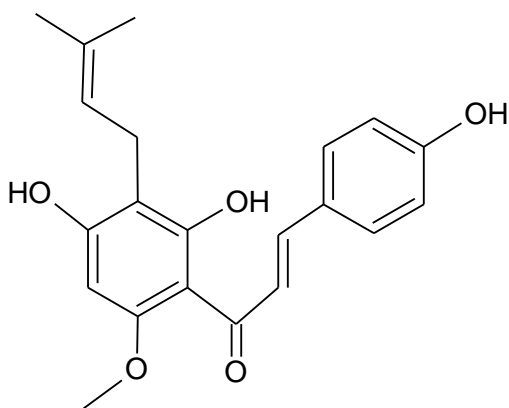
.

Table 5.1 The Stern-Volmer constant ( $K_{SV}$ ), the fraction of fluorophore accessible to the quencher ( $f_a$ ), the bimolecular quenching constants ( $k_q$ ), the dynamic quenching constant ( $K_D$ ) and the static quenching constant ( $K_S$ ) of the hFXR-LBD-ligand systems. These values were obtained by Equation 5.1 for IX and 8-PN, Equation 5.3 for GG (marked with \*), Equation 5.4 for XN (marked with \*\*) and Equation 5.2 for all ligands.

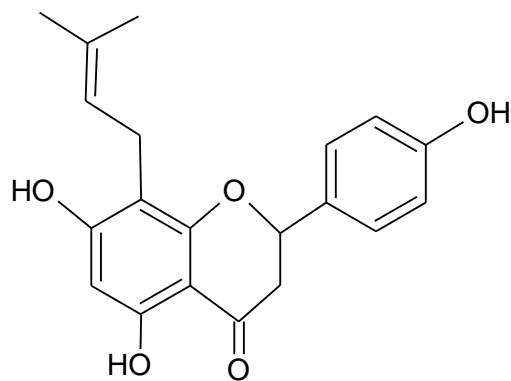
Table 5.2 Hill coefficient  $n_H$  and the apparent dissociation constant  $K_d$  ( $\mu\text{M}$ ) for different ligands with hFXR-LBD.  $K_d^*$  was calculated from  $K_{SV}$  or  $K_S$  which are the binding constants under the static quenching mechanism.

Table 5.3 Comparison of different ligand volumes. Volume values calculated from [www.chemicalize.org](http://www.chemicalize.org) (ChemAxon). The x-ray crystal structures of the FXR-LBD-ligand in group A are unavailable, whereas the x-ray crystal structures of the FXR-LBD-ligand complexes in group B are available.

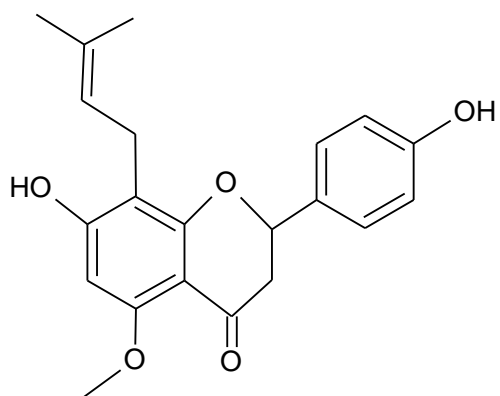
Figure 5.1



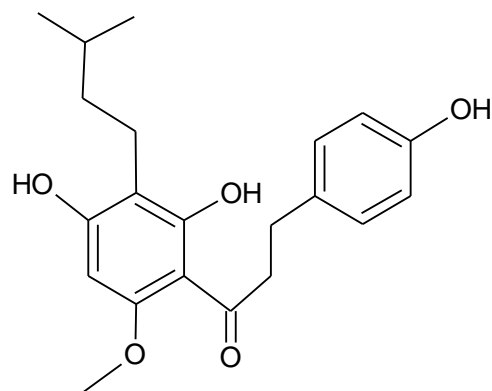
Xanthohumol (XN)



8-Prenylnaringenin (8-PN)



Isoxanthohumol (IX)



Tetrahydroxanthohumol (TX)

Figure 5.1 Chemical structure of the four ligands

Figure 5.2

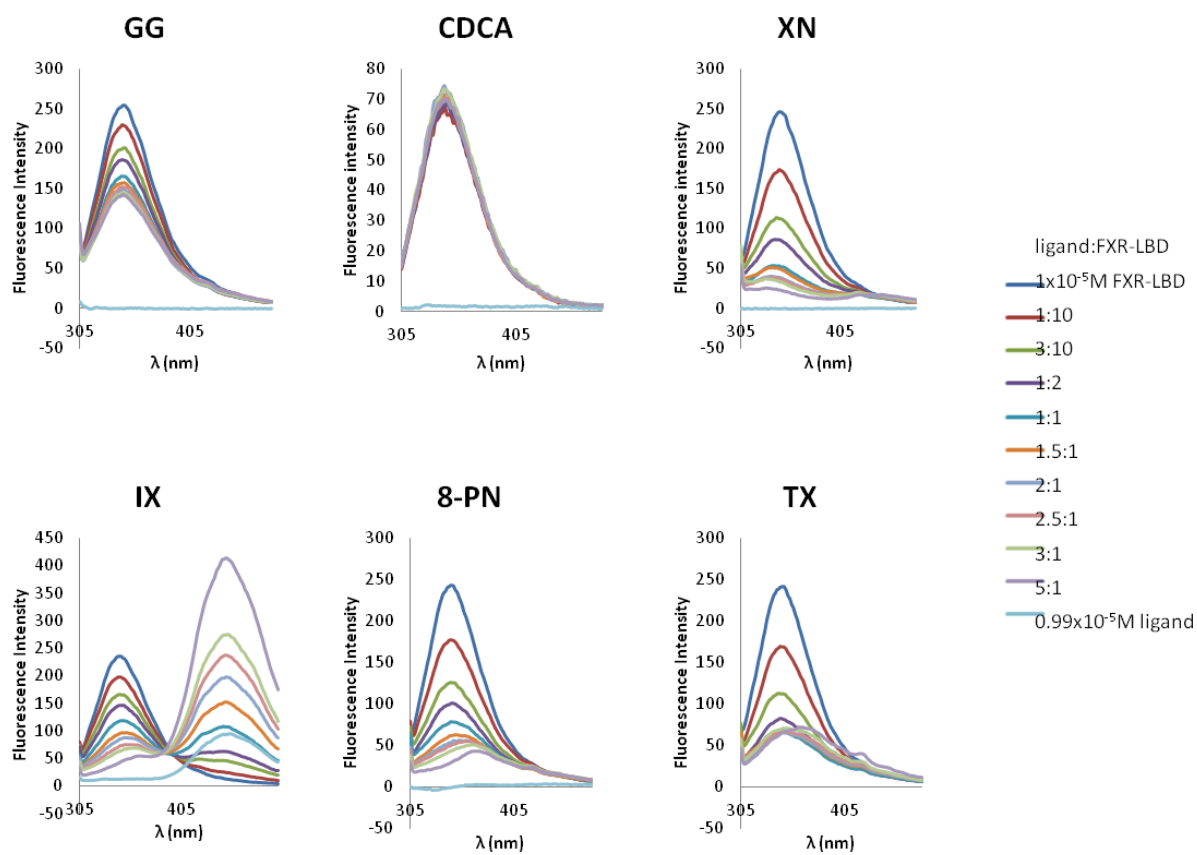


Figure 5.2 Fluorescence emission spectra of hFXR-LBD in the presence of different ligands

Figure 5.3

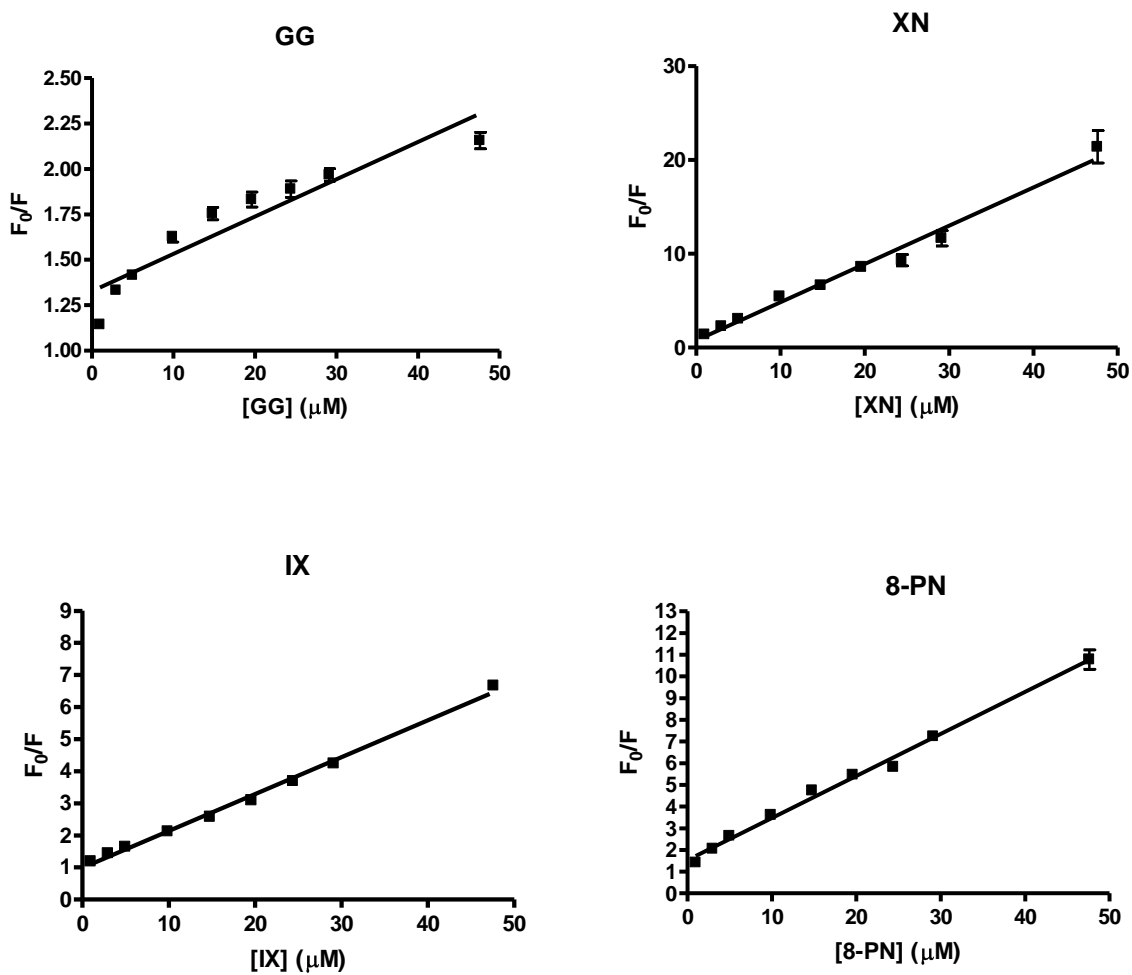


Figure 5.3 The Stern-Volmer plots of hFXR-LBD quenching by the different ligands

Figure 5.4

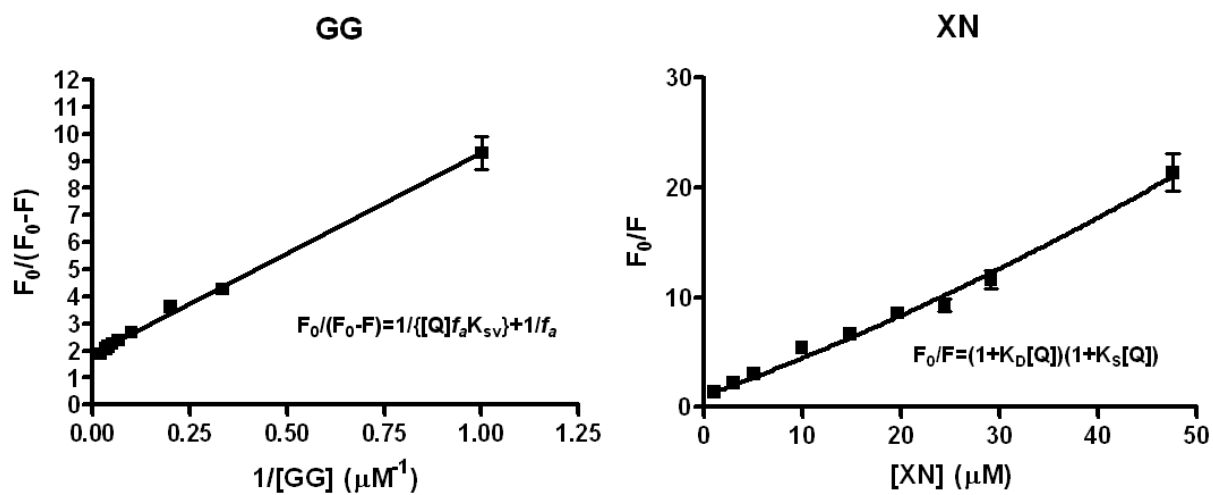


Figure 5.4 Modified Stern-Volmer plots for GG and XN quenching of hFXR-LBD



Figure 5.5

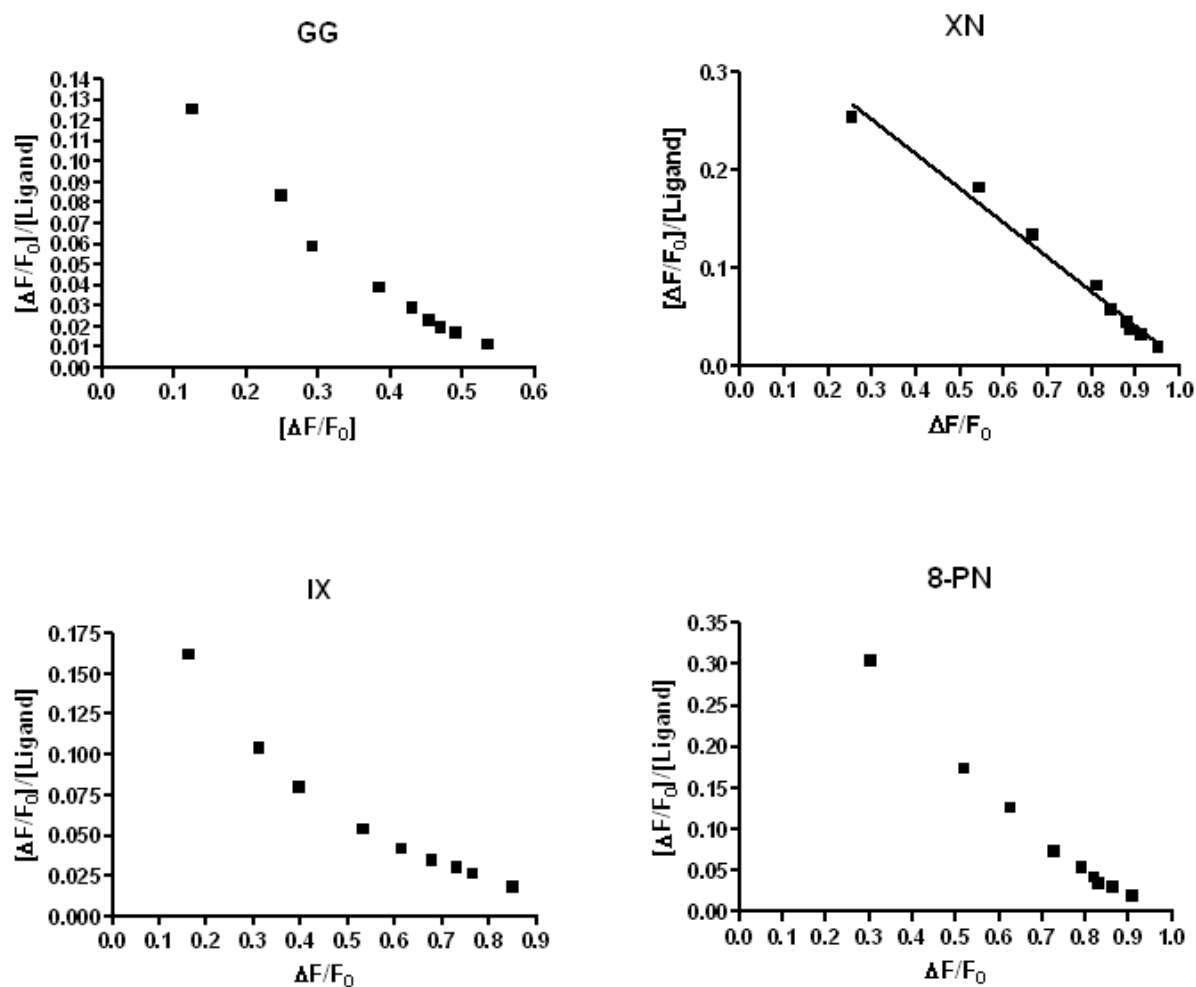


Figure 5.5 Scatchard plots of the hFXR-LBD-molecule binding data

Figure 5.6

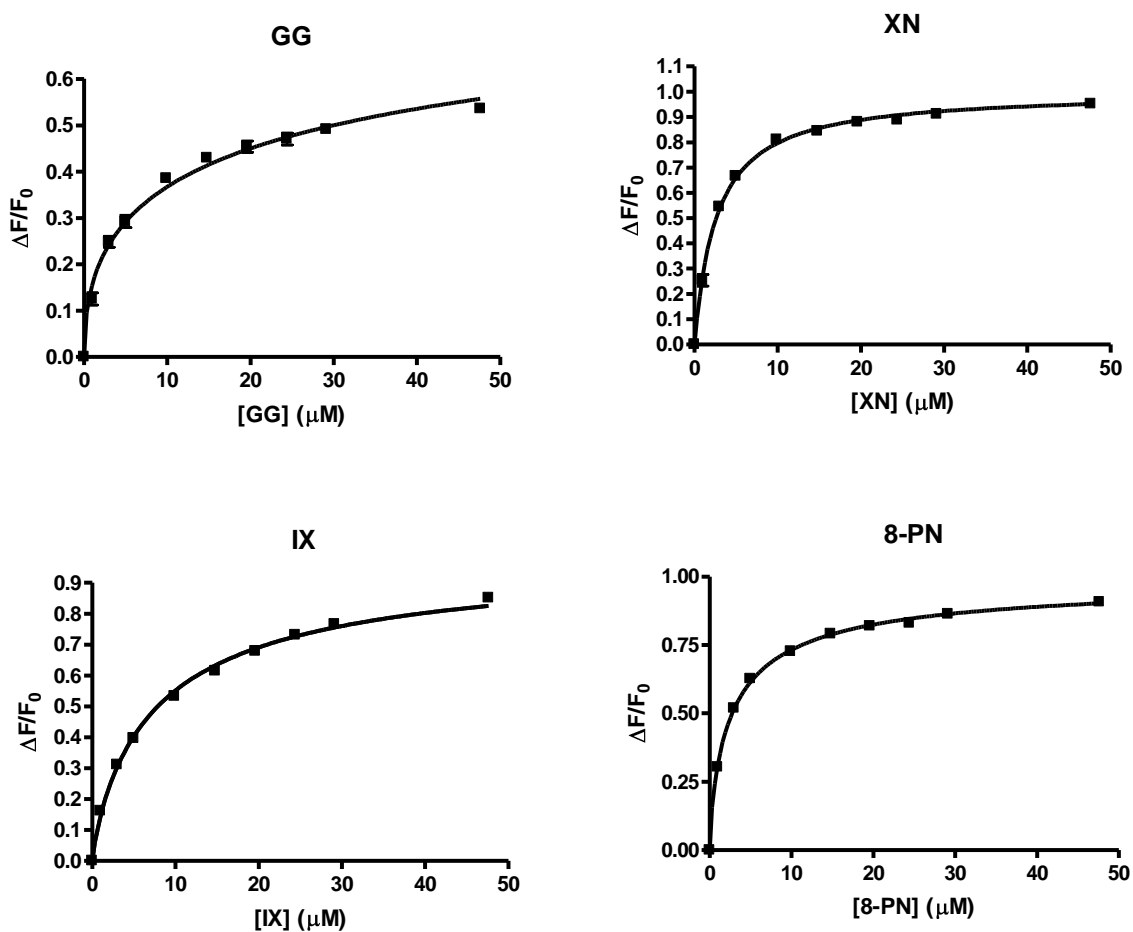


Figure 5.6 Hill plots of the hFXR-LBD-molecule binding data

Figure 5.7

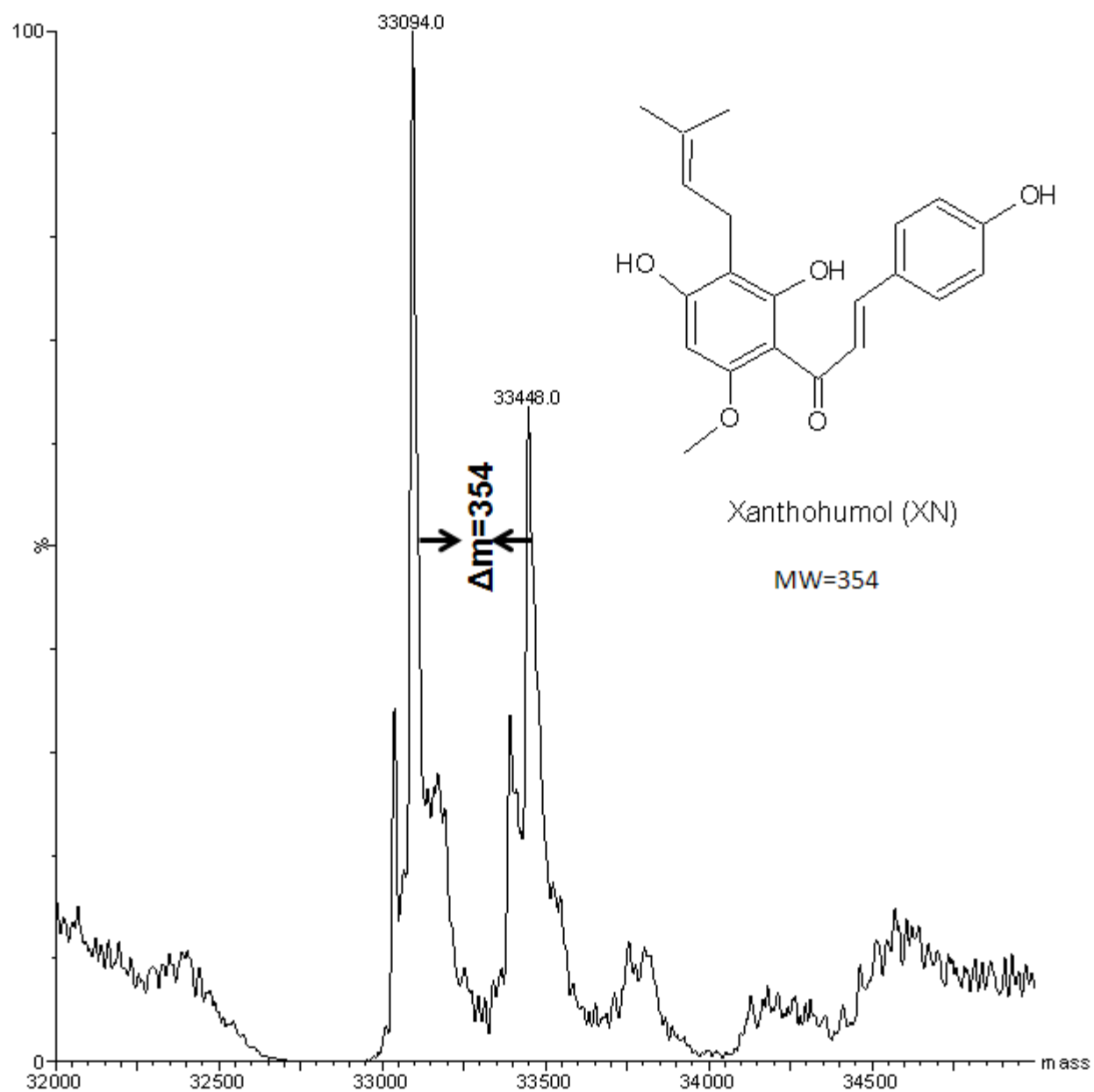


Figure 5.7 Mass spectra of XN exhibiting covalently binding to hFXR-LBD

Table 5.1

	$K_{SV} \times 10^5 \text{ (M}^{-1}\text{)}$	$f_a$	$K_S \times 10^5 \text{ (M}^{-1}\text{)}$	$k_q \times 10^{13} \text{ (M}^{-1}\text{S}^{-1}\text{)}$	$R^2$
GG*	2.53±0.13	0.53±0.02	-	8.43±0.43	0.9983
XN**	0.006±0.003 ( $K_D$ )	-	3.25±0.32	0.02±0.01	0.9931
IX	1.15±0.02	-	-	3.83±0.07	0.9922
8-PN	1.94±0.05	-	-	6.47±0.17	0.9952

Table 5.1 The Stern-Volmer constant ( $K_{SV}$ ), the fraction of fluorophore accessible to the quencher ( $f_a$ ), the bimolecular quenching constants ( $k_q$ ), the dynamic quenching constant ( $K_D$ ) and the static quenching constant ( $K_S$ ) of the hFXR-LBD-ligand

Table 5.2

	$n_H$	$K_d$ ( $\mu\text{M}$ )	$K_d^*$ ( $\mu\text{M}$ )	$R^2$
GG	0.50 $\pm$ 0.02	5.4 $\pm$ 0.3	4.0 $\pm$ 0.2	0.9832
XN	1.02 $\pm$ 0.02	2.7 $\pm$ 0.1	3.1 $\pm$ 0.3	0.9967
IX	0.86 $\pm$ 0.02	5.9 $\pm$ 0.3	8.7 $\pm$ 0.2	0.9964
8-PN	0.78 $\pm$ 0.01	2.2 $\pm$ 0.0	5.2 $\pm$ 0.1	0.9987

Table 5.2 Hill coefficient  $n_H$  and the apparent dissociation constant  $K_d$  ( $\mu\text{M}$ ) for different ligands with hFXR-LBD

Table 5.3

<b>Group A</b>	Ligands	GG	CDCA	XN	IX	8-PN	TX
	volume ( $\text{\AA}^3$ )	312.8	404.6	326.8	326.9	303.9	342.8

<b>Group B</b>	Ligands	6-ECDC	3-deoxyCDCA	GW4064	MFA-1	fexaramine	XL335	benzimidazolyl acetamide
	volume ( $\text{\AA}^3$ )	438.3	395.9	443.7	401.6	482.8	383.5	441.7

Table 5.3 Comparison of different ligand volumes

## 5.7 Reference

- [1] P. Lefebvre, B. Cariou, F. Lien, F. Kuipers, B. Staels, Role of bile acids and bile acid receptors in metabolic regulation, *Physiol Rev*, 89 (2009) 147-191.
- [2] S. Fiorucci, G. Rizzo, A. Donini, E. Distrutti, L. Santucci, Targeting farnesoid X receptor for liver and metabolic disorders, *Trends Mol Med*, 13 (2007) 298-309.
- [3] S. Westin, R.A. Heyman, R. Martin, FXR, a therapeutic target for bile acid and lipid disorders, *Mini Rev Med Chem*, 5 (2005) 719-727.
- [4] D. Merk, D. Steinhilber, M. Schubert-Zsilavecz, Medicinal chemistry of farnesoid X receptor ligands: from agonists and antagonists to modulators, *Future Med Chem*, 4 (2012) 1015-1036.
- [5] J.F. Stevens, A.W. Taylor, J.E. Clawson, M.L. Deinzer, Fate of xanthohumol and related prenylflavonoids from hops to beer, *J Agric Food Chem*, 47 (1999) 2421-2428.
- [6] J.F. Stevens, A.W. Taylor, M.L. Deinzer, Quantitative analysis of xanthohumol and related prenylflavonoids in hops and beer by liquid chromatography-tandem mass spectrometry, *J Chromatogr A*, 832 (1999) 97-107.
- [7] S.R. Milligan, J.C. Kalita, A. Heyerick, H. Rong, L. De Cooman, D. De Keukeleire, Identification of a potent phytoestrogen in hops (*Humulus lupulus* L.) and beer, *J Clin Endocrinol Metab*, 84 (1999) 2249-2252.
- [8] P. Zanolli, M. Zavatti, Pharmacognostic and pharmacological profile of *Humulus lupulus* L, *J Ethnopharmacol*, 116 (2008) 383-396.
- [9] P.J. Magalhaes, D.O. Carvalho, J.M. Cruz, L.F. Guido, A.A. Barros, Fundamentals and health benefits of xanthohumol, a natural product derived from hops and beer, *Nat Prod Commun*, 4 (2009) 591-610.
- [10] J.F. Stevens, J.E. Page, Xanthohumol and related prenylflavonoids from hops and beer: to your good health!, *Phytochemistry*, 65 (2004) 1317-1330.
- [11] H. Nozawa, Xanthohumol, the chalcone from beer hops (*Humulus lupulus* L.), is the ligand for farnesoid X receptor and ameliorates lipid and glucose metabolism in KK-A(y) mice, *Biochem Biophys Res Commun*, 336 (2005) 754-761.
- [12] J.Y. Yang, M.A. Della-Fera, S. Rayalam, C.A. Baile, Effect of xanthohumol and isoxanthohumol on 3T3-L1 cell apoptosis and adipogenesis, *Apoptosis*, 12 (2007) 1953-1963.
- [13] A. Casaschi, G.K. Maiyoh, B.K. Rubio, R.W. Li, K. Adeli, A.G. Theriault, The chalcone xanthohumol inhibits triglyceride and apolipoprotein B secretion in HepG2 cells, *J Nutr*, 134 (2004) 1340-1346.
- [14] C.J. Sinal, F.J. Gonzalez, Guggulsterone: an old approach to a new problem, *Trends Endocrinol Metab*, 13 (2002) 275-276.

- [15] J. Wu, C. Xia, J. Meier, S. Li, X. Hu, D.S. Lala, The hypolipidemic natural product guggulsterone acts as an antagonist of the bile acid receptor, *Mol Endocrinol*, 16 (2002) 1590-1597.
- [16] N.L. Urizar, D.D. Moore, GUGULIPID: a natural cholesterol-lowering agent, *Annu Rev Nutr*, 23 (2003) 303-313.
- [17] N.L. Urizar, A.B. Liverman, D.T. Dodds, F.V. Silva, P. Ordentlich, Y. Yan, F.J. Gonzalez, R.A. Heyman, D.J. Mangelsdorf, D.D. Moore, A natural product that lowers cholesterol as an antagonist ligand for FXR, *Science*, 296 (2002) 1703-1706.
- [18] R.B. Singh, M.A. Niaz, S. Ghosh, Hypolipidemic and antioxidant effects of *Commiphora mukul* as an adjunct to dietary therapy in patients with hypercholesterolemia, *Cardiovasc Drugs Ther*, 8 (1994) 659-664.
- [19] C. Ulbricht, E. Basch, P. Szapary, P. Hammerness, S. Axentsev, H. Boon, D. Kroll, L. Garraway, M. Vora, J. Woods, Guggul for hyperlipidemia: a review by the Natural Standard Research Collaboration, *Complement Ther Med*, 13 (2005) 279-290.
- [20] S. Rayalam, J.Y. Yang, M.A. Della-Fera, H.J. Park, S. Ambati, C.A. Baile, Anti-obesity effects of xanthohumol plus guggulsterone in 3T3-L1 adipocytes, *J Med Food*, 12 (2009) 846-853.
- [21] R. Deng, Therapeutic effects of guggul and its constituent guggulsterone: cardiovascular benefits, *Cardiovasc Drug Rev*, 25 (2007) 375-390.
- [22] B.Z. Yu, R. Kaimal, S. Bai, K.A. El Sayed, S.A. Tatulian, R.J. Apitz, M.K. Jain, R. Deng, O.G. Berg, Effect of guggulsterone and cembranoids of *Commiphora mukul* on pancreatic phospholipase A(2): role in hypocholesterolemia, *J Nat Prod*, 72 (2009) 24-28.
- [23] J.R. Lakowicz, SpringerLink (Online service), Principles of Fluorescence Spectroscopy, in, Springer Science+Business Media, LLC, Boston, MA, 2006.
- [24] D. Silva, C.M. Cortez, J. Cunha-Bastos, S.R. Louro, Methyl parathion interaction with human and bovine serum albumin, *Toxicol Lett*, 147 (2004) 53-61.
- [25] S. Bakkialakshmi, D. Chandrakala, A spectroscopic investigations of anticancer drugs binding to bovine serum albumin, *Spectrochim Acta A Mol Biomol Spectrosc*, 88 (2012) 2-9.
- [26] P.W. Chao, C.S. Chow, Monitoring aminoglycoside-induced conformational changes in 16S rRNA through acrylamide quenching, *Bioorg Med Chem*, 15 (2007) 3825-3831.
- [27] S.S. Lehrer, Solute perturbation of protein fluorescence. The quenching of the tryptophyl fluorescence of model compounds and of lysozyme by iodide ion, *Biochemistry*, 10 (1971) 3254-3263.
- [28] A.V. Hill, The Combinations of Haemoglobin with Oxygen and with Carbon Monoxide. I, *Biochem J*, 7 (1913) 471-480.



- [29] K.C. Han, J.H. Kim, K.H. Kim, E.E. Kim, J.H. Seo, E.G. Yang, Identification of farnesoid X receptor modulators by a fluorescence polarization-based interaction assay, *Anal Biochem*, 398 (2010) 185-190.
- [30] M. Moller, A. Denicola, Protein tryptophan accessibility studied by fluorescence quenching, *Biochem Mol Biol Edu*, 30 (2002) 175-178.
- [31] Z. Wang, X. Tan, D. Chen, Q. Yue, Z. Song, Study on the binding behavior of lysozyme with cephalosporin analogues by fluorescence spectroscopy, *J Fluoresc*, 19 (2009) 801-808.
- [32] P.B. Kandagal, S. Ashoka, J. Seetharamappa, S.M. Shaikh, Y. Jadegoud, O.B. Ijare, Study of the interaction of an anticancer drug with human and bovine serum albumin: spectroscopic approach, *J Pharm Biomed Anal*, 41 (2006) 393-399.
- [33] F.L. Cui, J. Fan, J.P. Li, Z.D. Hu, Interactions between 1-benzoyl-4-p-chlorophenyl thiosemicarbazide and serum albumin: investigation by fluorescence spectroscopy, *Bioorg Med Chem*, 12 (2004) 151-157.
- [34] F. Ding, W. Liu, F. Liu, Z.Y. Li, Y. Sun, A study of the interaction between malachite green and lysozyme by steady-state fluorescence, *J Fluoresc*, 19 (2009) 783-791.
- [35] A. Papadopoulou, R.J. Green, R.A. Frazier, Interaction of flavonoids with bovine serum albumin: a fluorescence quenching study, *J Agric Food Chem*, 53 (2005) 158-163.
- [36] F. Rasoulzadeh, H.N. Jabary, A. Naseri, M.R. Rashidi, Fluorescence quenching study of quercetin interaction with bovine milk xanthine oxidase, *Spectrochim Acta A Mol Biomol Spectrosc*, 72 (2009) 190-193.
- [37] J.R. Lakowicz, G. Weber, Quenching of fluorescence by oxygen. A probe for structural fluctuations in macromolecules, *Biochemistry*, 12 (1973) 4161-4170.
- [38] P. Somasundaran, A.T. Hubbard, *Encyclopedia of surface and colloid science*, Marcel Dekker, New York, 2002.
- [39] T. Nishimaki-Mogami, M. Une, T. Fujino, Y. Sato, N. Tamehiro, Y. Kawahara, K. Shudo, K. Inoue, Identification of intermediates in the bile acid synthetic pathway as ligands for the farnesoid X receptor, *J Lipid Res*, 45 (2004) 1538-1545.
- [40] T.P. Burris, C. Montrose, K.A. Houck, H.E. Osborne, W.P. Bocchinfuso, B.C. Yaden, C.C. Cheng, R.W. Zink, R.J. Barr, C.D. Hepler, V. Krishnan, H.A. Bullock, L.L. Burris, R.J. Galvin, K. Bramlett, K.R. Stayrook, The hypolipidemic natural product guggulsterone is a promiscuous steroid receptor ligand, *Mol Pharmacol*, 67 (2005) 948-954.
- [41] M.I. Kaldas, U.K. Walle, H. van der Woude, J.M. McMillan, T. Walle, Covalent binding of the flavonoid quercetin to human serum albumin, *J Agric Food Chem*, 53 (2005) 4194-4197.

- [42] T. Waku, T. Shiraki, T. Oyama, Y. Fujimoto, K. Maebara, N. Kamiya, H. Jingami, K. Morikawa, Structural insight into PPARgamma activation through covalent modification with endogenous fatty acids, *J Mol Biol*, 385 (2009) 188-199.
- [43] T. Waku, T. Shiraki, T. Oyama, K. Morikawa, Atomic structure of mutant PPARgamma LBD complexed with 15d-PGJ2: novel modulation mechanism of PPARgamma/RXRalpha function by covalently bound ligands, *FEBS Lett*, 583 (2009) 320-324.
- [44] M.A. Danielson, H.P. Biemann, D.E. Koshland, Jr., J.J. Falke, Attractant- and disulfide-induced conformational changes in the ligand binding domain of the chemotaxis aspartate receptor: a 19F NMR study, *Biochemistry*, 33 (1994) 6100-6109.
- [45] H.P. Biemann, D.E. Koshland, Jr., Aspartate receptors of *Escherichia coli* and *Salmonella typhimurium* bind ligand with negative and half-of-the-sites cooperativity, *Biochemistry*, 33 (1994) 629-634.
- [46] J.A. Lupisella, J.E. Driscoll, W.J. Metzler, P.R. Reczek, The ligand binding domain of the human retinoic acid receptor gamma is predominantly alpha-helical with a Trp residue in the ligand binding site, *J Biol Chem*, 270 (1995) 24884-24890.
- [47] U. Meyer, G. Costantino, A. Macchiarulo, R. Pellicciari, Is antagonism of E/Z-guggulsterone at the farnesoid X receptor mediated by a noncanonical binding site? A molecular modeling study, *J Med Chem*, 48 (2005) 6948-6955.
- [48] R. Deng, D. Yang, A. Radke, J. Yang, B. Yan, The hypolipidemic agent guggulsterone regulates the expression of human bile salt export pump: dominance of transactivation over farnesoid X receptor-mediated antagonism, *J Pharmacol Exp Ther*, 320 (2007) 1153-1162.
- [49] J. Cui, L. Huang, A. Zhao, J.L. Lew, J. Yu, S. Sahoo, P.T. Meinke, I. Royo, F. Pelaez, S.D. Wright, Guggulsterone is a farnesoid X receptor antagonist in coactivator association assays but acts to enhance transcription of bile salt export pump, *J Biol Chem*, 278 (2003) 10214-10220.
- [50] A.A. Bogan, F.E. Cohen, T.S. Scanlan, Natural ligands of nuclear receptors have conserved volumes, *Nat Struct Biol*, 5 (1998) 679-681.
- [51] L.Z. Mi, S. Devarakonda, J.M. Harp, Q. Han, R. Pellicciari, T.M. Willson, S. Khorasanizadeh, F. Rastinejad, Structural basis for bile acid binding and activation of the nuclear receptor FXR, *Mol Cell*, 11 (2003) 1093-1100.
- [52] A. Zhao, J. Yu, J.L. Lew, L. Huang, S.D. Wright, J. Cui, Polyunsaturated fatty acids are FXR ligands and differentially regulate expression of FXR targets, *DNA Cell Biol*, 23 (2004) 519-526.
- [53] W. Bourguet, P. Germain, H. Gronemeyer, Nuclear receptor ligand-binding domains: three-dimensional structures, molecular interactions and pharmacological implications, *Trends Pharmacol Sci*, 21 (2000) 381-388.

## **Chapter 6**

## **Conclusion**

This dissertation is centered on the development and application of Hydrogen Deuterium Exchange Mass Spectrometry (HDX-MS) for deciphering the effects of small molecule interactions on the conformational dynamics of the ligand binding domain (LBD) of the farnesoid X receptor (FXR) a nuclear receptor that regulates bile acid, lipid and glucose homeostasis. FXR has emerged as a highly researched and exciting pharmacological target. The pharmacological modulation of FXR by natural and/or synthetic ligands has great potential in the prevention and therapy of metabolic diseases, including metabolic syndromes and diabetes. This thesis research addressed the need of developing analytical strategies that allow obtaining structural description of FXR ligand complexes that provide molecular determinants for assisting structure-activity relationship (SAR) studies of FXR-targeting small molecule modulators with clinical potential.

Initial work demonstrates that HDX experiments in conjunction with mass spectrometry are capable of providing structural dynamics information for studying FXR ligand interactions. The HDX protection profiles for each FXR-LBD-ligand system revealed that the three regions encompassing the canonical binding pocket, 288-298 (Helix 3), 320-336 (Helix 5), and 361-375 (Helix 7), are protected by the molecular recognition of each ligand but the extent of exchange protection varies, suggesting that the FXR-LBD can harbor ligands of diverse chemotypes. Specifically, the synthetic high affinity agonist GW4064 presents distinct higher protection for regions containing contact residues and forming the ligand binding cavity in the FXR-LBD when compared to the low affinity agonist, CDCA, and the prenylflavonoid-type ligands, XN, IX, 8PN, and TX. The finding that exchange protection profiles reflect on the mode of ligand binding let us to speculate that the extent of exchange protection may hint towards binding modes that typify partial agonists.

Moreover, HDX experiments involving Z-guggulsterone, a recognized *in vitro* antagonist of FXR, resulted in protection profiles encompassing the partial sequences 201-278 and 388-396, which cover the H1-H2 loop and parts of helix H8 including the H8-H9 loop. The protection of these regions supports a model in which *in vitro* antagonism and modulation of FXR by GG may indeed involve a secondary noncanonical binding site as predicted previously.

Molecular docking studies resulted in models that predict that the prenylflavonoids tested can form hydrogen bonding interactions with residues Arg331 (Helix 5), Ser332 (Helix5), and Tyr369 (Helix 7), in accord with our HDX protection data that localized the molecular interaction of the diverse prenylflavonoids within the classical ligand binding cavity. Additionally, our research suggests that it is possible, starting from the metabolically unstable compound (XN), to obtain a more stable derivative (TX) with the same binding properties.

The fluorescence quenching titration data complemented our HDX and molecular docking studies. The fluorescence intensity changes in the tryptophan residues in FXR-LBD in the presence of the seven ligands suggest one high affinity ligand binding site in proximity to the tryptophan residues in the protein. The quenching mechanism of XN, IX, 8-PN, and GG binding to FXR-LBD was mainly caused by static quenching and, thus, indicating the formation of state-ground protein-ligand complexes. The quenching data analysis of XN binding with the FXR-LBD implied a combination of static and dynamic quenching, and the later might be caused by the covalent binding of XN, a weak electrophile, and FXR-LBD. The magnitude of the apparent dissociation constant  $K_d$  is in the micromolar range, suggesting that XN, IX, and 8-PN are low affinity ligands of the FXR-LBD. These results suggest that molecular size of the ligand and/or hydrophobicity could be contributing factors that affect the interaction between ligand and FXR LBD.

In conclusion, the current HDX-MS studies enabled obtaining unique insights into mechanisms of molecular recognition of diverse ligands by FXR. The exchange protection profiles reflected on the disparate mode of conformational stabilization of FXR LBD upon binding. Ligand-dependent modulation of the conformational dynamics of the LBD upon ligand binding has been reported for other nuclear receptors as well.

We foresee that HDX-MS as an analytical technique for profiling the modulation of conformational dynamics of FXR LBD by small molecule ligands will make important contributions to ongoing medicinal chemistry and SAR studies that aim to develop synthetic FXR ligands with acceptable pharmacological profiles.

## Abbreviation

6ECDCA	6 $\alpha$ -ethyl-chenodeoxycholic acid
6PN	6-prenylnaringenin
8-PN	8-prenylneringenin
AA	arachidonic acid
ASBT	the apical sodium-dependent bile acid transporter
BAAT	bile acid CoA–amino acid N-acetyltransferase
BACS	bile acid CoA synthase
BSEP	bile salt export pump
CDCA	chenodeoxycholic acid
CYP7A1	cytochrome P450 7A1
DA	docosahexaenoic acid
DC	direct voltage
DCA	deoxycholic acid
DDA	data dependent mode
DIA	data-independent acquisition
DMSO	Dimethylsulfoxide
ER	estrogen receptors
ESI	electrospray ionization
FAS	fatty acid synthase
FGF15	fibroblast growth factor 15

FGF4R	FGF4 receptor
FTICR	fourier-transform ion cyclotron resonance
FXR	farnesoic X receptor
G6Pase	glucose-6-phosphatase
GFP	glu-fibrinopeptide
GG	Z-guggulsterone
GR	glucocorticoid receptor
HDMS	high definition mass spectrometry
HDX	hydrogen deuterium exchange
IA	ion accounting
IBABP	ileal bile acid binding-protein
IM	ion-mobility
IMS	IM spectrometry
IPTG	isopropyl- $\beta$ -D-thiogalactopyranoside
IX	Isoxanthohumol
LA	and linolenic acid
LBC	ligand binding cavity
LBD	ligand binding domain
LCA	lithocholic acid
MALDI	matrix-assisted laser desorption/ionization
MDR2	multidrug resistance protein 2



MS	mass spectrometry
NR	nuclear receptor
NTCP	sodium taurocholate cotransporting polypeptide
OATP	organic anion transporting polypeptide
OST $\alpha$	organic solute transporter- $\alpha$
PBC	primary biliary cirrhosis
PEPCK	phosphoenolpyruvate carboxykinase
PLGS	proteinLynx Global Server
PPAR	peroxisome proliferator-activated receptor
Q	quadrupole
QIT	quadruple ion trap
RF	radio frequency
RXR	retinoid X receptor
SAR	structure-activity relationship
SDS-PAGE	sodium dodecyl sulfate –acrylamide gel electrophoresis
SHP	small heterodimer partner
SREBP1C	sterol-regulatory element-binding protein 1C
SULT2A1	bile acid-modifying enzymes sulphotransferase 2A1
TCEP	Tris (2-carboxyethyl) phosphine hydrochloride
THR	thyroid hormone receptor
ToF	time-of-flight

TWIM	traveling wave ion mobility
TX	Tetrahydroxanthohumol
UDCA	ursodeoxycholic acid
UGT2B4	UDP-glucuronosyltransferase 2B4
VDR	vitamin D receptor
VDR	vitamin D receptor
XN	Xanthohumol

## Bibliography

- [1] R. Abagyan, M. Totrov, and D. Kuznetsov. , ICM - A new method for protein modeling and design: applications to docking and structure prediction from the distorted native conformation, *J Comput Chem*, 15 (1994) 488-506.
- [2] R. Abagyan, M. Totrov, Biased probability Monte Carlo conformational searches and electrostatic calculations for peptides and proteins, *J Mol Biol*, 235 (1994) 983-1002.
- [3] K.R. Acharya, the advantages and limitations of protein crystal structure, *Trends in pharmacological sciences*, 26 (2005) 10-14.
- [4] A. Akwabi-Ameyaw, J.Y. Bass, R.D. Caldwell, J.A. Caravella, L. Chen, K.L. Creech, D.N. Deaton, S.A. Jones, I. Kaldor, Y. Liu, K.P. Madauss, H.B. Marr, R.B. McFadyen, A.B. Miller, F.N. Iii, D.J. Parks, P.K. Spearing, D. Todd, S.P. Williams, G.B. Wisely, Conformationally constrained farnesoid X receptor (FXR) agonists: Naphthoic acid-based analogs of GW 4064, *Bioorg Med Chem Lett*, 18 (2008) 4339-4343.
- [5] A. Akwabi-Ameyaw, J.Y. Bass, R.D. Caldwell, J.A. Caravella, L.H. Chen, K.L. Creech, D.N. Deaton, K.P. Madauss, H.B. Marr, R.B. McFadyen, A.B. Miller, F. Navas, D.J. Parks, P.K. Spearing, D. Todd, S.P. Williams, G.B. Wisely, FXR agonist activity of conformationally constrained analogs of GW 4064, *Bioorganic & Medicinal Chemistry Letters*, 19 (2009) 4733-4739.
- [6] A. Akwabi-Ameyaw, J.A. Caravella, L.H. Chen, K.L. Creech, D.N. Deaton, K.P. Madauss, H.B. Marr, A.B. Miller, F. Navas, D.J. Parks, P.K. Spearing, D. Todd, S.P. Williams, B. Wisely, Conformationally constrained farnesoid X receptor (FXR) agonists: Alternative replacements of the stilbene, *Bioorganic & Medicinal Chemistry Letters*, 21 (2011) 6154-6160.
- [7] M. Ananthanarayanan, N. Balasubramanian, M. Makishima, D.J. Mangelsdorf, F.J. Suchy, Human bile salt export pump promoter is transactivated by the farnesoid X receptor/bile acid receptor, *J Biol Chem*, 276 (2001) 28857-28865.
- [8] Y. Bai, J.S. Milne, L. Mayne, S.W. Englander, Primary structure effects on peptide group hydrogen exchange, *Proteins*, 17 (1993) 75-86.
- [9] S. Bakkialakshmi, D. Chandrakala, A spectroscopic investigations of anticancer drugs binding to bovine serum albumin, *Spectrochim Acta A Mol Biomol Spectrosc*, 88 (2012) 2-9.
- [10] J.Y. Bass, R.D. Caldwell, J.A. Caravella, L.H. Chen, K.L. Creech, D.N. Deaton, K.P. Madauss, H.B. Marr, R.B. McFadyen, A.B. Miller, D.J. Parks, D. Todd, S.P. Williams, G.B. Wisely, Substituted isoxazole analogs of farnesoid X receptor (FXR) agonist GW4064, *Bioorganic & Medicinal Chemistry Letters*, 19 (2009) 2969-2973.
- [11] J.Y. Bass, J.A. Caravella, L.H. Chen, K.L. Creech, D.N. Deaton, K.P. Madauss, H.B. Marr, R.B. McFadyen, A.B. Miller, W.Y. Mills, F. Navas, D.J. Parks, T.L. Smalley, P.K. Spearing, D. Todd, S.P. Williams, G.B. Wisely, Conformationally constrained farnesoid X receptor (FXR)

agonists: Heteroaryl replacements of the naphthalene, *Bioorganic & Medicinal Chemistry Letters*, 21 (2011) 1206-1213.

[12] E. Bertl, klmo, K., Heiss, E., Klenke, F., Peschke, P., Becker, H., Eicher, T., Herhaus, C., Kapadia, G., Bartsch, H., Gerhauser, C., , Identification of novel inhibitors of angiogenesis using a human in vitro anti-angiogenic assay, *International Journal of Cancer Prevention*, 1 (2004) 47-61.

[13] H.P. Biemann, D.E. Koshland, Jr., Aspartate receptors of *Escherichia coli* and *Salmonella typhimurium* bind ligand with negative and half-of-the-sites cooperativity, *Biochemistry*, 33 (1994) 629-634.

[14] M. Blumenthal, The complete german commission E monograph: therapeutic guide to herbal medicines., American botanical council, (1998) 147.

[15] M. Blumenthal, Goldberg, A., Brinckmann J., , *Herbal Medicine: Expanded Commission E Monographs.* , Integrative Medicine Communications, Newton, MA, (2000) 297-103.

[16] A.A. Bogan, F.E. Cohen, T.S. Scanlan, Natural ligands of nuclear receptors have conserved volumes, *Nat Struct Biol*, 5 (1998) 679-681.

[17] W. Bourguet, P. Germain, H. Gronemeyer, Nuclear receptor ligand-binding domains: three-dimensional structures, molecular interactions and pharmacological implications, *Trends Pharmacol Sci*, 21 (2000) 381-388.

[18] J. Bowe, X.F. Li, J. Kinsey-Jones, A. Heyerick, S. Brain, S. Milligan, K. O'Byrne, The hop phytoestrogen, 8-prenylnaringenin, reverses the ovariectomy-induced rise in skin temperature in an animal model of menopausal hot flashes, *J Endocrinol*, 191 (2006) 399-405.

[19] T.P. Burris, C. Montrose, K.A. Houck, H.E. Osborne, W.P. Bocchinfuso, B.C. Yaden, C.C. Cheng, R.W. Zink, R.J. Barr, C.D. Hepler, V. Krishnan, H.A. Bullock, L.L. Burris, R.J. Galvin, K. Bramlett, K.R. Stayrook, The hypolipidemic natural product guggulsterone is a promiscuous steroid receptor ligand, *Mol Pharmacol*, 67 (2005) 948-954.

[20] A.C. Calkin, P. Tontonoz, Transcriptional integration of metabolism by the nuclear sterol-activated receptors LXR and FXR, *Nat Rev Mol Cell Biol*, 13 (2012) 213-224.

[21] Y. Campbell, The effect of dietary compounds on human cathelicidin antimicrobial peptide gene expression mediated through farnesoid X receptor and its potential role in gastrointestinal health.

[22] S. Caron, C. Huaman Samanez, H. Dehondt, M. Ploton, O. Briand, F. Lien, E. Dorchies, J. Dumont, C. Postic, B. Cariou, P. Lefebvre, B. Staels, Farnesoid X receptor inhibits the transcriptional activity of carbohydrate response element binding protein in human hepatocytes, *Mol Cell Biol*, 33 (2013) 2202-2211.

[23] L.G. Carr, Westey, C., , Surviving folktales and herbal lore among the shinnecock Indians., *Journal of American Folklore*, 58 (1945) 113-123.

- [24] A. Casaschi, G.K. Maiyoh, B.K. Rubio, R.W. Li, K. Adeli, A.G. Theriault, The chalcone xanthohumol inhibits triglyceride and apolipoprotein B secretion in HepG2 cells, *J Nutr*, 134 (2004) 1340-1346.
- [25] M.J. Chalmers, B.D. Pascal, S. Willis, J. Zhang, S.J. Iturria, J.A. Dodge, P.R. Griffin, Methods for the Analysis of High Precision Differential Hydrogen Deuterium Exchange Data, *Int J Mass Spectrom*, 302 (2011) 59-68.
- [26] P.W. Chao, C.S. Chow, Monitoring aminoglycoside-induced conformational changes in 16S rRNA through acrylamide quenching, *Bioorg Med Chem*, 15 (2007) 3825-3831.
- [27] T.P. Charles, R.; Pruzanski, M.; Auwxr, J.; Schoonjans, K. , Targeting bile-acid signalling for metabolic diseases, *Nat Rev Drug Discovery*, 7 (2008) 678.
- [28] F. Chen, M. Ananthanarayanan, S. Emre, E. Neimark, L.N. Bull, A.S. Knisely, S.S. Strautnieks, R.J. Thompson, M.S. Magid, R. Gordon, N. Balasubramanian, F.J. Suchy, B.L. Shneider, Progressive familial intrahepatic cholestasis, type 1, is associated with decreased farnesoid X receptor activity, *Gastroenterology*, 126 (2004) 756-764.
- [29] H. Choi, H. Hwang, J. Chin, E. Kim, J. Lee, S.J. Nam, B.C. Lee, B.J. Rho, H. Kang, Tuberatolides, potent FXR antagonists from the Korean marine tunicate *Botryllus tuberatus*, *J Nat Prod*, 74 (2011) 90-94.
- [30] J.J. Chou, R. Sounier, Solution nuclear magnetic resonance spectroscopy, *Methods Mol Biol*, 955 (2013) 495-517.
- [31] E.C. Colgate, C.L. Miranda, J.F. Stevens, T.M. Bray, E. Ho, Xanthohumol, a prenylflavonoid derived from hops induces apoptosis and inhibits NF-kappaB activation in prostate epithelial cells, *Cancer Lett*, 246 (2007) 201-209.
- [32] R. Costa, R. Negrao, I. Valente, A. Castela, D. Duarte, L. Guardao, P.J. Magalhaes, J.A. Rodrigues, J.T. Guimaraes, P. Gomes, R. Soares, Xanthohumol modulates inflammation, oxidative stress, and angiogenesis in type 1 diabetic rat skin wound healing, *J Nat Prod*, 76 (2013) 2047-2053.
- [33] G. Costantino, A. Entrena-Guadix, A. Macchiarulo, A. Gioiello, R. Pellicciari, Molecular dynamics simulation of the ligand binding domain of farnesoid X receptor. Insights into helix-12 stability and coactivator peptide stabilization in response to agonist binding, *J Med Chem*, 48 (2005) 3251-3259.
- [34] M.L. Crawley, Farnesoid X receptor modulators: a patent review, *Expert Opin Ther Pat*, 20 (2010) 1047-1057.
- [35] J. Cui, L. Huang, A. Zhao, J.L. Lew, J. Yu, S. Sahoo, P.T. Meinke, I. Royo, F. Pelaez, S.D. Wright, Guggulsterone is a farnesoid X receptor antagonist in coactivator association assays but acts to enhance transcription of bile salt export pump, *J Biol Chem*, 278 (2003) 10214-10220.

- [36] S.Y. Dai, T.P. Burris, J.A. Dodge, C. Montrose-Rafizadeh, Y. Wang, B.D. Pascal, M.J. Chalmers, P.R. Griffin, Unique ligand binding patterns between estrogen receptor alpha and beta revealed by hydrogen-deuterium exchange, *Biochemistry*, 48 (2009) 9668-9676.
- [37] S.Y. Dai, M.J. Chalmers, J. Bruning, K.S. Bramlett, H.E. Osborne, C. Montrose-Rafizadeh, R.J. Barr, Y. Wang, M. Wang, T.P. Burris, J.A. Dodge, P.R. Griffin, Prediction of the tissue-specificity of selective estrogen receptor modulators by using a single biochemical method, *Proc Natl Acad Sci U S A*, 105 (2008) 7171-7176.
- [38] M.A. Danielson, H.P. Biemann, D.E. Koshland, Jr., J.J. Falke, Attractant- and disulfide-induced conformational changes in the ligand binding domain of the chemotaxis aspartate receptor: a <sup>19</sup>F NMR study, *Biochemistry*, 33 (1994) 6100-6109.
- [39] P.H. Dawson, *Quadrupole Mass Spectrometry and Its Applications.*, in, Springer, New York, 1995.
- [40] S. De Marino, R. Ummarino, M.V. D'Auria, M.G. Chini, G. Bifulco, B. Renga, C. D'Amore, S. Fiorucci, C. Debitus, A. Zampella, Theonellasterols and conicasterols from *Theonella swinhoei*. Novel marine natural ligands for human nuclear receptors, *J Med Chem*, 54 (2011) 3065-3075.
- [41] M. Delepierre, C.M. Dobson, M. Karplus, F.M. Poulsen, D.J. States, R.E. Wedin, Electrostatic effects and hydrogen exchange behaviour in proteins. The pH dependence of exchange rates in lysozyme, *J Mol Biol*, 197 (1987) 111-130.
- [42] L. Delmulle, A. Bellahcene, W. Dhooge, F. Comhaire, F. Roelens, K. Huvaere, A. Heyerick, V. Castronovo, D. De Keukeleire, Anti-proliferative properties of prenylated flavonoids from hops (*Humulus lupulus* L.) in human prostate cancer cell lines, *Phytomedicine*, 13 (2006) 732-734.
- [43] L. Delmulle, T. Vanden Berghe, D.D. Keukeleire, P. Vandenabeele, Treatment of PC-3 and DU145 prostate cancer cells by prenylflavonoids from hop (*Humulus lupulus* L.) induces a caspase-independent form of cell death, *Phytother Res*, 22 (2008) 197-203.
- [44] R. Deng, Therapeutic effects of guggul and its constituent guggulsterone: cardiovascular benefits, *Cardiovasc Drug Rev*, 25 (2007) 375-390.
- [45] R. Deng, D. Yang, A. Radke, J. Yang, B. Yan, The hypolipidemic agent guggulsterone regulates the expression of human bile salt export pump: dominance of transactivation over farnesoid X receptor-mediated antagonism, *J Pharmacol Exp Ther*, 320 (2007) 1153-1162.
- [46] Y. Deng, D.L. Smith, Identification of unfolding domains in large proteins by their unfolding rates, *Biochemistry*, 37 (1998) 6256-6262.
- [47] L.A. Denson, E. Sturm, W. Echevarria, T.L. Zimmerman, M. Makishima, D.J. Mangelsdorf, S.J. Karpen, The orphan nuclear receptor, shp, mediates bile acid-induced inhibition of the rat bile acid transporter, ntcp, *Gastroenterology*, 121 (2001) 140-147.

- [48] F.S. Di Leva, C. Festa, C. D'Amore, S. De Marino, B. Renga, M.V. D'Auria, E. Novellino, V. Limongelli, A. Zampella, S. Fiorucci, Binding mechanism of the farnesoid X receptor marine antagonist suvanine reveals a strategy to forestall drug modulation on nuclear receptors. Design, synthesis, and biological evaluation of novel ligands, *J Med Chem*, 56 (2013) 4701-4717.
- [49] F. Ding, W. Liu, F. Liu, Z.Y. Li, Y. Sun, A study of the interaction between malachite green and lysozyme by steady-state fluorescence, *J Fluoresc*, 19 (2009) 783-791.
- [50] M. Downes, M.A. Verdecia, A.J. Roecker, R. Hughes, J.B. Hogenesch, H.R. Kast-Woelbern, M.E. Bowman, J.L. Ferrer, A.M. Anisfeld, P.A. Edwards, J.M. Rosenfeld, J.G. Alvarez, J.P. Noel, K.C. Nicolaou, R.M. Evans, A chemical, genetic, and structural analysis of the nuclear bile acid receptor FXR, *Mol Cell*, 11 (2003) 1079-1092.
- [51] C. Eckers, A.M. Laures, K. Giles, H. Major, S. Pringle, Evaluating the utility of ion mobility separation in combination with high-pressure liquid chromatography/mass spectrometry to facilitate detection of trace impurities in formulated drug products, *Rapid Commun Mass Spectrom*, 21 (2007) 1255-1263.
- [52] S.W. Englander, N.R. Kallenbach, Hydrogen exchange and structural dynamics of proteins and nucleic acids, *Q Rev Biophys*, 16 (1983) 521-655.
- [53] S.W. Englander, T.R. Sosnick, J.J. Englander, L. Mayne, Mechanisms and uses of hydrogen exchange, *Curr Opin Struct Biol*, 6 (1996) 18-23.
- [54] M.A. Eriksson, T. Hard, L. Nilsson, On the pH dependence of amide proton exchange rates in proteins, *Biophys J*, 69 (1995) 329-339.
- [55] S. Feng, M. Yang, Z. Zhang, Z. Wang, D. Hong, H. Richter, G.M. Benson, K. Bleicher, U. Grether, R.E. Martin, J.M. Plancher, B. Kuhn, M.G. Rudolph, L. Chen, Identification of an N-oxide pyridine GW4064 analog as a potent FXR agonist, *Bioorg Med Chem Lett*, 19 (2009) 2595-2598.
- [56] J.B. Fenn, M. Mann, C.K. Meng, S.F. Wong, C.M. Whitehouse, Electrospray ionization for mass spectrometry of large biomolecules, *Science*, 246 (1989) 64-71.
- [57] L.S. Fenn, J.A. McLean, Enhanced carbohydrate structural selectivity in ion mobility-mass spectrometry analyses by boronic acid derivatization, *Chem Commun (Camb)*, (2008) 5505-5507.
- [58] M. Festa, A. Capasso, C.W. D'Acunto, M. Masullo, A.G. Rossi, C. Pizza, S. Piacente, Xanthohumol induces apoptosis in human malignant glioblastoma cells by increasing reactive oxygen species and activating MAPK pathways, *J Nat Prod*, 74 (2011) 2505-2513.
- [59] M. Festa, M. Caputo, C. Cipolla, C. D'Acunto, A. Rossi, M. Tecce, A. Capasso, The involvement of xanthohumol in the expression of annexin in human malignant glioblastoma cells, *Open Biochem J*, 7 (2013) 1-10.

- [60] A.C. Figueira, D.M. Saidenberg, P.C. Souza, L. Martinez, T.S. Scanlan, J.D. Baxter, M.S. Skaf, M.S. Palma, P. Webb, I. Polikarpov, Analysis of agonist and antagonist effects on thyroid hormone receptor conformation by hydrogen/deuterium exchange, *Mol Endocrinol*, 25 (2011) 15-31.
- [61] S. Fiorucci, G. Rizzo, A. Donini, E. Distrutti, L. Santucci, Targeting farnesoid X receptor for liver and metabolic disorders, *Trends Mol Med*, 13 (2007) 298-309.
- [62] B. Flatt, R. Martin, T.L. Wang, P. Mahaney, B. Murphy, X.H. Gu, P. Foster, J.L. Li, P. Pircher, M. Petrowski, I. Schulman, S. Westin, J. Wrobel, G. Yan, E. Bischoff, C. Daige, R. Mohan, Discovery of XL335 (WAY-362450), a Highly Potent, Selective, and Orally Active Agonist of the Farnesoid X Receptor (FXR), *Journal of Medicinal Chemistry*, 52 (2009) 904-907.
- [63] L. Frego, W. Davidson, Conformational changes of the glucocorticoid receptor ligand binding domain induced by ligand and cofactor binding, and the location of cofactor binding sites determined by hydrogen/deuterium exchange mass spectrometry, *Protein Sci*, 15 (2006) 722-730.
- [64] c. Gerhauser, Alt, A.P., Klimo, K., Knauf, J., Frank, N., Becker, H., Isolation and potential cancer chemopreventive activities of phenolic compounds of beer, *Phytochemistry Reviews*, 1 (2002) 369-377.
- [65] C. Gerhauser, Beer constituents as potential cancer chemopreventive agents, *Eur J Cancer*, 41 (2005) 1941-1954.
- [66] C. Gerhauser, Broad spectrum anti-infective potential of xanthohumol from hop (*Humulus lupulus* L.) in comparison with activities of other hop constituents and xanthohumol metabolites, *Mol Nutr Food Res*, 49 (2005) 827-831.
- [67] C. Gerhauser, A. Alt, E. Heiss, A. Gamal-Eldeen, K. Klimo, J. Knauf, I. Neumann, H.R. Scherf, N. Frank, H. Bartsch, H. Becker, Cancer chemopreventive activity of Xanthohumol, a natural product derived from hop, *Mol Cancer Ther*, 1 (2002) 959-969.
- [68] S.J. Geromanos, J.P. Vissers, J.C. Silva, C.A. Dorschel, G.Z. Li, M.V. Gorenstein, R.H. Bateman, J.I. Langridge, The detection, correlation, and comparison of peptide precursor and product ions from data independent LC-MS with data dependant LC-MS/MS, *Proteomics*, 9 (2009) 1683-1695.
- [69] M. Giles, C. McClenahan, E. Cairns, J. Mallet, An application of the Theory of Planned Behaviour to blood donation: the importance of self-efficacy, *Health Educ Res*, 19 (2004) 380-391.
- [70] B. Goodwin, S.A. Jones, R.R. Price, M.A. Watson, D.D. McKee, L.B. Moore, C. Galardi, J.G. Wilson, M.C. Lewis, M.E. Roth, P.R. Maloney, T.M. Willson, S.A. Kliewer, A regulatory cascade of the nuclear receptors FXR, SHP-1, and LXR-1 represses bile acid biosynthesis, *Mol Cell*, 6 (2000) 517-526.



- [71] V. Guixe, P.H. Rodriguez, J. Babul, Ligand-induced conformational transitions in *Escherichia coli* phosphofructokinase 2: evidence for an allosteric site for MgATP<sub>2</sub>, *Biochemistry*, 37 (1998) 13269-13275.
- [72] G.L. Guo, S. Santamarina-Fojo, T.E. Akiyama, M.J.A. Amar, B.J. Paigen, B. Brewer, F.J. Gonzalez, Effects of FXR in foam-cell formation and atherosclerosis development, *Bba-Mol Cell Biol L*, 1761 (2006) 1401-1409.
- [73] Y. Hamuro, S.J. Coales, J.A. Morrow, K.S. Molnar, S.J. Tuske, M.R. Southern, P.R. Griffin, Hydrogen/deuterium-exchange (H/D-Ex) of PPARgamma LBD in the presence of various modulators, *Protein Sci*, 15 (2006) 1883-1892.
- [74] K.C. Han, J.H. Kim, K.H. Kim, E.E. Kim, J.H. Seo, E.G. Yang, Identification of farnesoid X receptor modulators by a fluorescence polarization-based interaction assay, *Anal Biochem*, 398 (2010) 185-190.
- [75] E.A. Hanniman, G. Lambert, T.C. McCarthy, C.J. Sinal, Loss of functional farnesoid X receptor increases atherosclerotic lesions in apolipoprotein E-deficient mice, *Journal of Lipid Research*, 46 (2005) 2595-2604.
- [76] A. Hartkorn, F. Hoffmann, H. Ajamieh, S. Vogel, J. Heilmann, A.L. Gerbes, A.M. Vollmar, S. Zahler, Antioxidant effects of xanthohumol and functional impact on hepatic ischemia-reperfusion injury, *J Nat Prod*, 72 (2009) 1741-1747.
- [77] R.N. Hayes, M.L. Gross, Collision-induced dissociation, *Methods Enzymol*, 193 (1990) 237-263.
- [78] A. Heyerick, S. Vervarcke, H. Depypere, M. Bracke, D. De Keukeleire, A first prospective, randomized, double-blind, placebo-controlled study on the use of a standardized hop extract to alleviate menopausal discomforts, *Maturitas*, 54 (2006) 164-175.
- [79] A.V. Hill, The Combinations of Haemoglobin with Oxygen and with Carbon Monoxide. I, *Biochem J*, 7 (1913) 471-480.
- [80] R.Y. Huang, D.L. Rempel, M.L. Gross, HD exchange and PLIMSTEX determine the affinities and order of binding of Ca<sup>2+</sup> with troponin C, *Biochemistry*, 50 (2011) 5426-5435.
- [81] R.Y. Huang, J. Wen, R.E. Blankenship, M.L. Gross, Hydrogen-deuterium exchange mass spectrometry reveals the interaction of Fenna-Matthews-Olson protein and chlorosome CsmA protein, *Biochemistry*, 51 (2012) 187-193.
- [82] C.A. Hughes, J.G. Mandell, G.S. Anand, A.M. Stock, E.A. Komives, Phosphorylation causes subtle changes in solvent accessibility at the interdomain interface of methylesterase CheB, *J Mol Biol*, 307 (2001) 967-976.
- [83] L. Jin, X. Feng, H. Rong, Z. Pan, Y. Inaba, L. Qiu, W. Zheng, S. Lin, R. Wang, Z. Wang, S. Wang, H. Liu, S. Li, W. Xie, Y. Li, The antiparasitic drug ivermectin is a novel FXR ligand that regulates metabolism, *Nat Commun*, 4 (2013) 1937.

- [84] Josep Maria Del Bas<sup>1</sup>, Marie-Louise Ricketts<sup>2</sup>, Montserrat Vaqué<sup>1</sup>, Esther Sala<sup>1</sup>, Helena Quesada<sup>1</sup>, Anna Ardevol<sup>1</sup>, M. Josepa Salvadó<sup>1</sup>, Mayte Blay<sup>1</sup>, Lluís Arola<sup>1</sup>, David D. Moore<sup>2</sup>, Gerard Pujadas<sup>1</sup>, J.F.-L. and, C. Bladé<sup>1</sup>, Dietary procyanidins enhance transcriptional activity of bile acid-activated FXR in vitro and reduce triglyceridemia in vivo in a FXR-dependent manner, *Molecular Nutrition & Food Research*, 53 (2009) 805-814.
- [85] M.I. Kaldas, U.K. Walle, H. van der Woude, J.M. McMillan, T. Walle, Covalent binding of the flavonoid quercetin to human serum albumin, *J Agric Food Chem*, 53 (2005) 4194-4197.
- [86] T. Kanda, L. Foucand, Y. Nakamura, I. Niot, P. Besnard, M. Fujita, Y. Sakai, K. Hatakeyama, T. Ono, H. Fujii, Regulation of expression of human intestinal bile acid-binding protein in Caco-2 cells, *Biochem J*, 330 ( Pt 1) (1998) 261-265.
- [87] P.B. Kandagal, S. Ashoka, J. Seetharamappa, S.M. Shaikh, Y. Jadegoud, O.B. Ijare, Study of the interaction of an anticancer drug with human and bovine serum albumin: spectroscopic approach, *J Pharm Biomed Anal*, 41 (2006) 393-399.
- [88] A.B. Kanu, P. Dwivedi, M. Tam, L. Matz, H.H. Hill, Jr., Ion mobility-mass spectrometry, *J Mass Spectrom*, 43 (2008) 1-22.
- [89] M. Karas, Bachmann, D., Hillenkamp, F., Influence of the wavelength in high irradiance ultraviolet laser desorption mass spectrometry of organic molecules, *Anal Chem*, 57 (1985) 2935-2939.
- [90] C.R. Karnick, *Pharmacopoeial Standards of Herbal Plants*; Srisatgure Publications, Delhi, Vol. 1, Vol. 2 (1994) 183-184, 167.
- [91] A. Kassam, B. Miao, P.R. Young, R. Mukherjee, Retinoid X receptor (RXR) agonist-induced antagonism of farnesoid X receptor (FXR) activity due to absence of coactivator recruitment and decreased DNA binding, *J Biol Chem*, 278 (2003) 10028-10032.
- [92] K.S. Kim, C. Woodward, Protein internal flexibility and global stability: effect of urea on hydrogen exchange rates of bovine pancreatic trypsin inhibitor, *Biochemistry*, 32 (1993) 9609-9613.
- [93] J.S. Kirkwood, L.L. Legette, C.L. Miranda, Y. Jiang, J.F. Stevens, A metabolomics-driven elucidation of the anti-obesity mechanisms of xanthohumol, *J Biol Chem*, 288 (2013) 19000-19013.
- [94] J.R. Lakowicz, SpringerLink (Online service), *Principles of Fluorescence Spectroscopy*, in, Springer Science+Business Media, LLC, Boston, MA, 2006.
- [95] J.R. Lakowicz, G. Weber, Quenching of fluorescence by oxygen. A probe for structural fluctuations in macromolecules, *Biochemistry*, 12 (1973) 4161-4170.
- [96] A. Lanzini, M.G. De Tavonatti, B. Panarotto, S. Scalia, A. Mora, F. Benini, O. Baisini, F. Lanzarotto, Intestinal absorption of the bile acid analogue <sup>75</sup>Se-homocholeic acid-taurine is

increased in primary biliary cirrhosis, and reverts to normal during ursodeoxycholic acid administration, *Gut*, 52 (2003) 1371-1375.

[97] Y.M. Lee, K.H. Hsieh, W.J. Lu, H.C. Chou, D.S. Chou, L.M. Lien, J.R. Sheu, K.H. Lin, Xanthohumol, a Prenylated Flavonoid from Hops (*Humulus lupulus*), Prevents Platelet Activation in Human Platelets, *Evid Based Complement Alternat Med*, 2012 (2012) 852362.

[98] P. Lefebvre, B. Cariou, F. Lien, F. Kuipers, B. Staels, Role of bile acids and bile acid receptors in metabolic regulation, *Physiol Rev*, 89 (2009) 147-191.

[99] L. Legette, C. Karnpracha, R.L. Reed, J. Choi, G. Bobe, J.M. Christensen, R. Rodriguez-Proteau, J.Q. Purnell, J.F. Stevens, Human pharmacokinetics of xanthohumol, an antihyperglycemic flavonoid from hops, *Mol Nutr Food Res*, 58 (2014) 248-255.

[100] L.L. Legette, A.Y. Luna, R.L. Reed, C.L. Miranda, G. Bobe, R.R. Proteau, J.F. Stevens, Xanthohumol lowers body weight and fasting plasma glucose in obese male Zucker fa/fa rats, *Phytochemistry*, 91 (2013) 236-241.

[101] S.S. Lehrer, Solute perturbation of protein fluorescence. The quenching of the tryptophyl fluorescence of model compounds and of lysozyme by iodide ion, *Biochemistry*, 10 (1971) 3254-3263.

[102] J.L. Lew, A. Zhao, J. Yu, L. Huang, N. De Pedro, F. Pelaez, S.D. Wright, J. Cui, The farnesoid X receptor controls gene expression in a ligand- and promoter-selective fashion, *J Biol Chem*, 279 (2004) 8856-8861.

[103] G. Li, W. Lin, J.J. Araya, T. Chen, B.N. Timmermann, G.L. Guo, A tea catechin, epigallocatechin-3-gallate, is a unique modulator of the farnesoid X receptor, *Toxicol Appl Pharmacol*, 258 (2012) 268-274.

[104] J.D. Love, J.T. Gooch, S. Benko, C. Li, L. Nagy, V.K. Chatterjee, R.M. Evans, J.W. Schwabe, The structural basis for the specificity of retinoid-X receptor-selective agonists: new insights into the role of helix H12, *J Biol Chem*, 277 (2002) 11385-11391.

[105] J.T. Lundquist, D.C. Harnish, C.Y. Kim, J.F. Mehlmann, R.J. Unwalla, K.M. Phipps, M.L. Crawley, T. Commons, D.M. Green, W.X. Xu, W.T. Hum, J.E. Eta, I. Feingold, V. Patel, M.J. Evans, K. Lai, L. Borges-Marcucci, P.E. Mahaney, J.E. Wrobel, Improvement of Physiochemical Properties of the Tetrahydroazepinoindole Series of Farnesoid X Receptor (FXR) Agonists: Beneficial Modulation of Lipids in Primates, *Journal of Medicinal Chemistry*, 53 (2010) 1774-1787.

[106] J.A. Lupisella, J.E. Driscoll, W.J. Metzler, P.R. Reczek, The ligand binding domain of the human retinoic acid receptor gamma is predominantly alpha-helical with a Trp residue in the ligand binding site, *J Biol Chem*, 270 (1995) 24884-24890.

[107] K. Ma, P.K. Saha, L. Chan, D.D. Moore, Farnesoid X receptor is essential for normal glucose homeostasis, *J Clin Invest*, 116 (2006) 1102-1109.

- [108] P.J. Magalhaes, D.O. Carvalho, J.M. Cruz, L.F. Guido, A.A. Barros, Fundamentals and health benefits of xanthohumol, a natural product derived from hops and beer, *Nat Prod Commun*, 4 (2009) 591-610.
- [109] C.S. Maier, M.L. Deinzer, Protein conformations, interactions, and H/D exchange, *Methods Enzymol*, 402 (2005) 312-360.
- [110] C.S. Maier, O.H. Kim, M.L. Deinzer, Conformational properties of the A-state of cytochrome c studied by hydrogen/deuterium exchange and electrospray mass spectrometry, *Anal Biochem*, 252 (1997) 127-135.
- [111] C.S. Maier, M.I. Schimerlik, M.L. Deinzer, Thermal denaturation of Escherichia coli thioredoxin studied by hydrogen/deuterium exchange and electrospray ionization mass spectrometry: monitoring a two-state protein unfolding transition, *Biochemistry*, 38 (1999) 1136-1143.
- [112] M. Makishima, A.Y. Okamoto, J.J. Repa, H. Tu, R.M. Learned, A. Luk, M.V. Hull, K.D. Lustig, D.J. Mangelsdorf, B. Shan, Identification of a nuclear receptor for bile acids, *Science*, 284 (1999) 1362-1365.
- [113] B.A. Mamyrin, Karataev, V. I., Shmikk, D. V., Zagulin, V. A., The mass reflectron, a new nonmagnetic time-of-flight mass spectrometer with high resolution, *Soviet Phy JETP*, 37 (1973) 45-48.
- [114] J.G. Mandell, A. Baerga-Ortiz, S. Akashi, K. Takio, E.A. Komives, Solvent accessibility of the thrombin-thrombomodulin interface, *J Mol Biol*, 306 (2001) 575-589.
- [115] A. Mencarelli, S. Fiorucci, FXR an emerging therapeutic target for the treatment of atherosclerosis, *J Cell Mol Med*, 14 (2010) 79-92.
- [116] D. Merk, D. Steinhilber, M. Schubert-Zsilavecz, Medicinal chemistry of farnesoid X receptor ligands: from agonists and antagonists to modulators, *Future Med Chem*, 4 (2012) 1015-1036.
- [117] U. Meyer, G. Costantino, A. Macchiarulo, R. Pellicciari, Is antagonism of E/Z-guggulsterone at the farnesoid X receptor mediated by a noncanonical binding site? A molecular modeling study, *J Med Chem*, 48 (2005) 6948-6955.
- [118] L.Z. Mi, S. Devarakonda, J.M. Harp, Q. Han, R. Pellicciari, T.M. Willson, S. Khorasanizadeh, F. Rastinejad, Structural basis for bile acid binding and activation of the nuclear receptor FXR, *Mol Cell*, 11 (2003) 1093-1100.
- [119] S.R. Milligan, J.C. Kalita, A. Heyerick, H. Rong, L. De Cooman, D. De Keukeleire, Identification of a potent phytoestrogen in hops (*Humulus lupulus* L.) and beer, *J Clin Endocrinol Metab*, 84 (1999) 2249-2252.

- [120] C.L. Miranda, G.L. Aponso, J.F. Stevens, M.L. Deinzer, D.R. Buhler, Prenylated chalcones and flavanones as inducers of quinone reductase in mouse Hepa 1c1c7 cells, *Cancer Lett*, 149 (2000) 21-29.
- [121] C.L. Miranda, J.F. Stevens, A. Helmrigh, M.C. Henderson, R.J. Rodriguez, Y.H. Yang, M.L. Deinzer, D.W. Barnes, D.R. Buhler, Antiproliferative and cytotoxic effects of prenylated flavonoids from hops (*Humulus lupulus*) in human cancer cell lines, *Food Chem Toxicol*, 37 (1999) 271-285.
- [122] C.L. Miranda, J.F. Stevens, V. Ivanov, M. McCall, B. Frei, M.L. Deinzer, D.R. Buhler, Antioxidant and prooxidant actions of prenylated and nonprenylated chalcones and flavanones in vitro, *J Agric Food Chem*, 48 (2000) 3876-3884.
- [123] A. Miranker, C.V. Robinson, S.E. Radford, R.T. Aplin, C.M. Dobson, Detection of transient protein folding populations by mass spectrometry, *Science*, 262 (1993) 896-900.
- [124] M. Moller, A. Denicola, Protein tryptophan accessibility studied by fluorescence quenching, *Biochem Mol Biol Edu*, 30 (2002) 175-178.
- [125] L.B. Moore, D.J. Parks, S.A. Jones, R.K. Bledsoe, T.G. Consler, J.B. Stimmel, B. Goodwin, C. Liddle, S.G. Blanchard, T.M. Willson, J.L. Collins, S.A. Kliewer, Orphan nuclear receptors constitutive androstane receptor and pregnane X receptor share xenobiotic and steroid ligands, *J Biol Chem*, 275 (2000) 15122-15127.
- [126] S.J. Nam, H. Ko, M. Shin, J. Ham, J. Chin, Y. Kim, H. Kim, K. Shin, H. Choi, H. Kang, Farnesoid X-activated receptor antagonists from a marine sponge *Spongia* sp, *Bioorg Med Chem Lett*, 16 (2006) 5398-5402.
- [127] M.A. Neves, M. Totrov, R. Abagyan, Docking and scoring with ICM: the benchmarking results and strategies for improvement, *J Comput Aided Mol Des*, 26 (2012) 675-686.
- [128] K.C. Nicolaou, R.M. Evans, A.J. Roecker, R. Hughes, M. Downes, J.A. Pfefferkorn, Discovery and optimization of non-steroidal FXR agonists from natural product-like libraries, *Org Biomol Chem*, 1 (2003) 908-920.
- [129] T. Nishimaki-Mogami, M. Une, T. Fujino, Y. Sato, N. Tamehiro, Y. Kawahara, K. Shudo, K. Inoue, Identification of intermediates in the bile acid synthetic pathway as ligands for the farnesoid X receptor, *J Lipid Res*, 45 (2004) 1538-1545.
- [130] N. Novac, T. Heinzel, Nuclear receptors: overview and classification, *Curr Drug Targets Inflamm Allergy*, 3 (2004) 335-346.
- [131] H. Nozawa, Xanthohumol, the chalcone from beer hops (*Humulus lupulus* L.), is the ligand for farnesoid X receptor and ameliorates lipid and glucose metabolism in KK-A(y) mice, *Biochem Biophys Res Commun*, 336 (2005) 754-761.

- [132] L. Pan, H. Becker, C. Gerhauser, Xanthohumol induces apoptosis in cultured 40-16 human colon cancer cells by activation of the death receptor- and mitochondrial pathway, *Mol Nutr Food Res*, 49 (2005) 837-843.
- [133] A. Papadopoulou, R.J. Green, R.A. Frazier, Interaction of flavonoids with bovine serum albumin: a fluorescence quenching study, *J Agric Food Chem*, 53 (2005) 158-163.
- [134] C.H. Parker, C.R. Morgan, K.D. Rand, J.R. Engen, J.W. Jorgenson, D.W. Stafford, A Conformational Investigation of Propeptide Binding to the Integral Membrane Protein gamma-Glutamyl Carboxylase Using Nanodisc Hydrogen Exchange Mass Spectrometry, *Biochemistry*, 53 (2014) 1511-1520.
- [135] D.J. Parks, S.G. Blanchard, R.K. Bledsoe, G. Chandra, T.G. Consler, S.A. Kliewer, J.B. Stimmel, T.M. Willson, A.M. Zavacki, D.D. Moore, J.M. Lehmann, Bile acids: natural ligands for an orphan nuclear receptor, *Science*, 284 (1999) 1365-1368.
- [136] G. Paumgartner, U. Beuers, Ursodeoxycholic acid in cholestatic liver disease: mechanisms of action and therapeutic use revisited, *Hepatology*, 36 (2002) 525-531.
- [137] R. Pellicciari, S. Fiorucci, E. Camaioni, C. Clerici, G. Costantino, P.R. Maloney, A. Morelli, D.J. Parks, T.M. Willson, 6 $\alpha$ -ethyl-chenodeoxycholic acid (6-ECDCA), a potent and selective FXR agonist endowed with anticholestatic activity, *J Med Chem*, 45 (2002) 3569-3572.
- [138] R. Pellicciari, R.C. Rizzo, G. Costantino, M. Marinozzi, L. Amori, P. Guidetti, H.Q. Wu, R. Schwarcz, Modulators of the kynurenine pathway of tryptophan metabolism: synthesis and preliminary biological evaluation of (S)-4-(ethylsulfonyl)benzoylalanine, a potent and selective kynurenine aminotransferase II (KAT II) inhibitor, *ChemMedChem*, 1 (2006) 528-531.
- [139] M.S. Pepper, S.J. Hazel, M. Humpel, W.D. Schleuning, 8-prenylnaringenin, a novel phytoestrogen, inhibits angiogenesis in vitro and in vivo, *J Cell Physiol*, 199 (2004) 98-107.
- [140] R.S. Plumb, K.A. Johnson, P. Rainville, B.W. Smith, I.D. Wilson, J.M. Castro-Perez, J.K. Nicholson, UPLC/MSE; a new approach for generating molecular fragment information for biomarker structure elucidation (vol 20, pg 1989, 2006), *Rapid Commun Mass Sp*, 20 (2006) 2234-2234.
- [141] S.D.G. Pringle, K.; Wildgoose, J. L.; Williams, J. P.; Slade, S. E.; Thalassinou, K.; Bateman, R. H.; Bowers, M. T.; Scrivens,., An investigation of the mobility separation of some peptide and protein ions using a new hybrid quadrupole/travelling wave IMS/oa-ToF instrument, *International journal of mass spectrometry*, 261 (2007).
- [142] M. Rad, M. Humpel, O. Schaefer, R.C. Schoemaker, W.D. Schleuning, A.F. Cohen, J. Burggraaf, Pharmacokinetics and systemic endocrine effects of the phyto-oestrogen 8-prenylnaringenin after single oral doses to postmenopausal women, *Br J Clin Pharmacol*, 62 (2006) 288-296.

- [143] P. Rajendran, A.I. Kidane, T.W. Yu, W.M. Dashwood, W.H. Bisson, C.V. Lohr, E. Ho, D.E. Williams, R.H. Dashwood, HDAC turnover, CtIP acetylation and dysregulated DNA damage signaling in colon cancer cells treated with sulforaphane and related dietary isothiocyanates, *Epigenetics*, 8 (2013) 612-623.
- [144] F. Rasoulzadeh, H.N. Jabary, A. Naseri, M.R. Rashidi, Fluorescence quenching study of quercetin interaction with bovine milk xanthine oxidase, *Spectrochim Acta A Mol Biomol Spectrosc*, 72 (2009) 190-193.
- [145] H.M. Rawel, S.K. Frey, K. Meidtnr, J. Kroll, F.J. Schweigert, Determining the binding affinities of phenolic compounds to proteins by quenching of the intrinsic tryptophan fluorescence, *Mol Nutr Food Res*, 50 (2006) 705-713.
- [146] S. Rayalam, J.Y. Yang, M.A. Della-Fera, H.J. Park, S. Ambati, C.A. Baile, Anti-obesity effects of xanthohumol plus guggulsterone in 3T3-L1 adipocytes, *J Med Food*, 12 (2009) 846-853.
- [147] H.G.F. Richter, G.M. Benson, K.H. Bleicher, D. Blum, E. Chaput, N. Clemann, S. Feng, C. Gardes, U. Grether, P. Hartman, B. Kuhn, R.E. Martin, J.M. Plancher, M.G. Rudolph, F. Schuler, S. Taylor, Optimization of a novel class of benzimidazole-based farnesoid X receptor (FXR) agonists to improve physicochemical and ADME properties, *Bioorganic & Medicinal Chemistry Letters*, 21 (2011) 1134-1140.
- [148] H.G.F. Richter, G.M. Benson, D. Blum, E. Chaput, S. Feng, C. Gardes, U. Grether, P. Hartman, B. Kuhn, R.E. Martin, J.M. Plancher, M.G. Rudolph, F. Schuler, S. Taylor, K.H. Bleicher, Discovery of novel and orally active FXR agonists for the potential treatment of dyslipidemia & diabetes, *Bioorganic & Medicinal Chemistry Letters*, 21 (2011) 191-194.
- [149] R.J. Rodriguez, C.L. Miranda, J.F. Stevens, M.L. Deinzer, D.R. Buhler, Influence of prenylated and non-prenylated flavonoids on liver microsomal lipid peroxidation and oxidative injury in rat hepatocytes, *Food Chem Toxicol*, 39 (2001) 437-445.
- [150] O. Schaefer, M. Humpel, K.H. Fritzemeier, R. Bohlmann, W.D. Schleuning, 8-Prenyl naringenin is a potent ERalpha selective phytoestrogen present in hops and beer, *J Steroid Biochem Mol Biol*, 84 (2003) 359-360.
- [151] V. Sepe, G. Bifulco, B. Renga, C. D'Amore, S. Fiorucci, A. Zampella, Discovery of sulfated sterols from marine invertebrates as a new class of marine natural antagonists of farnesoid-X-receptor, *J Med Chem*, 54 (2011) 1314-1320.
- [152] V. Sepe, R. Ummarino, M.V. D'Auria, O. Tagliatela-Scafati, S.D. Marino, C. D'Amore, B. Renga, M.G. Chini, G. Bifulco, Y. Nakao, N. Fusetani, S. Fiorucci, A. Zampella, Preliminary structure-activity relationship on theonellasterol, a new chemotype of FXR antagonist, from the marine sponge *Theonella swinhoei*, *Mar Drugs*, 10 (2012) 2448-2466.
- [153] K. Shin, J. Chin, D. Hahn, J. Lee, H. Hwang, D.H. Won, J. Ham, H. Choi, E. Kang, H. Kim, M.K. Ju, S.J. Nam, H. Kang, Sterols from a soft coral, *Dendronephthya gigantea* as farnesoid X-activated receptor antagonists, *Steroids*, 77 (2012) 355-359.

- [154] T. Shiraki, N. Kamiya, S. Shiki, T.S. Kodama, A. Kakizuka, H. Jingami, Alpha,beta-unsaturated ketone is a core moiety of natural ligands for covalent binding to peroxisome proliferator-activated receptor gamma, *J Biol Chem*, 280 (2005) 14145-14153.
- [155] M.D. Shortridge, D.S. Hage, G.S. Harbison, R. Powers, Estimating protein-ligand binding affinity using high-throughput screening by NMR, *J Comb Chem*, 10 (2008) 948-958.
- [156] A.K. Shukla, J.H. Futrell, Tandem mass spectrometry: dissociation of ions by collisional activation, *J Mass Spectrom*, 35 (2000) 1069-1090.
- [157] A.I. Shulman, C. Larson, D.J. Mangelsdorf, R. Ranganathan, Structural determinants of allosteric ligand activation in RXR heterodimers, *Cell*, 116 (2004) 417-429.
- [158] D. Silva, C.M. Cortez, J. Cunha-Bastos, S.R. Louro, Methyl parathion interaction with human and bovine serum albumin, *Toxicol Lett*, 147 (2004) 53-61.
- [159] C.J. Sinal, F.J. Gonzalez, Guggulsterone: an old approach to a new problem, *Trends Endocrinol Metab*, 13 (2002) 275-276.
- [160] C.J. Sinal, M. Tohkin, M. Miyata, J.M. Ward, G. Lambert, F.J. Gonzalez, Targeted disruption of the nuclear receptor FXR/BAR impairs bile acid and lipid homeostasis, *Cell*, 102 (2000) 731-744.
- [161] R.B. Singh, M.A. Niaz, S. Ghosh, Hypolipidemic and antioxidant effects of Commiphora mukul as an adjunct to dietary therapy in patients with hypercholesterolemia, *Cardiovasc Drugs Ther*, 8 (1994) 659-664.
- [162] S.M. Soisson, G. Parthasarathy, A.D. Adams, S. Sahoo, A. Sitlani, C. Sparrow, J. Cui, J.W. Becker, Identification of a potent synthetic FXR agonist with an unexpected mode of binding and activation, *Proc Natl Acad Sci U S A*, 105 (2008) 5337-5342.
- [163] C. Soldani, M.G. Bottone, C. Pellicciari, A.I. Scovassi, Nucleolus disassembly in mitosis and apoptosis: dynamic redistribution of phosphorylated-c-Myc, fibrillarin and Ki-67, *Eur J Histochem*, 50 (2006) 273-280.
- [164] P. Somasundaran, A.T. Hubbard, *Encyclopedia of surface and colloid science*, Marcel Dekker, New York, 2002.
- [165] J.B. Sperry, R.Y. Huang, M.M. Zhu, D.L. Rempel, M.L. Gross, Hydrophobic Peptides Affect Binding of Calmodulin and Ca as Explored by H/D Amide Exchange and Mass Spectrometry, *Int J Mass Spectrom*, 302 (2011) 85-92.
- [166] J.B. Sperry, Z.C. Ryan, R. Kumar, M.L. Gross, Hydrogen/Deuterium Exchange Reflects Binding of Human Centrin 2 to Ca(2+) and Xeroderma Pigmentosum Group C Peptide: An Example of EX1 Kinetics, *Int J Mass Spectrom*, 330-332 (2012) 302-309.
- [167] K.G. Steven D. Pringle, Jason L. Wildgoose, Jonathan P. Williams, Susan E. Slade, Konstantinos Thalassions, Rober H. Bateman, Michael T. Bowers, James H. Scrivens, An



investigation of the mobility separation of some peptide and protein ions using a new hybrid quadrupole/travelling wave IMS/oa-TOF instrument, *International journal of mass spectrometry*, 261 (2006) 1-12.

[168] J.F. Stevens, Miranda, C.L., Buhler, D.R., Deinzer, M.L., *Chemistry and Biology of Hop Flavonoids*, *Journal of the American Society of Brewing Chemists*, 56 (1998) 136-145.

[169] J.F. Stevens, J.E. Page, Xanthohumol and related prenylflavonoids from hops and beer: to your good health!, *Phytochemistry*, 65 (2004) 1317-1330.

[170] J.F. Stevens, A.W. Taylor, J.E. Clawson, M.L. Deinzer, Fate of xanthohumol and related prenylflavonoids from hops to beer, *J Agric Food Chem*, 47 (1999) 2421-2428.

[171] J.F. Stevens, A.W. Taylor, M.L. Deinzer, Quantitative analysis of xanthohumol and related prenylflavonoids in hops and beer by liquid chromatography-tandem mass spectrometry, *J Chromatogr A*, 832 (1999) 97-107.

[172] A.Q. Sun, Y. Luo, D.S. Backos, S. Xu, N. Balasubramaniyan, P. Reigan, F.J. Suchy, Identification of functionally relevant lysine residues that modulate human farnesoid X receptor activation, *Mol Pharmacol*, 83 (2013) 1078-1086.

[173] L. Swint-Kruse, A.D. Robertson, Temperature and pH dependences of hydrogen exchange and global stability for ovomucoid third domain, *Biochemistry*, 35 (1996) 171-180.

[174] N. Tabata, M. Ito, H. Tomoda, S. Omura, Xanthohumols, diacylglycerol acyltransferase inhibitors, from *Humulus lupulus*, *Phytochemistry*, 46 (1997) 683-687.

[175] K. Tanaka, Waki, H., Ido, Y., Akita, s., Yoshida, Y., Yoshida, T., , Protein and polymer analyses up to  $m/z$  100 000 by laser ionization time-of-flight mass spectrometry., *Rapid Commun Mass Spectrom*, 2 (1988) 151-153.

[176] S. Titolo, E. Welchner, P.W. White, J. Archambault, Characterization of the DNA-binding properties of the origin-binding domain of simian virus 40 large T antigen by fluorescence anisotropy, *J Virol*, 77 (2003) 5512-5518.

[177] M. Totrov, Abagyan, R., Derivation of sensitive discrimination potential for virtual ligand screening proceedings of RECOMB99in ACM, Lyon, France, 1999, pp. 312-320.

[178] C. Ulbricht, E. Basch, P. Szapary, P. Hammerness, S. Axentsev, H. Boon, D. Kroll, L. Garraway, M. Vora, J. Woods, Guggul for hyperlipidemia: a review by the Natural Standard Research Collaboration, *Complement Ther Med*, 13 (2005) 279-290.

[179] N.L. Urizar, A.B. Liverman, D.T. Dodds, F.V. Silva, P. Ordentlich, Y. Yan, F.J. Gonzalez, R.A. Heyman, D.J. Mangelsdorf, D.D. Moore, A natural product that lowers cholesterol as an antagonist ligand for FXR, *Science*, 296 (2002) 1703-1706.

[180] N.L. Urizar, D.D. Moore, GUGULIPID: a natural cholesterol-lowering agent, *Annu Rev Nutr*, 23 (2003) 303-313.

- [181] B. Vanhoecke, L. Derycke, V. Van Marck, H. Depypere, D. De Keukeleire, M. Bracke, Antiinvasive effect of xanthohumol, a prenylated chalcone present in hops (*Humulus lupulus* L.) and beer, *Int J Cancer*, 117 (2005) 889-895.
- [182] T. Waku, T. Shiraki, T. Oyama, Y. Fujimoto, K. Maebara, N. Kamiya, H. Jingami, K. Morikawa, Structural insight into PPARgamma activation through covalent modification with endogenous fatty acids, *J Mol Biol*, 385 (2009) 188-199.
- [183] T. Waku, T. Shiraki, T. Oyama, K. Morikawa, Atomic structure of mutant PPARgamma LBD complexed with 15d-PGJ2: novel modulation mechanism of PPARgamma/RXRalpha function by covalently bound ligands, *FEBS Lett*, 583 (2009) 320-324.
- [184] T.E. Wales, J.R. Engen, Hydrogen exchange mass spectrometry for the analysis of protein dynamics, *Mass Spectrom Rev*, 25 (2006) 158-170.
- [185] H. Wang, J. Chen, K. Hollister, L.C. Sowers, B.M. Forman, Endogenous bile acids are ligands for the nuclear receptor FXR/BAR, *Mol Cell*, 3 (1999) 543-553.
- [186] Z. Wang, X. Tan, D. Chen, Q. Yue, Z. Song, Study on the binding behavior of lysozyme with cephalosporin analogues by fluorescence spectroscopy, *J Fluoresc*, 19 (2009) 801-808.
- [187] C. Weickhardt, Moritz, F., Grottemeyer, J. , Time-of-flight mass spectrometry: State-of-the-art in chemical analysis and molecular science, *Mass Spectrom Rev*, 15 (1996) 139-162.
- [188] D.D. Weis, J.R. Engen, I.J. Kass, Semi-automated data processing of hydrogen exchange mass spectra using HX-Express, *J Am Soc Mass Spectrom*, 17 (2006) 1700-1703.
- [189] S. Westin, R.A. Heyman, R. Martin, FXR, a therapeutic target for bile acid and lipid disorders, *Mini Rev Med Chem*, 5 (2005) 719-727.
- [190] J. Wu, C. Xia, J. Meier, S. Li, X. Hu, D.S. Lala, The hypolipidemic natural product guggulsterone acts as an antagonist of the bile acid receptor, *Mol Endocrinol*, 16 (2002) 1590-1597.
- [191] G. Xia, L.J. Boerma, B.D. Cox, C. Qiu, S. Kang, C.D. Smith, M.B. Renfrow, D.D. Muccio, Structure, Energetics, and Dynamics of Binding Coactivator Peptide to the Human Retinoid X Receptor alpha Ligand Binding Domain Complex with 9-cis-Retinoic Acid, *Biochemistry*, (2010).
- [192] G. Xu, L.X. Pan, H. Li, B.M. Forman, S.K. Erickson, S. Shefer, J. Bollineni, A.K. Batta, J. Christie, T.H. Wang, J. Michel, S. Yang, R. Tsai, L. Lai, K. Shimada, G.S. Tint, G. Salen, Regulation of the farnesoid X receptor (FXR) by bile acid flux in rabbits, *J Biol Chem*, 277 (2002) 50491-50496.
- [193] M. Yamashita, Fenn, J.B., Electrospray ion source. Another variation on the freejet theme., *J Phys Chem*, 88 (1984) 4451-4459.

- [194] X. Yan, M.L. Deinzer, M.I. Schimerlik, D. Broderick, M.E. Leid, M.I. Dawson, Investigation of ligand interactions with human RXRalpha by hydrogen/deuterium exchange and mass spectrometry, *J Am Soc Mass Spectrom*, 17 (2006) 1510-1517.
- [195] X. Yan, C.S. Maier, Hydrogen/deuterium exchange mass spectrometry, *Methods Mol Biol*, 492 (2009) 255-271.
- [196] X. Yan, E. Perez, M. Leid, M.I. Schimerlik, A.R. de Lera, M.L. Deinzer, Deuterium exchange and mass spectrometry reveal the interaction differences of two synthetic modulators of RXRalpha LBD, *Protein Sci*, 16 (2007) 2491-2501.
- [197] X. Yan, H. Zhang, J. Watson, M.I. Schimerlik, M.L. Deinzer, Hydrogen/deuterium exchange and mass spectrometric analysis of a protein containing multiple disulfide bonds: Solution structure of recombinant macrophage colony stimulating factor-beta (rhM-CSFbeta), *Protein Sci*, 11 (2002) 2113-2124.
- [198] C. Yang, Q. Li, Y. Li, Targeting nuclear receptors with marine natural products, *Mar Drugs*, 12 (2014) 601-635.
- [199] D. Yang, J. Yang, D. Shi, D. Xiao, Y.T. Chen, C. Black, R. Deng, B. Yan, Hypolipidemic agent Z-guggulsterone: metabolism interplays with induction of carboxylesterase and bile salt export pump, *J Lipid Res*, 53 (2012) 529-539.
- [200] J.Y. Yang, M.A. Della-Fera, S. Rayalam, C.A. Baile, Effect of xanthohumol and isoxanthohumol on 3T3-L1 cell apoptosis and adipogenesis, *Apoptosis*, 12 (2007) 1953-1963.
- [201] B.Z. Yu, R. Kaimal, S. Bai, K.A. El Sayed, S.A. Tatulian, R.J. Apitz, M.K. Jain, R. Deng, O.G. Berg, Effect of guggulsterone and cembranoids of *Commiphora mukul* on pancreatic phospholipase A(2): role in hypocholesterolemia, *J Nat Prod*, 72 (2009) 24-28.
- [202] P. Zanolli, M. Zavatti, Pharmacognostic and pharmacological profile of *Humulus lupulus* L, *J Ethnopharmacol*, 116 (2008) 383-396.
- [203] J. Zhang, M.J. Chalmers, K.R. Stayrook, L.L. Burris, R.D. Garcia-Ordonez, B.D. Pascal, T.P. Burris, J.A. Dodge, P.R. Griffin, Hydrogen/deuterium exchange reveals distinct agonist/partial agonist receptor dynamics within vitamin D receptor/retinoid X receptor heterodimer, *Structure*, 18 (2010) 1332-1341.
- [204] Y. Zhang, H.R. Kast-Woelbern, P.A. Edwards, Natural structural variants of the nuclear receptor farnesoid X receptor affect transcriptional activation, *J Biol Chem*, 278 (2003) 104-110.
- [205] Y.Q. Zhang, X.P. Wang, C. Vales, F.Y. Lee, H. Lee, A.J. Lusis, P.A. Edwards, FXR deficiency causes reduced atherosclerosis in *Ldlr*(-/-) mice, *Arterioscl Throm Vas*, 26 (2006) 2316-2321.
- [206] Z. Zhang, C.B. Post, D.L. Smith, Amide hydrogen exchange determined by mass spectrometry: application to rabbit muscle aldolase, *Biochemistry*, 35 (1996) 779-791.

- [207] Z. Zhang, D.L. Smith, Determination of amide hydrogen exchange by mass spectrometry: a new tool for protein structure elucidation, *Protein Sci*, 2 (1993) 522-531.
- [208] Z. Zhang, D.L. Smith, Thermal-induced unfolding domains in aldolase identified by amide hydrogen exchange and mass spectrometry, *Protein Sci*, 5 (1996) 1282-1289.
- [209] A. Zhao, J.L. Lew, L. Huang, J. Yu, T. Zhang, Y. Hrywna, J.R. Thompson, N. de Pedro, R.A. Blevins, F. Pelaez, S.D. Wright, J. Cui, Human kininogen gene is transactivated by the farnesoid X receptor, *J Biol Chem*, 278 (2003) 28765-28770.
- [210] A. Zhao, J. Yu, J.L. Lew, L. Huang, S.D. Wright, J. Cui, Polyunsaturated fatty acids are FXR ligands and differentially regulate expression of FXR targets, *DNA Cell Biol*, 23 (2004) 519-526.